Transcription analysis of an immune factor in a main African malaria vector *Anopheles funestus*

WITS
UNIVERSITY

Witness Ramashia

M.Sc. report submitted to the Faculty of Health Science, University of the Witwatersrand, Johannesburg, in fulfilment of the requirements for the degree of Master of Science in Medicine.

March 2022

Declaration

I, Witness Ramashia declare that this Dissertation is my own work. It is being submitted for M.Sc. (Medicine) degree in Health Sciences, University of the Witwatersrand, Johannesburg. It has not been submitted before for a degree or examination at any other university.

_____

Witness Ramashia

30/03/22

Dedication

This dissertation is dedicated to my late grandmother **Lorah Mtileni**.

There are no words on this earth to describe how much I miss you.

Thank you for the teachings and support you gave to me during your borrowed time on earth. Your desire for me to achieve more than what you were granted by life is the foundation with which my life is built, and your believing in me has made me embrace every opportunity in my life. This work is one of the signs of my gratitude to you.

Abstract

Anopheles funestus s.s. is one of the vectors that plays a major role in the transmission of malaria in sub-Saharan Africa, with *Plasmodium falciparum* the principal human malaria parasite, responsible for the majority of cases in Africa. Transmission of the malaria parasite to the human host depends on the successful completion of the parasite's sexual development in the *Anopheles* vector, however, the mosquito's immune system influences the plasmodial transmission cycle. The defensive immune response of the *Anopheles* contributes to decrease parasite numbers, but, certain factors in the immune response and blood meal favour infection. *Anopheles* C-type lectins (CTLs) are immune protein recognition receptors involved in the melanization process, the insect's prime immune reaction. CTLs, particularly *An. gambiae* CTL4 has been shown to inhibit melanization, thereby supporting the survival of ookinetes to oocysts and increasing the potential risk of infection. In this study, *An. funestus s.s.* CTL4 gene was successfully amplified and the analyzed protein was identified to consist of an N-terminal tri-cysteine (CXCPC) motif and one CTL domain with two calcium ions binding sites. Structural modelling revealed that this CTL4 domain is composed of two α-helices, five β-sheets and double-loop fold that are stabilized by two highly conserved disulphide bridges. In order to obtain sufficient number of fed adult females for infection/treatment studies, optimization of the feeding rate using an artificial feeding system was determined. Adult females provided with distilled water (dH_2O), 72 hours prior to blood feeding had an increased feeding rate ($p = 0.0117$), whereas the age at which adult females received their first blood meal had no impact on the feeding success rate. However, the cumulative probability of survival post blood feeding is affected by the age of the mosquitoes and reached 82, 66 and 50% at ages 5, 10 and 15 days old, respectively. Successful ingestion of infected *P. falciparum* (NF54 strain) blood by the laboratory *An. funestus s.s.* colony with was confirmed by the presence of the parasites' circumsporozoite protein (CPS) gene amplification. The mRNA expression level of the CTL4 in *P. falciparum* infected and uninfected mosquitoes were not significantly different ($p = 0.2560$). Sensitivity of *An. funestus s.s.* to antimalarial drug chloroquine (CQ) displayed no larvicidal activity, whereas CQ in the blood meal knocked down and killed *Anopheles* adults in a dose-dependent manner. Collectively, these observations show that it is feasible to obtain *P. falciparum* infected laboratory *An. funestus s.s.* using an artificial membrane feeding system. This can be used for comprehensive study on natural *Plasmodium-Anopheles* interactions that may provide novel malaria control strategies' including transmission-blocking vaccines. In addition, this study suggests that CQ interferes with the *Anopheles* immune system, compromising the defensive

response. This highlights the importance of understanding the impact that antimalarial drugs have on malaria parasite transmission in the *Anopheles* vector.

List of Congresses attended

W. Ramashia, R. L. Van Zyl, J. Reader, L.M. Birkholtz, L. L Koekemoer. Transcription analysis of an immune factor in a main African malaria vector *Anopheles funestus s.s.* **Oral presentation**. 26th Biennial SASBMB-FASBMB 8-11th July 2018, North-West University, Potchefstroom, South Africa. **Awarded** the Separations SASBMB-FASBMB 2018 Prize for Best Young Scientist presentation.

W. Ramashia, R. L Van Zyl, J. Reader, L.M. Birkholtz, L. L Koekemoer. Investigating the expression level of an immune factor: C-type lectin in *An. funestus s.s.*infected with *Plasmodium falciparum*. **Poster presentation**. Faculty of Health Science Research Day 6th September 2018, Wits University, Johannesburg, South Africa.

W. Ramashia, R. L Van Zyl, J. Reader, L.M. Birkholtz, L. L Koekemoer. Molecular characterization of an immune factor C-type lectin in a main African malaria vector *Anopheles funestus s.s.* **Poster presentation**. 4th Southern Africa Malaria Research Conference 30th July-1st August 2018, National Institute for Communicable Diseases, Johannesburg, South Africa.

Acknowledgements

I would like to thank:

My Creator and those that came before me for allowing me the opportunity to do this research project and giving me strength and perseverance to complete my project the best way I can.

To my supervisors **Prof. Lizette Leonie Koekemoer** and **Prof. Robyn Lynne Van Zyl,** thank you so much for the guidance, support, opportunity and advice you have given me throughout this project. It was a privilege for me to share your exceptional scientific knowledge and human qualities.

Prof. Lyn-Marie Birkholtz and **Dr. Janette Reader** for culturing the *Plasmodium* parasites, allowing me to perform my infection study in your laboratory and most of all for humouring me and the small chats during my experimental work.

Dr. Annette Bennett and **Erica Erlank** for the chats shared on the road and during the infection experimental work.

Prof. Riann Christian I am indebted and forever grateful for your academic experience and sharing your exceptional scientific knowledge with me. You have helped lay a foundation, supported and encouraged me to thrive to have a deeper understanding of scientific concepts.

My colleagues at WRIM and VCRL, the shared companionship you provided created a friendly working atmosphere. The chats and laughs helped made the journey lighter. Thank you for providing help wherever you could.

To **Mrs. Clowey Stevensons**, thank you for the effort in making sure that reagents and consumables for my experiments are available on time and the chats, laughs and sharing lifelong advice outside of scientific field.

To my mother, siblings and family at large, thank you for your prayers, support, unconditional love and encouragement. You all gave me strength when I did not have and told me I can do it. Thank you for listening.

To **Thembelihle and Busisiwe Msimango**, thank you for the support, encouragement and being my feet when I could not stand. I will forever be grateful for the unconditional love I received from you. Thank you for listening.

To my friends, you have been amazing. I would like to express my deepest gratitude for the encouragement, support and listening.

Special thanks for all financial support received from this project, National Research Foundation (NRF) chair (awarded to **Prof Lizette Koekemoer),** Pharmacology Division and Faculty Research Committee (FRC).

Table of Contents

List of Figures

List of Tables

List of Equations

List of Abbreviations

*Af*CTL4	*An. funestus s.s.*C-type lectin 4
AgDSCAM	*Anopheles gambiae* down syndrome adhesion cell molecule
An.	*Anopheles*
ANOVA	Analysis of variance
AMP	Antimicrobial peptide
bp	Base pair
BLAST	Basic Local Alignment Search Tool
CQ	Chloroquine
CDC	Centre for Disease Control and Prevention
cDNA	Complementary deoxyribonucleic acid
CTL	C-type lectin
CRD	Carbohydrate recognition domain
dH_2O	Distilled water
dNTP	Deoxyribonucleotide triphosphate
DDT	Dichlorodiphenyltrichloroethane
DMSO	Dimethyl sulfoxide
EDTA	Ethylenediaminetetraacetic acid
EPN	Glu-Pro-Asn (mannose) binding motif
FREP	Fibronectin related protein
FUMOZ	*Anopheles funestus* from Mozambique
G	Grams
g	Gravitational constant/G-force
GNBP	Gram-negative binding protein
IL-1,6	Interleukin-1,6
IFN-α	Interferon-α
IMD	Immune deficiency
IRS	Indoor residual spraying
JAK/STAT	Janus kinase signal transduction and activators of transcription
KD	Knock down
LD_{50}	Lethal dosage required to kill 50% of the population
µL	Microlitre
MEGA	Molecular Evolutionary Genetic Analysis
mL	Millilitre
mM	Millimolar
mRNA	Messenger RNA

MWM	Molecular weight marker
ng	Nanogram
NF-κB	Nuclear factor- kappa B
NTC	No template control
PAMP	Pathogen associated molecular pattern
PCR	Polymerase chain reaction
PRR	Pathogen recognition receptors
PGRP-LC	Peptidoglycan recognition protein
% w/v	Percentage weight per volume
PBS	Phosphate buffered saline
*Pf*CRT	*Plasmodium falciparum* CQ resistance transporter
PO	Phenoloxidase
PPAE	Prophenol oxidase activating enzyme
PDB	Protein Data Bank
PRR	Pathogen recognition receptors
QPD	Gln-Pro-Asp (galactose) binding motif
qPCR	Quantitative Polymerase Reaction
RDT	Rapid diagnostic testing
RBC	Red blood cell
RNA	Ribonucleic acid
RNAi	RNA interference
ROS	Reactive oxygen species
STAT	ssignal transduction and activators of transcription
TAE	Tris, Acetic acid, EDTA
TEP	Thioester containing protein
TLR	Toll-like receptors
WHO	World Health Organization
WNDf	Trp-Asn-Asp motif
w/v	weight per volume

CHAPTER ONE

1 Introduction

Mosquitoes are invertebrate anthropods that are classified under the Diptera order (Service, 1996). There are approximately 3,600 species of mosquitoes that have been identified, 41 of which belong to the Culicidae family (Service, 2008; Coetzee, 2017). The Culicidae family is comprised of three subfamilies, Anophelinae, Culicinae and Toxorhynchitinae; these mosquitoes are distributed throughout tropical and temperate regions worldwide. Mosquitoes are of major medical importance because they transmit various deadly diseases including chikungunya, dengue fever, filariasis, Japanese encephalitis, West Nile virus, yellow fever, zika virus and malaria being the most predominant (Service, 2008; Foster and Walker, 2019).

1.1 Malaria

Malaria is a vector borne infectious disease that is spread by an infected *Anopheline* mosquito and is caused by a protozoan parasite, which invades the erythrocyte of an infected individual. Approximately half of the world's population is at risk of malaria, most living in the tropical regions of Africa, Southeast Asia and central South America (Figure 1.1). In 2021, the World Health Organization (WHO) annual report disclosed that in 2020, 241 million cases and 627,000 deaths of malaria occurred globally (WHO, 2021). The WHO African region was home to 95% of the global cases of malaria in 2020, of which 96% were fatal. Malaria is a leading cause of death in developing countries and results in a global burden on the government and affected individuals. Pregnant women and children are the most vulnerable group affected by malaria and in 2020 children under the age of five accounted for 80% of the global deaths (WHO, 2020).

Malaria control programs aim to prevent transmission of malaria by 1) early diagnosis, 2) effective treatment and 3) effective vector control (WHO, 2015). Early and accurate diagnosis of malaria is important for disease management and surveillance, thus the WHO recommends the use of microscopy or rapid diagnostic testing (RDT) for patients suspected to have malaria before treatment is administered (WHO, 2019). Nucleic acid amplification based diagnostic testing detects low density of parasites, thus, the WHO urges that it should only be used for epidemiological research, as well as in surveys that map submicroscopic infections (WHO 2019). Antimalarial drugs are critical for the control and elimination of malaria, therefore, it is essential that they are efficient in treating malaria. The efficacy of antimalarial drugs has been reported to be threatened by *Plasmodium* parasites developing resistance to the drug.

Resistance has been reported in commonly used drugs and these include artemisinin, antifolates (pyrimethamine, sulfadoxine) and quinolones (chloroquine (CQ), mefloquine) (Fitch, 1970; Wilson *et al*., 1989; Wang *et al*., 1997; Gay, 1994; Plowe *et al*., 1998). Thus, the WHO urges for the continuous monitoring of the efficacy of the antimalarial drugs.

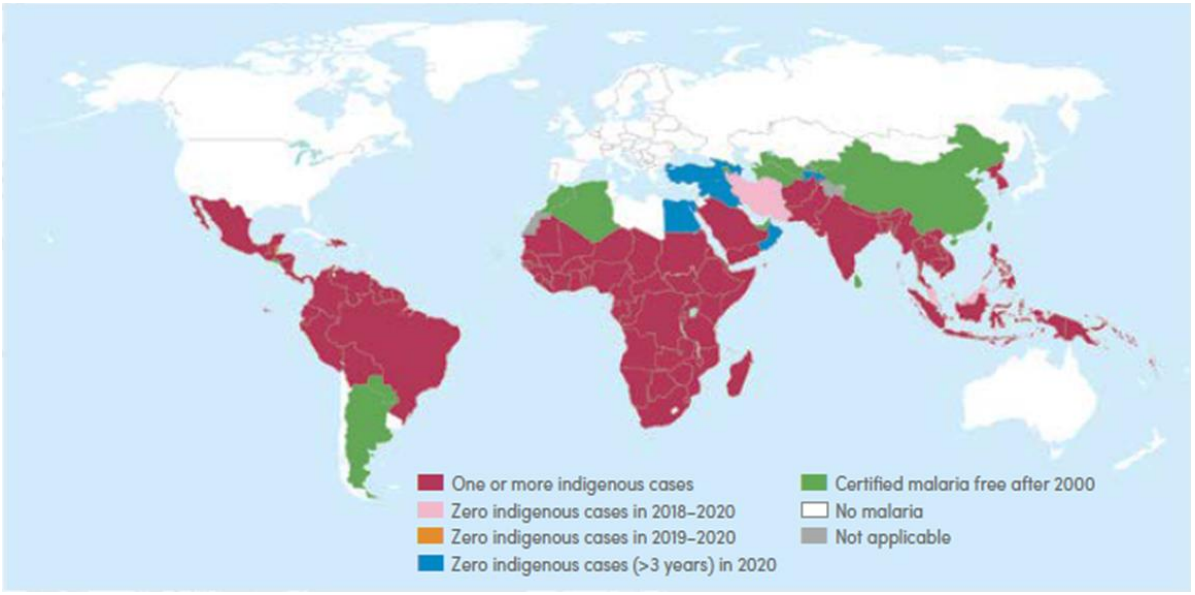

Figure 1.1: Worldwide distribution and cases of malaria showing Africa and South Africa with high prevalence annually (WHO, 2020).

1.1.1 Vector control

In order to prevent the transmission of malaria, the disease and the vector needs to be managed. In Africa, vector control programs have been primarily dependent on indoor residual spraying (IRS) and long lasting insecticidal nets (LLIN) that target the adult mosquitoes (WHO, 2019). Pyrethroids are the only insecticides approved for use on LLIN, this is due to their low mammalian toxicity and ability to rapidly immobilize and kill insects. In 2018, 50% of the people living in Africa who were at risk of contracting malaria were protected by LLINs (WHO, 2019). The IRS protection has decreased globally across all WHO regions from 5% in 2010 to 2% in 2018 (WHO, 2019). Other WHO approved IRS classes of insecticides includes organoclorines, carbamates, neonicotinoid and organophosphates (Mnzava *et al*., 2015; WHO, 2012; WHO, 2020). In addition to interventions to control adult vector populations, larval vector population control can be achieved by environmental management that involves educating the community, chemical insecticides and the introduction of biological control in aquatic breeding sites (WHO, 2013; Dambach *et al*., 2014; Chen *et al*., 2019).

Despite the efforts of biological control and insecticide centered management control programs, insecticide resistance by vectors of malaria undermines the efficacy of these control programs and poses a major threat in the potential number of people that may contract malaria (Ranson *et al*., 2009).

1.2 Malaria parasite

The *Plasmodium* parasite requires a vertebrate host and an invertebrate mosquito vector to complete its lifecycle. Different *Plasmodium* parasite species have adapted to a different vertebrate host ranging from birds to mammals (Garnham, 1966). Interestingly, the infection process between parasite and vertebrate host has remained similar throughout the *Plasmodium* parasite genus (Garnham, 1966). Approximately 200 species of *Plasmodium* parasites are known to infect birds, mammals and reptiles (Rich and Ayala, 2006), five of which, namely, *P. falciparum*, *P. knowlesi*, *P. malariae*, *P. ovale*, and *P. vivax* have been identified to infect humans. The most lethal is *P. falciparum* causing the highest mortality (WHO, 2019). *Plasmodium falciparum* was found to be responsible for 99.7% of the estimated malaria cases in 2018 in the WHO African region (WHO, 2019).

The lifecycle of the *P. falciparum* comprises of three stages of cell division and development (Figure 1.2). These includes the exo-erythrocytic cycle (Figure 1.2A), intra- erythrocytic cycle (Figure 1.2B) and sporogonic cycle (Figure 1.2C) (Burkot and Graves, 2000; CDC, 2019). During these stages, the parasite undergoes 10 morphological transitions where it proliferates asexually and propagates sexually following transmission from human to mosquito (Figure 1.2).

1.2.1 The vertebrate host

During a blood meal, the female *Anopheles* vector inoculates sporozoites from her salivary glands into the bloodstream of the human host (Figure 1.2-1) where sporozoites use the host's circulatory system to rapidly travel to the liver and invade the hepatocytes (Figure 1.2-2) (Shin *et al*., 1982). Sporozoites mature and undergo asexual reproduction known as the exo-erythrocytic schizogony (Figure 1.2A) where they develop into schizonts (Figure 1.2-3). After 9-16 days schizonts multiply via mitosis, this results in the rapture of the hepatocyte that releases thousands of merozoites (Figure 1.2-4) into the blood to invade erythrocytes/red blood cells (RBCs) (Figure 1.2-5).

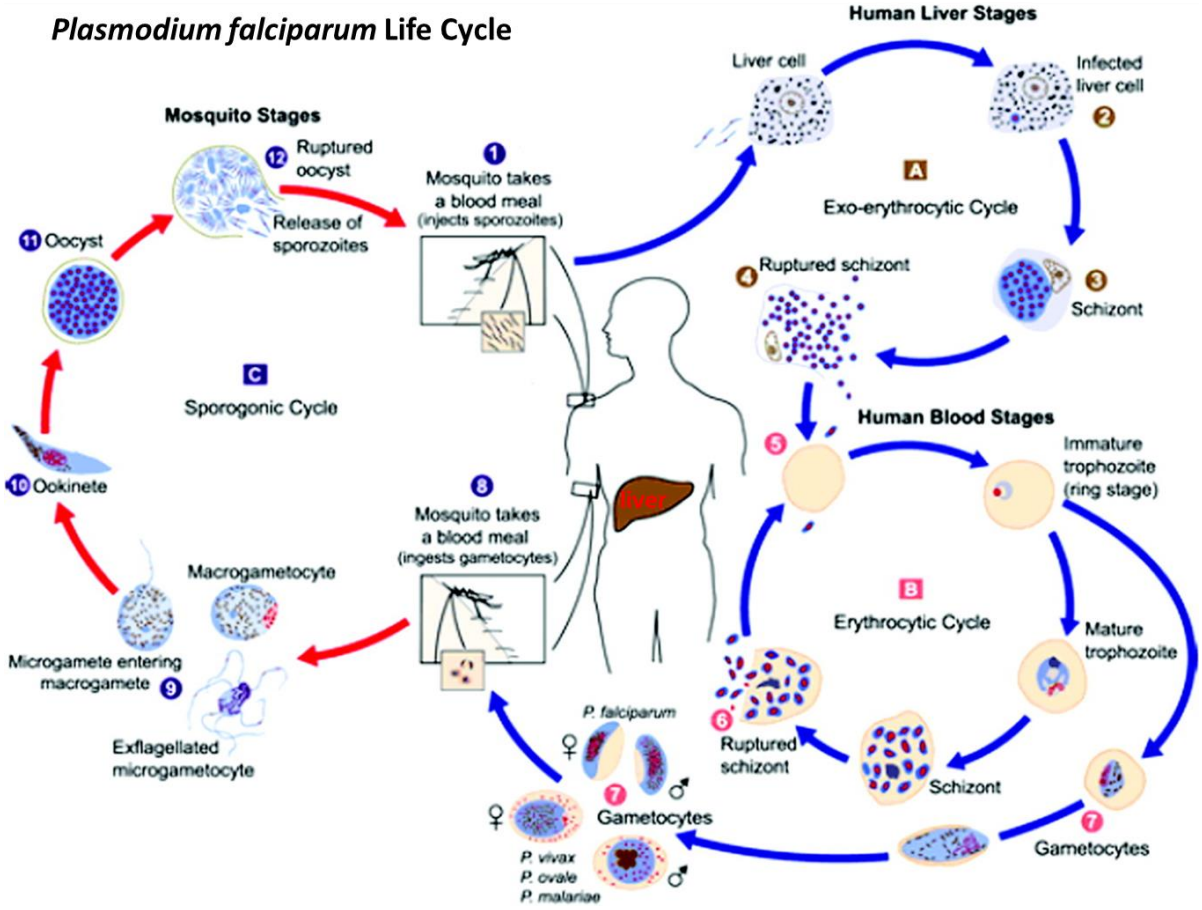

Figure 1.2: Life cycle of *P. falciparum* (stages 1-12). The development of *P. falciparum* in vertebrate (right, stages 1-7) and invertebrate (left, stages 8-12) host. The distinctive stages showing different parasite forms: sporogonic cycle (1.2C), exo-erythrocytic cycle (1.2A) and erythrocytic cycle (1.2B) and the morphology of *P. falciparum* gametocytes (step 7) is different to the other human *Plasmodium* species (CDC, 2019).

The merozoites invade the erythrocytes and undergo further asexual reproduction in the host erythrocyte, differentiating into distinct developmental stages: rings, trophozoites and schizonts over approximately 48 hours only in *P. falciparum* (24 hours in *P. knowlesi* and 72 hours in *P. malariae*). At the end of the first erythrocytic cycle, lysis of the original erythrocyte occurs and up to 32 progeny merozoites (only in *P. falciparum*) are released into the bloodstream where subsequent invasion of more RBCs takes place (CDC, 2019). This mass release of merozoites marks the pathogenesis of the disease and is characterized by flu-like symptoms associated with malaria (CDC, 2019). Some merozoites differentiate into sexual precursor cells, called gametocytes. This is achieved when the invasive stage, intra-erythrocytic cycle (Figure 1.2B) is slowed down due to stress response factors from the host (Bennink *et al*., 2016), such as anemia, parasite density, host immune response or drug treatment (Kuhen and Pradel, 2010).

1.2.2 Invertebrate host

The sexual reproduction stage (Figure 1.2C) of the *P. falciparum* begins immediately when the male microgametocyte and female macrogametocyte are ingested by the female *Anopheles* vector during her blood meal. Gametogenesis is initiated by changes in environmental conditions in the mosquito midgut less than two minutes following ingestion. These changes include: (i) a drop in temperature by approximately 5°C which is mandatory for gametocyte activation; (ii) presence of compounds such as xathurenic acid (XA) which is a mosquito-derived metabolic intermediate of tryptophan catabolism; (iii) an increase in pH from 7.2 to approximately 8 (Bennink *et al*., 2016); (iv) a decrease in glucose concentration and (v) an increase in Na^+ and HCO^-_3/Cl^- ion exchange shuttle (Figure 1.3A) (Kawamoto *et al*., 1992; Alano and Billker, 2005). Following this, the activated microgametocytes and macrogametocytes begin to egress from the enveloping human RBC and transform into fertile gametes, this occurs for 5 to 10 minutes after activation (Sologub *et al*., 2011). The egress vesicles are known to contain plasmodial pore-forming perforin protein (PPLP2), which is able to penetrate the extracellular matrix (ECM) on the parasite six minutes post gametocyte activation (Figure 1.3A). Fifteen minutes post blood intake, the extracellular matrix opens up to release fertile micro- and macrogametes. The microgamete exflagellates by replicating its genome three times by mitosis to form eight haploid microgametes which detach from the male residual body in search of a macrogamete for sexual reproduction (Figure 1.3B). This attachment (micro- and macrogamete) is facilitated by the parasites lumulus coagulating factor C (LCCL-domain) proteins and surface proteins of the 6-cysteine rich gene family of proteins including, Ps47, Ps48/45 and Ps230, where the latter two are considered as potential candidates for transmission -blocking vaccines (Pradel, 2007).

Fertilization takes place ~2 hours post blood intake and results in the rapid generation of a zygote, which over the next 20 to 24 hours differentiates into motile elongated ookinetes (Figure 1.3C). Over the next 19 to 36 hours, the ookinetes invade the mosquito midgut epithelium and lodge under the basal lamina to develop into oocysts (Figure 1.3D) (Bennink *et al*., 2016; Simoes *et al*., 2017). Midgut invasion by the ookinetes is facilitated by specialized secretory micronemal proteins (Figure 1.3D) of the protozoan body that are important for gliding motility and host cell adhesion and invasion (Bennink *et al*., 2016). Sebastian *et al*. (2012) identified 91 proteins in zygotes that were only synthesized following fertilization, most of these proteins are involved in motile and invasion attributes by the ookinetes. During the next 10-15 days, the oocyst matures and raptures to release sporozoites into the haemocoel that migrate to and invade the salivary glands.

Sporozoites are then transferred to the next host when the mosquito has her next blood meal, this marks the complete lifecycle of the parasite (Figure 1.2C and 1.3E). The mosquito stages of *P. falciparum* are completed in 10-15 days (Smith *et al*., 2014), however this may vary depending on the vector species and climate.

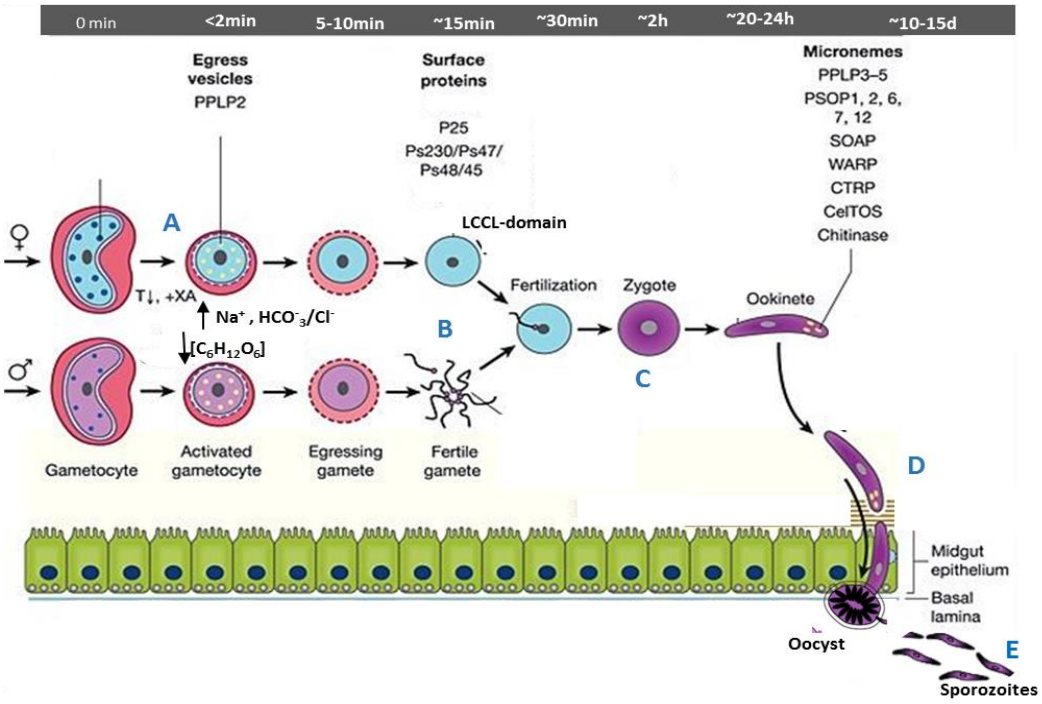

Figure 1.3: Development of the *P. falciparum* in the midgut of the *Anopheles* vector. The sequence of parasite development and the approximate time for each step within the mosquito is summarized in steps A-E. **Abbreviations of molecules involved:** CelTOS; cell-traversal protein for ookinetes and sporozoites, CTRP; circumsporozoite and thrombospondin-related adhesive protein-related protein, $C_6H_{12}O_6$; glucose, LCCL; lumulus coagulating factor C, PPLP2; *Plasmodium* perforin-like protein, POS1-10; putative ookinete surface-associated protein 1-10, PSOP1/2/6/7/12; putative secreted ookinete protein 1/2/6/7/12, SOAP; secreted ookinete adhesive protein, WARP; von Wilebrand factor A domain-related protein, XA; xanthurenic acid (Adapted from Bennink *et al*., 2016).

1.3 *Anopheles* vector

Female mosquitoes from the anopheline genus are well known vectors of human malaria (Gillies and De Meillon, 1968). In 1897, Sir Ronald Ross confirmed that the *Anopheles* mosquito is a vector of malaria by using the avian malaria parasite, *P. relictum* and suggested that an infected *Anopheles* female is responsible for transmission of the malaria parasite (Garnhan, 1966; Brindha, 2014).

There are over 400 species of *Anopheles* mosquitoes known worldwide, only 40 have been identified to be vectors of malaria (Blandin and Levashina, 2004a; Sinka *et al*., 2010). In Africa, *An. arabiensis*, *An. gambiae s.s.*, *An. coluzzii* and *An. funestus s.s* are the four major vectors responsible for the the bulk of the transmission of malaria. *Anopheles arabiensis, An. gambiae s.s.* and *An. coluzzii* belong to the *An. gambiae* complex which is comprised of nine sibling species that are morphologically indistinguishable (Gillies and De Meillon, 1968; Gillies and Coetzee, 1987; Coetzee *et al*., 2013; Barron *et al*., 2019; Coetzee, 2020). *Anopheles funestus s.s.* belongs to the *An. funestus* group that is recognized by eleven African sibling species that are morphological similar (Harbach, 2004; Cohuet *et al*., 2003; Spilling *et al*., 2009).

The *Anopheles* vector goes through four distinct stages of its lifecycle: egg, larva, pupa and adult, which are recognized by different morphological characteristics (Figure 1.4). The length of each stage is dependant on the type of species and environmental conditions including temperature and food supply. The first three stages are aquatic and lasts about 5-14 days, briefly, adult mosquitoes lay a raft of eggs on water surfaces which hatch into larvae within 3-5 days. The larvae futher undergoes four stages (L1-L4) that last between 5-10 day. Eventually larvae will develop into pupa, which remains at the surface of the water and responds to stimuli only (Figure 1.4). The adult mosquito develops inside the pupa and emerges after 3-5 days.

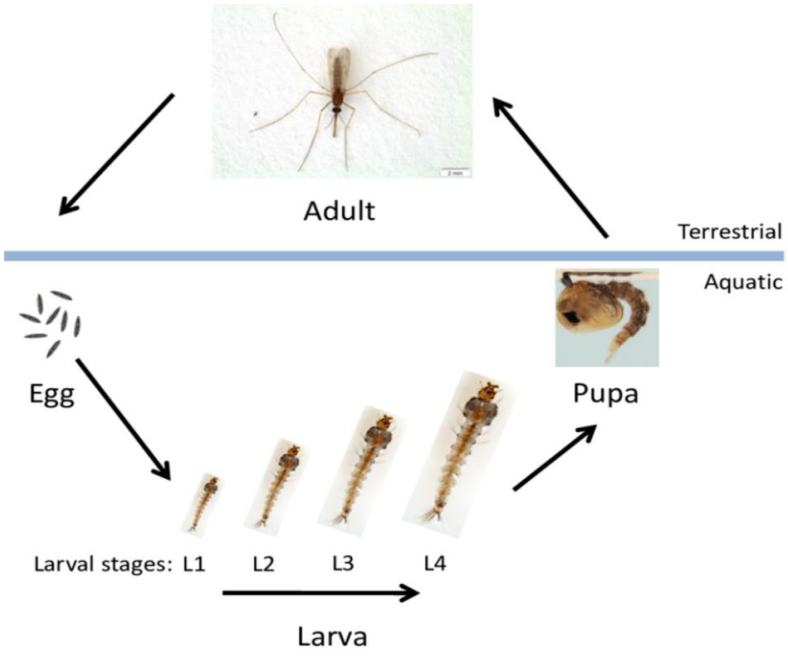

Figure 1.4: The Lifecycle of the *Anopheles* mosquito (Williams and Pinto, 2012).

1.3.1 *Anopheles funestus* group

Historically, the *An. funestus* group was comprised of nine African sibling species *An. aruni*, *An. brucei*, *An. confusus*, *An. funestus s.s.*, *An. fuscivenosus*, *An. leesoni*, *An. parensis*, *An. rivulorum* and *An. vaneedeni* (Gillies and De Meillon, 1968; Gillies and Coetzee, 1987). In 2003, a new species was identified in Cameroon by Cohuet *et al*. (2003) and name *An. rivulorum-like*. In addition, Spilling *et al*. (2009) identified another new species named *An. funestus-like*. The identification of these two species expanded this group to 11 African sibling species.

Anopheles funestus s.s., which is the focus of this study, is the most predominant vector of this group and is widespread throughout the tropical regions (Gillies and De Meillon, 1968; Sinka *et al*., 2010). This vector is (i) smaller and darker in color in comparison with members of the *An. gambia*e complex; (ii) has a longer generation time, where depending on the environmental conditions, it takes on average two to three weeks from egg to develop into adult stage, in contrast to members of the *An. gambiae* complex (one to two weeks); and (iii) adults have a longer lifespan of up to 40 days (Gillies and Coetzee, 1987; Fontenille and Simard, 2004; Lo, 2014). *Anopheles funestus s.s.* is highly anthropophilic (feeds on humans) and endophilic (indoor resting), thus making it easy to control using appropriate insecticides (Gillies and De Meillon, 1968; Dadzie *et al*., 2013). The other members of this group are mainly zoophilic (feeds on animals). However, *An. rivulorum*, *An. vaneedeni* and *An. parensis* have been implicated as minor vector species and their role and impact in malaria transmission needs further research (Wilkes *et al*., 1986; Kawada *et al*., 2012; Burke *et al*., 2017; Burke *et al*., 2019).

1.4 Vector-parasite interaction

During its sexual reproduction, the *Plasmodium* parasite and its *Anopheles* vector engage in a series of interactions, which include invasion and migration by the *Plasmodium* parasite through the *Anopheles* epithelial tissues (Dimopoulos *et al*., 2001). During these interactions, the *Plasmodium* parasite encounters and triggers the *Anopheles* robust innate immune system, which is capable of activating a plethora of defense reactions (Dimopoulos *et al*., 2001; Christophides *et al*., 2002). These reactions result in major parasite losses (Figure 1.5) and in some cases, can stop the development of the parasite and lead to total refractoriness by the *Anopheles* (Blandin and Levashina, 2004a). Not all ingested gametocytes develop into mature ookinetes in the midgut epithelium (Figure 1.5A), significant parasite losses also occur when ookinetes invade and transverse the midgut epithelium and only a minority develop into oocycts (Figure 1.5B-C).

When the oocysts mature and rapture, only a fraction of the released sporozoites successfully ends up in the salivary glands (Figure 1.5D). These dramatic parasite losses are attributed to:

1) Midgut epithelium defense reactions such as digestive enzymes including phenoloxidase (PO), dopa decarboxylase and dopachrome conversion enzyme resulting in melanization and lytic events that destroy the parasite (Hillyer, 2010),
2) Reactions in the haemocoel compartment are mounted to parasites that were not neutralized and immune responses involve immune factors secreted by the haemocytes, fat body and pericardial cells and
3) Salivary glands mainly form a physical barrier that must be crossed by the sporozoites before they are transmitted to the next host, defense reactions includes the production of AMPs and serine protease inhibitors by the salivary glands to limit gland invasion (Hillyer, 2010).

Successful transmission of the *Plasmodium* parasite depends on several *Anopheles* immune factors and molecules at cellular and molecular levels, thus understanding how they interact at different parasite developmental stages is important. Furthermore, identification of the *Anopheles* immune molecules that have a vital role in regulating *Plasmodium* parasites has redirected and informed new strategies to control and prevent *Plasmodium* parasite development and progression in the mosquito (Blandin *et al*., 2004b). In addition to the mosquitoe's immune factors (regulating the transmission of the *Plasmodium* parasite), several external factors in the veterbrates blood meal have been reported to interfere with the development of the *Plasmodium* parasite in the *Anopheles* mosquito (Ichimori *et al*., 1990; Hogh *et al*., 1998; Abrantes *et al*., 2005). Increased infectivity by the *Plasmodium* parasite to the *Anopheles* mosquito has been attributed to the presence of antimalarial drugs, such as CQ in the blood meal. It is proposed to inhibit some *Anopheles* immune-related proteins, highlighting a need to understand the impact that antimalarial drugs have on transmission of the *Plasmodium* parasite (Ichimori *et al*., 1990; Hogh *et al*., 1998; Abrantes *et al*., 2005).

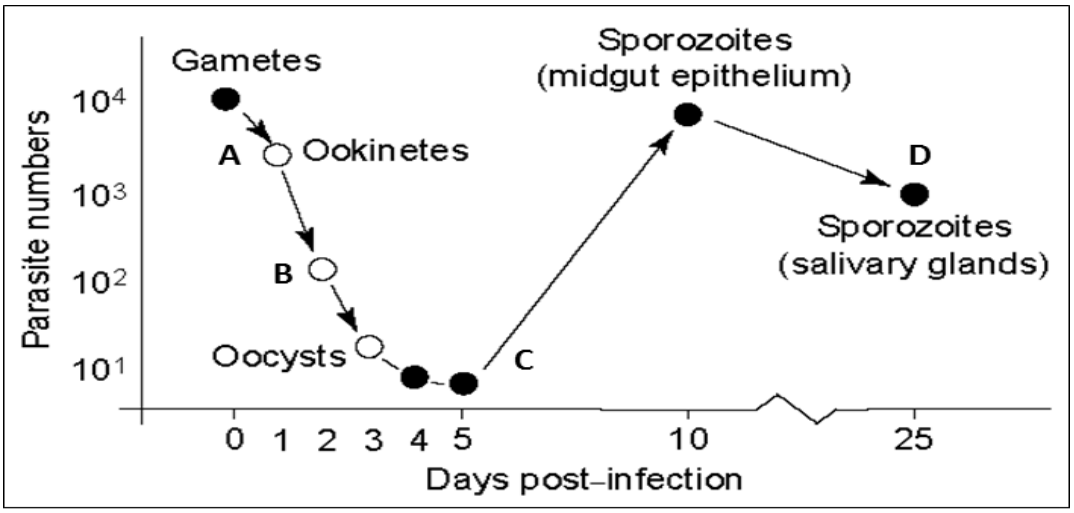

Figure1.5: Major bottle necks of *Plasmodium* parasite and amplification in the *Anopheles* vector. Significant parasite loses during critical developmental stages. The initial number of ingested *Plasmodium* parasites was approximately 10^4, major parasite losses between 1-3 days post infection were observed (Blandin and Levashina, 2004a).

1.5 Mosquito immune system

The mosquito's immune system has gained more attention since the 1990s as a potential alternative method to enhance and complement existing vector control tools (Ndo *et al*., 2016). The mosquito's immune system can be categorized into three major compartments for malaria parasites, namely, the midgut epithelium, haemocoel, and within the salivary glands. These compartments include physical and physiological barriers linked with antimicrobial peptides (AMPs), pathogen recognition receptors (PRRs), immune signaling pathways and mechanisms that parasites must overcome in order to complete its development in the mosquito (Figure 1.6 and Figure 1.7).

Female mosquitoes are anautogenous, where they require a blood meal for egg production and this exposes them to several pathogens that can go through complex development stages inside the mosquito (Hillyer, 2010). Pathogen entry into the mosquito can be acquired through ingestion in cases such as those involving the malaria parasite or cuticle breakage in cases involving entomopathogenic fungi or other microbial infections (Hillyer, 2010). In the latter, immune responses such as coagulation, haemocyte degranulation, melanization and scar formation are induced to prevent pathogen entry. If the pathogen is able to enter, the mosquito has an effective innate immune system comprising of cellular and humoral responses that are capable of fighting the pathogen (Figure 1.6A and Figure 1.6B).

Cellular immune responses are mainly facilitated by haemocytes (blood cells) (Figure 1.6B), meanwhile the AMPs, PRRs and the PO cascade form part of the humoral immune response (Figure 1.6A) (Hillyer, 2010).

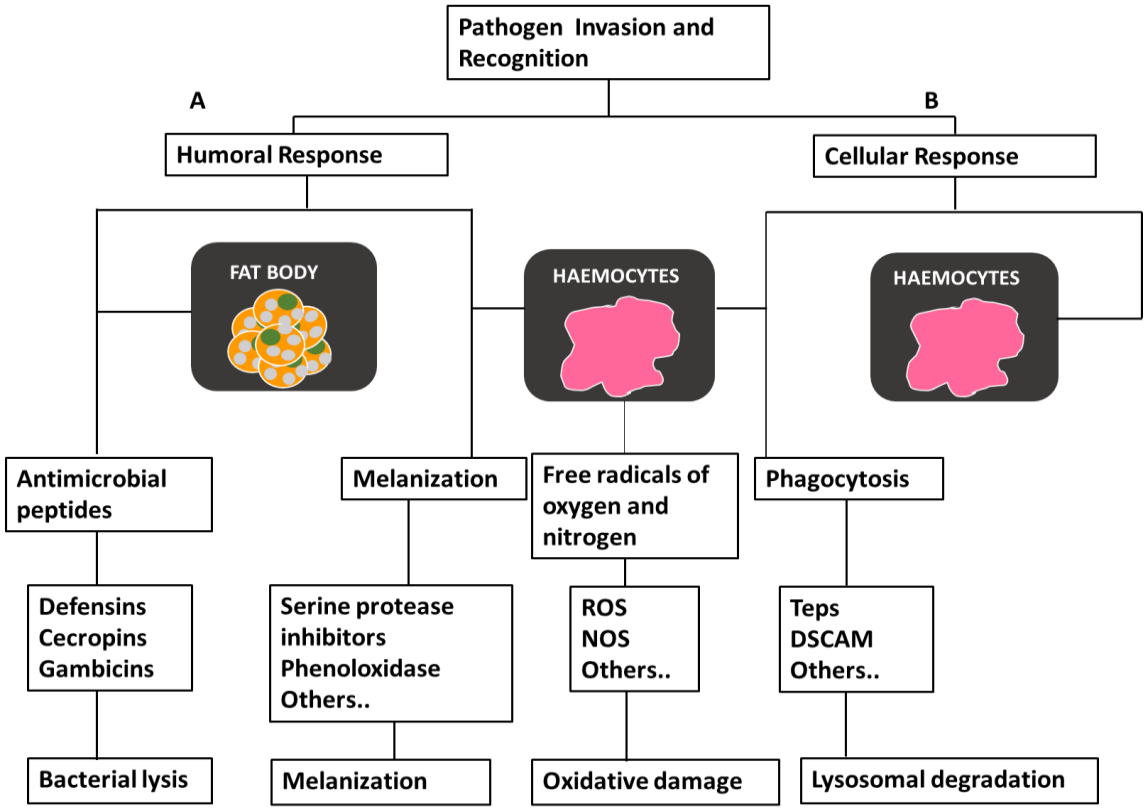

Figure 1.6 : Outline of cellular and humoral immune responses in female mosquitoes upon pathogen recognition. (A) Humoral response includes soluble components of the haemolymph in which PRR binds to pathogen cell surfaces resulting in the activation of AMPs in the fat body, oxidative stress by haemocytes leading to bacterial lysis, melanization and oxidative damage. **(B)** Cellular immune response is mainly mediated by haemocytes where recognition of pathogens induces encapsulation and phagocytosis (Redrawn from Hillyer, 2010). **Abbreviations:** ROS; reactive oxygen species, NOS; nitric oxide, Tep; thioester-containing protein and DSCAM; down syndrome cell adhesion molecule.

The discovery and development of technologies such as deep sequencing has revealed that mosquitoes, like all animals and plants are holobionts, comprising of a diverse community of organisms (Bartholomay and Michel, 2018). These include protozoa (Xu *et al*., 2005; Pinto *et al*., 2008; Osta *et al*., 2004; Graumans *et al*., 2017), bacteria (Warr *et al*., 2008; Pan *et al*., 2012; Akorli *et al*., 2016), viruses (Sang *et al*., 2003; Saiyasombat *et al*., 2011; Bolling *et al*., 2015), fungi (Andreadis, 2005; Beenel *et al*., 2005) and nematodes (Paily and Balarama, 2000).

Obtaining sufficient mosquitoes experimentally infected with *Plasmodium* parasites has been one of the most challenging steps in understanding *Plasmodium-Anopheles* interactions. Although this has recently become a standard technique in most laboratories, the technique remains challenging. Thus, for this section, available *Plasmodium* interactions which could be sourced from the available literature will be discussed. Exception will be given to other mosquito species including *Aedes aegypti* and other microorganisms including bacteria and viruses, since the immune response following a challenged by these microbes has been studied in detail, thus can be used to understand the mosquito immune system (Scott *et al*., 1990; Dimopoulos *et al*., 1997; Dong *et al*., 2009a; Schnitger *et al*., 2009).

1.5.1 Barriers to infection

For pathogens to successfully establish infection, it is important that they overcome the physical (Figure 1.7A-C) and physiological barriers (Figure 1.7D-G) of the mosquito defense compartments, midgut epithelium, haemocoel and salivary glands (Kumar *et al*., 2018a).

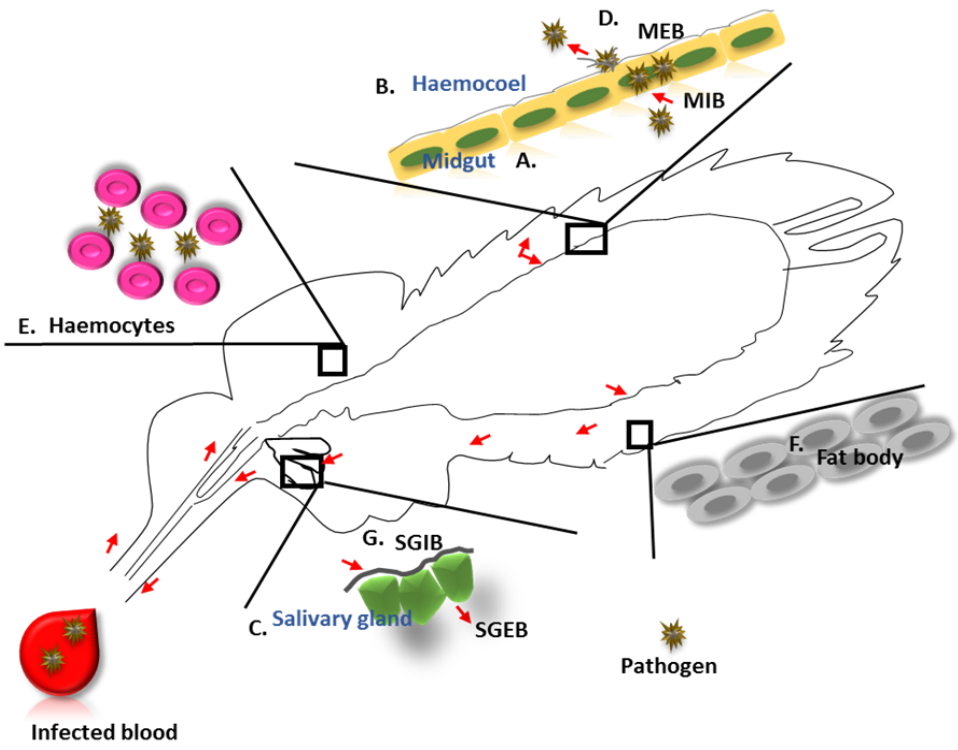

Figure 1.7: Schematic representation of infection barriers in the mosquito. Physical and physiological barriers to infection include midgut epithelium, haemocoel and salivary glands. Arrows represents path followed by ingested pathogens in and out of the mosquito. **Abbreviations for physiological barriers:** MIB; midgut infection barrier, MEB; midgut escape barrier, SGIB; salivary gland infection barrier and SGEB; salivary gland escape barrier. (Figure redrawn from Kumar *et al*., 2018).

1.5.1.1 Physical barrier

1.5.1.1.1 Midgut barrieir

The midgut epithelium barrier comprises of a narrow anterior region that has prominent microvilli, smooth endoplasmic reticulum and a well-developed basal labyrinth. This region is involved in the absorption of sugar and a wider posterior region, which is involved in blood absorption and is comprised of noticeable rough endoplasmic reticulum and high numbers of mitochondria (Franz *et al*., 2015; Kumar *et al*., 2018). Drastic structural changes in the midgut have been observed following acquisition of a blood meal and these include the condensation of the nuclei, enlargement of the mitochondria and concentric whorls in the rough endoplasmic reticulum begin to form (Franz *et al*., 2015; Kumar *et al*., 2018). The concentric whorls of the rough endoplasmic reticulum have been reported to be reserves for synthesis of enzymes when the mosquito is under stress (Staublet *et al*., 1964). Furthermore, following the acquisition of a blood meal, the midgut epithelium secretes a sac-like thick structure comprised of chitin, protein and glycoprotein, known as the peritrophic matrix, which lines the digestive tract of most invertebrates (Shao *et al*., 2001; Dinglasan *et al*., 2008). The peritrophic matrix thickens and surrounds the entire blood bolus and is known to prevent ingested pathogens from adhering to the midgut epithelial cells (Franz *et al*., 2015).

In addition, pathogens including *Plasmodium* parasites ingested with a blood meal must secret hydrolytic enzymes such as chitinase to "open a hole" or lyse the matrix in order to transverse and escape (Vinetz *et al*., 2000; Dinglasan *et al*., 2008). The role of chitinase in allowing ookinetes to transverse the peritrophic matrix has been reported where ultrasound studies demonstrated that *Plasmodium* ookinetes were able to penetrate and disrupt the peritrophic matrix (Sieber, *et al*., 1991). This important role was further demonstrated when mutations or deletion of chitinase in *P. berhgei* and *P. falciparum* impared the infectivity of the parasites for mosquitoes (Dessens *et al*., 2001; Tsai *et al*., 2001). Moreover, the thickening of the peritrophic matrix has been shown to reduce *Plasmodium* infectivity (Billingsley and Rudin, 1992). A complementary study reported that inhibition of chitinase by enzymes or antibodies results in major reduction of *Plasmodium* invasion of the midgut epithelium (Langer *et al*., 2002; Li *et al*., 2004).

1.5.1.1.2 Haemocoel barrier

The haemocoel (open body cavity) is a barrier to the salivary glands and consists of visceral organs. It is delineated by the outer cuticle and the basal lamina surrounding internal tissues (Hillyer, 2010). The basal lamina has a dense matrix that prevents "free flow" of pathogens and its thickness varies between mosquito species and strains (Vogels *et al*., 2017).

1.5.1.1.3 Salivary gland barrier

A physical barrier that pathogens must cross to complete their lifecycle, the salivary glands of a female mosquito is comprised of three lobes, where two lateral lobes are further divided into proximal and distal regions and one medial lobe that is connected to the main salivary duct (Figure 1.6C) (Pinto *et al*., 2008; Vogels *et al*., 2017). The lobes are enriched with epithelial cells and bound by basal lamina, which forms thick layers that are difficult for microbes to penetrate (Kumar *et al*., 2018a).

1.5.1.2 Physiological barriers

These are "protect" barriers that defend the mosquito against pathogens by creating an environment that is not suitable for the survival and replication of the pathogens (Figure 1.7D -G). The degree to which the physiological barriers restricts the passage of pathogens can depend on various factors, such as the inoculum of pathogens ingested, nutritional status, host strain, time post-ingestion, temperature and the production of immune factors from the cellular and humoral responses (Hillyer, 2010; Oviedo *et al*., 2011).

1.5.1.2.1 Midgut infection barrier and midgut escape barrier

In the midgut infection barrier, pathogens are unable to replicate or infect the midgut epithelial cells. This may be due to 1) host cell surface receptors required by pathogens to bind and initiate infection; 2) midgut epithelial cells being non-permissive to infection; or 3) strong immune response against the pathogen (Kumar *et al*., 2018a). This infection barrier was evident in *An. gambiae* G3 strain which was refractory to *P. gallinaceum*, where ookinete death was observed following an infected blood meal (Figure 1.7D) (Vernick *et al*., 1995). A secondary barrier, namely the midgut escape barrier is present in case pathogens were able to infect and escape the midgut infection barrier. The secondary barrier prevents pathogens from escaping and making their way to the salivary gland (Kumar *et al*., 2018a). The effectiveness of the midgut escape barrier was evident in *An. gambiae* G3 strain, where 100% refractoriness was observed against several *Plasmodium* species including, *P. cynomolgi* (ceylon strain), *P. gallinaceum* (8A strain), *P. gunderi* and *P. inui* (N34 strain).

Whilst, 80-100% refractory was observed against *P. berghei* (NK strain) and some human *Plasmodium,* including *P. knowlesi* (H strain), *P. vivax* (NK, Chesson and ONG strains) and *P. falciparum* (SL, 7G8 and Indo3 strains). Refractoriness was attributed to the encapsulation of *Plasmodium* oocysts in the midgut epithelium (Collins *et al*., 1986). However, *Plasmodium* parasites of some *Anopheles* strains escape both the midgut infection and escape barriers and develop into oocysts. The oocysts then mature and rapture to release sporozoites that enter the haemocoel, which is a primary body cavity found in most invertebrates, containing circulatory fluid or a nutrient rich medium, that is comprised of immune cells and humoral immune factors that are produced by haemocytes, pericardial cells and fat body (Hillyer, 2010). These latter cells and organ are multifunctional and essential for the mosquito's immunity:

i. Haemocytes are blood cells involved in immune surveillance and are found circulating in the haemolymph or attached to the visceral tissues (Figure 1.7E). Based on the enzymatic activity, lectin- binding properties and morphology, mosquito haemocytes were divided into adipohemocytes, granulocytes, oenocytoids and thrombocytoids (Hillyer and Christensen, 2002). However, it was later realized that adipohemocytes and thrombocytoids are not true haemocytes based on functional and comparative studies. Haemocytes initiate immune responses upon pathogen recognition and are involved in the secretion of humoral factors, as well as sequestration of pathogens through phagocytosis and nodulation. A number of immune factors are produced by the haemocytes including AMPs, PRRs, phagocytosis elements and proteins, melanization modulators and enzymes, stress response proteins and signal transduction proteins. Granulocytes are adhesive by nature and account for 95% of the circulating population of haemocytes. They produce proteins of humoral immune system, namely, nitric oxide, serine protease and serine protease inhibitors (Castillo *et al*., 2009; Hillyer and Estevez-Lao, 2010). In addition, they display acid phosphatase activity, bind strongly to artificial substances and engage in phagocytosis of *Plasmodium* sporozoites and bacterial pathogens within five minutes of recognition (Hillyer *et al*., 2003). Oenocytoids account for 5% of the haemocytes and are known to produce phenoloxidase and phenylalanine hydroxylase, which are key enzymes in the melanization process.

ii. Pericardial cells are large binucleate cells flanking the heart of the mosquito and mediate both cellular and humoral immune responses, such as lytic activity and phagocytosis in response to yeast (Hernández-Martínez *et al*., 2013), bacterial and *Plasmodium* (Hillyer *et al*., 2007). Immune challenge has been reported on the surface of the heart (Jones, 1954).

iii. The fat body or otherwise known as the energy storage organ, exclusively mediates humoral immune responses (Figure 1.7F). The fat body of a mosquito is a multifunctional organ lining the integument of the mosquito and is comprised of loosely assembled cells that are rich in glycogen and lipids. The synthesis of precursors of vitellogenin (required for egg production) takes place in fat cells. In addition, the fat body also facilitates the production of AMPs, reactive oxygen species (ROS) and reactive nitrogen species associated immune responses (Hillyer *et al*., 2002).

1.5.1.2.2 Salivary gland infection barrier and salivary gland escape barrier

The molecular mechanism underlying the salivary gland infection and salivary gland escape barrier is not well defined (Figure 1.7G). The salivary gland infection barrier was identified when Scott *et al*. (1990) investigated the susceptibility of *A. albopictas* to eastern equine encephalomyelitis virus. After acquisition of viraemic blood, the following was deduced: the posterior region of the midgut epithelium is thought to be the initial site of eastern equine encephalomyelitis virus replication after which it disseminates into the haemocoel, where the secondary replication takes place in the fat body. The eastern equine encephalomyelitis virus was, however, unable to establish infection in the salivary gland, thus showing the active effect of the salivary gland infection barrier (Scott *et al*., 1990). The presence of the salivary gland escape barrier was shown in *A. hendersoni* when infection of the salivary gland infection barrier by La Crosse virus was successful. However, La Crosse virus was not secreted in the saliva, thus failing to be transmitted orally (Grimstad *et al*., 1985). Interestingly, some parasites and viruses are able to infect and escape this barrier due to their ability to modify the cytoskeleton of the epithelial salivary glands (Kumar *et al*., 2018a). In addition, an immune factor serine protease inhibitor 6 (SRPN6) produced by the salivary glands was found to be present near the epithelium cells of the distal lateral lobes when *P. berghei* were present (Pinto *et al*., 2008). Furthermore, a gene knockdown study by Pinto *et al*. (2008) using RNA interference (RNAi) showed that SRNP6 limits gland invasion in *An. gambiae*. Knockdown of the SRNP6 protein resulted in an increased number of sporozoites nine days post knockdown (i.e. 19 days post infected blood meal), sporozoites numbers were 3,541 and 8,196 for controls and 7,142 and 10,734 for SRNP6 knockdown 15 and 19 days post infection i.e. a 2.05 amd 1.31 fold difference 15 and 19 days post infection, respectively (Pinto *et al*., 2008).

1.6 Molecular basis of immunity

1.6.1 Recognition

The mosquito has effective molecules that can recognize and interact with pathogens when they are being invaded. These mosquito-derived molecules, PRR's are mostly located on the midgut epithelium and haemocoel of the mosquito. Pattern recognition receptors bind specifically to pathogen cell surface structures known as pathogen associated molecular patterns (PAMPs) resulting in the activation of downstream events that may lead to the destruction of the pathogen (Das *et al*., 2009). Approximately 150 putative PRRs were identified in *An. gambiae* of which most were found to be secreted proteins with adhesive domains that interact with PAMPs. These include thioester-containing proteins (TEPs), fibronectin related proteins (FREPs), Gram-negative binding proteins (GNBPs), immunoglobulin superfamily (Ig) and C-type lectins (CTLs) (Das *et al*., 2009).

1.6.1.1 Thioester-containing protein

These receptors are generally found in the haemolymph, their main role is to lead pathogens to neutralization. Christophides *et al*. (2002) identified 19 TEPs in *An. gambiae* genome and the thioester-containing protein-1 (TEP1). PRR is the most studied in *Drosophila melanogaster*, *An. gambiae* and *Aedes aegypti* (Lagueux *et al*., 2000; Blandin *et al*., 2004b; Cheng *et al*., 2011). TEP1 is an acute phase glycoprotein secreted by haemocytes (in the haemolymph) as a single peptide chain that is activated following a proteolytic cleavage (Blandin and Levashina, 2004a). The activated TEP1 recognizes and binds to surfaces of Gram-negative bacteria and targets them for clearance by phagocytosis (Levashina *et al*., 2001). This receptor can also recognize and bind *P. berghei* parasites in susceptible and refractory *An. gambiae* (Blandin *et al*., 2002). Blandin *et al*. (2002) showed that TEP1 binds to *P. berghei* ookinetes surface protein P28 (Figure 1.3) in infected susceptible *An. gambiae* mosquitoes, where this recognition was more pronounced 48 hours post infection until ookinetes finished invading the midgut. When using the refractory *An. gambiae* strain, TEP1 completely aborts the development of *Plasmodium* parasites including *P. gallinaceum* (Vernick *et al*., 1995), *P. cynomolgi*, *P. berghei* and *P. falciparum* (Collins *et al*., 1986), TEP1 bound to *P. berghei* in a time-dependent manner, inducing perturbation of the P28 signal, condensation and degradation of ookinete nuclei followed by melanization of parasites (Blandin *et al*., 2004b).

1.6.1.2 Fibronectin Related Proteins

Fibronectin related proteins (FREPs) also known as fribrinogen domain immunolectins (FBNs), represent the largest gene family of PRRs in *An. gambiae*. FBNs are mostly located in the abdomen, haemolymph and haemocytes, with approximately 59 putative FREPs identified to interact with bacteria, fungi and *Plasmodium* following an immune challenged (Waterhouse *et al*., 2007). All FBNs comprise of a pathogen binding fibrinogen-like (FBG) domain at their C-terminus, whereas the N-terminus sequence is proposed to be involved in the interaction with other FBNs. This interaction results in the formation of a multimeric protein bundle with potentially high affinity and specificity for pathogens, thus increasing the recognition repertoire. The FBN gene family is classified into clusters (R, G, P, B and X) based on their location in the chromosome and FBGG domain (Dong *et al*., 2009). Dong *et al*. (2009) investigated the expression of 38 FBNs following an immune challenge with Gram-negative *Escherichia coli*, Gram-positive *Staphylococcus aureus* bacteria, *P. berghei* and *P. falciparum*.

The findings of the study indicated that; i) FBN-4, -6 and -22 were up-regulated by both bacteria; ii) FBN-3, -6, -8, -9, -13, -22 and -37 were up-regulated following both *Plasmodium* species challenges; iii) FBN-6, -9, -22 and -24 were up-regulated in response to bacterial and *Plasmodium* challenges. RNAi mediated gene silencing of FBN-39 showed i) an increase of 99% across four Gram-negative bacterial species, *Serratia sp*, *Asia bogorensis*, *Pseudomonas veronii* and *Sphingomonas sp* and ii) RNAi mediated gene silencing of FBN-6 and FBN-9 resulted in an overall increase in 55 and 68%, respectively in oocyst number of *P. berghei*. However, silencing both genes FBN 6/9 resulted in a significant increase of 82% oocyst number of *P. berghei*. Furthermore, silencing FBN-8, -9 and -39 in *P. falciparum*-infected mosquitoes resulted in an increase in oocyst numbers between 51-81%, whereas silencing all genes including FBN-6 resulted in the significant increase of 95% oocyst number. These observations suggest that members of the FBN gene family function synergistically against *Plasmodium* infection. Amongst all FBNs, FBN-9 was shown to have antimicrobial and anti-*Plasmodium* activity (Dong *et al*., 2009).

1.6.1.3 Gram-negative binding proteins

Gram-negative binding proteins (GNBPs) are membrane bound receptors that are located on different tissues of the mosquito, these include haemocytes, midgut and salivary glands and are up-regulated following infection by bacteria or *Plasmodium* infection (Dimopoulos *et al*., 1997).

The *An. gambiae* genome contains six members of the GNBP gene family which belong to subfamily A (GNBPA1 and GNBPA2) and subfamily B (GNBPB1, GNBPB2, GNBPB3 and GNBPB4) (Warr *et al*., 2008). Subfamily A is present in all known fruit flies and moths, whereas subfamily B is specific to mosquitoes. GNBPB1 are mostly expressed in the salivary gland and abundant in the thorax.

The *An. gambiae* GNBP family is expressed in the following mosquito tissues, all six aforementioned GNBPs are highly expressed in the posterior region of the female midgut in contrast to the cardia. Furthermore, high expression levels were observed in the haemocytes compared to the whole mosquito. GNBPB1 is highly expressed in the salivary glands and thorax, but expressed in less amounts in the head, GNBPB4 is highly expressed in the fat body, whereas the head and midgut contains less amounts of this protein (Warr *et al*., 2008). *Anopheles gambiae* GNBPs primarily responds to exogenous immune challenges. RNAi mediated gene silencing of GNBPA2, GNBPB1, GNBPB3 and GNBPB4 resulted in a significant increase in the mortality of mosquitoes following an immune challenge with *E. coli* (Figure 1.8A-D). Depletion of GNBPB4 resulted in a significant increase in mosquito mortality reaching ±18% of survival six days post an immune challenge by *E. coli,* in comparison to the GFP control that showed ±57% (Figure 1.8D) (Warr *et al*., 2008). In addition, the depletion of GNBPB4 in mosquitoes challenged with *S. aureus* increased mosquito mortality (Figure 1.7D). GNBPB4 has been found to neutralize *E. coli*, *S. aureus*, *P. berghei,* but not *P. falciparum* (Dimopoulos *et al*., 1997). GNBPA2 however was able to neutralize *P. falciparum* (Warr *et al*., 2008). For *Plasmodium* immune challenge, gene silencing of GNBPA2 significantly increased the number oocyst approximately 2.43 fold in the midgut following *P. falciparum* infection, whereas silencing of GNBPB4 and GNBPB3 significantly increased *P. berghei* oocyst to 2.44-fold and 2.86- fold, respectively. The fold difference for the positive control for *P. falciparum* was 3.0 whereas a 4.49 fold was observed in *P. berghei* infection compared to their respective controls (Warr *et al*., 2008).

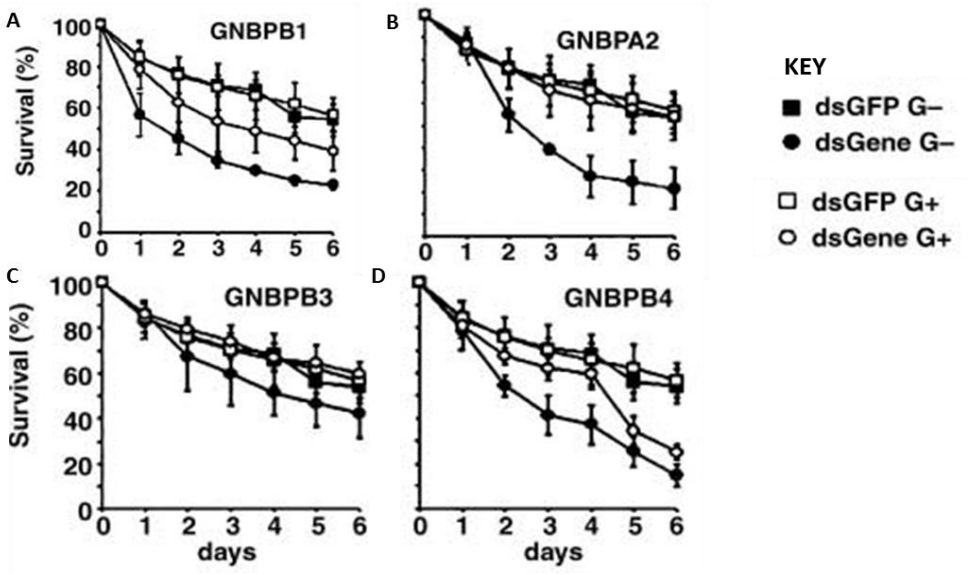

Figure 1.8: The role of *An. gambiae* GNBPs in defense against Gram-negative and Gram-positive bacteria. Transcripts of four GNBPs were independently depleted in an adult female *An. gambiae* following dsRNA injection: Mosquitoes were immune challenged with *E. coli* (G+) or *S. aureus* (G-) 4 days thereafter, and the survival rate was monitored for 6 days post dsRNA injection. dsGFP were used as positive controls for this study. (Warr *et al*., 2008).

1.6.1.4 Immunoglobulin superfamily

The *An. gambiae* mosquito contains 135 of genes from this gene family, 85 of which were found to be overexpressed following an immune challenge (Hillyer, 2010). Although their location is not clear, six of these 85 identified genes have been characterized. *Anopheles gambiae* down syndrome cell adhesion molecule (AgDSCAM) is a member of the immunoglobulin (Ig) gene superfamily known to be hypervariable because it undergoes alternative splicing, which enables it to produce a broad repertoire of 31,920 splice sites containing variable combinations of Ig domain that have different recognition and binding sites (Dong *et al*., 2006a). The structure of the Ig domain is known to be ideal for ligand binding, recognizing non-self molecules and promotes their elimination (Garver *et al*., 2008). Alternative splicing of the AgDSCAM gene has been reported in response to a bacterial or *Plasmodium* immune challenge. RNAi mediated gene silencing of AgDSCAM following Gram-negative bacterial challenge showed that AgDSCAM is essential for antimicrobial activity. Following the depletion of the AgDSCAM, there was a significant proliferation of Bacterium HPC1068 (89%), *A. bogorensis* (97%), *P. veroni*i bacteria and (99%) (Dong *et al*., 2006a). Furthermore, the RNAi gene silencing of AgDCAM in mosquitoes provided with a blood meal infected with *P. berghei* showed a 65% overall increase in oocyst number (Dong *et al*., 2006a).

In addition, AgDCAM has been implicated in phagocytosis where thisdepletion significantly decreases the phagocytic capacity of Sua5B cells in response to *S. aureus* (55%) and *E. coli* (60%), respectively. Garver *et al*. (2008) showed that the depletion of two immunoglobulin's IRID4 and IRID6 significantly doubled the number of *P. falciparum* oocysts with a fold change of 1.71 and 2.56, respectively, IRID6 was able to limit *P. berghei* infection (Garver *et al*., 2008).

1.6.1.5 C-type lectins

Lectins are glycoproteins that are present in all organisms and are a gene family comprising of selectins, collectins, endocytic receptors and proteoglycans (Varki *et al*., 2009). Lectins interact with glycans on the cell surfaces were they mediate processes including cell-cell adhesion, glycoprotein turnover, pathogen recognition and opsonisation (Drickamer and Taylor, 1993; Varki *et al*., 2009; Wang *et al*., 2018). Lectins contain the carbohydrate recognition domain (CRD) or also known as C-type lectin (CTL) domain (CTLD), with which they bind with high affinity to carbohydrate structures (Drickamer and Taylor, 1993). Classical CTLs are a group of CTLs that share primary and secondary structural homology, where the CRDs depend on calcium ions for activity (Drickamer and Taylor, 1993). Calcium is responsible for maintaining the structural intergrity of the CTLD, which is necessary for optimal function and are directly involved in ligand binding (Cambi *et al*., 2005). Not all CTLDs require calcium for activity, some may participate in protein interactions and bind inorganic surfaces and lipids (Zelensky and Gready, 2005). One CTL may contain more than one CTLD, where a single CTLD consists of approximately 110-130 amino acid residues that adopts a prototypic lectin fold composed of five anti-parallel β-sheets (β1-β5) and two α-helices (α1-α2). In addition, the CTLD loops are stabilized by two or more disulphide bonds between a pair of cysteine residues (Zelensky and Gready, 2003; Rao *et al*., 2015; Bishnoi *et al*., 2019). *Ostrina furnacalis*, an Asian corn borer moth has been reported to contain a CTL with more than one CTLD (Shen *et al*., 2018); whilst different species may contain four calcium-binding sites at typical locations within the CTLD of the protein (Figure 1.9A-B). Sites one, two and three are located in the upper lobe (Figure 1.9B), whereas site four is located in the lower lobe (Figure 1.9A) (Zelensky and Gready, 2005). The sugar binding specificity of CTLs is governed by key conserved motifs in the CTLD, which interact with cognate monosaccharades via calcium coordination and a network of four hydrogen bonds (Zelensky and Gready, 2005). CTLDs with calcium-binding site-2 consist of the Gln-Pro-Asp (QPD) motif, which is characteristic for galactose binding. Similarly, CTLDs with a Glu-Pro-Asn (EPN) motif is characteristic of mannose binding; whereas the Trp-Asn-Asp (WND)

motif is characteristic for calcium binding in site-2 (Weis *et al*., 1992; Weis and Drickamer 1994; Zelensky and Gready 2005 and Iwanga and Lee, 2005; Zhang *et al*., 2009).

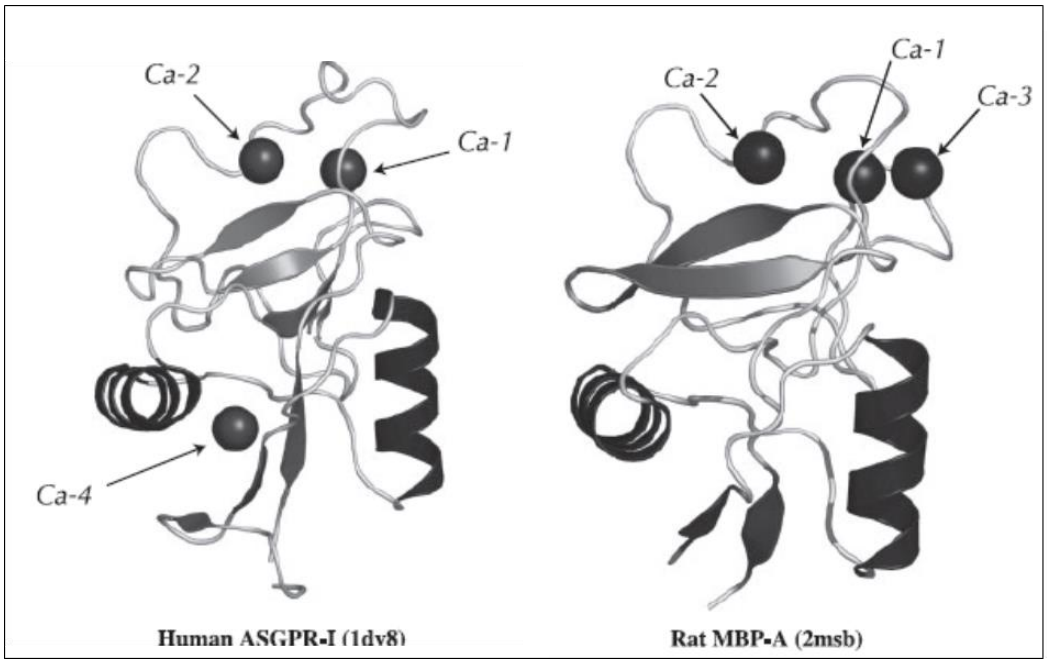

Figure 1.9: Calcium ion binding sites in the C-type lectin domain. Ribbon diagrams representing CTLD structures of human ASGPR-I and rat MBP-A demonstrate the four locations of the Ca^{2+} binding sites (Ca-1 to Ca-4). The black spheres represent the calcium ion and the numbered arrows represent the differet sites (Zelensky and Gready, 2005).

Anopheles gambiae CTL gene family comprises of 22 members that are classified into four groups, galactose-binding (GCTLA), mannose-binding (CTLM), selectins and other CTLs based on sequence specific features (Christophides *et al*., 2002). Two *An. gambiae* C-type lectin proteins CTL4 and CTLMA2 have been identified (Osta *et al*., 2004). These two genes are up-regulated following bacterial and *Plasmodium* immune challenge and have been implicated with protecting the *Plasmodium* parasite from the mosquito's immune response. Functional knockout of the CTL4 and CTLMA2 gene in *An. gambiae* that are susceptible to *P. berghei* infections, respectively resulted in significant melanization of 97% and 53% of invading ookinetes. In contrast a double knockout of both genes resulted in melanization of 88% of invading ookinetes (Osta *et al*., 2004). This double knockout additive effect of CTL4 and CTLMA2 was similar to the knockout of CTL4 alone. Collectively these observertions suggest that both CTLs function to protect parasites against melanisation and that CTL4 may be the key "driver" of protecting *P. berghei* (Osta *et al*., 2004). Although these lectins have a protective function to *P. berghei*, they are required for Gram-negative antimicrobial activity (Schnitger *et al*., 2009).

Schnitger *et al*. (2009) showed that CTL4 has antimicrobial activity against *E*. *coli* in *An*. *gambiae*. The depletion of the CTL4 and CTLMA2 resulted in a significant increase of 4.6 and 4.3-fold bacterial proliferation of *E*. *coli*, respectively, while no additive antibacterial activity was observed when silencing both genes (Schnitger *et al*., 2009).

1.7 Immune signaling

The molecular basis of the mosquito innate immunity involves a series of signal transductions, which regulate the natural microbiota and most importantly protect the mosquito from continuous exposure to invading pathogens (Kumar *et al*., 2018a). The recognition of microoganisms by PRRs can lead to the killing of the pathogen through 1) constitutive effector mechanisms, including melanization and phagocytosis and/or 2) activation of intracellular immune-signalling pathways, which induce the production of effector molecules including AMPs or reactive species to neutralize the invading pathogens (Hillyer, 2010; Kumar *et al*., 2018a). There are three major pathways within the mosquito innate immune system i.e. Toll, immune deficiency (IMD) and the Janus kinase signal transducers and activators of transcription in the JAK/STAT pathway (Figure 1.10A-C) (Cirimotich *et al*., 2010; Hillyer, 2010). These immune signaling pathways have been shown to be activated by pathogens including fungi, Gram-positive bacteria, *Plasmodium* and viruses (Kumar *et al*., 2018a).

1.7.1 Toll pathway

Initially identified in *Drosophila melanogaste*r during genetic screening of genes involved in the embryonic development, the Toll pathway has been shown to be induced by Gram-positive bacteria, fungi and some *Plasmodium* parasites including *P*. *falciparum* and *P*. *knowlesi*, and viruses. Induction led to the activation of cellular immune response and the production of AMPs (Gwadz *et al*., 1989). Furthermore, this pathway is controlled by Relish (Rel1), an NF-κβ transcription factor (Figure 1.10A). In larval and female adult mosquitoes, Rel1 has two isoforms, Rel1-A and Rel1-B, that are induced following bacterial immune challenge (Cirimotich *et al*., 2010). Some of the immune related genes with antibacterial, antifungal and antiparasitic activity include AMPs defensin, gambisin and cecropin.

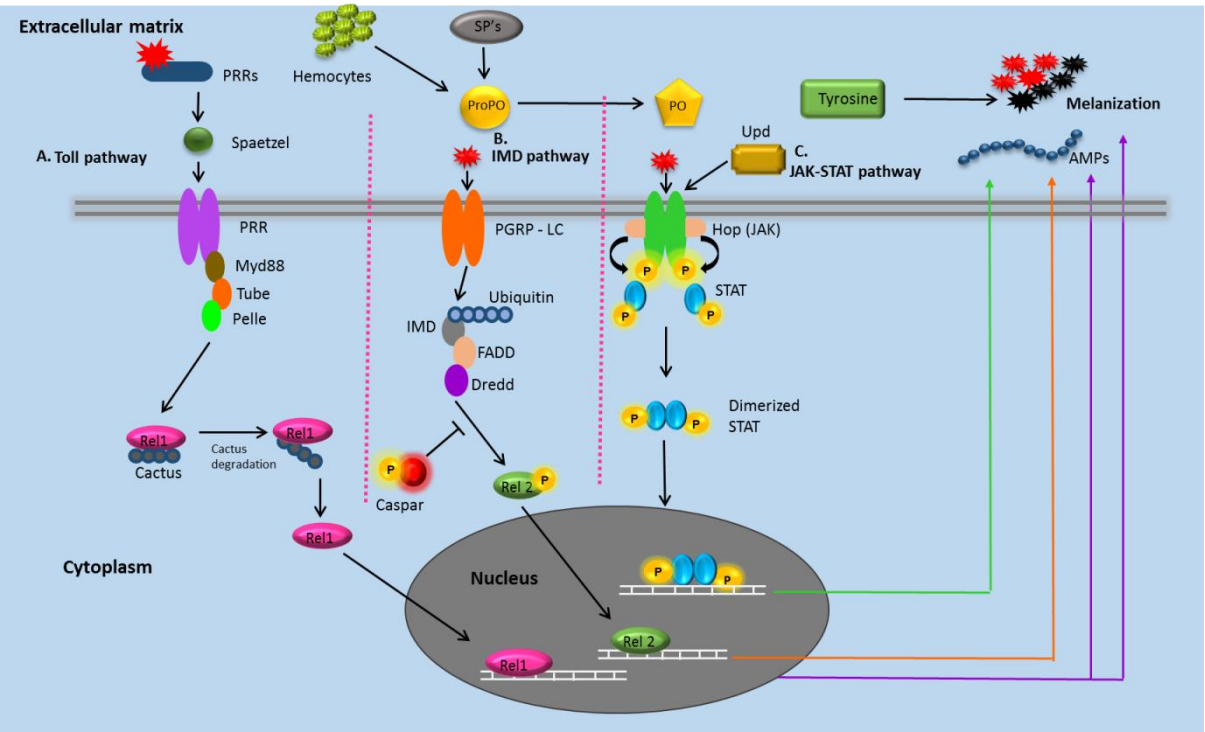

Figure 1.10: Immune signaling pathways in mosquitoes. Briefly, the (A) Toll pathway is activated by the recognition of PAMPs by PRRs, which trigger proteolytic cleavage of spaetzel. Spaetzel binds to the Toll receptors, which induce signaling via the Myd88, Tube and Pelle adapter proteins. This leads to the inhibition of cactus protein that is phosphorylated and targeted for degradation. This allows Rel1 to be translocated to the nucleus and activates the transcription of AMPs related to the Toll pathway. The (B) IMD detects a pathogen through the PGRP-LC receptors, which leads to cascades of signalling events through IMD, FADD, Dredd. Rel2 is phosphorylated by Dredd and is translocated to the nucleus resulting in the activation of the production of AMPs in this pathway. The (C) JAK/STAT is initiated when the Upd protein binds to the Dome receptor. This leads to the activation of the Hop protein that phosphorylates STAT proteins and allows for STAT dimerization. The dimer is translocated to the nucleus were it activates the transcription of JAK/STAT related genes. **Abbreviations:** AMP; antimicrobial peptides, Dome; domeless, Dredd; death related ced-3/Nedd 2-like caspase, FADD; Fas-associated protein with death domain, Hop (JAK); JAK tyrosine kinase Hopscotch, IMD; immune deficiency, JAK/STAT; Janus kinase signal transducers and activators of transcription, Myd88; myeloid differentiation primary response protein , PAMP; pathogen-associated molecular patterns, PO; phenoloxidase, proPO; pro-phenol oxidase, PRR; pathogen-recognition receptors, IMD; immune deficiency, PGRP-LC; peptidoglycan-recognition protein, Rel; relish, STAT; signal transducers and activators of transcription, SP; serpin,UPD; unpaired. (Redrawn from Kumar *et al*., 2018a).

1.7.2 Immune deficiency pathway

Induction of the IMD pathway begins when PRR recognizes a foreign pathogen and is reportedly the most effective pathway in immune responses against *P. falciparum* (Kumar *et al*., 2018a). The IMD pathway also has a NF-κβ transcription factor Rel2, which plays a central role in this pathway by regulating cecropin 1 and AMP (Cirimotich *et al*., 2010; Garver *et al*., 2012). When Rel2 undergoes alternative splicing, two isoforms are produced, the short length (Rel2–S) protein and the full length (Rel2–F) protein that contains a carboxy-terminal ankyrin, ANK and death domain. Rel2–F has been reported to modulate the intensity of infection in mosquitoes (Figure 1.10B). When the negative regulator of Rel2 (Caspar) was silenced, an overexpression of Rel2 was observed and this rendered complete resistance of *An. albimanus, An. gambiae* and *An. stephens*i against laboratory cultured *P. falciparum* (Kumar *et al*., 2018a). Some of the immune genes with antiparasitic action related to the IMD pathway include TEP1, CTL and FBN-9.

1.7.3 JAK/STAT pathway

There is limited information available on this pathway as far as mosquito immunity is concerned (Figure 1.10C). The JAK/STAT pathway comprises of four major components, unpaired (Upd) peptide ligand, transmembrane protein receptor (Dome), Janus kinase (JAK) and STAT proteins. Induction of the JAK/STAT pathway begins when Upd binds to the extracellular terminal of the Dome receptor, which results in dimerization of receptors and leads to the phosphorylation of Janus kinase (Kumar *et al*., 2018a). The activation of the Janus kinase in turn phosphorylates the C-terminal side of the receptors and produces a binding pocket for the STAT protein. The STAT proteins become phosphorylated when they bind to the JAK-Dome complex, this activates the STAT proteins leading its dimerization and translocation to the nucleus where they regulate the expression of target genes (Kumar *et al*., 2018a). This pathway mediates the transcriptional activation of the nitric oxide synthase in response to *Plasmodium* infection, which in turn leads to the production of reactive nitrogen species.

1.8 Mosquito effectors

1.8.1 Antimicrobial peptides

The AMPs are positively charged, low molecular weight proteins that are produced by the fat body and haemocytes that are involved in humoral immune responses (Figure 1.6A) (Blandin *et al*., 2002).

Mosquito AMPs are classified into three groups, defensins, cecropins and gambicins based on structure and amino acid sequence (Gwadz *et al*., 1989; Dong *et al*., 2006b). Cecropins are the largest AMP group in mosquitoes with a broad spectrum of antimicrobial and anti-*Plasmodium* activity and these include cecropin A, B and C (Wu *et al*., 2018). The antibacterial activity of cecropins is to lyse bacterial cell membranes leading to the leakage of cellular contents that eventually leads to the death of the bacterial. Furthermore, Gwadz *et al*. (1989) showed that an up-regulation of cecropin *B* in *An. gambiae* infected with *P. falciparum* or *P. knowlesi* disrupts oocysts development, there was a significant increase of 85% and 94% in the number of destroyed oocysts, respectively. Defensins are small variable cationic arginine-rich peptides with six conserved cysteine residues and are induced in response to bacteria, but are mostly effective against Gram-positive bacteria, *Bacillus subtilis* (Blandin *et al*., 2002). The RNAi mediated gene silencing of defensin in *An. gambiae* challenged with *B. subtilis* resulted in killing 85% of the mosquitoes one day post-immune challenge and all by day two (Blandin *et al*., 2002). The *An. gambiae* gambicin exist in two forms, the oxidized form with high antibacterial activity and non-oxidized form (Vizioli *et al*., 2001). Oxidized gambicin inhibits *E. coli* at minimal concentrations (6.25-12.5µM). Both forms of gambicin have antifungal activity because their up-regulation reduced the elongation of *Neurospora crassa* hyphae, delaying the germination of spores. Furthermore, both forms of gambicin showed a dose-dependent effect on anti-*Plasmodium* development in *An. gambiae*, where 54.6% and 65.2% of *P. berghei* ookinetes were respectively killed with 10µM and 50µM of gambicin (Vizioli *et al*., 2001). In addition, gene silencing of gambicin resulted in a 80% increase in *P. berghei* oocysts formation (Dong *et al*., 2006b).

1.8.2 Reactive species

Reactive species are products of oxidative stress produced by the innate immune response system (Figure 1.6A and B) (Betteridge, 2000). These oxidative by-products are potentially toxic to the host and must be generated transiently and kept localized (Molina-Cruz *et al*., 2008). ROS and reactive nitrogen species are associated with killing of mosquito non-self-entities. ROS facilitates some cellular processes including apoptosis, digestion of the blood meal, intercellular signaling and cell growth regulatory pathways (Valko *et al*., 2006). ROS activity against Gram-negative bacteria showed that the refractory *An. gambiae* mosquito, which exhibits high levels of ROS, survives bacterial challenges. This is in contrast to susceptible strains where 90% of these susceptible mosquitoes died eight days post bacterial challenge.

When vitamin C (ascorbic acid), an anti-oxidant, was administered to susceptible bacteria, all mosquitoes died by day three (Molina-Cruz *et al*., 2008). This suggests that ROS is required for antibacterial activity.

1.9 Immune effector mechanisms

1.9.1 Phagocytosis

Phagocytosis is an evolutionary conserved immune cellular process known to effectively neutralize and remove microorganisms. In the mosquito, phagocytosis is mainly regulated by PRR, transmembrane receptors and other signaling proteins. The TEP1 and LRMI1 were identified as major recognition peptides involved in the phagocytic degradation of microorganisms due to their ability to opsonize microorganisms (Schitger *et al*., 2009). Phagocytosis is initiated when proteins on the plasma membrane recognizes a foreign agent and is engulfed by a phagocytic cell resulting in the formation of a phagosome (a cell that carries foreign targets or microoganisms). The phagosome is then internalized into a membrane delimited phagosome, which fuses with the lysososme in the cytosol. This leads to the neutralization of the target by hydrolytic enzymes in the lysosome (Hillyer *et al*., 2003; Kumar *et al*., 2018).

1.9.2 Melanization

Melanization is the major effector immune response of the immune system that consists of enzymatic and non-enzymatic reactions (Gonzalez-Santoyo and Cordoba-Aguilar, 2011). It is activated locally in response to cuticle injury or systemically following pathogen invasion in the haemocoel (Nakhleh *et al*., 2017). The melanization process has dual function, 1) in development such as cuticle hardening, egg chorion tanning and 2) immunity (Hillyer, 2010). As part of the immunity of the mosquito, melanization is responsible for encapsulating multicellular microorganisms, repairing injured tissue and defending the mosquito against pathogens. The melanization process is characterized by the formation of a thick dark melanin rich proteinaceous layer that surrounds the invading pathogen (Figure 1.11B and C).

The melanization process begins with a proteolytic cleavage of pro-phenol oxidase zymogen (proPO) following recognition of PAMPs, peptidoglycans or lipopolysaccharides by clip domain serine protease (CLIP) to an active form called the PO enzyme (Nakhleh *et al*., 2017). Although not well defined, this interaction activates the serine protease pathway where the cleavage of the proPO is thought to be facilitated by the activation of a serine proteinase, pro-phenol oxidase activating enzyme (PPAE) at specific sites of the peptide bond near the amino terminus (Kanost, 1999).

The activation of the PO enzyme subsequently initiates the formation of melanin. Briefly, phenylalanine undergoes hydroxylation by phenylalanine hydroxylase to form tyrosine, which is also hydroxylated by PO to form Dopa. Dopa becomes oxidized to form dopaquinone that undergoes a spontaneous non-enzymatic structural rearrangement and is converted to dopachrome which undergoes decarboxylation to form 5,6- dihydroxyindole (DHI) (Gonzalez-Santoyo and Cordoba-Aguilar, 2011). The DHI is then oxidized by PO to form indole-5, 6-quinone that cross links with proteins in the haemolymph to form a malanitic capsule (Hillyer *et al*., 2010; Gonzalez-Santoyo and Cordoba-Aguilar, 2011). The production of melanin by-products and its intermediates (quinones, diphenols, hydrogen peroxide, reactive nitrogen and superoxide) results in a highly oxidative environment. This is lethal for the pathogens, but becomes detrimental to the mosquito. However, this is tightly controlled by mosquito gene families including C-type lectins or serine protease inhibitors and enzymes that prevent excess melanization. One such enzyme is the NADPH–dependent thioredoxin reductase, which can neutralize oxidative molecules such as quinones. The NADPH-glutathione reductase catalyzes the reduction of glutathione disulphide to glutathione, thereby neutralizing oxidative molecules (Figure 1.11). The mosquito NADPH–dependent thioredoxin reductase employs a similar process (Bauer *et al*., 2002).

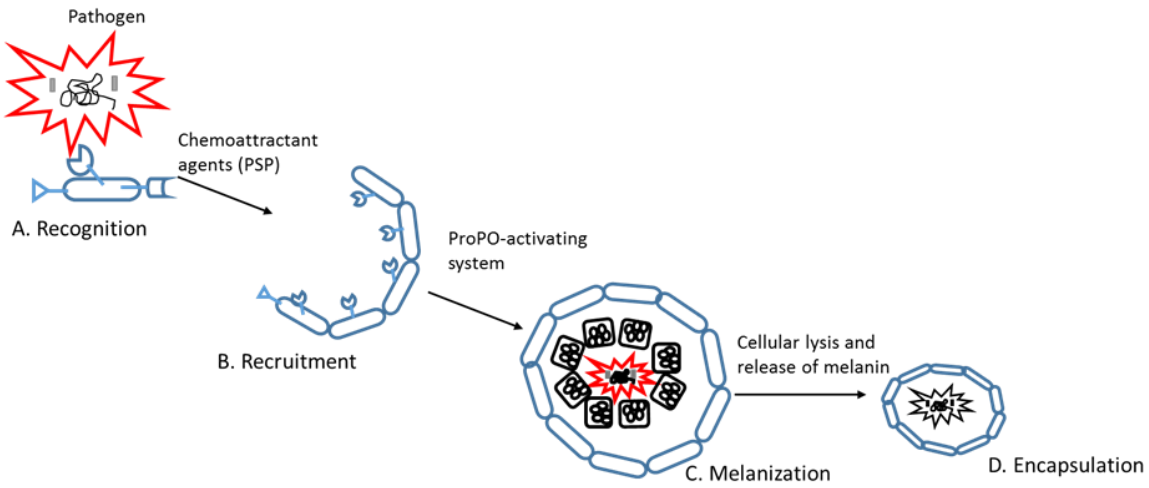

Figure 1.11: Overview of the melanization process. (**A**) Recognition of pathogens by PRRs (**B**) recruitment of hemocytes surround the pathogen and release chemoattractant proteins PSP which recruit plasmatocytes (**C**) internal layers of the plasmatocytes begin to thicken and become dark due to the production of melanin which occur within hemocytes (**D**) Melanin is deposited to the foreign target thereby creating unfavorable living conditions for the pathogen, this results in the prevention of growth of the of the foreign target and eventually leads to its death. **Abbreviations:** PSP; plasmatocyte spreading peptide (Redrawn from Gonzalez-Santoyo and Cordoba-Aguilar, 2011).

1.10 Immunomodulators

Immunomodulators include a wide range of immune activators and suppressors aimed at restoring normal immune function and can be indigenous or synthetic (Bascones-Martinez *et al*., 2014). Antimalarial drugs such as chloroquine (CQ), artemisinin and pyrimethamine are also immunomodulators and range from immune suppressors to activators depending on the target (Kim *et al*., 2015; Hou and Huang, 2016; Oh *et al*., 2016). The presence of antimalarial drugs such as CQ in the blood meal ingested by the *Anopheles* mosquito has been reported to interact with the *Anopheles* immune system and interfere with the development of the *Plasmodium* parasite in the mosquito (Abrantes *et al*., 2005).

1.10.1 Chloroquine

CQ is a 4-aminoquinoline antimalarial drug discovered by Hans Andersig in the early 1900s. It has been used as an antimalarial drug for many decades due to its low cost, efficacy against the asexual stages of *P. falciparum* parasite and its safety. However, the development of resistance by the malaria parasite has greatly reduced it clinical use (Krogstad *et al*., 1987). In South Africa, CQ is not used for malaria treatment because the principal parasite, *P. falciparum* is resistant to CQ. However, CQ is still effective against other *Plasmodium* species including *P. malariae*, *P. ovale* and *P. vivax* (WHO, 2019). CQ is not only an antimalarial drug, it is also also used in the management of rheumatoid arthritis and lupus erythematosus (Fox, 1996; Al-Bari, 2015; Schrezenmeier and Dorner, 2020). In addition, preliminary studies have reported that CQ may be an effective drug against the new SARS-coronavirus 2 (Vincent *et al*., 2005; Fantini *et al*., 2020; Gbinigie *et al*., 2020).

1.10.2 Mechanism of action of CQ against *P. falciparum*

During the intra-erythrocytic cycle of the *P. falciparum* parasite, approximately 60-80% of the host erythrocyte cytoplasm is consumed into the cytosome where haemoglobin is ingested and transported to the digestive food vacuole by transport vesicles (Figure 1.12) (Chemaly *et al*., 2007). The acidic food vacuole (pH 5.0 to 5.4) is maintained by the proton gradient and activated by an ATPase pump and proteolytic enzymes (Coranado *et al*., 2014). Degradation of haemoglobin produces amino acids that are used by the parasite to produce proteins, as well as, a release of haem-Fe(II). Haem-Fe(II) is oxidized to form haematin-Fe(III). This subsequently results in the production of hydrogen peroxide, which together with haem are toxic to the parasite. The parasite then detoxifies haematin to form an insoluble, inert, crystalline haemozoin that is not toxic to the parasite. This is crucial for the survival and growth of the parasite, enabling it to continue its cycle by utilizing host molecules and invading new cells (Chemaly *et al*., 2007; Coranado *et al*., 2014).

Additionally, haemoglobin degradation involves two parasite aspartic enzymes in the *P. falciparum* food vacuole, plasmepesin I and II, and a cysteine protease falcipain. These enzymes function at an optimal pH of approximately 5.0, indicating their role in haemoglobin degradation (Coranado *et al*., 2014).

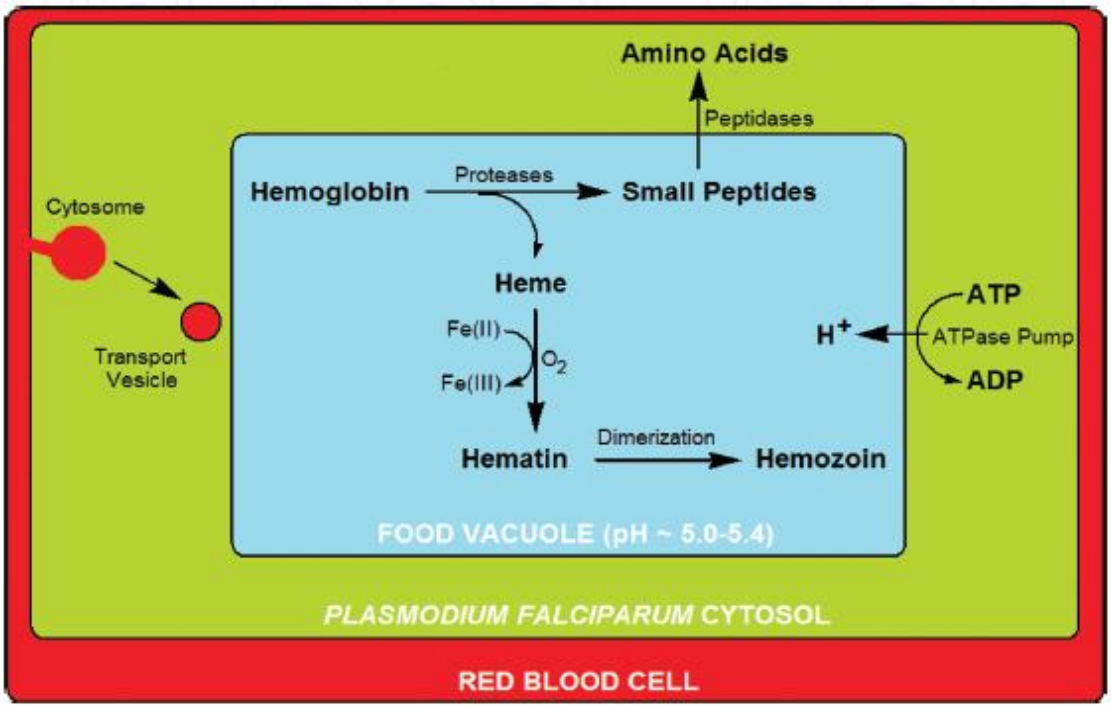

Figure 1.12: Haemoglobin degradation by *P. falciparum* and haemozoin formation in RBC (Vanderesse *et al*., 2016).

The proposed mechanism of action of CQ is attributed to its ability to prevent the formation of haemozoin (Figure 1.13). At a physiological pH of 7.4, unprotonated CQ enters an infected RBC by diffusion where it becomes protonated to CQ^{2+} (Aoi and Marunaka, 2014; Coronado *et al*., 2014) and, due to the ionised state is prevented from leaving the parasite. CQ binds to the free haem, preventing bio-crystallization to haemozoin; and as a result, the toxic haem accumulates in the cell and the environment becomes unfavourable for the parasite. The resulting CQ-haem complex is highly toxic, generating free radicals that induce lipid peroxidation leading to haemolysis and eventually auto-digestion by the host immune cells killing the infected RBC (Golberg, 1993; O'Neill *et al*., 2012; Parhizga and Tahghighi, 2017). Resistance in the parasite is due to the efflux of CQ out of the parasite's digestive food vacuole and is known to be associated with a parasite protein, namely *Plasmodium falciparum* CQ resistance transporter (*Pf*CRT) found in the digestive food vacuole membrane (Hayward *et al*., 2006; Ecker *et al*., 2012). After many years of drug pressure, various mutations have emerged to protect the parasite by alterating the membrane protein physiochemical properties, thereby modifying CQ uptake in resistant parasites (Ecker *et al*., 2012).

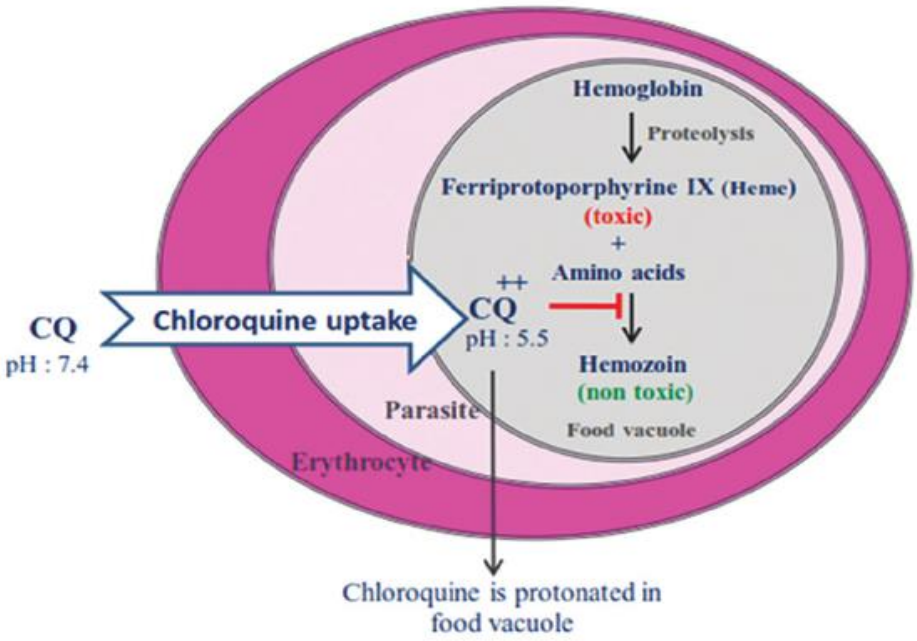

Figure 1.13: Proposed mode of action of CQ on *P. falciparum* (Parhizga and Tahghighi, 2017).

1.10.3 The use of CQ on anti-inflammatory diseases

Rheumatic arthritis and systemic lupus erythematosus (hereafter referred to as lupus erythematosus) are auntoimmune diseases. Rhematic arthritis causes pain, swelling, stiffness and damage of joints throughout the body and lupus erythematosus causes permanent chronic kidney disease and permanent renal damage (Lee *et al*., 2011). Therapy for patients with renal damage includes corticosteroids, immune suppressive agents and antihypertensive medication. The first use of an antimalarial drug in a patient with lupus erythematosus occurred in 1630 when it successfully treated tertian fever (malaria) and, in the 1800, quinine successfully induced pallor in a patient diagnosed to have a lupus rush (Figure 1.14) (Lee *et al*., 2011). Furthermore, during World War II, quinine was used as malaria prophalaxis by soldiers. Interestingly, soldiers with inflammatory arthritis and cutaneous lupus had symptomatic impovements while they were taling quinine. Collectively, these observertions led to studies on the use of antimalarial drugs to treat patients with rheumatic diseases. CQ and hydrochloroquine (CQ analogue) were later introduced and approved for medicinal use; this was due to great efficacy and tolerability in comparison to quinine. CQ and hydrochloroquine are still commonly used antimalarial drugs administered to manage patients with rheumatic diseases (Lee *et al*., 2011; Al-Bari, 2015; Schrezenmeier and Dorner, 2020).

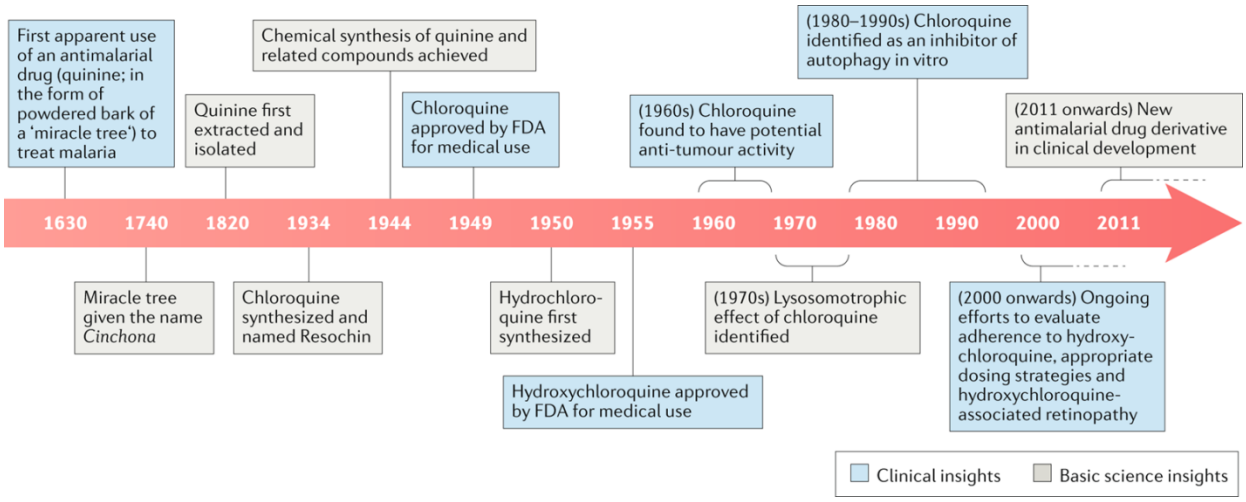

Figure 1.14: History of CQ and CQ analogue, hydroxychloroquine introduction (Schrezenmeier and Dorner, 2020).

1.10.4 Anti-inflammatory mechanism of action of CQ

The specific mechanism of action of CQ and its analogues in reducing anti-inflammation is still unclear. However, the immunomodulatory effects of CQ and hydroxychloroquine are mediated by actions that can be summerized in Figure 1.15.

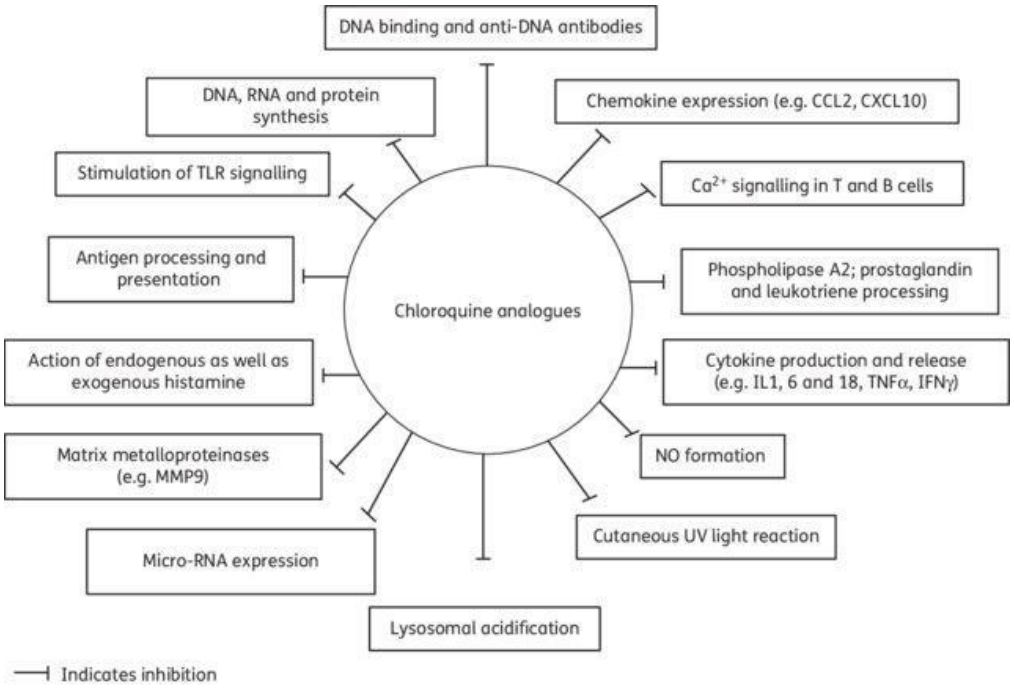

Figure 1.15: Proposed anti-inflammatory and immunomodulatory effects of CQ and its analogues (Al-Bari, 2015). **Abbreviations:** CCL2: Chemokine (C-C motif) ligand 2; CXCL10: C-X-C motif chemokine ligand 10; TLR: Toll- like receptor; NO: Nitric oxide; IL1,6: Interleukin-1,6 ; TNFα: tumor necrosis factor-alpha; IFNγ: Interferon-gamma; UV: ultra-violet.

The proposed mechanism of action of CQ is dependant on its weak base properties which allow it to accumulate in acidic vesicles to elicit its anti-inflammatory effects. This is initiated when unprotonated CQ (pH 7.4) diffuses freely and rapidly across cell membranes to acidic cytoplasmic vesicles (lysosomes) in inflammatory cells and, once protonated becomes trapped. Lysosomes are cellular compartments that contain acid hydrolases that digest macromolecules (Al-Bari, 2015). The pH of the lysosome is maintained at approximately 5.0 by lysosomal H^+-ATPase, this is for optimal activity of hydrolases. The ATP-dependent lysosomal H^+-ATPase pumps H^+ ions into the acidic vesicle, CQ then diffuse from the cells cytoplasm into the acidic lysosome. This action causes a partition due to the difference between the pH gradient that ultimately leads to the irreversible accumulation of CQ in the lysosome and increases the pH (Al-Bari, 2015). CQ and its analogues interfer with the acidic environment in the lysosome and inhibits processes including enzyme function, antigen presentation and phagocytosis.

1.10.4.1 Blockade of Toll-like receptor signalling pathways

Toll-like receptors (TLR) are pattern recognition cellular receptors that recognize foreign invading pathogens and endogenous molecules from damaged tissue and induce inflammatory responses by activating the human immune system (Lee *et al*., 2011; Gao *et al*., 2017). During auto-immunity endogenous molecules (cellular debris) can activate Toll-like receptor signalling pathway causing plasmacytoid dendritic cells and antigen presenting cells to produce large amounts of interferon-α (IFN-α) and stimulate B-cells to increase the production of immunoglobulins and cytokines that repair damaged tissue and fight invading pathogens (Gao *et al*., 2017; Schrezenmeier and Dorner, 2020). However, excessive activation of the Toll-like receptors disrupts homeostasis by sustained pro-inflammatory chemokines and cytokines, at most times, consequently leading to the development of auto-immune diseases (Gao *et al*., 2017). In antigen presenting cells, CQ/hydroxychloroquine reduces inflammatory responses by inhibiting the activation of Toll-like receptors, which prevents the production of cytokines, including: TNF, IFNγ, IL-6 and IL-1 (Figure 1.16A). In plasmacytoid dendritic cells (Figure 1.16B), CQ/hydroxychloroquine also inhibits antigen processing and major histocompatibility complex class II presentation to T-cell, which prevents the activation of T-cells. This subsequently prevents the differentiation and expression of the transmembrane type II protein, CD154, as well as the reduction in production of cytokines by T-cells (TNF, IFNγ, IL-6 and IL-1) and B-cells (BAFF, TNF, IL-6 and IL-1) (Schrezenmeier and Dorner, 2020).

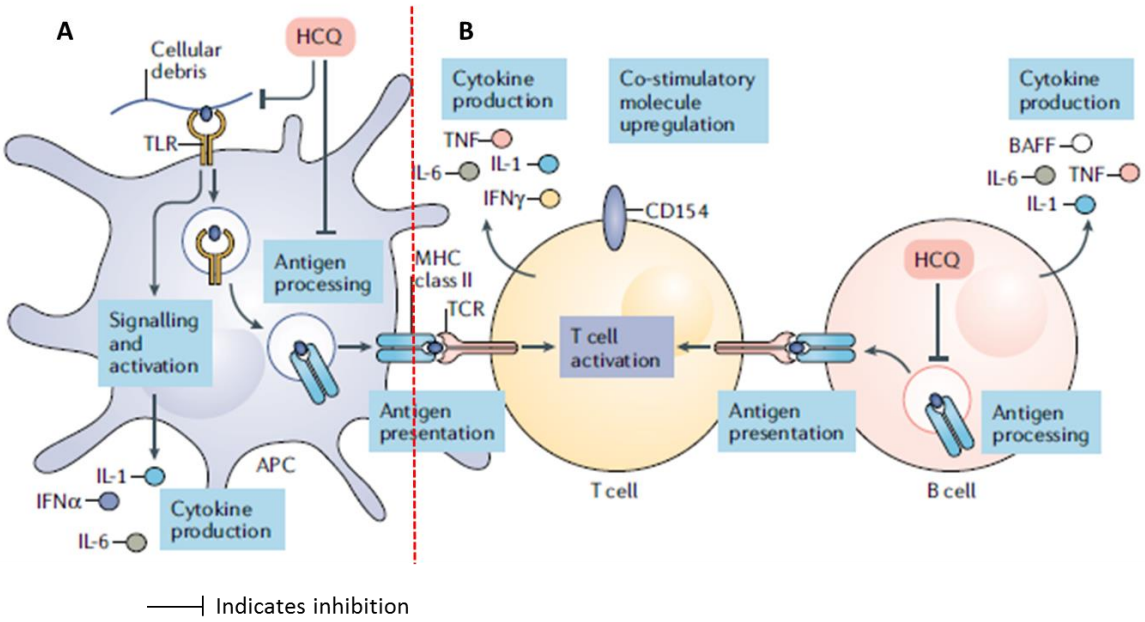

Figure 1.16: Proposed cellular mechanism of action of hydroxychloroquine during auto-immunity. A) Antigen presenting cells and B) plasmacytoid dendritic cells, **Abbreviations:** APC; antigen presenting cells, BAFF; B-cell activating factor, HCQ; hydroxychloroquine, IL-1,-6; interleukin, INFα/INFγ; interferon alpha/gamma, MHC calss II; major histocompatibility complex class II, TNF; tumor necrosis factor, TCR; t-cell receptor (Schrezenmeier and Dorner, 2020).

1.10.4.2 Antigen processing and presentation

Autophagy is a conserved transport pathway that is essential to maintain cellular homeostasis (Mauthe *et al*., 2017). Cellular homeostasis is achieved through sequestration, delivery and degradation of damaged tissue (cargo) and organelles into lysososme. The ultimate aim of autophagy is the degradation of cargo (Figure 1.17). Dysregulation of the autophagy disrupts immune homeostasis and has been implicated in inflammatory, lysosomal disorders, cancer, muscle dystrophies and neurodegeneration (Shintani and Klionsky, 2004; Levine and Klionsky, 2004; Mizushima *et al*., 2008; Levine *et al*., 2011). Antigen processing is a pH-dependent phenomena which is interfered with by CQ/hydroxychloroquine affecting lysosomal acidification by increasing the pH inside the lysososme (Al-Bari, 2015). This interference turns off the process of antigen presentation and leads to a decrease in the number of autoantigentic peptides appearing on the cell surface (i.e. reduces binding of antigenic peptides to class II major histocompatibity complex molecules (MHC class II) (Figure 1.17) (Al-Bari, 2015; Schrezenmeier and Dorner, 2020).

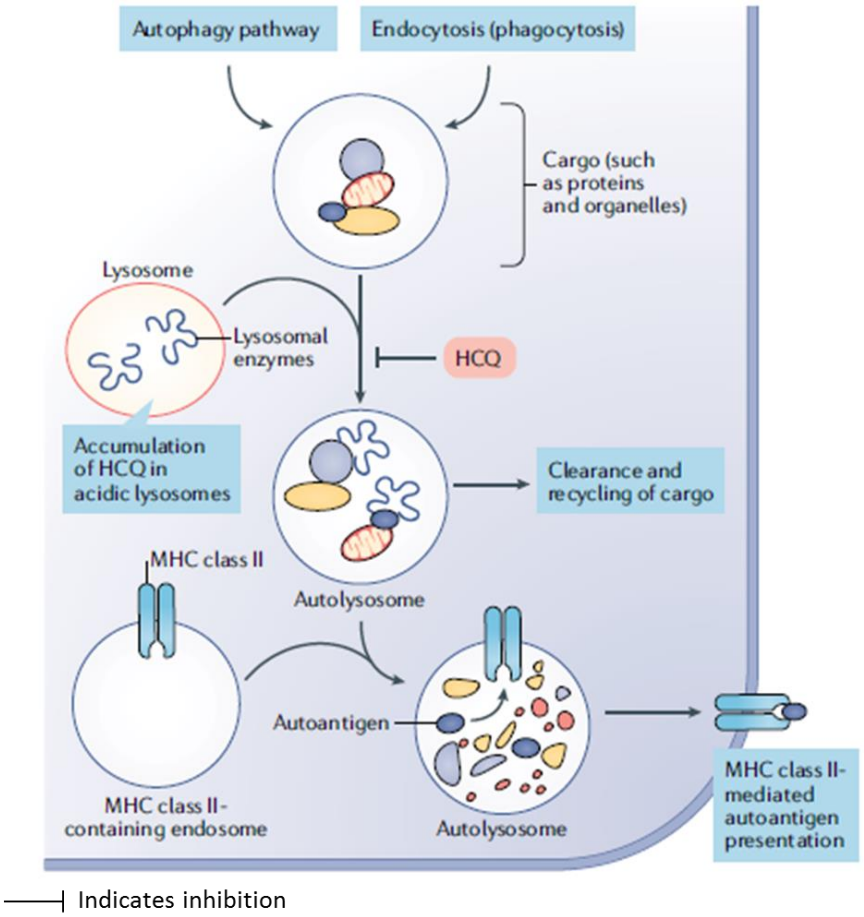

Figure 1.17: Proposed molecular mechanism of CQ analogue, hydroxychloroquine (HCQ) during auto-immunity. (Schrezenmeier and Dorner, 2020).

1.11 Melanization, C-type lectin and immunomodulators

The understanding of the interaction between the *Plasmodium* parasite and its *Anopheles* vector has led to many studies that target major developmental stages of the parasite in the vector. In addition, the gain of knowledge of the mosquito immune system clearly shows that this robust defense system is capable of eliminating invading pathogens. The melanization response is a tightly controlled process in mosquitoes (Section 1.9.2), controlled by gene families that inhibit excessive melanization preventing excessive production of melanization by products/intermediates that will be detrimental to the insect (Shin *et al*., 2011). It has been reported that two genes (CTL4 and CTLMA2) of the C-type lectin family inhibit excessive melanization during an immune challenge by *P. berghei*. This inhibitory process from the CTLs is the hosts' way of protecting itself from death, but in turn prevents the destruction of the *Plasmodium* parasites (Section 1.6.1.5) (Osta *et al*., 2004).

Shin *et al*. (2011) reported on the discovery of the CLSP2 gene in *Aedes aegypti* mosquito that encodes for modular proteins with a C-type lectin and elastase-like serine protease domain that is controlled by NF-κβ of the Toll and IMD pathway. The CLSP2 gene is up-regulated following an immune challenge with avian malaria parasite *P*. *gallinecaum* and *Enterobacter cloacae*. RNAi mediated gene silencing of CLSP2 resulted in the proteolytic cleavage of proPO 24 hours post infection, which leads to the melanization of *P*. *gallinecaum* ookinetes and *E*. *cloacae* bacterial cells. However, when the proPO enzyme was depleted, CLSP2 accumulation was detected and this prevented the melanization of *P*. *gallinecaum* and *E*. *clocae* (Shin *et al*., 2011). Wang *et al*. (2015) reported on the CLSP2 gene to function extracellularly as a PRR in which the lectin domain binds to fungal components of *Beauveria bassiana conida*. RNAi mediated gene silencing of the CLSP2 gene in *Ae*. *aegypti* mosquitoes infected with *B. bassiana* led to the up-regulation of genes encoding FBNs, TEPs and serine proteases that are involved in melanisation this increased refractory of *Ae*. *aegypti* against *B. bassiana* (Wang *et al*., 2015). These findings suggest that PRR containing the lectin domain act as negative regulators of the melanization process.

In addition to C-type lectins acting as negative regulators and promoting *Plasmodium* development, CQ has been shown to increase *Plasmodium* infectivity to the *Anopheles* vector (Abrantes *et al*., 2005). Abrantes *et al*. (2005) showed that CQ down regulates the expression of immune related genes including AMPs, gambicin and defensin . This effect was found to be dose-dependant in *An*. *gambiae* when mosquitoes were provided with a blood meal supplemented with CQ (10 and 50mg/kg). The cohort provided with 50mg/kg of CQ was able to suppress gambicin and defensin with a fold change of -1.69 and -1.9, respectively. Moreover, Abrantes *et al*. (2008) showed a down-regulation (suppression) of gambicin in *An*. *gambiae* previously treated with 50mg/kg of CQ and infected with *P*. *berghei* with a fold change of -1.63. This study suggests that CQ interferes with signalling pathways of the mosquitos' innate immune system at a transcriptional level and understanding these interactions can provide new strategies to control malaria (Abrantes *et al*., 2005). In addition, it has previously been shown that glucocorticoids are able to inhibit the transcription of AMPs by inducing the synthesis of Iκβa, which can inhibit the activity of NF-κβ (Simmaco *et al*., 1997). The actions of glucocorticosteroids are not always immunosuppressive, but can also be immune-enhancing. Tan *et al*. (2014) showed that glucocorticosteroids enhanced the expression of AMP genes to amplify the immune response of the fly embryo to bacterial infections.

1.12 Rationale/ research motivation

Insecticide resistance conferred by the *Anopheles* vector and drug resistance by the *Plasmodium* parasite undermines the efficacy of the current intervention used for malaria control. Understanding the biological interactions between the *Anopheles* vector and *Plasmodium* parasite can enable potential possibilities for disrupting the transmission cycle. Available research on the transmission cycle between the *Anopheles* vector and its *Plasmodium* parasite has shown potential targets as an alternative in the reduction of the number of deaths caused by malaria. Molecular and biological research of the transmission cycle has been studied in great detail in *An. gambiae* and murine parasite, *P. berghei*. Vector-parasite interactions have been limited in *An. funestus s.s.*, primarily due to the difficulty of rearing of this mosquito species in the laboratory and acquiring sufficient *Plasmodium* infected mosquitoes experimentally.

The establishment of the *An. funestus s.s.* colony by Hunt *et al.* (2005) has opened new research opportunities. The *An. funestus s.s.* FUMOZ colony is routinely reared using guinea pigs for a blood meal. However, to initiate *P. falciparum* infection studies, whereby this colony needs to feed on an artificial standard membrane feeding system, optimised blood feeding will be needed to ensure adults feeds adequately for subsequent studies. Considering the significant role the mosquito immune system plays in the transmission of the malaria parasite, the interaction between the mosquito and *P. falciparum* can be used as an approach to interrupt transmission. The putative *An. funestus s.s.* CTL4 has been identified from an automated projection (bioinformatics resource center) from *An. gambiae* CTL4 (https://www.vectorbase.org/). Therefore, it was hypothesized that:

1) *An. funestus s.s.* CTL4 is up-regulated following immune challenge by *P. falciparum* and this plays a significant role in the transmission cycle of the malaria parasites, particularly by protecting malaria parasites from immune response through the inhibition of immune processes such as melanization.

2) The immune system of *An. funestus s.s.* can be modulated by compounds to inhibit CTL4 and this would allow for specific targeting of malaria-infected mosquitoes. By inhibiting CTL4, this will allow for melanization to occur and the subsequent production of quinones that would result in death of the mosquito and at the same time inhibit the transmission of the malaria parasite.

1.13 Aim and Objectives

1.13.1 Aim

This study aimed to understand the effect that *P. falciparum* and an immune-modulator, CQ, have on the expression profile of the putative immune factor CTL4 in the main African malaria vector *An. funestus s.s.*

1.13.2 Objectives

1. Identify *An. funestus s.s.* CTL4 transcript.
2. Optimize *An. funestus s.s.* feeding rate.
3. Infect *An. funestus s.s.* with *P. falciparum*.
4. Evaluate the transcript level of CTL4 in *P. falciparum* infected and uninfected *An. funestus s.s.*
5. Investigate the preliminary toxicological profile of CQ on *An. funestus s.s.* larvae and adult females.
6. Evaluate the transcript level of CTL4 in CQ-treated and untreated adult *An. funestus s.s.*

CHAPTER TWO

2. Materials and Methods

2.1 Identification of *An. funestus s.s.* CTL4 gene

2.1.1 Bioinformatics analysis

The CTL4 gene has been shown to play a major role in the development of the *Plasmodium* parasite in *An. gambiae*, however, has not yet been studied in *An. funestus s.s*. In order to identify the molecular, structural, functional and conformational characteristics of *An. funestus s.s*. CTL4, the approach included the use of bioinformatics tools (Table 2.1). As such, genomic DNA (gDNA), complementary DNA (cDNA) and amino acid sequences were used to investigate structural, functional and conformational features, gene specific primers were designed at coding regions (exons).

2.1.1.1 Obtaining *An. funestus s.s.* CTL4 sequences

The *An. funestus s.s*. CTL4 (AFUN10847) nucleotide, cDNA and amino acid sequences were retrieved from the VectorBase (https://www.vectorbase.org/). Analysis of the deduced cDNA and amino acid sequences including general features in cDNA, molecular weight, signal peptide and domain organization were performed by Pfam, PredictProtein, Prosite, InterPro, SignalP and SMART (Table 2.1). Furthermore, the deduced amino acid sequence was submitted to Quark, RaptorX and Phyre servers for prediction of the tertiary structure (Table 2.1). These servers were selected because they are not only free and accessible but have been shown to perform well in the CRISPR associated protein 9 experiment (CAS-9) which will enable the generation of a more accurate structure (Kallberg *et al*., 2012; Xu and Zhang *et al*., 2012; Xu and Zhang *et al*., 2013; Kelly *et al*., 2015). The generated protein data bank (PDB) files which is a texual file format that describes the three-dimensional structures of a molecule were submitted to ProSA and PROCHECK for assessment of the predicted tertiary structures and visualized with Pymol Molecular Graphics V1.8 software.

2.1.1.2 Sequence alignment and phylogeny

Amino acid sequences for *An. funestus s.s*. CTL4 orthologs were retrieved from VectorBase and multiple sequence alignment was carried out using multiple sequence comparison by log expectation (MUSCLE) program available in MEGA X (Kumar *et al*., 2018) with the following default parameters: refining alignment; gap opening penalty of -2, 9; gap extension penalty of 0; hydrophobicity multiplier of 1, 2; maximum interactions of 100; clustering method (for interactions 1, 2) = unweighted pair group method with arithmetic mean

(UPGMB) and minimum diagonal length of 24. Additionally, multiple sequence alignment by Clustal O (https://www.ebi.ac.uk/Tools/msa/clustalo/) between *An. funestus s.s.* CTL4 and other C-type lectins that have been studied was employed to determine conserved functional domains in *An. funestus s.s.* CTL4 (Zelensky and Gready, 2003). Phylogeny was performed in order to evaluate the evolutionary relationship amongst *An. funestus s.s.* CTL4 and its orthologs. The resulted alignments were used to construct a phylogenetic tree with the aid of the neighbour joining (NJ) available in MEGA X software package. In order to construct the NJ phylogenetic tree, the following parameters were set: gaps were treated as characters; complete deletion of gaps or missing data; poison model; uniform rates and statistical analysis was performed using bootstrap trails with, 1,000 replicates (https://www.megasoftware.net/).

2.1.1.3 Primer design

All primers used in this study were designed with the aid of bioinformatic tool, Primer3 (http://bioinfo.ut.ee/primer3-0.4.0/) and are listed in Table 2.2. This excludes primers in Table 2.3, which were previously designed by other members in the lab and have become standards. This tool provided the most optimal primer sequences with G-C content between 50-60% and an annealing temperature ranging between 55°-60°C, however for some primer sequences, the G-C content is low as a result of the A-T rich base that is characteristic of the *Plasmodium* genome (used in Section 2.5.2). Prior to use, the lyophilized oligo primers where briefly centrifuged to pellett the lyophilized content to the bottom and a 100µM stock was prepared by dissolving the pellet in deionized water as instructed by the manufacturer (Inqaba biotec, Pretoria, South Africa). The concentration of the stock primers were determined by measuring the absorbance of the DNA at 260nm whereas the purity was determined by using the ratio 260nm/280nm ($A_{260nm/280nm}$) aided by a NanoDrop™ OneC spectrophotometer (Thermo Scientific™, USA: 840274200). For identification, the deduced *An. funestsus s.s.* CTL4 (AFUN10847) nucleotide was retrieved from VectorBase (https://www.vectorbase.org/) as a FASTA format sequence and exon sequences were uploaded on Primer3 for primer design. Additionally, exon two was only 80bp long and segments of the introns were included so that sequencing without the need for cloning can be possible. Sequencing of small fragments are problematic and therefore primers were designed to amplify fragments between 200 - 1,000bp.

2.2 Biological Materials

Mosquito strain: wild-caught females (n>200) were collected by other members of the unit from house searches in southern Mozambique and colonized in 2000 (Hunt *et al*., 2005). Adults and larvae that make up the FUMOZ colony are maintained in the insectary in the

WITS Research Institute for Malaria, Faculty of Health Sciences, University of the Witwatersrand under standard insectary condition: 25 ± 1°C, 80% humidity and a 12 hour day-night, 45 minutes dusk-dawn cycle (Hunt *et al*., 2005). Adults were provided with 10% (w/v) sugar water solution, whereas larvae were fed on 2:1 ratio of finely crushed Beeno® dog biscuits to brewers yeast.

All ethical clearance certificates for the study were obtained from the University of the Witwatersrand Ethics Committees (Appendix - Section A.1).

Table 2.1 List of databases and bioinformatics tools used during *in silico* characterization of *An. funestus s.s.* CTL4. Servers were used to characterize the CTL4 protein, more than one server was used since each server uses specific properties in the analysis of the cDNA and amino acid sequences.

Software name	Website/ URL link	Reference(s)
Sequences (nucleotide/amino acid)		
VectorBase	https://www.vectorbase.org/	Giraldo-Calderón *et al*., 2015.
GeneBank	https://www.ncbi.nlm.nih.gov/genbank/	Benson *et al*., 2013.
Sequence alignment		
ClustalO	https://www.ebi.ac.uk/Tools/msa/clustalo/	Sievers *et al*., 2011.
Domain organization		
Pfam	http://pfam.xfam.org/	El-Gebali *et al*., 2019.
PredictProtein	https://www.predictprotein.org/	Yachdav *et al*., 2014.
Prosite	https://prosite.expasy.org/	Sirgrist *et al*., 2013.
SMART	https://smart.embl.de/	Letunic *et al*., 2014; Letunic *et al*., 2017.
InterPro	https://www.ebi.ac.uk/interpro/protein/	Mitchell *et al*., 2019.
SignalP	http://www.cbs.dtu.dk/services/SignalP/	Armenteros *et al*., 2019.
Tertiary structure prediction/homology modelling		
RaptorX	http://raptorx.uchicago.edu/	Kallberg *et al*., 2012.
Quark	https://zhanglab.ccmb.med.umich.edu/QUARK/	Xu and *Zhang et al*., 2012; Xu and Zhang *et al*., 2013.
Phyre	http://www.sbg.bio.ic.ac.uk/phyre2/html/page.cgi?id=index	Kelly *et al*., 2015.
Protein quality assessment		
ProSA	https://prosa.services.came.sbg.ac.at/prosa.php	Sippl, 1993. Wiederstein and Sippl, 2007.
PROCHECK	http://servicesn.mbi.ucla.edu/PROCHECK/	Laskowski *et al*., 1993; 1996.

Table 2.2 Primers sequences designed as part of this study. The sequence, length of the oligo primers, melting temperature of each primer pair (Tm) and the expected amplicon size.

Primer		Sequence (5'-3')	Length (nt)	Tm (°C)	Expected amplicon size (bp)
Primers used to amplify *An. funestsus s.s.* CTL4 protein coding regions					
Exon 1	**E1F** **E1R**	CGTACGCACTTT CAGAGGGA TGGGCTAAATG TTGGTTCTGT	20 21	62.45 58.66	188
Exon 2	**E2F** **E2R**	AAGAACTGCGC TCGGTAAAT CACGCATGTTTG GTACGGTA	20 20	58.35 60.40	158
Exon 3	**E3F** **E3R**	ACACTGCAACT CGATCGGTA CGGCACTGATG TTGGATTCC	20 20	62.45 60.40	226
Primers used to detect An. funestus gDNA					
Intron1	**I1F** **I1R**	CGGCCATTTCT GGCTTACTA GCAACATACGA CGGGTGAAT	20 20	60.22 60.79	413
Primers used for confirmation of *P. falciparum* infection					
CSP	**CSPF** **CSPR**	CAAATGACCC AAACCGAAAT CACTACATGG GGACCATTCA	20 20	47.68 51.78	150

2.2.1 Isolation and amplification of *An. funestus s.s.* CTL4

2.2.1.1 DNA extraction

Prior to DNA extraction, live adult female (n=10) *An. funestus s.s.* from the FUMOZ colony were obtained from the insectary and killed by freezing at -20°C for no more than 10 minutes, samples were then desiccated on silica gel and placed at room temperature. Genomic DNA (gDNA) was extracted from leg/wing of each *An. funestus s.s.* sample using a DNA extraction prepGEM® Insect kit (ZyGEM, New Zealand: 95044-104) as instructed by the manufacturer. Briefly, a leg/wing from each sample was placed in a DNA extraction master mix comprising of 10x black buffer, 1µL prepGEM® that lyses sample leg/wing by removing nucleoproteins from DNA (ZyGEM, New Zealand: 95044-104) and an addition of deionized water to make up a total volume of 10µL per leg/wing.

Samples were then incubated in a thermal cycler (T100™, Bio-Rad, USA: 1861096) with the following cycling conditions: proteinase activation step for 15 minutes at 75°C followed by a proteinase deactivation step at 95°C for 5 minutes. The resultant gDNA samples were stored at -20°C until needed.

2.2.1.2 Amplification and sequencing

Singleplex polymerase chain reaction (PCR) was used for the amplification of the target CTL4 exons (Table 2.2). The principle of the singleplex PCR is that a single target sequence is amplified in a single reaction tube in contrast to multiple targets being amplified in one reaction tube. The PCR was optimized by evaluating the following: primer concentrations between 1- 3.5pmol, annealing temperature between 53-57°C, as well as the amount of template used (between 0.5-2µL). For the amplification of the CTL4 exons, the master mix comprised of a 20µL reaction of 10x PCR buffer (100mM Tris-HCl (pH 8.3)), 500mM KCl), 25mM $MgCl_2$, 2.5mM deoxyribonucleotide (each containing 2.5mM of each dATP, dTTP, dCTP and dGTP), 3.3pmol of each primer pair, 0.5 units *Taq* DNA polymerase enzyme (TaKaRa Taq™, China: R001AM) and 9.8µL of deionized water, gDNA was added to give a total volume of 22µL. Samples were placed in a thermal cycler (T100™, Bio-Rad, USA:1861096) with the following cycling conditions: an initial denaturation step at 94°C for 2 minutes, followed by 29 cycles of denaturation at 94°C for 30 seconds, annealing at 55°C for 30 seconds, extension at 72°C for 30 seconds and a final extension for 5 minutes at 72°C. In order to visualize the PCR products, samples were mixed in a 5:1 ratio with 6x TriTrack loading dye (10mM Tris-HCl (pH 7.6); 0.03% (w/v) bromophenol blue; 0.03% (w/v) xylene cyanol FF; 60% (w/v) glycerol; 60 mM ethylenediaminetetraacetic acid (EDTA)) (Thermo Scientific™, USA: R0611). The PCR products, 12.5µL, were electrophoresed with a 0.1µg/uL 100bp ready-to-use DNA ladder (containing 6x TriTrack loading dye; Thermo Scientific™, USA: SM0244) in a 2% (w/v) TAE SeaKem® LE agarose gel (Lozna, USA: 50004) that was stained with 10mg/mL ethidium bromide (Sigma, USA: 1239-45-8) and submerged in a 1x TAE buffer (40mM Tris, 20mM acetic acid and 1mM EDTA, pH 7.2) at 110V/400Amps 1 hour 20 minutes. The PCR products were sent to Macrogen (Amsterdam, Netherlands) for Sanger sequencing to confirm that the correct sequences were being amplified (Sanger *et al*., 1977).

2.2.1.3 Sequence analysis

Sequences from the PCR products were obtained from Macrogen and uploaded into a Molecular Evolutionary Genetics Analysis tool (MEGA X software package) for analysis of the electropherogram of the nucleotide sequences (Kumar *et al*., 2018). Some nucleotide

sequences had baseline signals on either the 5' or 3' -ends that could have resulted from signal saturation, G/C degradation, G/C compression and these were removed (ThermoFisher Scientific, 2016). The edited sequences (query sequences) were deposited into the VectorBase (https://www.vectorbase.org/) where the Basic Local Alignment Search Tool (BLASTn) for nucleotides was used to align the sequences against available *Anopheles* sequences in the database. This was to confirm that the sequenced PCR products were indeed from *An. funestus s.s.* CTL4 from the database, and the following parameters were considered: The resultant percentage identity between query sequence and sequences in the database must be greater than 98%, a maximum e-value of 10 (i.e. range between 10 and 10^{-80} and 95-100% coverage of sequence alignment (https://www.vectorbase.org/). Additionally, MEGA X package (Kumar *et al*., 2018b) was used for phylogenetic analysis of the *An. funestus s.s.* CTL4 and its orthologs (Appendix Section B, Table B1). Evolutionary history was estimated by the Neighbour-Joining (NJ) methods, the topology of the of the generated tree was assessed by default settings were test was based on 1000 replicates and evolutionary distance were computed using Poison correction (Kumar *et al*., 2018b).

2.3 Optimization of the feeding rate of the *An. funestus s.s.*

In order to obtain maximal number of emerging adults for the feeding optimization and infection/treatment studies, the FUMOZ colony was scaled up (Figure 2.1). Subsequently, optimal feeding conditions were determined to ensure sufficient engorgement *An. funestus s.s.* females were obtained. In addition to this, females need to survive for at least 10 day's post infection feeding to ensure that sufficient samples will be available for infection/treatment studies (see objectives 3 and 5). Three parameters were evaluated:

1) Does starvation (no sugar water) increase feeding rate?

2) Does an increase in starvation period influence feeding rate?

3) What is the impact of adult female age on feeding rate and survival post feeding?

2.3.1 Artificial membrane system

The system comprised of a water bath chamber which was attached to two tubes connected to six glass feeders in series (Figure 2.2) and maintained at 37°C constant temperature (Kasap *et al*., 2003). Calf collagen casing was thoroughly rinsed to remove the salt that is used for its storage, rinsed and cut into 7x7cm square segments that were stretched at the bottom of each glass feeder and secured using a rubber band.

Defibrinated cow blood (whole blood) obtained in 15mL falcon tubes from Vector Control Reference Laboratories (VCRL, Johannesburg, South Africa, Mr O. Wood) were kept at -20°C for not more than 3 months for feeding adult female *An. funestus s.s.* mosquitoes. Prior to each assay, the blood meal was allowed to thaw at room temperature, after which 1mL of the blood meal was added into each glass feeder and warmed to 37°C for not more than 5 minutes before feeding the mosquitoes.

Figure 2.1: *Anopheles funestus s.s.* colony in the Maureen Coetzee Insectary, WRIM, University of the Witwatersrand, Johannesburg, South Africa. The emerging adults of the *An. funestus s.s.* colony were transferred from larval/pupal bowls to 5L and BugDorm-1 holding cages. **(A)** Larval bowls, 21.5cm length by 4cm breadth were used to house early second instar larvae **(B)** larval bowls 40cm length by 28cm breath enclosed with nylon mesh were used to house third-fourth instar larvae and pupae, **(C)** cages 5L and 29.98cm length x 29.98cm width BugDorm-1 were used to house adult mosquitoes after they emerge from the pupal stage and are provided with 10% (w/v) sugar water at all times.

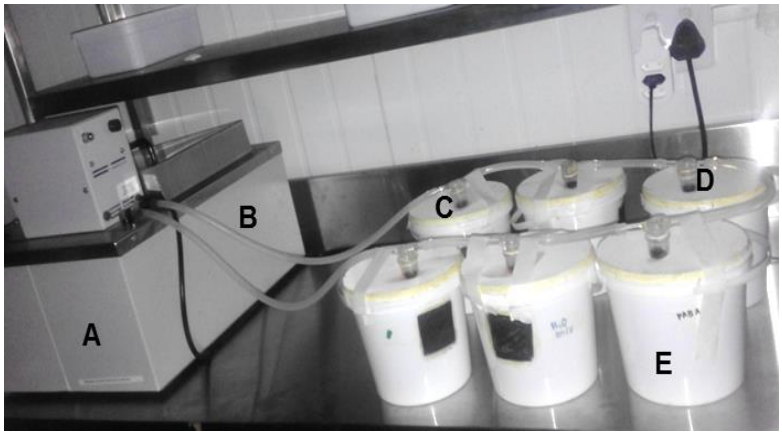

Figure 2.2: Overview of a multiple artificial glass feeding membrane system. (A) water bath with dH_2O was kept at 37°C, **(B)** the water inlet and outlet tubes connected the circulating system and allowed for the flow of water to keep the blood meal warm, **(C)** nylon mesh covered the cages enabled the female *An. funestus s.s.* to use their serrated proboscis to pierce through the mesh and the membrane. Temperature of the blood meal was regulated at 37°C inside the glass feeder and collagen sausage casing, **(D**, **E)** blood meal and adult female *An. funestus s.s.* in 2.5L cages.

2.3.2 Starvation of mosquitoes (no sugar water) increases the feeding rate

In order to increase the success feeding rate, it was necessary to optimize the diet required by the laboratory adult female *An. funestus s.s.* prior to their first blood meal. As such, a 48 hours starvation period was used by members of the unit for infection studies of members of the *An. gambiae* complex and these conditions were evaluated on *An. funestus s.s.* A total of 300 (males and females adults) were fed with a 10% (w/v) sugar water solution for eight days in a 5L holding cage to allow them to mate (Figure 2.3A). Mating is known increase blood feeding in females (Dahalan *et al*., 2019). Forty-eight hours prior to blood feeding, ±50 laboratory adult females were removed from the holding cage and separated into three different sandpapered 2.5L treatment cages (Figure 2.3B). The first group received 10% (w/v) sugar water solution the second group's the energy source (sugar water) was withdrawn i.e. received plain dH_2O and the third group did not receive anything, it was fully starved (Figure 2.3B).

Prior to the blood meal, 20 10-days old adult female *An. funestus s.s* mosquitoes were randomly selected from each diet treatment and were introduced into 250mL sandpapered polystyrene cups with a top diameter of 77mm and a height of 92mm (Figure 2.3C). This assay was repeated three times having three biological replicates and for each of the replicates, there were two technical replicates which totals to six technical replicates for each diet treatment (Figure 2.3C).

The polystyrene cups were covered with a nylon mesh net on the opening of the cup and secured with a rubber band (Appendix A.6, Figure A1). Subsequently, *An. funestus s.s.* adult females were left to acclimate for not more than 60 minutes. In each case, female mosquitoes were allowed to feed for 30-45 minutes. For recording experimental outcomes only fully engorged (midgut/blood bolus of a mosquito is completely filled with ingested blood meal) mosquitoes were used, partially engorged (midgut/blood bolus of a mosquito partly contains ingested blood meal) and non-engorged (did not feed) mosquitoes were killed by freezing at -20°C and then
discarded. The blood feeding success rate was calculated using Equation 2.1.

$$\text{Percentage blood feeding success rate} = \frac{\text{Number of fully fed mosquitoes}}{\text{Total number of mosquitoes tested}} \text{X100}$$

Equation 2.1 The blood feeding success rate calculation.

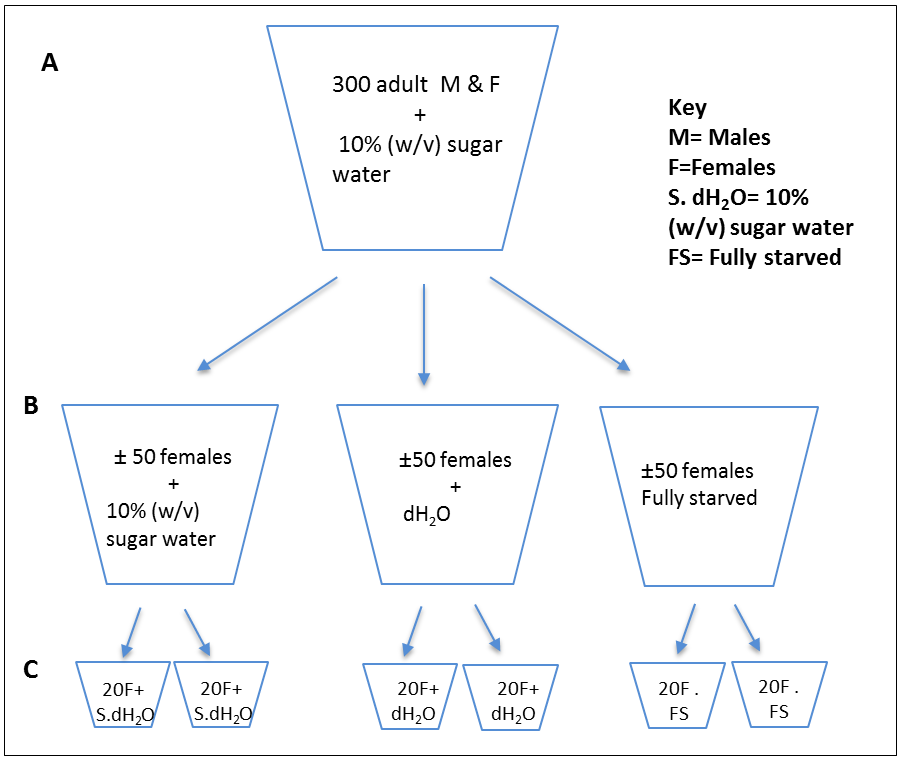

Figure 2.3: Experimental set up to assess starvation in feeding rate of various diets provided 48 hours prior to blood feeding adult female *An. funestus s.s.* **(A)** Adult *An. funestus s.s.* males (M) and females (F) were collected and housed in 5L holding cage and provided with 10% (w/v) sugar (S). Distilled water (dH_2O) for eight days. **(B)** Adult females (± 50) were transferred to 2.5L cages and where treated as follows: one group was provided with 10% (w/v) sugar water (S. dH_2O), second group dH_2O and the third group were fully starved (FS). (C) The experiment was repeated three times (three biological replicates with two technical replicates for each biological replicate).

2.3.3 An increase in the starvation period influences the feeding rate

Based on the outcome from (Section 2.3.2), the starvation period was determined to identify the optimal starvation period that will result in increased feeding rate for *An. funestus s.s.* adult females, without resulting in increased mortality. Approximately 230 adult female mosquitoes were collected from a 5L holding cage comprising of adult male and female mosquitoes that were kept at standard insectary conditions (Hunt *et al.*, 2005). Adult females were provided with 10% (w/v) sugar water solution and split into ±45 mosquitoes which were then introduced in 2.5L treatment cages where they received a cotton pad soaked in dH_2O for 24 hours, 48 hours, 72 hours and 96 hours (Figure 2.4), the remaining 45 were treated as controls (0 hours) that received 10% (w/v) sugar water solution. Blood feeding was peformed as per (Section 2.3.2)

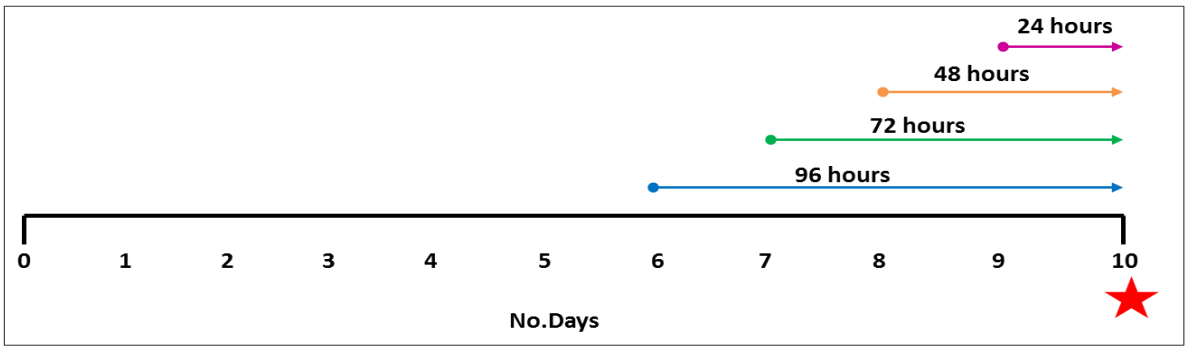

Figure 2.4: Schematic diagram illustrating the conditions used to investigate the starvation period. Adult female *An. funestus s.s.* were starved at different time points 24, 48, 72 and 96 hours shown in purple, orange, green and blue respectively such that on of blood meal they are 10 days old. Controls were kept on 10% (w/v) sugar water solution until blood feeding day which is indicated by a red star.

2.3.4 Adult female age has an influence on feeding rate and survival of mosquitoes post feeding

Anopheles funestus s.s. has a longer generation time in comparison to mosquitoes from the *An. gambiae* complex (Lo, 2014). During colony maintenance at the Maureen Coetzee Insectary, adults from *An. gambiae* complex are blood fed between 4-5 days post emergence. This is however different for *An. funestus s.s.*, which receive their blood meal 5-7 days post emergence, this results in feeding, however, only a few adults feed (unpublished observation, Prof. L. Koekemoer). This optimization step was performed for two main reasons: 1) to determine the optimal age that will result in an increased blood feeding rate i.e. is there any relationship between age of *An. funestus s.s.* and blood feeding success, 2) whether *An. funestus s.s.* blood fed at different ages will have different survival periods i.e. is there any relationship between age at which *An. funestus s.s.* blood feed and longevity. The latter was performed to find out if the laboratory *An. funestus s.s.* fed at different ages can survive throughout the life cycle of the *P. falciparum* as outlined (Smith *et al.*, 2014). To initiate these experiments, 80 adult female *An. funestus s.s.* from each cohort 5-, 10- or 15- days old were prepared as described for Section 2.3.2 and 2.3.3 based on the outcome: 10% (w/v) sugar water solution provision after emergence followed by an exclusive dH_2O starvation diet 72 hours prior to blood feeding. Mosquitoes were collected such that they would be 5, 10 and 15 days old on the day the feeding assay was to be conducted (Figure 2.5B).

Blood feeding was peformed as per Section 2.3.2, subsequently a 10% (w/v) sugar water solution was given to the mosquitoes and refreshed after every two days. Mortality was monitored daily up to 18 days post the blood meal.

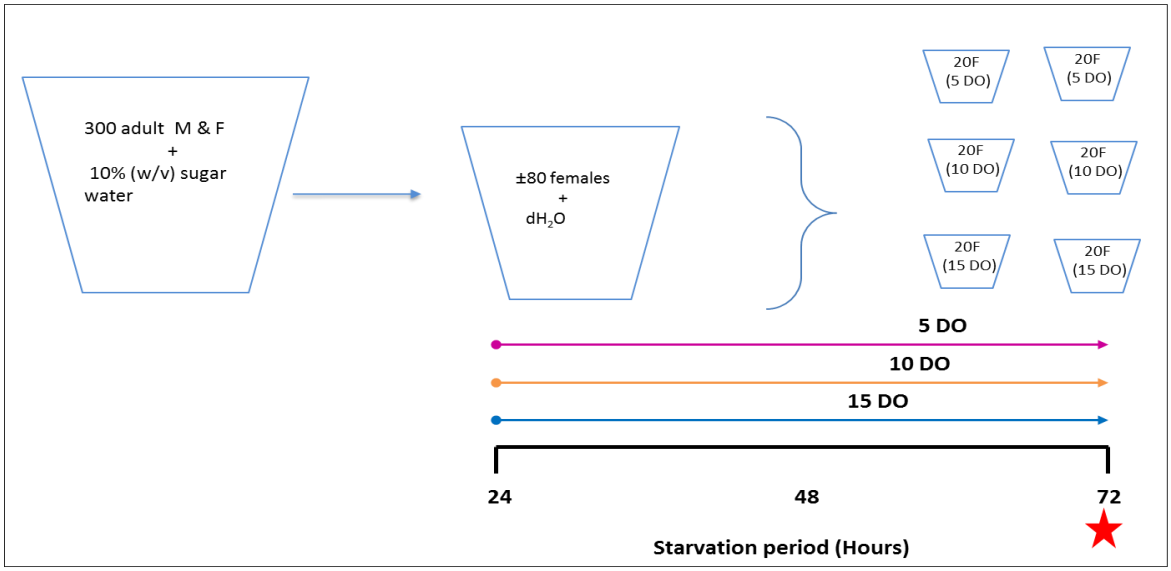

Figure 2.5: Illustration of the strategy used for investigating the impact of age on *An. funestus s.s.* blood feeding. Adult females at ages 5, 10 and 15 days old were starved for 72 hours prior to blood meal. Controls were kept on 10% (w/v) sugar water solution until blood feeding day which is indicated by a red star.

2.4 *Anopheles funestus s.s.* immune challenged with *P. falciparum*

2.4.1 Biological material:

Mosquito strain: Laboratory female adult *An. funestus s.s.* (FUMOZ colony) was prepared as summerized in (Section 2.3). **Malaria parasite:** *Plasmodium falciparum* (NF54 strain) infected human blood with gametocyte percentage between 4-6% was provided by the Prof L-M Birkholtz, University of Pretoria (Reader *et al*., 2015; 2021).

2.4.2 *Anopheles* infection with *P. falciparum*

A total of 320 adult female *An. funestus s.s.* prepared as described in Section 2.3. Briefly, adult females were provided with dH_2O for 72 hours and were immune challenged with a blood meal infected with *P. falciparum* at 10 days old. A total of 160 mosquitoes were introduced into two separate 2.5L sandpapered cages where one cohort (n = 160) received a blood meal infected with *P. falciparum* and the other cohort, control (n = 160) received a blood meal without *P. falciparum*. Briefly, adult female *An. funestus s.s.* mosquitoes (n = 160) received 1mL of infected and uninfected blood meal for 45 minutes using an artificial glass

feeding membrane system (Figure 2.2; Appendix Section A.2, Figure A2, showing *An. funestus s.s.* blood feeding) (Reader *et al*., 2021).

Females that did not feed or partially engorged with a blood meal were removed using a manual aspirator and killed by freezing at -20°C and dicarded. Only those that were fully engorged with a blood meal were maintained on 10% (w/v) sugar water solution.

2.4.3 RNA stabilization

Twenty four hours post feeding with *P. falciparum* infected blood meal or CQ-treatment, 15 mosquitoes (±1,000ng/µL RNA) from each biological replicate were removed from 2.5L cages and preserved using two different RNA stabilizing solutions: RNAlater (RNA Stabilizing Reagent, Qiagen, Germany: 76106) or TRIzol Reagent™ (Chomczynski, 1993; Invitrogen, USA: 15596018) depending on availibilty at the time. Samples could then be used later for downstream transcript analysis (Section 2.5; 2.7). Briefly, mosquitoes from each biological replicate were first immobilized by freezing at -80°C for not more than 3 minutes, which does not kill the mosquito nor destroy the RNA, samples were prepared for RNA isolation as follows:

1) RNA was stabilized using TRIzol Reagent™ (Invitrogen, USA: 15596018): This is a monophasic solution employed to isolate RNA, but can also maintain the integrity of RNA during tissue homogenization. Briefly, 15 infected vs. uninfected (designated as *P. falciparum* A and control A) and treated vs. untreated (designated as CQA-C and control A-C) mosquitoes were introduced to a sterile microcentrifuge tube containing 0.5mL TRIzol Reagent™ (Invitrogen, USA: 15596018) was added. Mosquitoes where manually homogenized using a sterile plastic RNaseZap™ (Sigma Life Science, USA: SLBQ7780V) treated pestle. The homogenates were placed at -20°C for later use.
2) RNA stabilization using RNAlater (Qiagen, Germany: 76106): Individual infected vs. uninfected mosquitoes from two biological replicates designated as samples *P. falciparum* B and C and control B and C where immersed in 100% ethanol for approximately half a second. Subsequently, mosquitoes were gently placed on filter paper for two seconds to remove excess ethanol. Ethanol decreases the hydrophobicity of the adults and ensures more permeability of the stabilizing solution. Five ethanol treated mosquitoes were transferred into a sterile microcentrifuge tube containing 0.5mL RNAlater (RNA Stabilizing Reagent, Qiagen, Germany: 76106), which is an aqueous non-toxic tissue storage reagent that stabilizes and protects cellular RNA in specimens

and enables the use of specimens later. The tubes were placed at -4°C overnight and transferred to -80°C until required.

2.5 Transcription analysis

2.5.1 Sample preparation

2.5.1.1 RNA extraction

Mosquitoes samples that were stored at -80°C in RNAlater (RNA Stabilizing Reagent, Qiagen, Germany: 76106) where thawed at room temperature, the RNAlater was discarded and the excess solution was removed using a paper towel, samples that were homogenized in TRIzol Reagent™ (Invitrogen, USA: 15596018) as per manufacturers instructions were removed from -20°C and allowed to thaw at room temperature. RNA was extracted as follows: samples that were in RNAlater (RNA Stabilizing Reagent, Qiagen, Germany: 76106) were transferred in a sterile tube, manually homogenized in 0.5mL of TRIzol Reagent™ (Invitrogen, USA: 15596018) and incubated at room temperature for five minutes, to allow for complete dissociation of nucleoprotein complexes. Following this, 0.2mL chloroform was added to the homogenates (Trizol and RNAlater stabilized samples) and incubated at room temperature for 2-3 minutes. Samples were centrifuged for 15 minutes at 12,000g at 4°C to separate out the aqueous mix into 3 phases. The upper aqueous layer containing RNA was transferred into a new sterile microcentrifuge tube, whereas the interphase and red-pheno-indyl containing DNA and protein were stored at -20°C.

RNA was precipitated by the addition of 0.5mL isopropanol solution (ACE, France: 161054014) at room temperature to an aqueous phase and incubated at room temperature for 10 minutes, before being centrifuged at 4°C for 10 minutes at 12,000g. The supernatant was discarded and the RNA pellet was washed with 75% ethanol, briefly vortexed and centrifuged at 4°C for five minutes at 7,500*g*. The supernatant was discarded and the RNA pellet air-dried at room temperature for not more than 5 minutes. The RNA pellet was resuspended in 50µL RNase-free water (Qiagen, Germany: 157013852) and incubated in a heating block at 57°C for 15 minutes, to allow for complete dissociation of the pellet. Thereafter, the pellet was immediately placed on ice and stored at -80°C for downstream analysis (Section 2.5 and 2.7).

2.5.1.2 Quality and quantity assessment of RNA samples

The concentration of the RNA was determined using NanoDrop™ OneC spectrophotometer (Thermo Scientific™, USA: 840274200) by measuring the A280/A260 ratio, a ratio between

1.8 and 2.0 is generally accepted for pure RNA whereas the range outside 1.8-2.0 is a result of contaminants including phenols and protein. (Thermo Scientific™, USA: 302-479-7707). In saddition, a 1% (w/v) 0.5x TBE (54g Tris base, 27.5g boric acid, 0.5M EDTA) SeaKem® LE (Lozna, USA: 50004) denaturing agarose gel was used to assess the integrity of the extracted RNA (Ogino *et al*., 1990). Briefly, 0.5g of agarose was dissolved in 0.5x TBE buffer. The gel was stained with 0.1ng/µL ethidium bromide in order to allow visualization of the RNA. One µg of RNA sample was mixed in a 1:1 ratio with 2x RNA loading dye (95% formamide; 0.025% (w/v) SDS; 0.02% (w/v) bromophenol blue; 0.025% (w/v) xylene cyanol FF; 0.025% (w/v) ethidium bromide and 0.5µM EDTA; Thermo Scientific™, USA: R0641). The latter RNA-loading dye samples were incubated at 70°C in a thermal cycler for 10 minutes and then loaded in a 1% (w/v) agarose gel and electrophoresed at 70V for 45 minutes with a 1kb RNA ladder (Thermofisher, USA: R064127) to determine the size of the resolved RNA fragments. The gel was photographed under an ultraviolet illuminutesescence. RNA was regarded to be of good quality if it comprised the 28S+16S 5.8S and 5S ribosomal fragments (Winnebeck *et al*., 2010; Machaira *et al*., 2015).

2.5.1.3 cDNA synthesis

Prior to cDNA synthesis, RNA was thawed on ice and the concentration of the RNA samples re-measured, since RNA degrades at room temperature and may degrade the concentration during the freeze-thaw process. A reverse transcriptase enzyme was used to convert RNA to complementary DNA (cDNA) using a High Capacity RNA-to-cDNA kit (Applied Biosynthesis, USA: 4387404) as instructed by the manufacturer. The reaction mix comprised of 2µg total RNA per 20µL reaction mix with 2x buffer mix, 20x enzyme mix and nuclease-free water, whereas the control reaction had no enzyme. The RT reactions were performed by incubation at 37°C for 60 minutes and terminated by heating at 95°C for 5 minutes. The concentration and purity of the synthesized cDNA was determined with a NanoDrop™ OneC spectrophotometer (Thermo Scientific™ USA: 840274200) and then immediately stored at -80°C until required.

2.5.1.4 Assessment of the quality of the cDNA

The quality of the synthesized cDNA was assessed by conventional singleplex PCR and agarose gel electrophoresis. During primer design of the CTL4 exons (Section 2.2.1.3, Table 2.2), primers for intron one were designed, primer pair CTL4I1-F and CTL4I1-R (Table 2.1), to assess if cDNA was intron (gDNA) free. The assessment of the cDNA was as follows: PCR of 2µg of the synthesized cDNA samples from mosquitoes that fed on a *P. falciparum* infected and uninfected blood meal and the CTL4 intron one was performed using the

extracted gDNA (Section 2.1.1.2) as a positive control. The PCR master mix for the amplification of the *An. funestus s.s.* CTL4 intron comprised of a 20µL reaction with 10x PCR buffer (100mM Tris-HCl, pH 8.3), 25mM $MgCl_2$, 2.5mM dNTPs (each containing 2.5mM of each dATP, dTTP, dCTP and dGTP), 10µM of each primer pair, 0.5 units of Taq DNA polymerase enzyme (TaKaRa Taq™, China: R001AM) and 9.8µL dH_2O. Samples were placed in a thermal cycler and the cycling conditions comprised of an initial denaturation step at 94°C for 2 minutes, followed by 29 cycles of denaturation at 94°C for 30 seconds, annealing at 48°C for 30 seconds, extension at 72°C for 30 seconds and a final auto-extension for 5 minutes at 72°C. In order to visualize the expected 403bp amplicon, PCR products were mixed in a 5:1 ratio with 6xTriTrack loading dye (Thermo Scientific™, USA: R0611). The PCR products were then electrophoresed with a 0.1µg/µL 100bp ready-to-use DNA ladder (containing 6x TriTrack loading dye; Thermo Scientific™, USA: SM0244) in a 2.5% (w/v) 1x TAE SeaKem® LE agarose gel (Lozna, 50004, USA) that was stained with 10mg/mL ethidium bromide and submerged in a 1x TAE buffer at 100V/400 A for 90 minutes.

2.5.2 Confirmation of *P. falciparum* infection in *An. funestsus s.s.*

In order to confirm the presence of *P. falciparum* parasites 24 hours post feeding, the presence of the circumsporozite transcript (CSP) in *An. funestsus s.s.* midguts was amplified by PCR. *Plasmodium falciparum* CSP is required for the successful transmission of the sporozoites to the mammalian vector and was previously detected during sporozoite stages has recently been detected during ookinete stages (Oakley *et al.*, 2018). The PCR was conducted with the NF54 strain of *P. falciparum* as the positive control (Prof R. L. Van Zyl, University of the Witwatersrand) and the DNA was extracted using the DNeasy® Blood and Tissue kit (Qiagen, Germany: 69504) as per manufacturer instructions.

Briefly, 100µL *P. falciparum* containing blood was lysed in a mix containing 40mAU/mg of proteinase K and phosphate buffered saline (PBS; pH 7.3) in a total volume of 220µL. The PBS was prepared with 136.89 mM NaCl (Merck), 4.1 mM $Na_2HPO_4.2H_2O$ (Riedel-de Haën®), 4.02 mM KCl (Sigma-Aldrich®), and 1.47 mM KH_2PO_4 (Fluka) in Milli-Q® water, autoclaved and stored at room temperature.

A total of 200µL buffer AL was added to the mix and vortexed, briefly before being incubated at 56°C for 10 minutes 100% (w/v) of 200µL of ethanol was added thereafter. Purification of the DNA included binding and washing of the sample with 99% ethanol, buffer AW1 and AW2 and centrifugation steps between 6,000*g* and 20,000*g*. Finally 100µL DNA was eluted using buffer AE (10mM Tris.Cl, 0.5mM EDTA, pH 9.0).

Plasmodium falciparum circumsporozoite (PF3D7_0304600) nucleotide sequence was obtained from PlasmoDB (https://plasmodb.org/plasmo/). Primer3 (http://bioinfo.ut.ee/primer3-0.4.0/) was used to design the circumsporozoite specific primer pairs CSPF and CSPR (Table 2.2) at protein coding regions. Briefly, the PCR was performed with a 21µL reaction total volume and was comprised of 10x PCR buffer (100mM Tris-HCl, pH8.3); 25mM $MgCl_2$; 2.5mM dNTPs (each containing 2.5mM of each dATP, dTTP, dCTP and dGTP); 10µM of each primer pair; 0.5 units of Taq DNA polymerase enzyme (TaKaRa Taq™, China: R001AM); 150ng/µL i.e.1µL template cDNA and 9.8µL deionized water. Samples were placed in a thermal cycler with the following cycling conditions: cycling: an initial denaturation step at 94°C for 2 min, followed by 32 cycles of denaturation at 94°C for 30 seconds, annealing at 53°C for 30 seconds, extension at 72°C for 30 seconds and a final extension for 5 minutes at 72°C.

In order to visualize the 150bp amplicon, PCR products were mixed in a 5:1 ratio with 6x TriTrack loading dye (10mM Tris-HCl (pH 7.6); 0.03% (w/v) bromophenol blue, 0.03% (w/v) xylene cyanol FF, 60% (w/v) glycerol and 60mM EDTA) (Thermo Scientific™, USA: R0611). The PCR products were electrophoresed with a 0.1µg/uL of 100bp ready-to-use DNA ladder (containing 6x TriTrack loading dye; Thermo Scientific™, USA: SM0244) in a 2% (w/v) 1x TAE buffer SeaKem® LE agarose gel (Lozna, USA: 50004) that was stained with 10mg/L ethidium bromide and submerged in a 1x TAE buffer at 110V/400A for 90 minutes.

2.5.3 Quantitative real time qPCR

2.5.3.1 Reference gene selection

In order to select the candidate genes to normalize data samples of *P. falciparum* immune challenged and control mosquitoes, four (n = 4) *An. funestus s.s.* reference genes (Table 2.3) were screened. These genes have been previously used as internal controls for transcript analysis (Christian *et al.*, 2011; Lo, 2014).

Prior to reference gene selection some of the cDNA from the three biological replicates was pooled, this was done to normalize variation within replicates and produce a standard curve, the pooled concentration was measured with an aid of a NanoDrop™ OneC spectrophotometer (Thermo Scientific™ USA: 840274200). The pooled cDNA was then serially diluted to give a final concentration of 1,000ng/µL which was further diluted 2-fold to a final concentration of 1.95ng/µL. The remaining cDNA products independently from the

three biological replicates were diluted to a working stock solution of 100ng/µL for transcript level analysis.

In order to ensure a sterile working environment, the workspace was wiped with 75% ethanol and 15% (w/v) bleach. A singleplex qPCR for reference gene selection was performed in a 25µL total volume comprising of 1.2mM 2x SYBR® (antibody-mediated-hot start, iTaq DNA polymerase, dNTPs and $MgCl_2$) (Bio-Rad, USA: 17-8880), 3µM of forward and reverse primers, 100ng/µL of template cDNA and a range (1.95ng/µL-1,000ng/µL) of different concentration in the case of the standard curve and an addition of 3.5µL nuclease free water (Ambion®, USA: AM9937). Amplification of each gene was performed using CFX96 qPCR Bio-Rad machine (CFX connect real time system, USA: 184-5096). All reactions were performed in triplicates (n = 3), where each biological replicate comprised of three technical replicates (n = 3). Samples in a 96 well plate were subjected to the following PCR condition: an initial denaturation step at 94°C for 2 minutes followed by 38 cycles of denaturation at 94°C for 30 seconds, annealing of primers at 55°C for 30 seconds, extension at 72°C for 30 seconds, final extension at 72°C for 10 minutes and a dissociation curve between 72-95°C at 0.5°C increments for 5 seconds.

In order to visualize and confirm the qPCR products, samples were mixed in a 5:1 ratio with 6x TriTrack loading dye (Thermo Scientific™, USA: R0611). The qPCR products were then electrophoresed with a 0.1µg/µL 100bp ready-to-use DNA ladder (containing 6x TriTrack loading dye; Thermo Scientific™, USA: SM0244) in a 2.5% (w/v) 1x TAE buffer SeaKem® LE agarose gel (Lozna, USA: 50004) that was stained with 10mg/mL ethidium bromide and submerged in a 1x TAE buffer at 110V/400 A for 90 minutes.

Table 2.3 Primers used during reference gene selection.

Gene Name	Accession ID	Sequence (5'---3')	Expected Amplicon size (bp)
ND_5**	AY727672.1	TAGAATTTTATTAGGGTGGGATGG GCATTATCAAATCGAATTGGAGAT	122
RPS7*	AFUN007153	TTACTGCTGTGTACGATGCC GATGGTGGTCTGCTGGTT	134
RPS26**	AFUN003198	GATAAGGCAATCAAGAAGTTCG TACACAGGCGACGCAACAC	160
RPL19**	AFUN005878	GAAACACCAACTCCCGACA TCAACAGGCGACGCAACAC	223

*RPS7 was used as an internal control by Christian, 2011. **ND_5, RPS26 and RPL19 were used by Lo, 2014. RPS7: 40S ribosomal protein S7, ND_5: NADH dehydrogenase subunit 5, RPS26: 40S ribosomal protein S26 and RPL19: 60S ribosomal protein L19.

NormFinder, a statistical software algorithm that identifies the optimal normalization gene between a set of candidate genes was used to identify the optimal reference genes based on the gene with the lowest stability value (numerical) in comparison to the other candidate genes (Andersen *et al*., 2004). This was achieved when raw Cq values of infected and uninfected target and candidate reference genes were used.

2.5.3.2 Transcript level analysis

The *An. funestus s.s*. CTL4 transcript analysis was performed in *P. falciparum* immune challenged mosquitoes. The CTL4 transcript level was normalized with the top three stable candidate reference genes, RPS7, RPS26 and RPL19 that were identified in Section 2.5.3.1 (Gimeno *et al*., 2014). Quantification of the *An. funestus s.s* CTL4 transcript was performed in a CFX96 qPCR Bio-Rad machine (CFX connect real time system, USA, 184-5096) where a standard curve for the target and reference genes was generated (Section 2.5.3.1). The reaction conditions were performed as in Section 2.5.3.1. The following critical factors were used to validate the efficiency of the qPCR: a linear standard curve of (R^2 > 0.980 or r-| -0.990|), consistency across all replicates and an efficiency value between 90 – 110% (Taylor *et al.*, 2010). The expression of the CTL4 transcript was determined using raw Cq values in several methods including: i) Livak method $2^{-\Delta\Delta Ct}$, ii) Error of propagation and iii) REST 2009 relative expression software tool (www.qiagen.com) to ensure the correct expression was reported.

2.5.3.3 Confirmation of qPCR products

Prior to transcript level analysis confirmation of the qPCR products for the expected amplicon size of 226, 160, 134 and 223bp long for CTL4, RPS26, RPS7 and RPL19, respectively was undertaken using agarose gel electrophoresis. Where the qPCR products were mixed in a 5:1 ratio with 6x TriTrack loading dye (Thermo Scientific™, USA: R0611) and electrophoresed with a 0.1µg/µL 100bp ready-to-use DNA ladder (containing 6X TriTrack loading dye; Thermo Scientific™, USA: SM0244) in a 2.5% 1x TAE buffer SeaKem® LE agarose gel (Lozna, 50004, USA) that was stained with 10mg/mL ethidiun bromide and submerged in a 1x TAE buffer at 110V/400 A for 90 minutes. Following gel electrophoresis, qPCR products were sent to Inqaba Biotech, Pretoria, South Africa for Sanger sequencing (Sanger *et al*., 1977).

2.6 Investigating toxicological effect of CQ on *An. funestus s.s.* larvae and adult females

Prior to the immune challenge of the adult female *An. funestus s.s.* mosquitoes with CQ, the toxicological properties of CQ were assessed against 3rd-4th instar larvae and adult female mosquitoes using the WHO recommended guidelines (WHO, 2005). Table 2.4 shows the properties of the compounds used in the toxicological assays.

Table 2.4 Properties of compounds used in the toxicological assays of *An. funestus s.s.* (Sigma-Aldrich® USA, 2020a; 2020b).

Compound	Emperical formulae	Molecular weight (g/mol)	Structural formulae**
Chloroquine	$C_{18}H_{26}ClN_3 \bullet 2H_3PO_4$	515.86	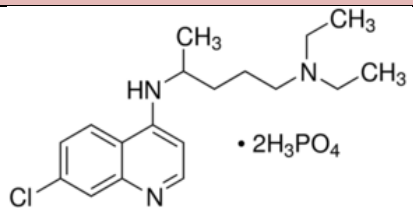
4,4' DDT	$C_{14}H_9C_{l5}$	354.49	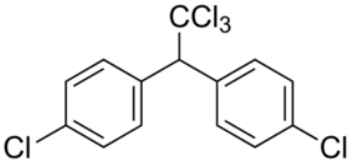

** Only CQ was used in adulticidal assays.

2.6.1 Preparation of compounds

Stock solutions, 500mM DDT (0.177g/mL) (Sigma, USA: 50-29-3) and CQ (0.257g/mL) (Sigma, USA: 50-63-5) (Table 2.4) were prepared in 1mL dimethyl sulfoxide (DMSO; ENSURE®ACS; Merck, USA: 67-68-5) for the larvacidal assays. The stock solutions were mixed thoroughly to give a homogenous mixture and were then stored at -80°C.

Prior to the larvicidal assays, serial dilutions including a 10x dilution factor ranging from 500µM to 5×10^{-8}µM were prepared in DMSO. In addition, 100mg/mL of CQ (5×10^{5}µM) was prepared by dissolving 0.140g of weighed CQ in 1.4mL PBS (pH 7.3) due to the isotonic and non-toxic properties of PBS (pH 7.3) to cells (Section 2.5.2). This was further dissolved in PBS (pH 7.3) to give the following concentrations: 5, 10, 25 and 50mg/mL for the adulticidal toxicity assessment.

2.6.2 Larvicidal assay

Larvicidal bioassays were conducted as described by WHO (2013) and Kweka *et al*. (2016) with slight modifications. Briefly, 24.75mL normal laboratory larval rearing water (dH_2O) was added to 250mL plastic cups. Batches of twenty 3^{rd}-4^{th} instar *An*. *funestus s.s*. larvae from the same generation were added to each cup and allowed to assimilate for not more than 15 minutes. Varying concentrations of DDT or CQ (Section 2.6.1) were added to the water in each cup and mixed to ensure even distribution of the compound.

The cups were then enclosed with a nylon mesh net and secured with a rubber band (Figure 2.6). A small dose of larval food (Section 2.1) was provided to the larvae once a day to prevent starvation. Each assay was repeated five times with two controls: one with a mix of dH_2O and 250µL 1% (w/v) DMSO (Merck, USA: 67-68-5) and the second containing only dH_2O to assess the effect of the solvent on the larvae. The assay was kept at 25-27°C for 72 hours and the mortality and morphological appearance of the larvae was recorded every 24 hours. Larvae that were unable to rise to the surface when the water was disturbed were considered dead, whilst morbid larvae, i.e. inability to show characteristic diving reaction, were also recorded as dead. If the mortality of the controls was between 5-20%, the assay was not discarded, it was corrected by using Abbotts formula in Equation 2.2. (Abbott, 1925).

$$\%\ Mortality\ =\ [(X-Y)\ /\ Y]\ \times\ 100$$

Equation 2.2 Abbotts formula, where X = percentage survival in untreated control and Y = percentage survival in treated sample (WHO, 2005).

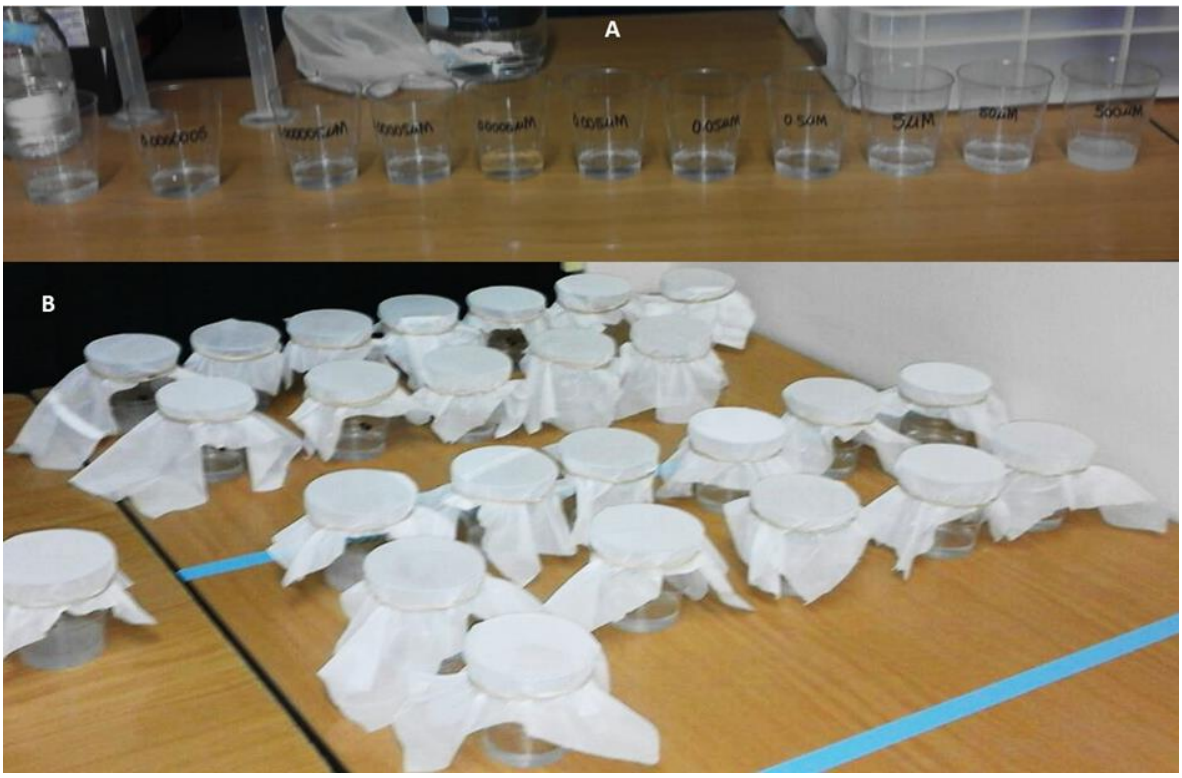

Figure 2.6: Larvicidal bioassay for testing toxicological effects of DDT and CQ. Experimental step up for larvicidal assay during incubation with compounds **(A)** 3rd-4th instar *An. funestsus s.s.* larvae exposed to different concentrations of DDT. **(B)** Larval cups enclosed with a nylon mesh and secured with rubber band in case larvae progresses to the adult stage.

2.6.3 Adulticidal assay

The CQ concentration used in the pilot adulticidal assay was determined based on the larvacidal assay (Section 2.6.2). To screen the CQ dosage of 0.025g/mL, it was added to the blood meal for the adult female *An. funestus s.s.* mosquitoes using an artificial Hemotek membrane feeding system (Discovery Workshops, Accrington, UK). This feeding system used an electric power unit/source that maintained a constant temperature at 37°C that regulated the temperature of the blood meal (Figure 2.7). Connected to the power unit were six feeders, calf collagen casing was prepared as described in Section 2.3 (Figure 2.7). The rinsed collagen casing was cut and stretched across the bottom of the Hemotek heated-blood reservoir with a surface area of 9.6cm^2 and secured with a hard rubber band. One millilitre of 100% human blood obtained from three different donors constituting three biological replicates was transferred into the Hemotek heated-blood reservoir (Gunathilaka *et al*., 2017). Adult female mosquitoes were prepared as described in Section 2.3. One hour before being evaluated, mosquitoes received the CQ-treated blood meal, 20 adult female *An. funestus s.s.* were introduced in 250mL sand papered polyester cups in order for them to assimilate.

This assay was conducted with two controls: one blood meal contained PBS (pH 7.3) and the other was an untreated blood meal. Adults that were not fully engorged with the blood meal were removed and knockdown i.e. mosquitoes that died or those that were alive, but unable to fly 10-15 minutes post ingestion of CQ-treated blood meal was recorded, the mortality was recorded 24 hours post blood feeding.

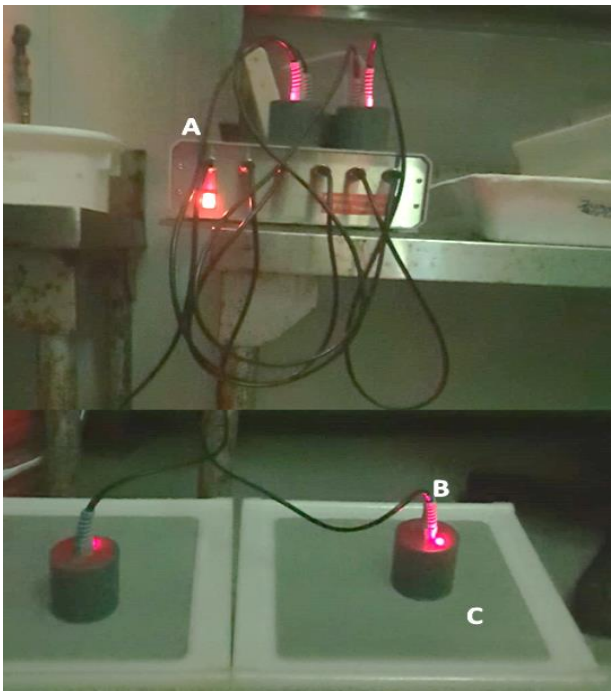

Figure 2.7: Overview of Hemotek artificial membrane feeding system. (A) Power unit source, **(B)** blood meal in a feeder, **(C)** cage with adult mosquitoes.

2.7 Evaluation of the effect of CQ on *An. funestus s.s.* CTL4

2.7.1 *Anopheles* treatment with CQ

A total of 320 adult female *An. funestus s.s.* prepared as optimized (Section 2.3) were immune challenged with a blood meal treated with a dose of 5mg/mL of CQ as determined by the pilot assay (Section 2.6.3). A total of 160 mosquitoes were introduced into two separate 2.5L sandpapered cages; where one cohort (n = 160) received a blood meal treated with CQ and the other control cohort (n = 160) received a blood meal with PBS (pH 7.3). Briefly, adult female *An. funestus s.s.* mosquitoes received 1mL of treated and untreated blood meal for 30-45 minutes using an artificial Hemotek membrane feeding system (Discovery Workshops, Accrington, UK). Females that did not feed or were partially engorged were discarded, only those that were fully engorged were maintained on 10% (w/v) sugar water.

Twenty-four hours post chloroquine treatment, RNA was stabilized using TRIzol Reagent™ (Invitrogen, USA: 15596018) as described in Section 2.4.3. RNA extraction, nucleic acid

quality assessment and CTL4 transcript abundance were performed as described in Sections 2.5.1 and 2.5.3). The control group included the CQ-untreated mosquitoes. In order to improve the efficiency of the reference genes in the qPCR, optimization included; 1) testing primer concentrations between 1µM-3.5µM; 2) test different volumes of 100ng/µL cDNA template between 0.5µL-2µL in the reaction mix; 3) using different annealing temperatures for primers between 45°C-60°C, and 4) change of reagents and consumables. These were reactions were repeated severally after which an introduction of the S7 and 18S primers were used.

2.8 Statistical analysis

Data analysis for the optimization of the feeding rate of *An. funestus s.s.* was performed using GraphPad Prism® version 5 (GraphPad Software, USA). One way analysis of variance (ANOVA), Dunnetts' multiple comparison test for difference in mean was used to analyze differences between treatments. Kaplan Meier survival curves analyzed the percentage survival across different age *An. funestus s.s.*; the Log-rank (Mantel-Cox) test was used to compare the difference in means between different treatments and, Spearmans Rank test was used to test for correlation. Reference gene selection and relative quantification were determined using NormFinder v20 and REST 2009 software, respectively; where the two-way Student T- test was used for relative quantification. The larvicidal dose required to cause 50% lethality (LD_{50}) was determined using IBM SPSS statistics 22 software package (IBM corp, USA), two way ANOVA was used to compare the difference in means of treatments and survival of the larvae during the incubation period from GraphPad Prism® version 5 (GraphPad Software, USA). Adulticidal assays were determined using Chi squared (Fisher's exact) test. A $p< 0.05$ was considered significantly different for all tests conducted in this study.

CHAPTER THREE

3. Results

3.1 Characterization of *An. funestus s.s.* CTL4

The CTL4 transcript has not yet been characterized structurally and functionally in *An. funestus s.s.* mosquitoes. In this regard, the approach involved the use of computational tools (Table 2.1) to:

1) Identify and obtain the *An. funestus s.s.* CTL4 nucleotide sequence and cDNA information,
2) Use bioinformatics analysis (Section 2.1.1.2) to further obtain full length of the *An. funestus s.s.* CTL4 amino acid sequences and determine the conserved residues involved in domain functioning and structural conformation,
3) Isolate and amplify the exons by PCR and
4) Confirm the presence of the CTL4 in colonized *An. funestus s.s.* FUMOZ mosquitoes.

3.1.1 *In silico* characterization of *An. funestus s.s.* CTL4

3.1.1.1 General features of cDNA and domain organization

The *An. funestus s.s.* CTL4 cDNA is 721bp long with a 534bp open reading frame (ORF), 177 amino acids, a 157bp 5' untranslated region (UTR) and a 30bp 3' UTR (Figure 3.1). The 721bp cDNA codes for three exons namely, E1 (97bp), E2 (80bp) and E3 (357bp). The resultant protein contains a signal peptide (SP) between 1-22 amino acids at the N-terminal, a single CTLD between 53-177 amino acids (Figure 3.1 and Figure 3.2). Additionally, the other regions that are present are highlighted by different colours (Figure 3.2B), namely, the cleavage site between amino acids 24-25 (shown by a broken red line) and the SP contains the following regions: nitrogen (N) region that constitutes a stretch between 1-5, hydrogen (H) region that constitutes a stretch between 6-17 residues a carbon (C) region that constitutes a stretch between 18-22 amino acids.

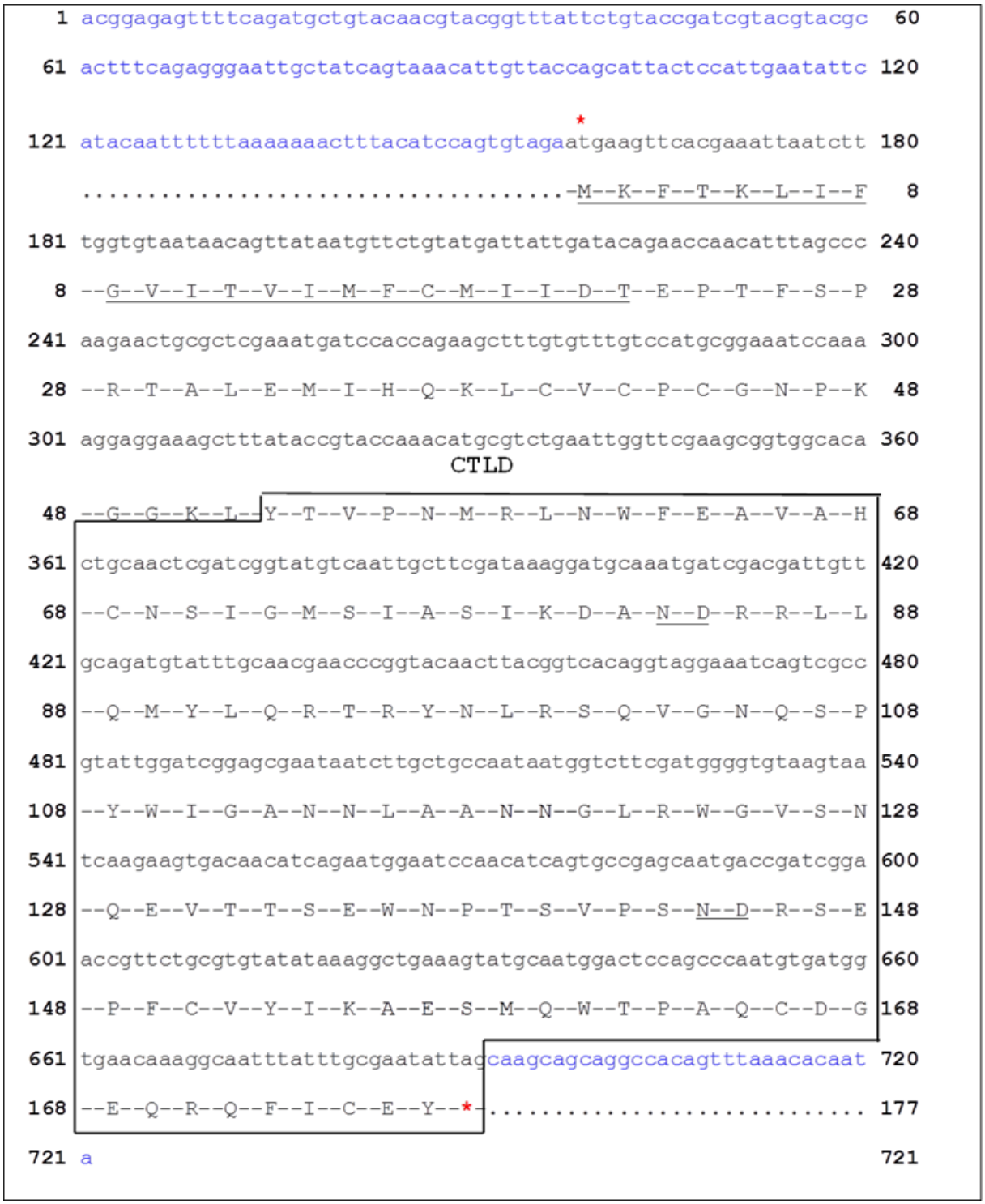

Figure 3.1: Sequence analysis of *An. funestus s.s.* CTL4 cDNA. Nucleotide sequence open reading frame and deduced amino acid sequence. The signal peptide is underlined, the start (ATG) and stop (TAG) codon are shown by asterisk red stars, the 5' and 3' untranslated reagions (UTR) in blue with 157bp and 30bp long. The putative C-type lectin domain (CTLD) (124aa) is indicated in a box. The ND motif that contains calcium binding sites is underlined.

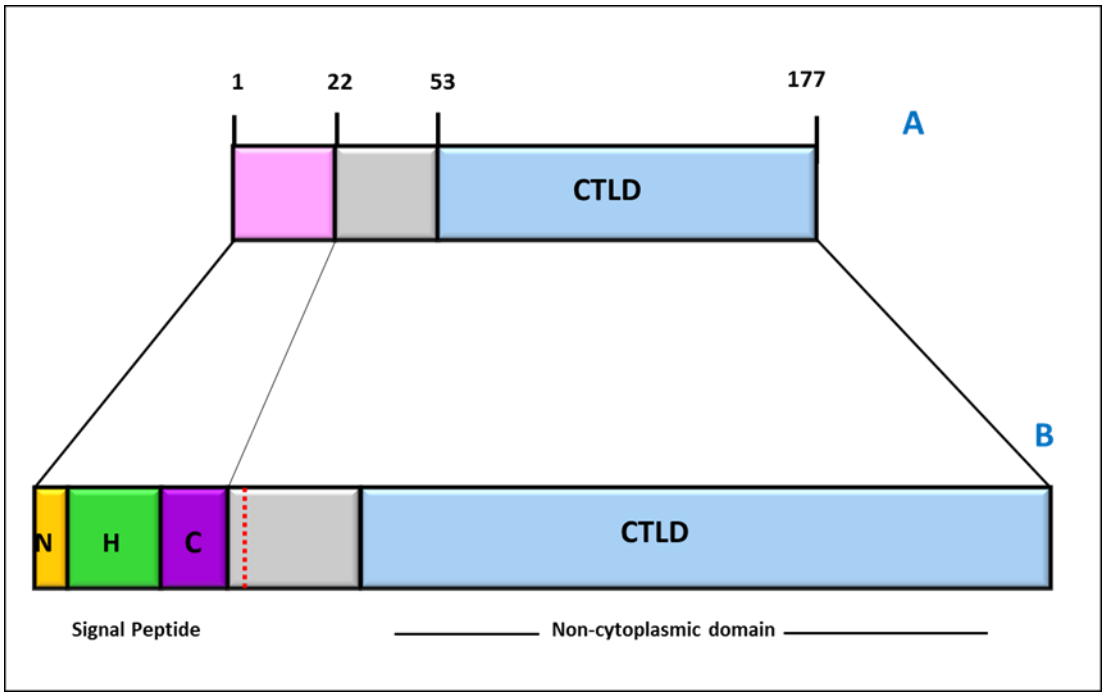

Figure 3.2: Domain organization of *An. funestus s.s.* CTL4 protein. (A) The numbers above the domain indicates the corresponding location of amino acid residues in the protein sequence. Signal peptide region coloured in lavender and C-type lectin domain is coloured in light blue and the grey region is undefined. **(B)** Other domain features: N region in yellow, H region in green and C region in purple. The protein cleavage site shown as a broken in red line and the CTLD is a non-cytoplasmic domain.

3.1.1.2 Molecular features and phylogeny relationship of CTL4

In order to identify essential amino acid residues that may be involved in the functioning of the *An. funestus s.s.* CTL4, a multiple sequence alignment between *An. funestus s.s.* CTL4 and other studied proteins with CTLD was conducted (Figure 3.3). In addition, multiple sequence alignment of *An. funestus s.s.* CTL4 orthologs of other mosquitoes are displayed (Figure 3.4A-B). Mammalian CTLDs were used since their crystalized protein structures are available and could be used to analyze key structural properties of CTLDs (Zelensky and Gready, 2003). *Anopheles funestus s.s.* CTL4 CTLD lacks the EPN (mannose binding motif) and QPD (galactose binding motif) motif, but may contain the WND motif with a substitution from tryptophan (W) to alanine (A) shown in a blue box as AND (Figure 3.3), there is one ND motif indicated by a double line in the *An. funestus s.s.*, this motif may be a stand alone since hydrophobic W was substituted with the polar uncharged serine (S) (Figure 3.3). The CTLD of *An. funestus s.s.* CTL4 is stabilized by disulphide bonds two pairs of cysteine residues between Cys-1 and Cys-4 (bond one) and Cys-2 and Cys-3 (bond two), these are highlighted

in purple and are positions: C^{32} and C^{138} for bond one and C^{114} and C^{129} for bond two (Figure 3.3) whereas C^{69} and C^{175} for bond one and C^{151} and C^{166} for bond two (Figure 3.4A-B).

In addition, *An. funestus s.s.* CTLD structural features includes: the small hydrophobic core contributed by α1 and β2, primary hydrophobic core (PHC) contributed by β5 isoleucine (I), long loop hydrophobic core (LLHR) contributed by β2, β3 and β4, negatively charged aspartic acid (D) substituting glutamic acid (E) at α2, hydrophobic residues at β1 and β5, highly conserved β1'(β1'V, β1'A or β1'L), a WIGL motif and lastly β2' and β2" forming a hairpin (Figure 3.3).

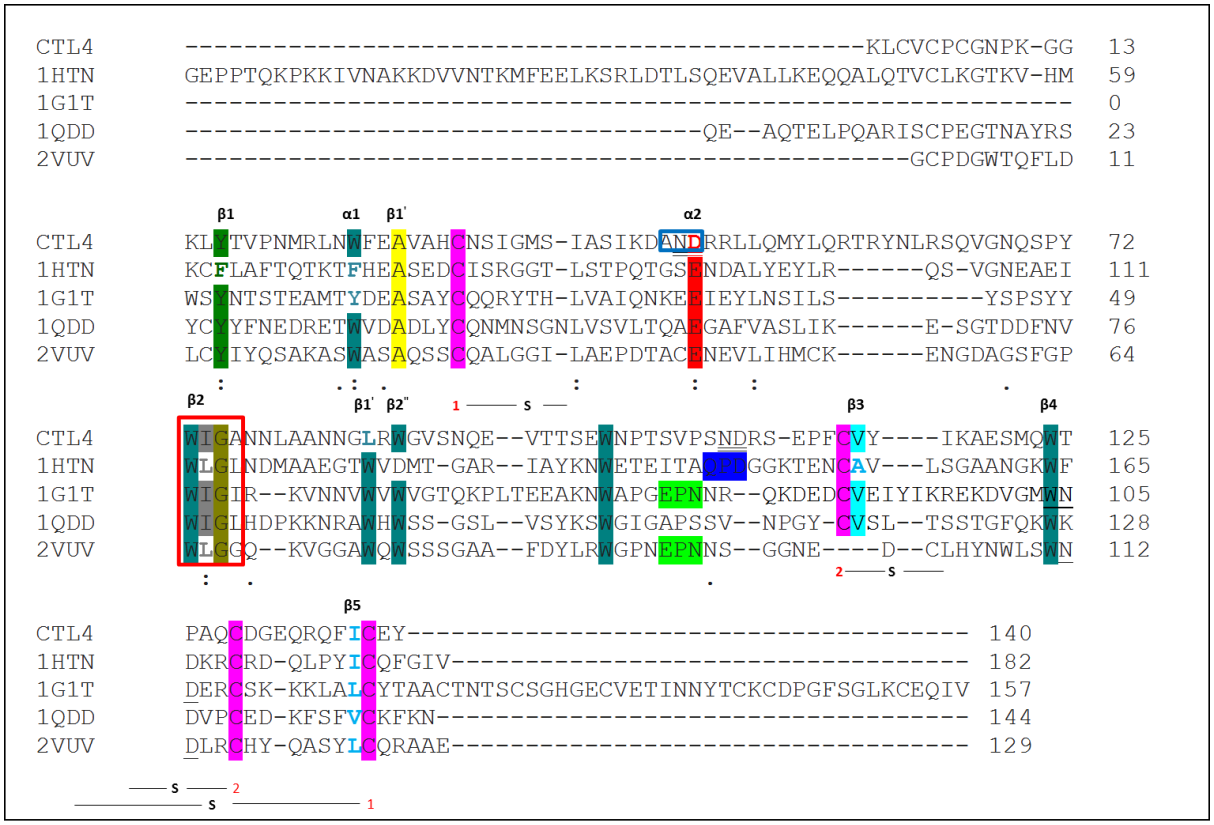

Figure 3.3: Multiple sequence alignment of *An. funestus s.s.* CTLD with four CTLDs from other species (*Homo sapiens* (1g1t, 2vuvand 1qdd) and *Codakia orbicularis* (1htn)). Conserved amino acid residues are highlighted by different colours with substitutes written in corresponding colours. Numbers to the right represent positions to residues, canonical motifs are double underlined, and disulphide bridges are shown at the bottom of the sequences at cysteine residues and the secondary structural features shown above sequences. Percentage identity matrix of reference sequences to *An. funestus s.s* CTLD is 21%, 17%, 18% and 23% for 1g1t, 2vuv, 1qdd and 1htn respectively.Other conserved residues involved in either calcium or carbohydrate binding are indicated by:/. symbols.

In addition, *An. funestus s.s.* CTL4 has a tri-cysteine $C^{41}XC^{43}XC^{45}$ at the N-terminus which may form a disulphide bridge heterodimer with *An. funestus s.s.* CTLMA4 (boxed in pink in Figure 3.4A) (Schnitiger *et al*., 2009). The aspartic acid (D^{81} in the *An. funestus s.s.* CTL4) is conserved across almost all orthologs, excluding *An. albimanus* and *An. darling*. The Trp-Ile-Gly-Leu WIGL motif in *An. funestus s.s.* CTL4 orthologs has a substitution from leucine to alanine resulting in a WIGA motif (boxed in red in Figure 3.4A), except for *Ae. aegypti* which has glycine as a substitute.

Interestingly, *Ae. aegypti* not only possess the EPN, but also the WND motifs in its CTLD (shown by a double line in Figure 3.4A-B). The absence of the EPN motif in other mosquito species may be due that these proteins are evolutionary distant from each other and between different mosquito species. The QPD motif is proposed to be possessed by *An. stephensi* and *An. maculatus* with a D amino acid substitution to E (QPE). In addition, predicted ligand binding amino acids of the *An. funestus s.s.* CTL4 (red colour in Figure 3.4B). Other highly conserved amino acids are also highlighted (Figure 3.4A-B).

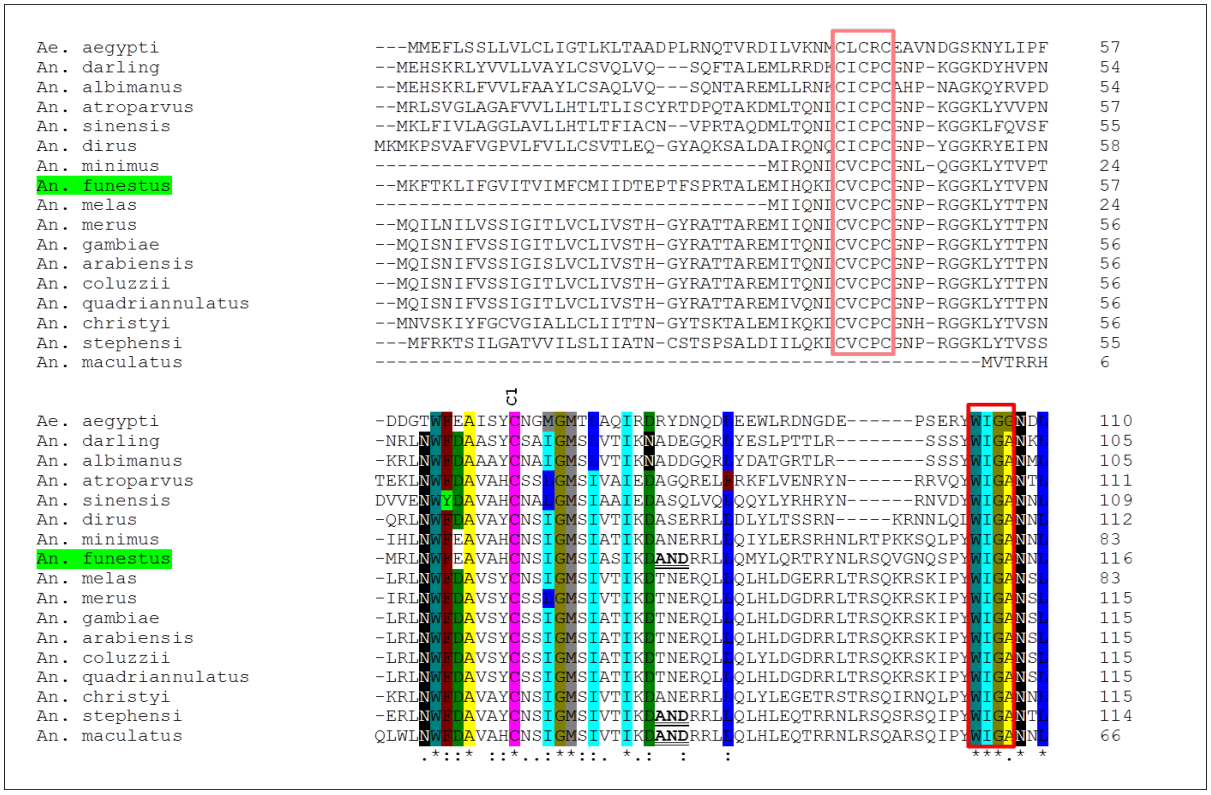

Figure 3.4A: Multiple sequence alignment of *An. funestus s.s.* CTL4 orthologs. The different amino acid sequences from different vector species are aligned, showing tri-cycteine residues (boxed in pink).The WIGA motif is boxed in red whereas the carbohydrate binding WND motif of *Ae. aegypti* is underlined and substituted by AND motif. Gene accession numbers of each mosquito vector and percentage similary to *An. funestus s.s* CTL4 are reported in Appendix Section B, Table B1.

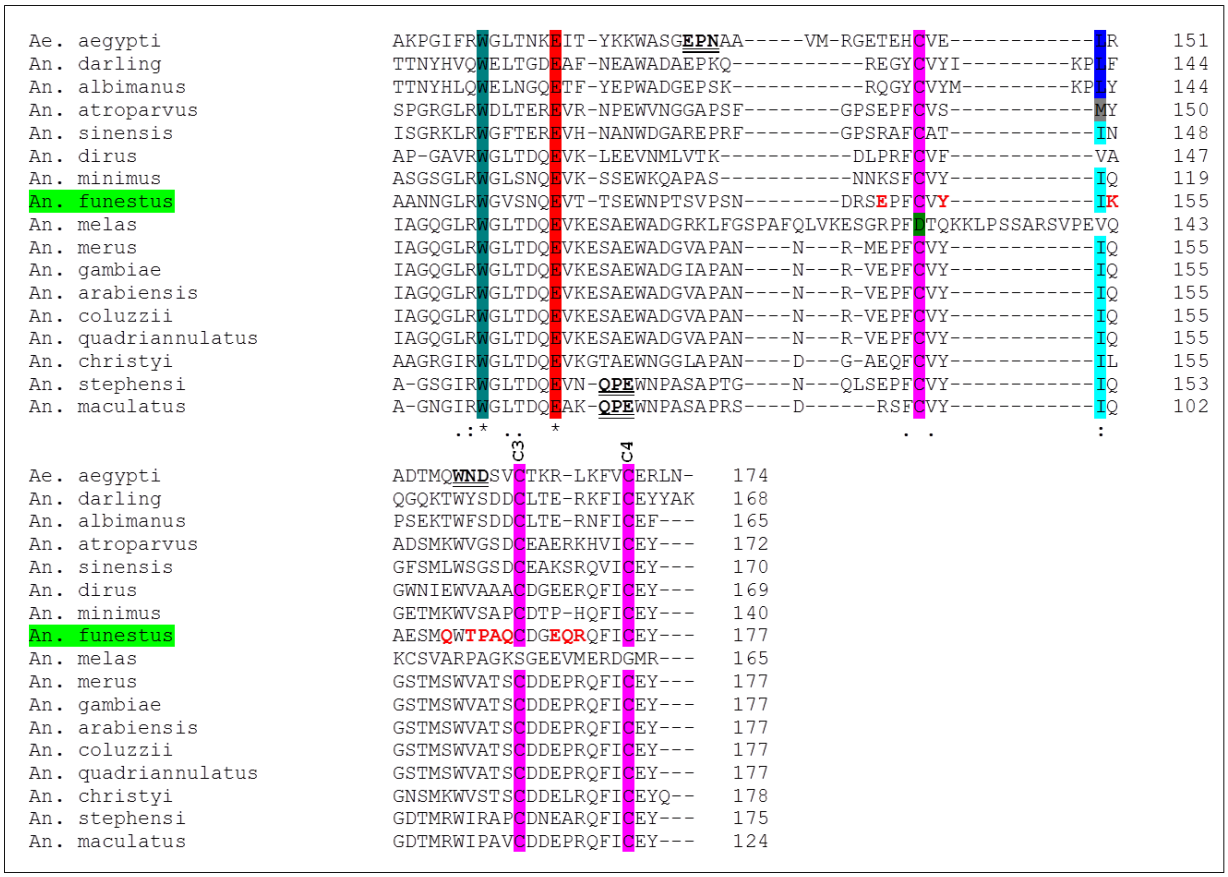

Figure 3.4B: Multiple sequence alignment of *An. funestus s.s.* CTL4 orthologs. The different amino acid sequences from different vector species are aligned, showing highly conserved cysteine residues responsible for the formation of disulphide bonding (purple). The galactose binding QPD motif is substituted by the QPE motif (underlined). Ligand binding residues are bold in red. Gene accession numbers of each mosquito vector are reported in Appendix Section B, Table B1.

To investigate the evolutionary relationship between *An. funestus s.s.* CTL4 and its orthologs, a neighbour joining tree was used (Figure 3.5). Results showed that *An. funestus s.s.* CTL4 is closely related to *An. minimus*, this was expected since the percentage similarity is the highest of all the orthologs with 68.57% sequence identity (https://www.vectorbase.org/). Members of the *An. gambiae* complex shown in blue are clustered together in Figure 3.5 (Scott *et al.*, 1993; Barron *et al.*, 2019). Although all proteins from different mosquito species emerge from the same ancestor, it is interesting that *An. funestus s.s.* and *An. christyi* whose sequence homology percentage is 61.24%, but the proteins are evolutionary distant (Figure 3.5).

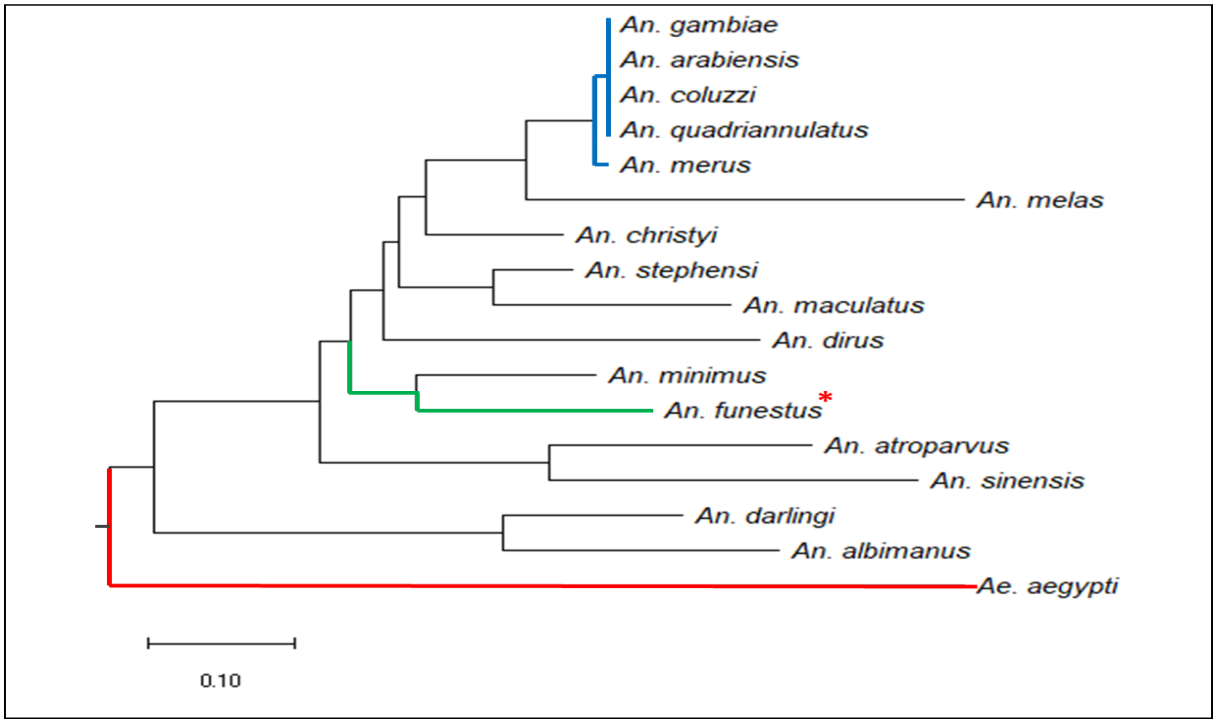

Figure 3.5: Phylogenetic analysis between *An. funestus s.s.* CTL4 orthologs. *Anopheles funestus s.s.* CTL4 shown by the green line is closely related to *An. minimus* they evolve from the same ancestor, *Ae. aegypti* shown by the red line is an outlier, and members of the *An. gambiae* complex shown by the blue lines and are closely related. Evolutionary history was inferred by NJ method, bootstrap test was based on 1000 replicates. Evolutionary distances were computed using the Poison correction method where all positions containing gaps were completely deleted. Gene accession numbers can be found in Appendix Section B, Table B1.

3.1.1.3 Conformational tertiary structure predictions

In order to extrapolate the conformational characteristics of the *An. funestus s.s.* CTL4, the overall three dimensional (3D) structure was analysed with the aid of bioinformatics tools (Table 2.1), to determine the protein fold of the conserved residues. A total of seven models demonstrating the tertiary structural folding of the CTL4 were resolved, five ranked from top to least model ($M1_Q$-$M5_Q$) were resolved from Quark, one from RaptorX ($M1_R$) and one from Phyre ($M1_P$). The lower ranked Quark models $M4_Q$ and $M5_Q$ were discarded. Template based server RaptorX used PDB 5e4k, 5xtS, 1htn, 1SI6 and 2VV templates to predict the 3D fold of *An. funestus s.s.* CTL4 summarized Table 3.1. The quality of the resolved model is assessed using the following measures: a *P*-value less than1x 10^{-3} and 1x 10^{-4} for mainly alpha and beta proteins respectively, score value which measure the alignment between template and query protein with an alignment score of 0 indicating very poor quality and the unnormalized global distance test score (uGDT/GDT) which measures the absolute quality of the model in which proteins with residues > 100 (*An. funestus s.s.* CTL4 has 177), a uGDT > 50 indicates a good quality (Table 3.1). Whereas template based server Phyre produced 120 PDB templates

but c5ao6A, c5e41B and c4yliA were amongst the top ranking with confidence of 100, 99.9 and 99.9 respectively and a percentage sequence of 22%, 25% and 24% respectively. Residues involved in the CTLD fold are shown in purple, yellow and green for models $M1_Q$-$M3_Q$, $M1_R$ and $M1_P$ respectively (Figure 3.6). Characteristically, *An. funestus s.s.* CTL4 CTLD has two α-helices and two pairs of antiparallel β-sheets (excluding the $M2_Q$ and $M3_Q$, which only have a pair of antiparallel β-sheets) (Zelensky and Gready, 2005). These resolved models compared to the preliminary experimentally determined *An. gambiae* CTL4 (Figure 3.6D) adopts similar conformational protein folds (Bishnoi *et al*., 2019).

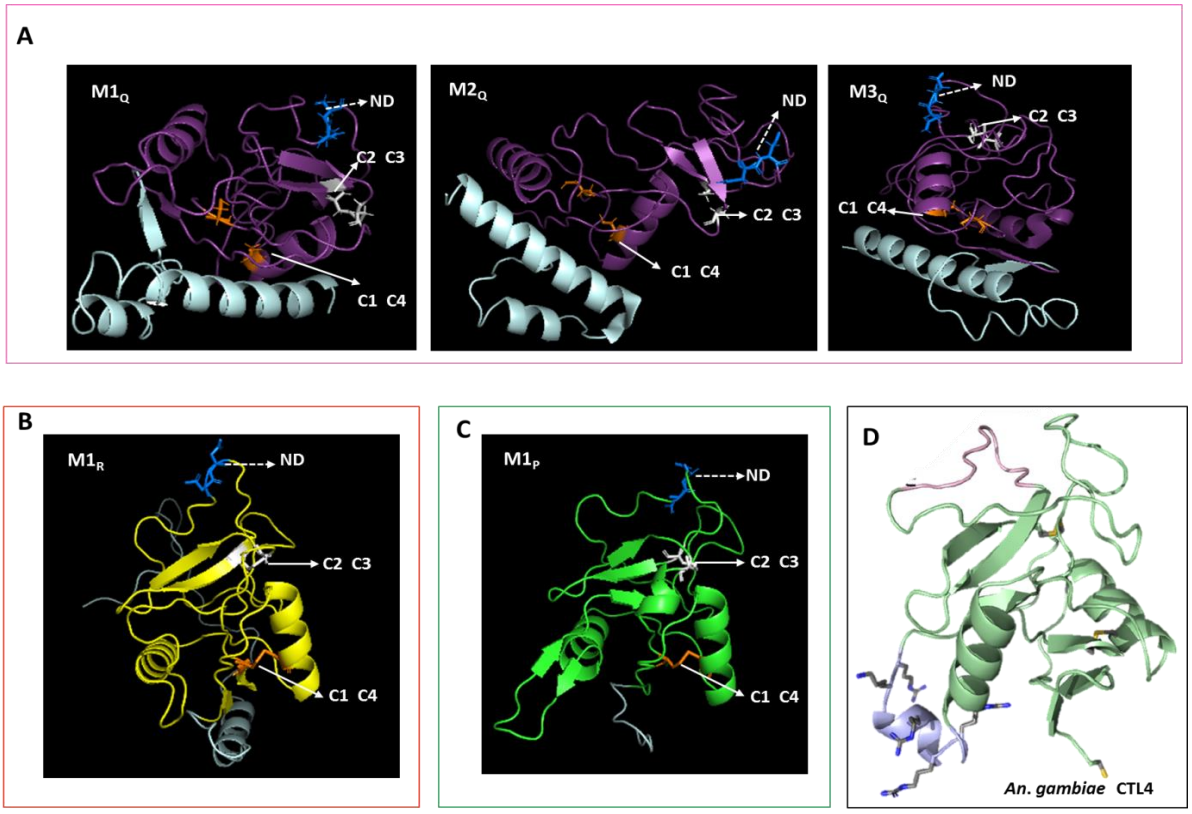

Figure 3.6: Tertiary structure of *An. funestus s.s.* CTL4. Models resolved by Quark, RaptorX and Phyre respectively **(A-C)**. Shown are tertiary representations of the CTL4 with CTLD, residues not involved in CTLD fold shown in cyan; The calcium binding ND-motif is shown as blue sticks and indicated by white broken arrow. The cysteine residues for the formation of the disulphide bonds are shown as grey and orange sticks and are also indicated by white solid arrows. Theoretical tertiary structures predicted through alignment with PDB structures, PDB ID: 5e4k, 5aO6, 1SI6, and 5xtS. Structures were viewed by Pymol. Disclaimer: Please note thatstructures $M1_R$ and $M1_P$ are theoretical predictions based on experimentally crystallized structures, laboratory experimentations is required for the final determination of the tertiary structure. **(D)** Tertiary structure of *An. gambiae* CTL4 (Bishnoi *et al*., 2019).

Table 3.1 RaptorX model quality score assessment.

Rank	p-value	Score	uGDT/GDT	uSeqID/SeqID	Model Name	Template (s)
1	$1.1x10^{-07}$	110	92/52	26/15	5e4kA-440640_1	5e4kA
2	$3.1x10^{-07}$	104	90/51	25/14	5xtsA-440640_1	5xtsA
3	$5.2x10^{-07}$	101	92/52	28/16	1htnA-440640_1	1htnA
4	$8.6x10^{-07}$	98	91/51	21/12	2vuvA-440640_1	2vuvA
5	$5.6x10^{-07}$	100	87/49	27/15	1s16A-440640_1	1s16A

3.1.1.4 Tertiary structure quality assessment

Since the tertiary structure of the *An. funestus s.s.* CTL4 has not yet been experimentally determined, quality assessment of the predicted tertiary structures was carried out in order to evaluate local and global energy and the stability of the resolved models (Figure 3.6). Analysis from ProSA web server indicates a deviation of the predicted models from experimentally determined crystalized or NMR native protein structures that have been submitted to the PDB and the local stability of the models resolved from Quark, RaptorX and Phyre, respectively (Figure 3.7A-C). A Z-score outside the a range that is characteristic for native proteins indicates erroneous structures, energy plot shows energy as a function of amino acid sequence generally, positive values corresponds to the problematic erroneous parts of a protein structure whereas negative corresponds to the stable parts of the protein structure. All models resolved from Quark fall within the NMR region i.e. and the Z-scores are -2.97, -4. 33 and-3.98 for models $M1_Q$, $M2_Q$ and $M3_Q$, respectively (Figure 3.7Ai-iii). The local energy of these models shows that $M1_Q$ and $M2_Q$ are the least stable models since most amino acid residues do not fall in the negative region. However, $M3_Q$ appears to be the most stable (of the top three Quark models) where most of its amino acid residues fall within the negative region (Figure 3.7 iv-vi). Model $M1_R$ falls within the NMR region with a Z-score of -4.05, the energy of the model shows stability in most of amino acid residues that are involved in the CTLD fold (Figure 3.1; 3.2) since they fall in the negative region (Figure 3.7B (i-ii)). Instability in model $M1_R$ occurs in amino acid residues found in the positive region of the graph and contribute to the disorder in the secondary structure between amino acid residues 1-31, 144-145 and 177 (Figure 3.8A). Model $M1_P$ falls within the NMR region with a Z-score of -4.09 and is a stable model since most of its amino acid residues fall in the negative region (Figure 3.9), instability in model $M1_P$ occurs in amino acid residues found in the positive region of the graph and contribute to the disorder in the secondary structure between amino acid residues at high confidence 73-74, 95-96, 98, 100-102, 104-105, 118, 137-140, 142-146 and 176 (Figure 3.9).

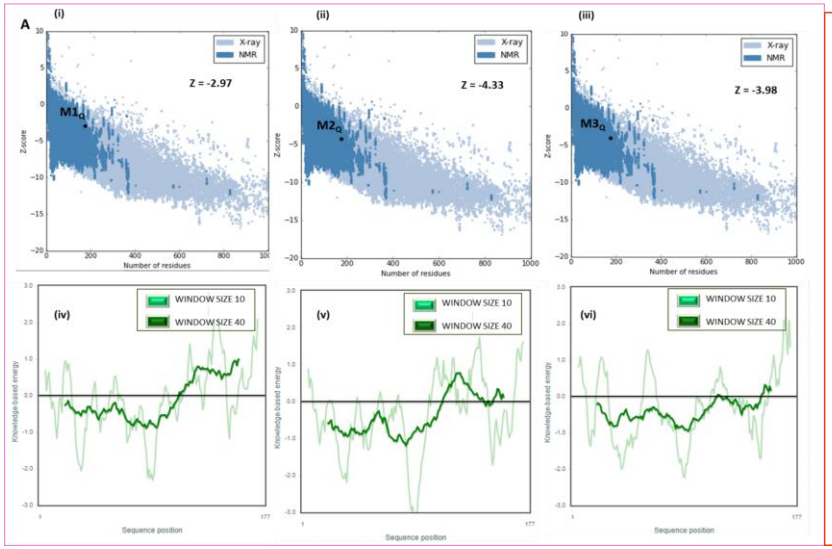

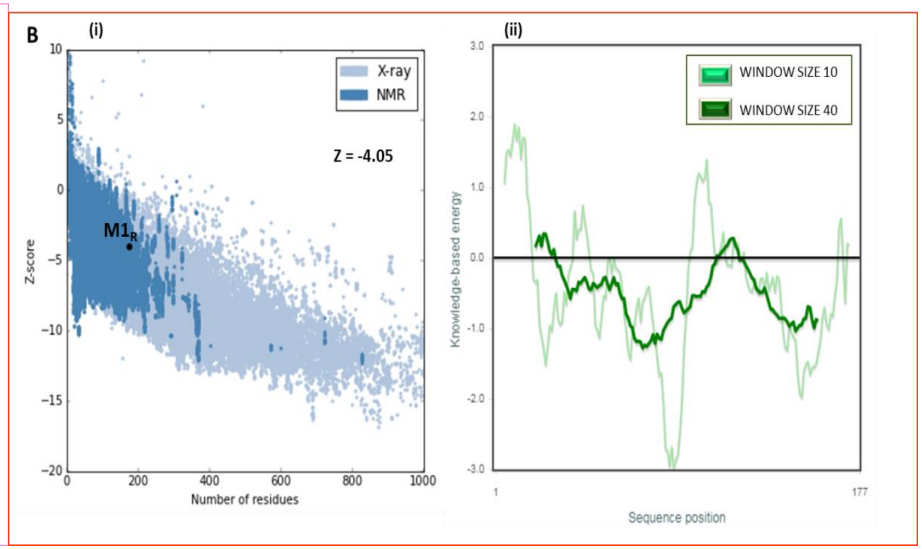

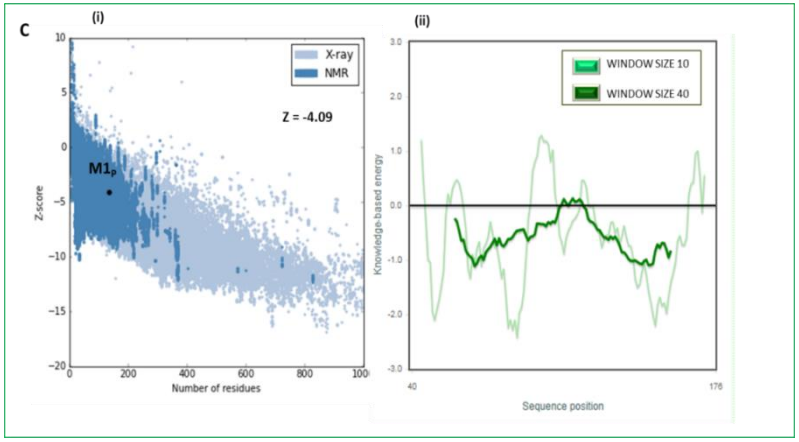

Figure 3.7 Structural quality assessment of the theoretical predicted tertiary structure of *An. funestus s.s.* CTL4. (A): (i-iii) shows the Z-score plot in comparison to PDB structures fall within NMR region. **(iv-vi)** local energy plot M1Q and M2Q as the least stable, most of the residues are found in the positive region whereas M3Q energy for residues has low overlap to the positive region. The size of the protein is indicated by the window size, a default of 40 is generally used. **(B): (i)** Shows the Z-score plot in comparison with PDB structures were M1R falls within the NMR region, **(ii)** local energy plot, M1R residues 1-38 and 141-147 have disorder and do not fall in the negative region. The size of the protein is indicated by the window size, a default of 40 is generally used. **(C): (i)** Shows the Z-score plot in comparison with PDB structures were M1P falls within the NMR region, **(ii)** local energy plot, most residues fall in the negative region. The size of the protein is indicated by the window size, a default of 40 is generally used.

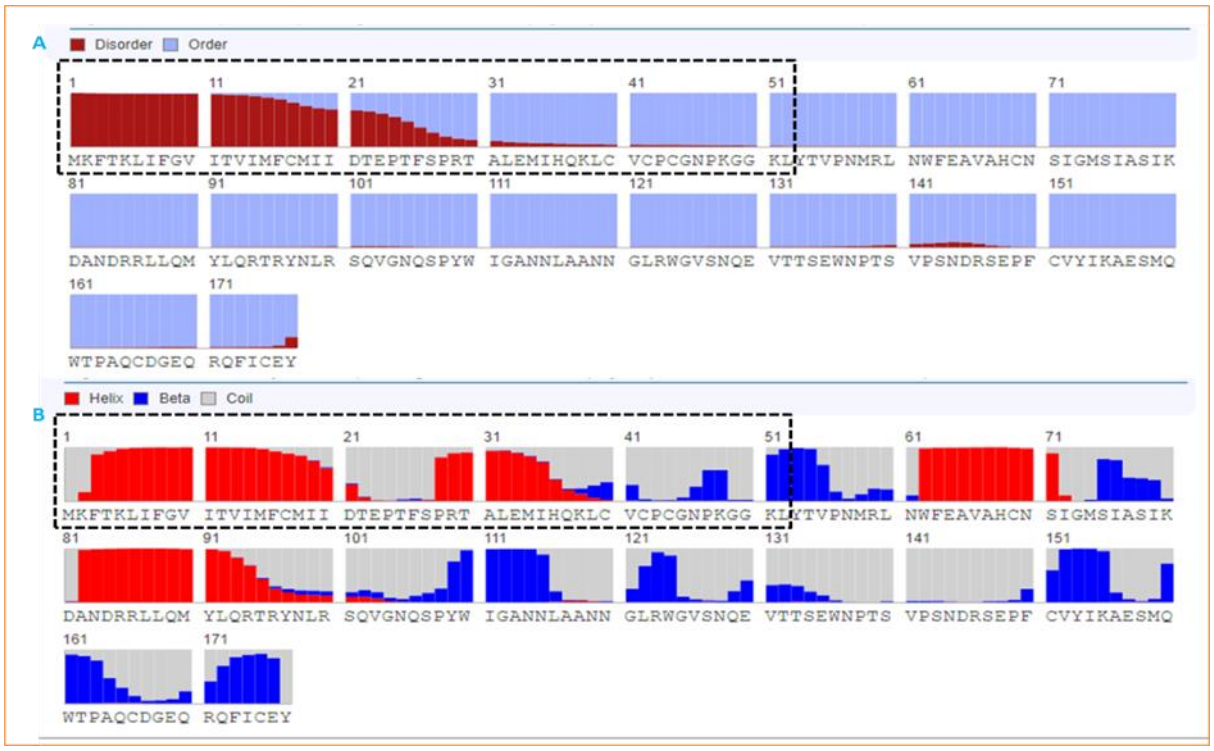

Figure 3.8: Summary of secondary structure properties of *An. funestus s.s.* CTL4 predicted by RaptorX. (A) Hovering on top of the amino acid residues is the predicted distribution of stability that affects the tertiary structure. Approximately 23% residues of the overall structure have disorder shown by maroon bars that affect the stability of the tertiary structure whereas only 7% of the CTLD are disordered. The amino acid residues that are ordered are shown by the light blue bars. **(B)** Secondary structure components involved in the folding of the tertiary structure, there are four helices shown by the red bars, five beta strands are shown by the dark blue bars and the coils are shown by the grey bars. The residues that are not part of the CTLD fold are boxed in black broken line.

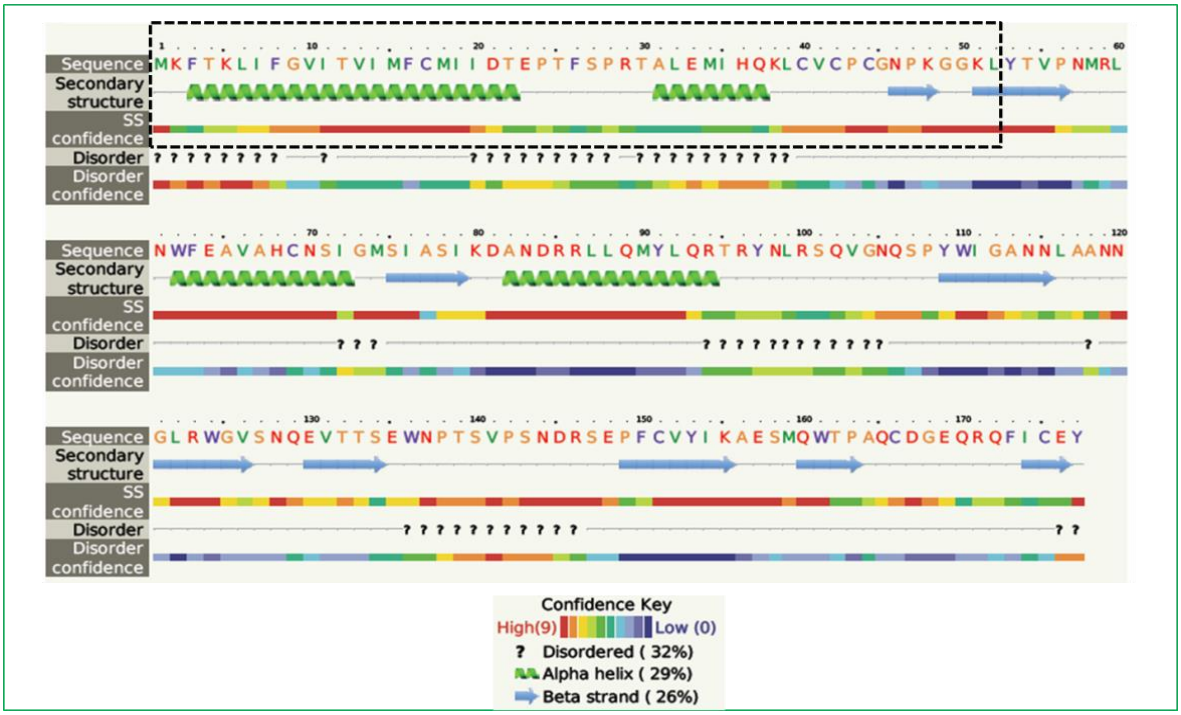

Figure 3.9: Summary of secondary structure properties of *An. funestus s.s.* CTL4 predicted by Phyre. The predicted secondary structure that affects the folding and stability of the tertiary structure, there is high confidence in the helices (total of four) shown in green and most beta strands (total of nine) shown in blue. The disordered residues of the overall structure are shown by a question mark symbol making up 32% whereas 28% residues of the CTLD are disordered. The residues that are not part of the CTLD are boxed in black broken line.

Additionally, the quality of the predicted models was evaluated by the use of the Ramachandran's plot. This was to determine the steriochemical quality of the resolved protein models via assessing psi and phi angles of amino acid residues which shows energetically allowed regions in the amino acid residues. Figure 3.10A-C shows the Ramachandran's plot for the predicted *An. funestus s.s.* CTL4 models wherein quadrant I (top left), quadrant II (top right), quadrant III (bottom left) and quadrant IV (bottom right). Ramachandran's analysis for all the resolved models is summerized in (Table 3.2). Briefly, the most favoured region, additionally allowed region, generously allowe region and disallowed regions of the Ramachandran's plots corresponds to quadrants I-IV respectively (Figure 3.10). Models resolved from template servers $M1_R$ and $M1_P$ have over 80% of their amino acid residues in the most favoured regions (QI) and the least amount in the disallowed region (QIV) whereas models resolved from template free $M1_Q$-$M3_Q$ have at most 54% residues in the most favoured region and over 4% of residues in the disallowed region (Table 3.2).

Table 3.2 Analysis for the arrangement of amino acid residues in Ramachandran's plot.

Model	Quadrant I	Quadrant II	Quadrant III	Quadrant IV
$M1_Q$	47.1%	37.4%	10.3%	5.2%
$M2_Q$	49.7%	36.1%	10.3%	3.9%
$M3_Q$	54.2%	31.6%	8.4%	5.8%
$M1_R$	84%	13.5%	1.9%	0.6%
$M1_P$	80.5%	11.9%	5.1%	2.5%

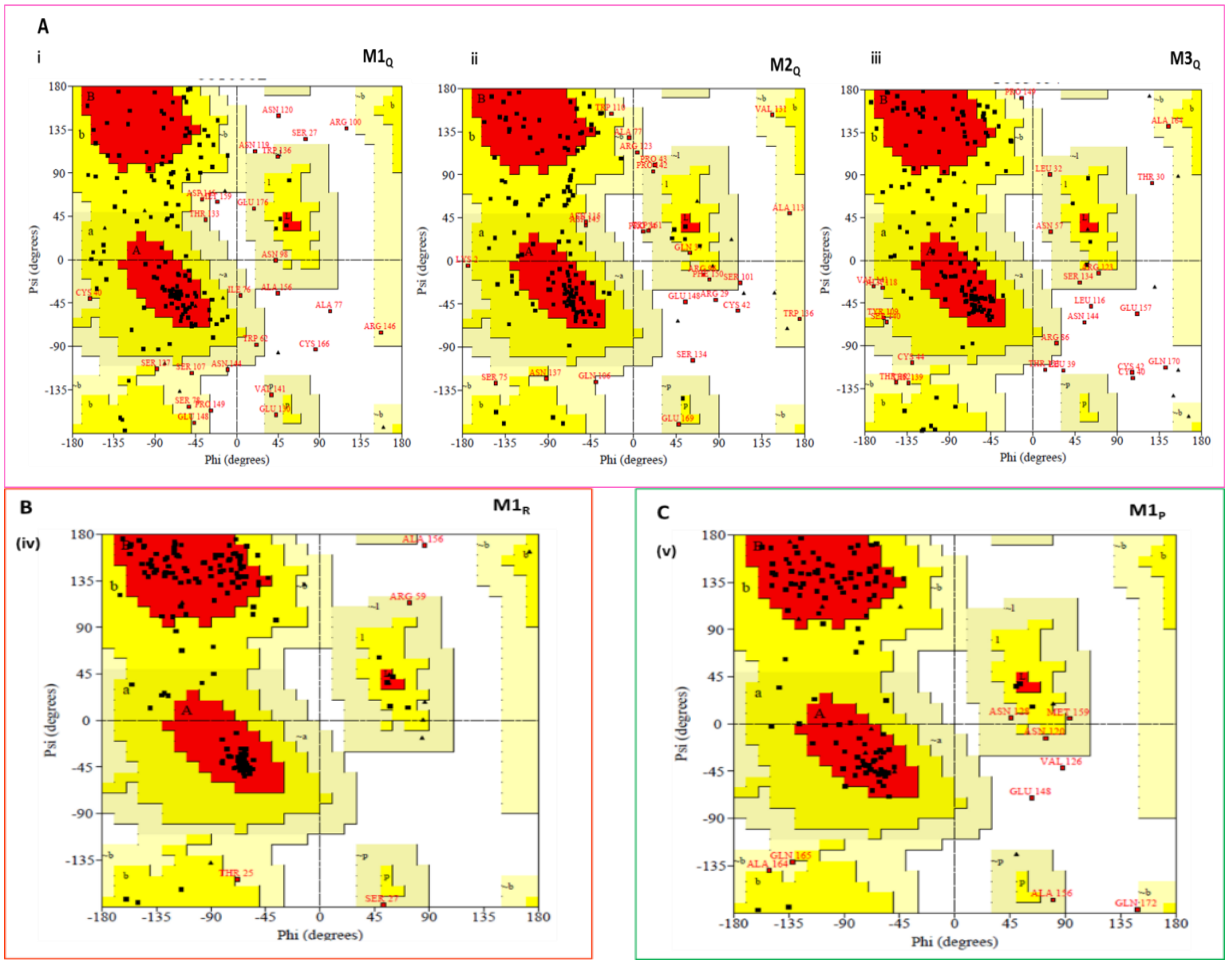

Figure 3.10: Ramachandran's plot for theoretically predicted tertiary structures of the *An. funestus s.s.* CTL4. Plot showing the distribution of energetically allowed amino acid residues (A) (i) M1Q has a total of 94.8% residues in energetically allowed regions (QI-QII) with 5.2% outlier residues in energetically disallowed region (QIV) (ii) M2Q has a total of 96.1% residues in energetically allowed regions (QI-QII) with 3.9% outlier residues in energetically disallowed region whereas(QIV) (iii) M3Q has a total of 94.2% residues in energetically allowed regions (QI-QII)with 5.8% outlier residues in energetically disallowed region(QIV). **(B)** $M1_R$ has a total of 99.4% residues in energetically allowed regions (QI-QII) with 0.6% outlier residues in energetically disallowed region (QIV) whereas **(C)** $M1_P$ has a total of 97.5% residues in energetically allowed regions (QI-QII) with 2.5% outlier residues in energetically disallowed region (QIV).

3.1.2 Confirmation that CTL4 is present in laboratory *An. funestus s.s.*

In order to confirm whether the CTL4 gene is present in *An. funestus s.s.*, conventional PCR was conducted using gene specific primer pairs (Figure 3.11). These primer pairs were designed to amplify specific regions of the translated nucleotide sequence (Figure 3.11). The electrophoresed PCR products from CTL4 exons indicate single distinctive PCR products of 188, 158 and 226bp depicting exons one, two and three, respectively, and a template free negative control for each primer pair (Figure 3.12). Each primer pair was optimised to ensure a single amplicon with high yield was achieved and that amplicons produce fragments of expected sizes. There was no amplification in the template free negative control, suggesting that there was no contamination in the mastermix.

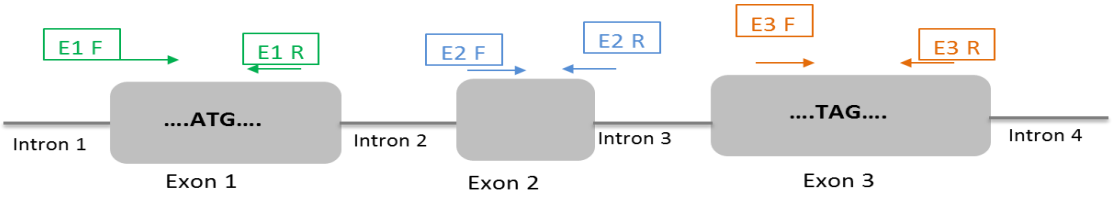

Figure 3.11: Graphical representation of gene specific primer pairs binding sites of CTL4. *Anopheles funestus s.s* CTL4 start and stop codon indicated by ATG and TAG respectively, introns are indicated by the grey lines between exons. Primer pairs are indicated by the same colour.

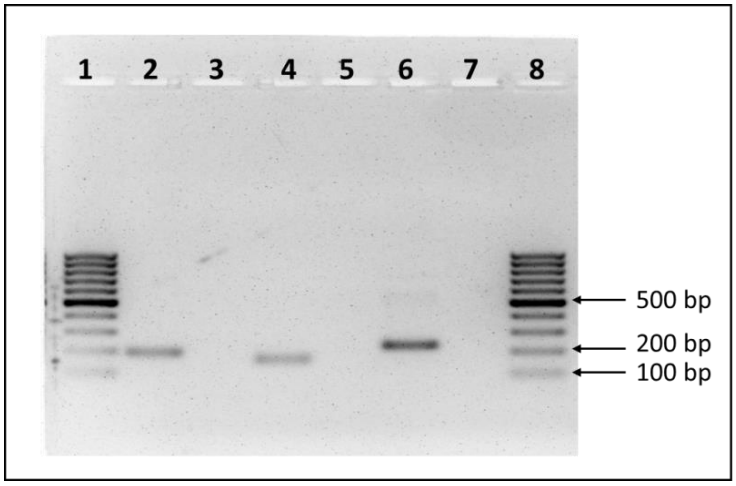

Figure 3.12: Amplification of *An. funestus s.s.* CTL4 in laboratory FUMOZ colony. Amplification of CTL4 exons in *An. funestus s.s.* gDNA. DNA fragments of the PCR products were visualized on a 2% (w/v) non-denaturing agarose gel, sizes were estimated by comparison with a 100bp DNA molecular weight marker (MWM). PCR products were loaded as follows: lanes 1 and 8 with MWM, lanes 2, 4 and 6 indicates exons one, two and three, respectively. The no template negative control (NTC) for each PCR reaction is indicated by lanes 3, 5 and 7 for each exon, respectively.

Subsequently, sequence analysis of these PCR products was conducted to confirm identity to the *An. funestus s.s.* CTL4 (AFUN010847). Visual inspection of the amplicons after electrophoresis (Figure 3.12), revealed that one of the PCR products, exon three (226bp), performed better and was used to investigate the *An. funestus s.s.* CTL4. MEGA X software was used to edit the chromatogram from Sanger sequencing of the PCR products. BLASTn tool from Vectorbase was then used to search chromatogram nucleotide sequence against nucleotide sequences of members of the anophiline mosquitoes. BLASTn results identified the *An. funestus s.s.* CTL4 (AFUN010847) which showed a 98.7% identity, 100% sequence alignment of 155bp of the edited sequence and an E-value of $1x10^{-73}$ between query (chromatogram nucleotide sequence) and sequence in the database.

3.2 Optimization of the feeding rate

Optimization of the feeding rate to carry out infection/treatment studies was performed. The *An. funestus s.s.* FUMOZ colony is reared using guinea pig as a source of blood meal, therefore the development of a successful artificial feeding system was essential for *P. falciparum* transmission studies. The use of an artificial feeding system is not only blood efficient, but also maintains constant temperature of the blood meal (Luo, 2014).

This study focused on determining whether 1) starvation increases the feeding rate, 2) an increase in starvation influences the feeding rate and 3) the impact of adult female age on feeding rate and survival post feeding.

3.2.1 Starvation increases the feeding success rate

Table 3.3 shows data on *An. funestus s.s.* adult females blood fed on cow blood who received different diet treatments 48 hours prior to blood meal. The mean percentage number of individual mosquitoes that were fully fed (Section 2.2 now designated as fed), significantly differed between different diet treatments (One-way ANOVA; $F = 5.26$, $p < 0.05$, n=3) (Figure 3.13). Interestingly, the number of mosquitoes that fed in the control and H_2O treatment is similar. Dunnett's multiple comparisons analysis showed that there was no significant difference between the mean of the control vs. H_2O treatment ($p = 0.99$). However, there was a significant difference in the means between control vs. fully starved treatment ($p = 0.0244$, n=3).

Table 3.3 Feeding success of *An. funestus s.s.* adult females provided with different diets.

Treatment	Sample size before feeding	Mean % feeding rate ± SD (n)	95% CI Lower	Upper
Control (10% (w/v))	120	44^{a} ± 9.7 (53)	33.98	54.35
H_2O	120	44 ± 16.5 (53)	26.79	61.54
Fully starved (48 hours)	78	22^{b} ± 12.9 (27)	8.91	36.08

Different superscript letter ($^{a/b}$) within columns indicates statistical difference between means.

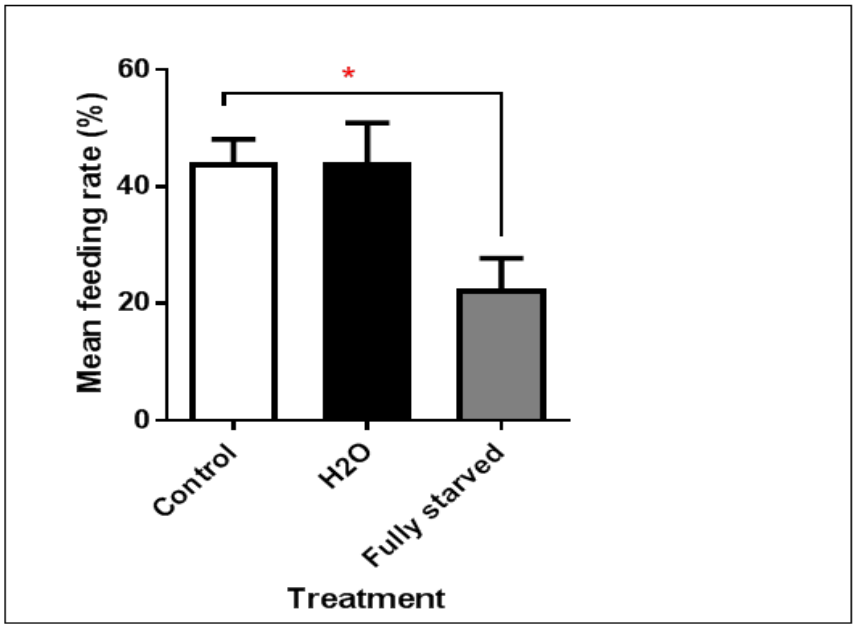

Figure 3.13: Average blood feeding success rate of *An. funestus s.s.* females provided with different diets. Graph represents the mean success feeding rate from three independent biological replicates, error bars show the mean ± SD. *; (p= 0.0244).

3.2.2 An increase in starvation period influences the success feeding rate

It was hypothesized that adult females that are starved for longer periods of time will have a higher feeding rate in contrast to those that are starved for a shorter period of time. In addition, this assay was also performed to increase the low percentage feeding rate obtained (Section 3.2.1). Moreover, a total of 42 individual mosquitoes in the fully starved treatment (Section 3.2.1) died, this resulted in less number of individual mosquitoes before feeding (Figure 3.13), and for this reason diet treatment with H_2O was used for the starvation period objective. Data on success feeding rate at different starvation periods is summarized in (Table 3.4).

Adults starved for 72 hours resulted in higher feeding rates than the control group (Figure 3.14). Additionally, the majority of mosquitoes starved for 72 hours were partially fed, probably required more time to feed, they were however not included in the analysis. There was a statistical significant difference in mean percentage feeding success rates between different starvation periods (One-way ANOVA; F = 3.09, $p < 0.05$, n=3). Dunnett's multiple comparisons showed a statistical difference in means between controls vs. mosquitoes starved for 72 hours (Table 3.4). Lastly, mosquitoes with a 96 hour water starvation period had high mortality and resulted in fewer mosquitoes available for blood feeding (Table 3.4). Variation between the control feeding rate of this experiment and those presented in table 3.1, might be due to difference in blood stocks used, insectary conditions, etc. and should be investigated in future.

Table 3.4 Feeding success rates of *An. funestus s.s.* females across different starvation periods.

Treatment (starvation period)	Sample size	Mean % feeding rate ± SD (n)	95% CI	
Control (10% (w/v))	120	14^{a} ± 7.36 (17)	6.44	21.89
24 hours	120	27 ± 18.62 (32)	7.12	46.21
48 hours	120	31 ± 15.30 (37)	14.77	46.89
72 hours	120	39^{b} ± 11.58 (47)	21.01	51.32
96 hours	100	20 ± 7.76 (14)	7.39	32.10

Different superscript letter ($^{a/b}$) within columns indicates statistical difference between means.

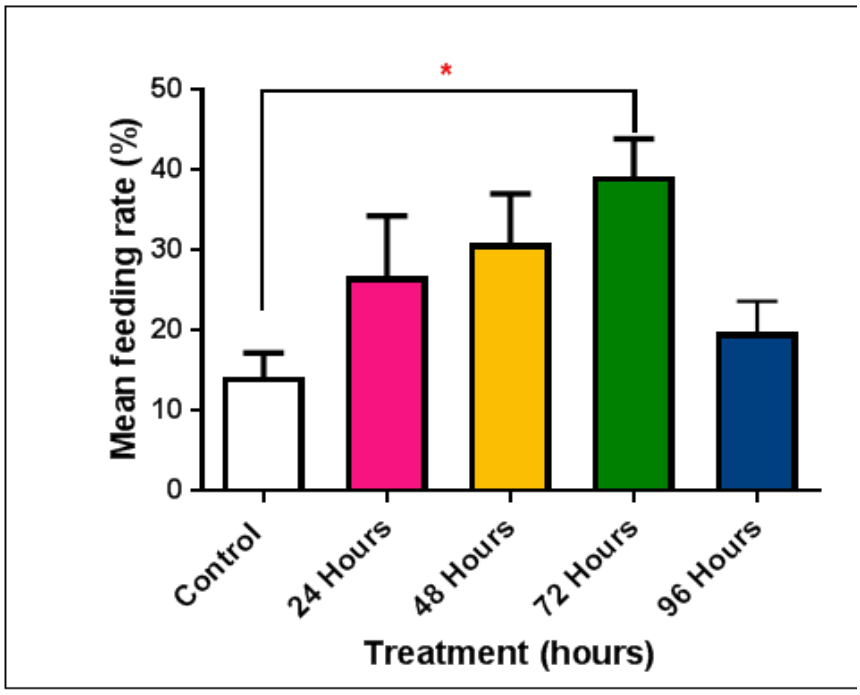

Figure 3.14: Percentage feeding success rate of *An. funestus s.s.* starvation period. Mean number of individual mosquitoes that fully engorged the blood meal following starvation for 24, 48, 72 and 96 hours, mosquitoes starved for 72 hours had a mean feeding rate of 9. Graph represents the mean feeding rate from three independent biological replicates, error bars show the mean ± SD. *; (p = 0.0117).

3.2.3 Adult female age has an impact on the feeding rate and survival post feeding

The percentage success feeding rate of *An. funestus s.s.* blood fed on cow blood at different ages 5, 10 and 15-days old is summarized in Table 3.5. There was no statistical significant difference in means between of feeding rates and age at which *An. funestus s.s.* have their first blood meal (One-way ANOVA; F = 1.32, p = 0.2968, n=3) (Figure 3.15). The lack of statistical significance might be due to the high level of variation observed and increasing the sample size might decrease the variation observed here. In addition, the feeding rate was directly proportional to the age at which adult females have their first blood meal. As such, correlation between 5 vs. 10 days old adults was r = 0.8824 at p = 0.0361, whereas no correlation was found between 10 vs. 15 days old r = 0.4928 at p = 0. 3278 (Figure 3.15).

Table 3.5 Feeding success rates of *An. funestus s.s.* females of different age groups.

Age of blood feeding	Sample size	Mean % feeding rate ± SD (n)	95% CI	
			Lower	Upper
5 days old	120	43 ± 19.92 (52)	22.43	64.23
10 days old	120	63 ± 36.98 (75)	23.69	101.30
15 days	120	68 ± 21.39 (81)	45.05	89.95

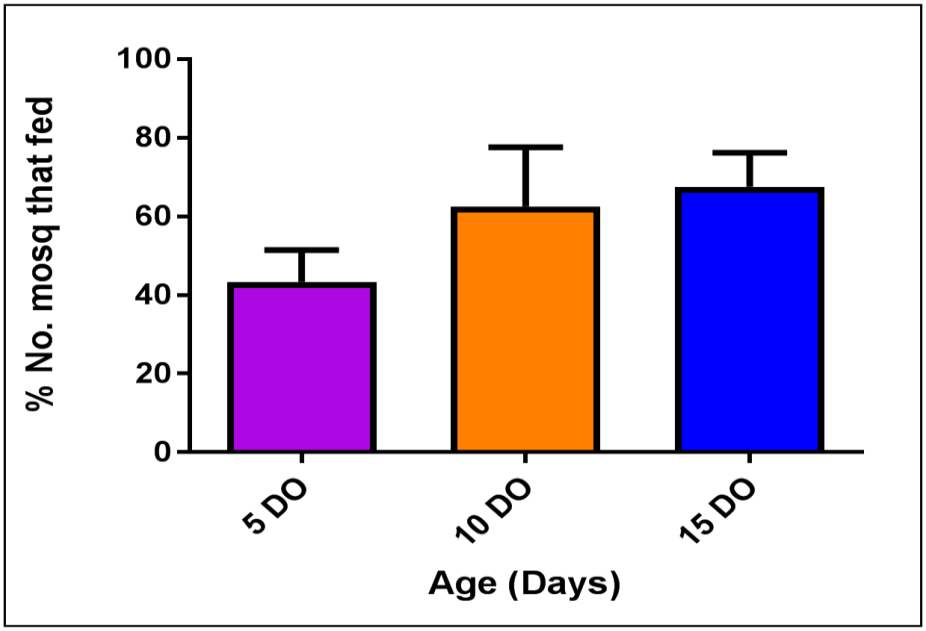

Figure 3.15: Average feeding success rate of *An. funestus s.s.* of different ages. There was no statistical difference in mean between the feeding rates of mosquitoes of different ages. Graph represent the mean feeding rate from three independent biological replicates, error bars show the mean ± SD. (p = 0. 2968).

Data for longevity of *An. funestus s.s.* fed on cow blood at different ages (5, 10 and 15 days old is summarized in Figure 3.16. Results show that female survival proportion ranges from 100-28%; 100-20% and 100-16% with median survival rate of 15; 14.5 and 10 for adults aged 5; 10 and 15 days old, respectively from 1-18 days post blood meal. There was no significant statistical difference of adult females across the different ages (Log-rank Mantel-Cox test, Chi-square 19.2, DF = 2, p = 0.3839).

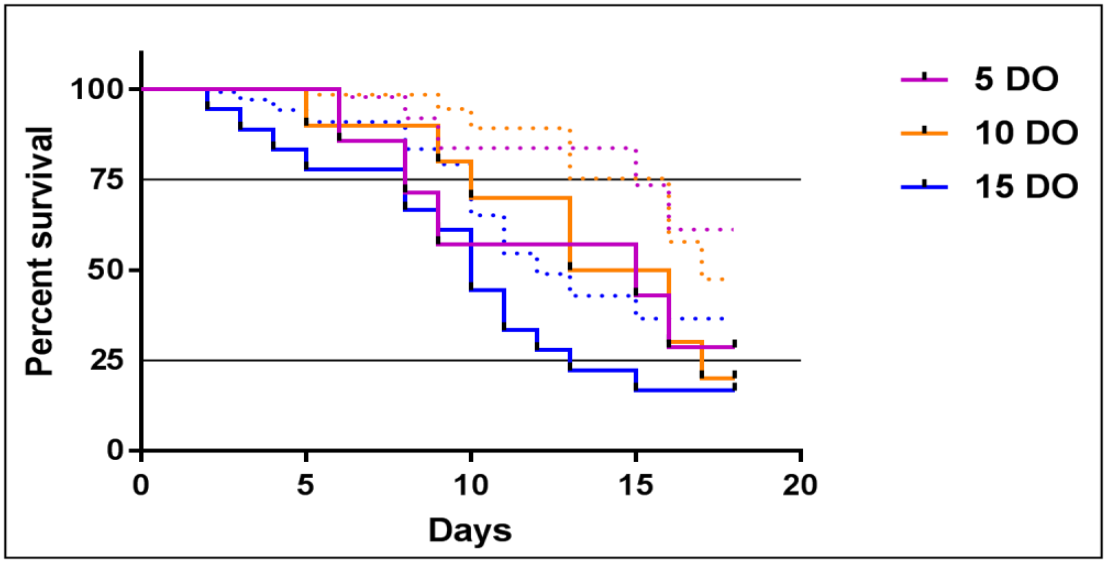

Figure 3.16: Percentage survival rates of mosquitoes of different ages post blood meal. Graph represents the cumulative survival across the indicated time points for all three replicates, (p = 0.3839). Dotted lines indicate the 95% confidence intervals and the solid horizontal lines indicate the upper 75% and lower 25% percentiles.

3.3 *Anopheles funestus s.s.* infection with *P. falciparum*

Ingestion of *Plasmodium* infected blood meal by *An. gambiae s.s.* has been associated with an up-regulation of the CTL4 gene which leads to the protection of the parasite against the *An. gambiae s.s.* immune system (Osta *et al.*, 2004). In order to obtain *An. funestus s.s.* CTL4 gene (AFUN010847) transcript i.e. of exon 3, total RNA was extracted 24 hours post feeding. The messenger RNA (mRNA) was converted to cDNA for downstream trancript abundance analysis. Additionally, since *An. funestus s.s.* mosquitoes ingested a human blood meal infected with *P. falciparum* parasites, nucleic acid (mRNA or gDNA) that is extracted from the mosquito will contain the parasites'genetic material. Therefore, in order to confirm that *P. falciparum* parasites were ingested by adult female *An. funestus s.s.* mosquitoes, PCR was used to amplify the parasites circumsporozoite gene .

3.3.1 RNA quality assessment

The purity of the RNA was determined by measuring the absorbance of the total extracted RNA. A summary of the optical densit at A_{260}/A_{280} of the RNA samples from mosquitoes that were immune challenged with a parasitic-infected blood meal and uninfected controls are reported in Table 3.6. An absorbance value between 1.8-2.0 is generally accepted as good quality RNA with no contaminants (Taylor *et al*., 2010). The yield in RNA samples stabilized RNA using Trizol Reagent™ was higher in comparison to samples whose RNA was stabilized with RNAlater and closer to the desired concentration (Section 2.5.1).

Table 3.6 Summary of readings showing optical density ratios from extracted RNA fed on *P. falciparum* infected blood.

Sample ID	Nucleic Acid Yield (ng/µL)	A260/A280
P. falciparum* A	838.59	2.01
***P. falciparum* B**	780.93	1.99
***P. falciparum* C**	667.01	1.98
Control A*	835.56	1.94
Control B	562.81	1.98
Control C	509.00	1.94

* RNA samples stabilized using Trizol Reagent™.

The integrity of the RNA samples was assessed using denaturing agarose gel electrophoresis, since the concentrations of all RNA samples were >350ng/µL, which is high enough to be viewed by gel electrophoresis (Machaira *et al*., 2015). Figure 3.17 shows electrophoresed RNA samples which typically indicate a strong 18S rRNA (~2,000bp) profiling due to the co-migration of the 28S rRNA which cleaves with the 18S rRNA under denaturing conditions to form one distinctive bright band, a faint 5.8S (200bp) and 5S (~120bp) (Ogino, 1990; Winnebeck *et al*., 2010; Machaira *et al*., 2015). The fragments of the ribosomal subunits in samples whose RNA was stabilized using Trizol Reagent™, indicated by red arrows in (Figure 3.17), was more apparent in comparison to samples stabilised in RNAlater.

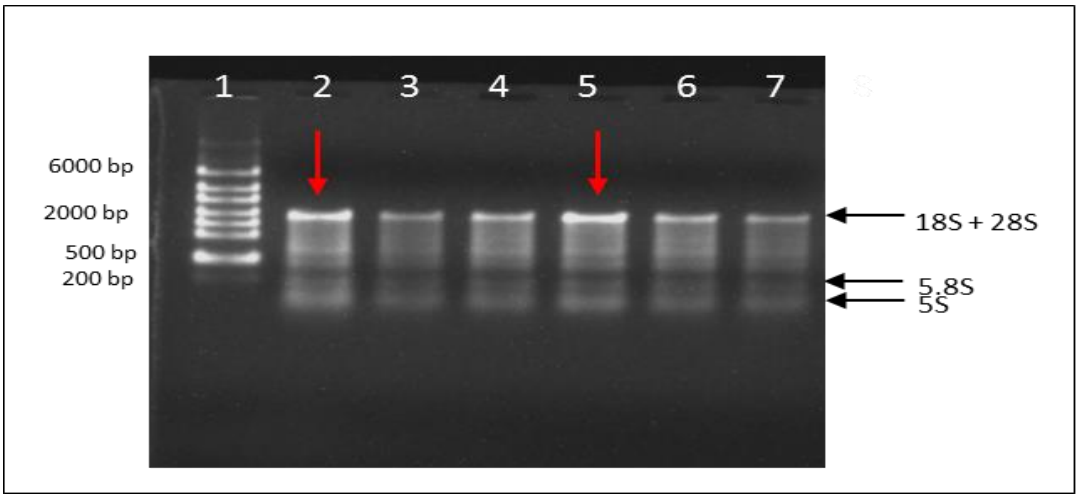

Figure 3.17: Total RNA extraction migration patterns in *P. falciparum*-challenegd *An. funestus s.s.* rRNA fragments were visualized on a 1% (w/v) denaturing agarose gel. Sizes were estimated by comparison to a 1kb RNA ladder (MWM). Sample RNA was loaded as follows: lane 1 MWM, lanes 2, 3 and 4 mosquitoes provided with *P. falciparum* infected blood meal whereas lanes 5, 6 and 7 mosquitoes provided with uninfected blood meal.

3.3.2 cDNA quality assessment

The quality of the synthesized cDNA was assessed by screening for gDNA contamination via PCR and agarose gel electrophoresis. Figure 3.18 displays the region at which primer pairs for intron-1 region anneal. The intron was not amplified in all *P. falciparum* infected blood meal and uninfected samples (Intron-1 primers in Table 2.2) in comparison to the mosquito gDNA (positive control) which resulted in a 403bp (red arrow in Figure 3.19). Additionally, BLASTn results for the mosquito gDNA intron confirmed the sequence match to the *An. funestus s.s.* CTL4 intron region.

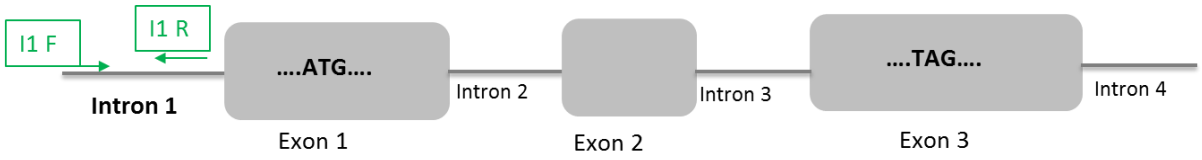

Figure 3.18: Graphical representation of gene specific primer pairs binding sites of CTL4. *Anopheles funestus s.s* CTL4 start and stop codon indicated by ATG and TAG respectively, introns are indicated by the grey lines between exons. Primer pair for intron-1 is indicated by a green colour.

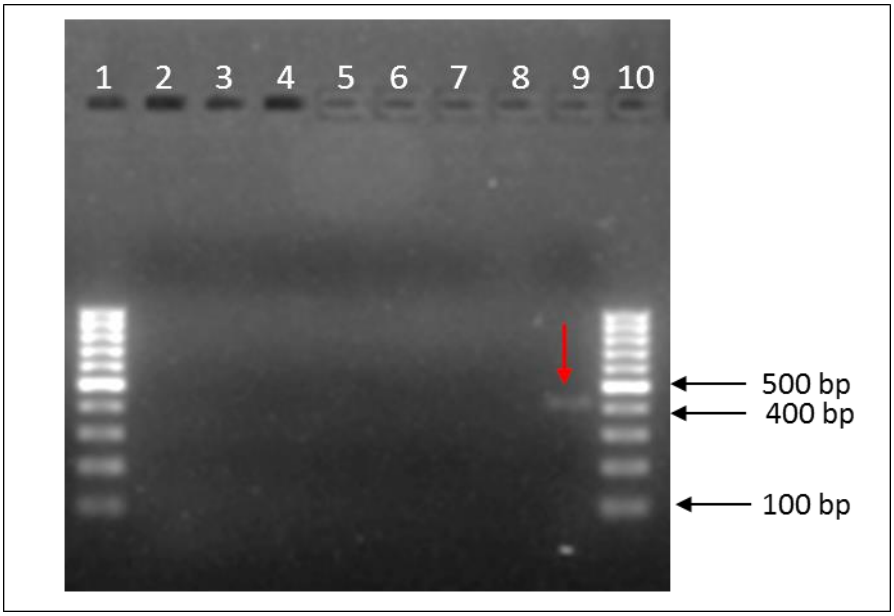

Figure 3.19 : Nucleic acid assessment in *P. falciparum* immune challenged *An. funestus s.s.* Amplification of intron 1 cDNA fragments were visualized on a 2% (w/v) non-denaturing agarose gel, sizes were estimated by comparison to a 100bp DNA ladder (MWM). PCR product was loaded as follows: lanes 1and 10 MWM, lanes 2, 3 and 4 are mosquitoes provided with *P. falciparum* infected blood meal, lanes 5, 6 and 7 are mosquitoes provided with uninfected blood meal, lane 8 no template negative control whereas lane 9 is gDNA positive control. The 403bp intron 1 band is faint and pointed by the red arrow.

3.3.3 Confirmation of *P. falciparum* infection in *An. funestus s.s.*

The presence of *P. falciparum* parasites in the ingested blood meal can be detected using various assays including qPCR, PCR and morphology. A morphologically based assay for the viability of the parasites was not necessary for this study, however, other members of the research unit conducted morphological assays, 8 and 10 days post infection which showed that infection was established based on the different stages of the parasite development (data not shown, as per personal communiation with Prof L Koekemoer (SHIP project)). In order to confirm the presence of the *P. falciparum* parasites in the cDNA, PCR was used to analyze the presence of the circumsporozite transcript in *An. funestus s.s.* 24 hours post ingestion of an infected blood meal. Amplification of the circumsporozite 150bp was detected in parasites mosquitoes, but no amplification was detected in mosquitoes provided with an uninfected blood meal (Figure 3.20).

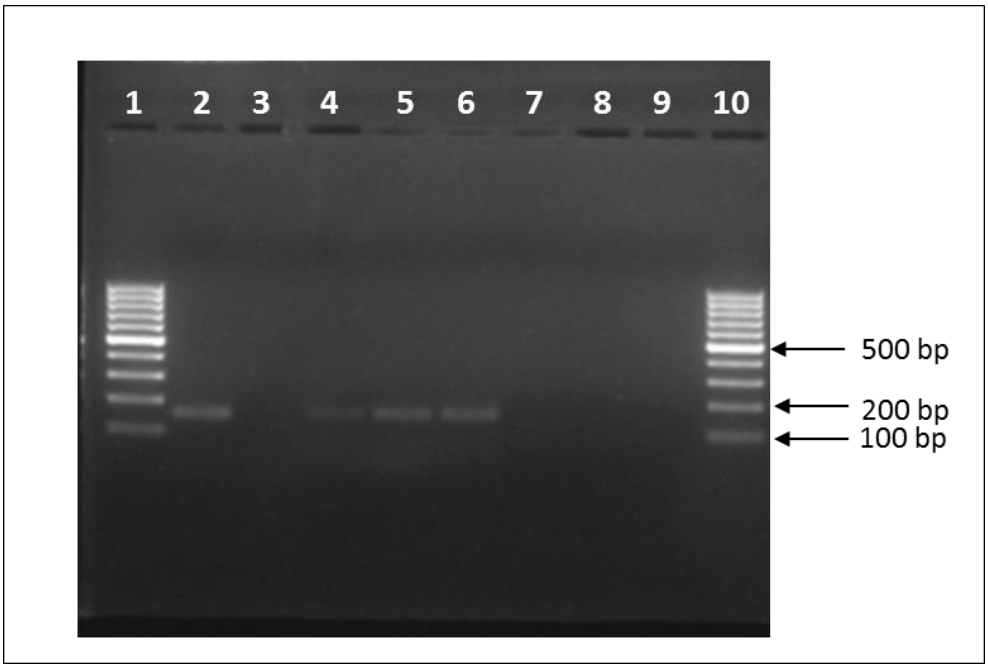

Figure 3.20: Screening for *P. falciparum* parasites in *An. funestus s.s.* PCR products were visualized on a 2% non-denaturing agarose gel. Sizes were estimated by comparison to a 100bp DNA ladder (MWM). PCR product was loaded as follows: lanes 1 and 10 MWM, lane 2 depicts *P. falciparum* positive control (150bp), lane 3 depicts no template negative control, lanes 4, 5 and 6 depicts transcript of mosquitoes provided with *P. falciparum* infected blood meal; whereas lanes 7,8 and 9 depicts product of mosquitoes provided with uninfected blood meal.

3.4 Quantitative real time PCR (qPCR)

3.4.1 Reference gene selection

qPCR was used to quantify the *An. funestus s.s.* CTL4 transcript 24 hours post *P. falciparum* infected blood meal. The accuracy of the qPCR is influenced by the stability of the reference genes to normalize the *An. funestus s.s.* CTL4 mRNA levels (Vandesomple *et al*., 2002). In this regard, candidate reference genes were first screened to find the suitable reference genes. Selection of potential reference genes was based on genes with the lowest stability value, a numerical value that is the lowest in comparison to the others. Figure 3.21A shows the ranking of candidate reference genes from the most to the least stable, reference gene RPS26 was the most stable of the screened reference genes with a stability value of 0.010; RPS7 and RPL19 were equally stable with a stability value of 0.017; whereas ND_5 was the least stable with a stability value of 0.031. In addition, Normfinder also estimated intergroup variation between reference genes (Figure 3.21B) which revealed that ND_5 is the least stable of the four candidate reference genes with a stability value of above zero (0.029); whereas RPS7, RPS26

and RPL19 stability values where below zero as -0.009, -0.008 and -0.012, respectively. This further supports the values in Figure 3.21A, the top 3 ranked genes will be used for normalizing CTL4.

A

Rank	Gene name	Stability value	*P.f* [Cq (mean±SEM)]	C [Cq (mean±SEM)]
1	RPS26	0.010	22.16 ± 0.027	23.62 ± 0.045
2	RPS7	0.017	21.05 ± 0.106	22.50 ± 0.067
3	RPL19	0.017	20.18 ± 0.027	21.68 ± 0.109
4	ND_5	0.031	21.73 ± 0.018	21.51 ± 0.065

P. f = *P. falciparum*; C = Controls; Cq [(mean±SEM)] = arithmetic mean ± standard error of mean.

B

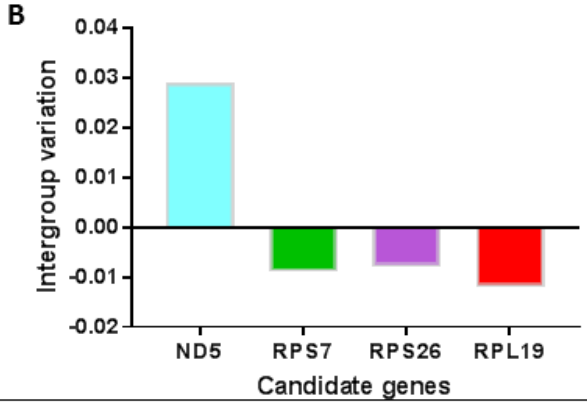

Figure 3.21: Reference gene selection and intergroup variation in *P. falciparum* infected *An. funestus s.s.* (A) Ranking of candidate reference genes according to their expression stability by Normfinder. **(B)** Graphical representation showing that RPS7, RPS26 and RPL19 intergroup values fall below zero, indicating that they are stable in comparison to ND_5 which has a value above zero.

3.4.2 Relative quantification

The amplification of the reference genes and target gene for qPCR analysis was successful. Optimization of the qPCR included determining the optimal annealing temperature and primer concentrations for all genes. All reactions resulted in good exponential curves (Figure 3.22). The reaction efficiencies for all three independent replicates were between 96-100%, R^2 values were greater than 0.992 and a slope between -3.311 to -3.418 (Appendix Section B; Figure B2 [A-D (ii)]). Additionally, a dissociation curve and peak were used to evaluate the formation of primer dimers as well as non-specific amplification, the melt peak for all transcripts show a single peak at different template concentration indication that a single

qPCR product was Figure 3.22 (i-ii) (Taylor *et al*,. 2010). The qPCR reactions were performed with a no template control (NTC) and reaction with SYBR with H_2O as negative controls, did not have any amplification indicating that reagents were free of contaminants. Individual amplification, standard, melt peaks and curves for each gene can be found in (Appendix Section B; Figure B2 [A-D (ii)]).

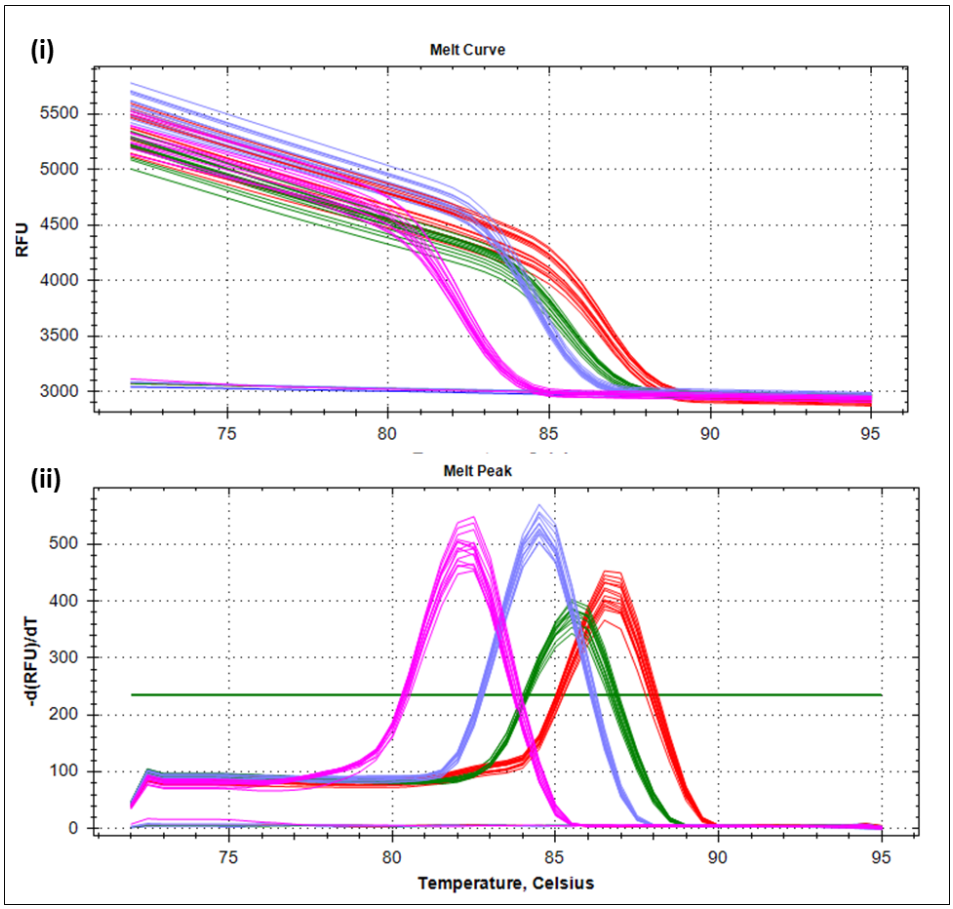

Figure 3.22: Curves of reference gene selection in *P. falciparum* infected *An. funestus s.s.* Graphical representations of dissociation (i) curve and (ii) peak showing single peaks indicating amplification of a single qPCR product. Negative controls are shown by the blue line at the bottom of the curves. Gene identifications are as follows: CTL4 shown in pink, RPS26 shown in blue, RPS7 shown in green and RPL19 shown in red. The NTC and SYBR + H_2O are shown in light blue at the bottom of the curves.

3.4.3 Confirmation of qPCR products

In order to confirm that the correct amplicons were being amplified, qPCR products were electrophoresed (Figure 3.23) and sent for sequencing. The qPCR cDNA profiling was as follows: 226bp, 160bp, 134bp and 223bp for CTL4, RPS26, RPS7 and RPL19 respectively. All reactions included a NTC, which did not have any amplicon and a SYBR with H_2O

negative controls, both these controls did not have amplification indicating that primers/reagents were working efficiently and are void of contaminants. Additionally, a BLASTn search in Vectorbase resulted in 100% coverage of the edited sequences from the chromatogram (Sanger sequencing) that where aligned with those in the database and very high negative E values between 10^{-38} - 10^{-54} and a sequence similarity identity score between 97.8-100%.

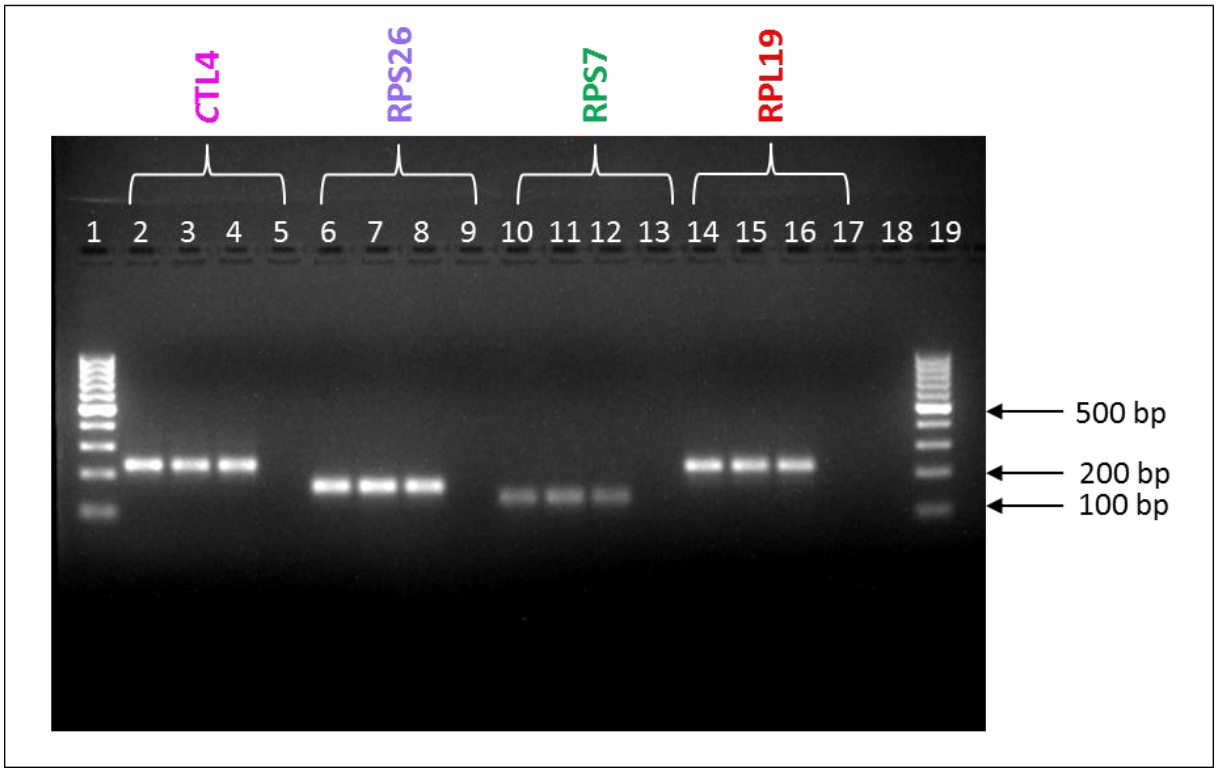

Figure 3.23: Amplification of qPCR products in *An. funestus s.s.* immune challenged with *P. falciparum* infected blood meal. cDNA fragments of qPCR products were visualized in a 2% (w/v) non-denaturing agarose gel, sizes were estimated by comparison to a 100bp DNA ladder (MWM). qPCR products was loaded as follows: lanes 1 and 19 MWM; lanes 2, 3 and 4 CTL4, lane 5 CTL4 NTC; lanes 6, 7 and 8 RPS26, lane 9 RPS26 NTC; lanes 10, 11 and 12 RPS7, lane 13 RPS7 NTC, lanes 14, 15 and 16 RPL19, lane 17 RPL19 NTC and lane 17 SYBR with H_2O negative control.

3.4.4 Expression analysis of *An. funestus s.s.* CTL4 transcript 24 hours post *P. falciparum* infected blood meal

Several C-type lectins have been implicated in innate immune responses in vertebrate and invertebrates. In invertebrates, it has been reported that there is a change in gene expression following ingestion of *Plasmodium* parasites (*P. berghei*) infected blood meal (Osta *et al.*, 2004).

In order to investigate the impact that *P. falciparum* has on *An. funestus s.s.* CTL4 gene expression, qPCR was used to measure the CTL4 transcript abundance which was normalized by RPS26, RPS7 and RPL19 reference genes (Ct values Appendix Section B, Figure B1). The *An. funestus s.s.* CTL4 transcript in *P. falciparum* infected blood meal is not significantly differentially expressed (p = 0.256) in comparison to uninfected controls, implying that the expression profile is similar to the uninfected controls 24 hours post-infected (PI) blood meal (Figure 3.24).

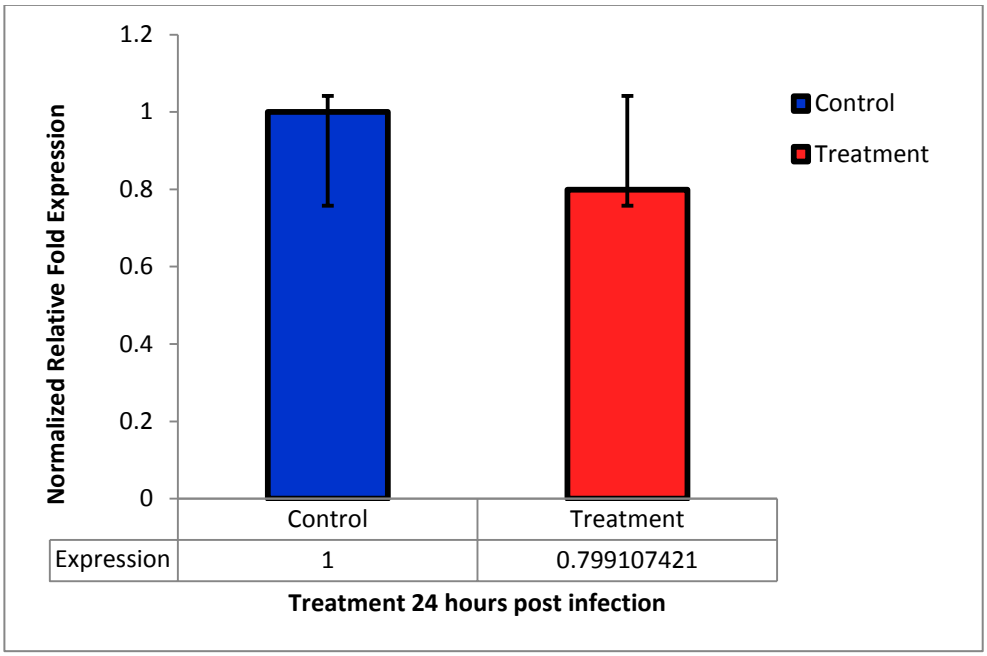

Figure 3.24: Effect of *P. falciparum* on the transcript level of *An. funestus s.s.* CTL4. Transcript level was determined in mosquitoes immune challenged with blood meal infected with *P. falciparum* (red) and controls (blue) 24 hours post blood meal. Ordinate depicts relative expression between cohorts where means were calculated from three independent biological replicates. Error bars represent ± standard error mean of relative quantity. Statistical significance was determined using the Student's T-test with a (p = 0.256).

3.5 Toxicity of CQ

Vector control at larval or adult stage of the *Anopheles* mosquito plays a major role in the reduction of malaria transmission (WHO, 2016). Thus, continual testing of insecticides and novel compounds is essential in identifying efficient and ineffective compounds, as well as those compound that have lost their effectiveness. In this study, the potency of DDT and CQ were determined on larval and adult stages of *An. funestus s.s.* female mosquitoes.

3.5.1 Larvicidal toxicity

The larvicidal activity of CQ against *An. funestus s.s.* larvae showed that 0.5µM CQ did not possess any larvicidal activity (0% mortality) in comparison to 0.5µM DDT that was able to induce a total 85%, 92% and 100% mortality at 24, 48 and 72 hours post incubation, respectively (Figure 3.25).

Additionally, morphological effects of 0.5µM CQ on third instar larva were investigated at 24 hours post incubation. The progression of the larvae to pupal stage was observed 24-72 hours post incubation and from larvae to adult stage, 72 hours post incubation in CQ-treated larvae. Chloroquine-treated larvae retained their physical and mobility characteristics, whereas DDT-treated larvae showed impairment of the physical and mobility characteristics (Table 3.7).

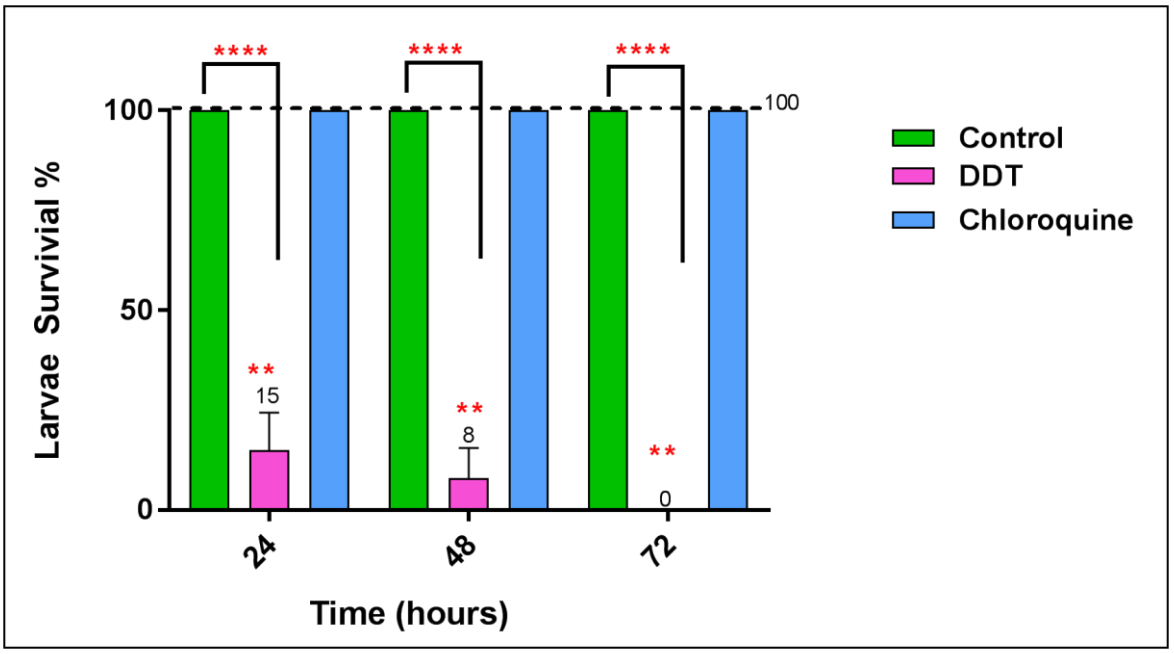

Figure 3.25: Average survival percentage rate 24-72 hours post incubation with test compounds at 0.5µM. Graph representation of the average survival rate of *An. funestus s.s.* larvae from five independant biological replicates. Error bars show the mean ± SD. ****; (p = 0.0001) and **; (p = 0.0064).

3.5.2 Adulticidal assay

In order to determine the concentration of CQ to add in the blood meal, a pilot adulticidal assay was conducted. Mosquitoes given CQ (5mg/mL) had a relatively high feeding rate of 65% in comparison to the other treatments (10, 25 and 50mg/mL) (Figure 3.26).

Additionally, mosquitoes that received a 50mg/mL treatment had the second highest feeding rate (Figure 3.26). This may have been due to various factors, including the fitness of the mosquito, the blood meal itself and its scent; however this observation warrants further investigation. Subsequently, adult females that recieved a blood meal containing CQ were knocked down during the time of feeding i.e. mosquitoes that died or those that were alive, but were unable to fly 10-15 minutes post-treated blood meal. Knockdown was increased with high concentrations of CQ in the blood meal, in comparison to the no knockdown effect observed in the controls. Knockdown persisted and the mortality was recorded 24 hours post CQ-treated (25 and 50mg/mL) blood meal in adults. Adults that were knocked down when 10mg/mL and 5mg/mL of CQ was added in the blood meal recovered 24 hours post blood meal and the mortality increased with increased CQ concentration (Table 3.8).

Table 3.7 Morphological changes in *An. funestus s.s.* larvae 24 hours post incubation with 0.5µM of CQ at 100X magnification, Δ indicates change in.

Treat-ment	Morphological changes	Stage progression	*An. funestus s.s.* larvae
Control	No Δ in size (A) Antennae hair is visible. (B) Integrity of abdomen is retained. (C) Anal brush is visible. (D) Prominent lateral and caudal hair (abdominal segment II-III).	No pupae developed	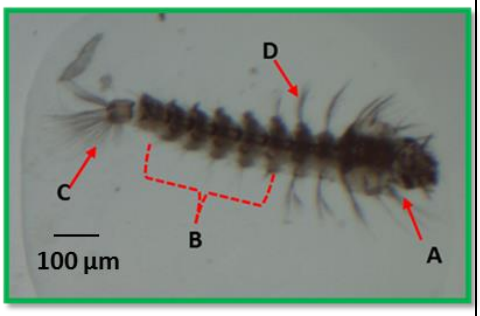
DDT	No Δ in size (A) Antennae hair loss and weakening of head from thorax. (B) Abdominal segment (III) increased in size. (C) Anal brush is not visible/ weakening. (D) Loss of lateral and caudal hair (abdominal segment II-III). (E) Loss of abdominal integrity.	No pupae developed. Growth was inhibited.	
CQ	No Δ in size (A) Antennae hair is visible. (B) Integrity of abdomen is retained. (C) Anal brush is visible. (D) Prominent lateral and caudal hair (abdominal segment II-III).	Pupae developed. Progressed to adult stage.	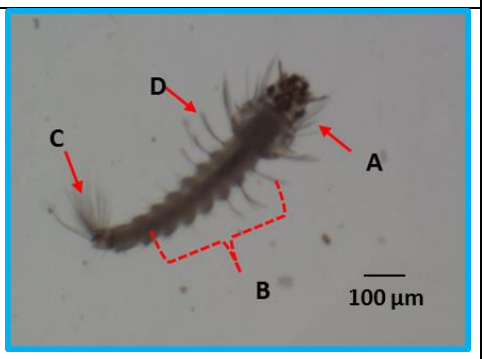

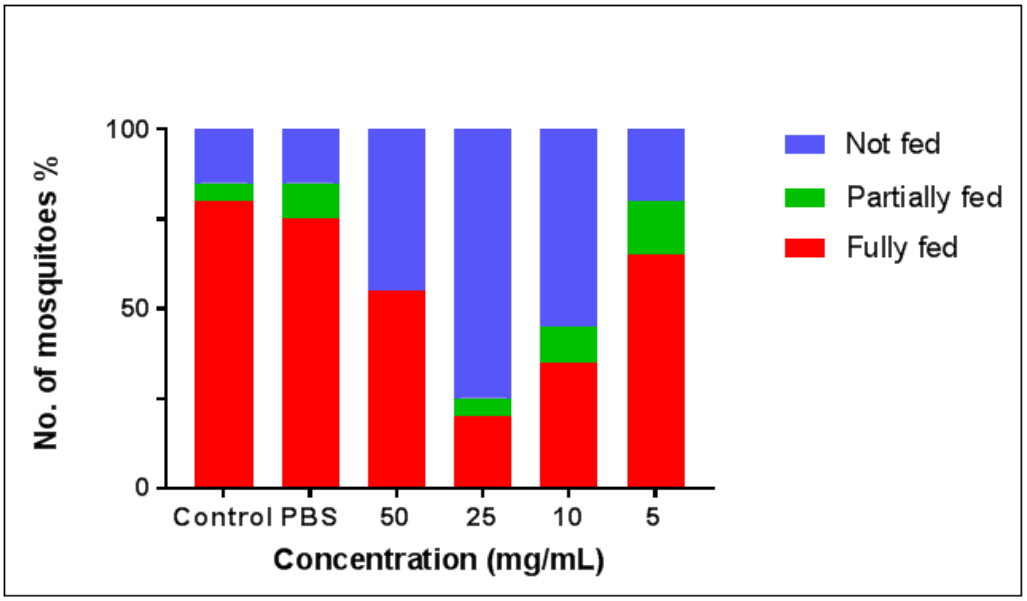

Figure 3.26: Feeding success of CQ-treated blood meal. Graphical representation of the mean of the fully, partially and not fed *An. funestus s.s.* adult females, χ^2; (p = 0.0001).

Table 3.8 Susceptibility of adult *An. funestus s.s.* females in response to CQ uptake in blood meal.

CQ treatment (mg/mL)	Sample size	Knockdown 10-15 minutes post treatment	% Mortality 24 hours post treatment
Control	100	0	0
PBS	100	0	0
5	100	8	0
10	100	29	0
25	100	75	50
50	100	73	73

3.5.3 *Anopheles funestus s.s.* treatment with CQ

From the adulticidal pilot assay (Section 2.6.3 and Section 3.5.2), 5mg/mL of CQ was identified as the most suitable concentration to be used in this study, based on that it did not result in the mortality of the mosquitoes and that it relatively produced a higer feeding rate (Table 3.8). The impact that ingested CQ-treated blood has on *An. funestus s.s.* CTL4 transcript was investigated by qPCR.

3.5.3.1 RNA quality assessment

The purity of the RNA was determined by measuring the absorbance of the total extracted RNA, absorbance ($A_{260/280}$) values were within the accepted range of 1.8-2.0 (Table 3.9) (Taylor *et al*., 2010). The concentrations of all samples were closer to the desired concentration as described in Section 2.4.3 (Table 3.9).

Table 3.9 Summary of readings showing optical density ratios from extracted RNA of *An. funestus s.s.* provided with CQ-treated blood meal.

Sample ID	Nucleic Acid (ng/µL)	A260/A280
CQA	1,027.50	1.96
CQB	956.80	1.96
CQC	798.60	1.99
Control A	822.20	1.93
Control B	657.70	1.91
Control C	704.30	2.00

Additionally, the integrity of the RNA samples was assessed by a denaturing agarose gel electrophoresis as described in Section 3.3.1, The remaining electrophoresed RNA samples can be found in Appendix Section B; Figure B3.

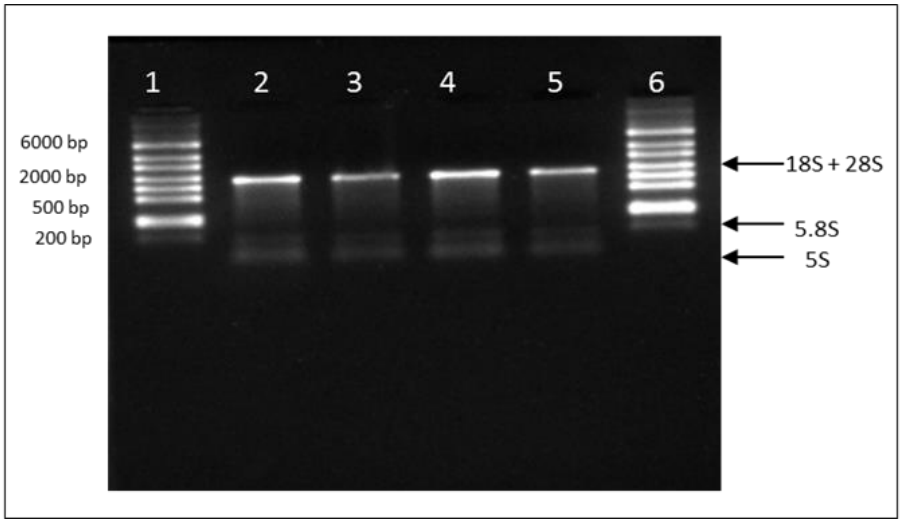

Figure 3.27: Total extracted rRNA migration patterns in CQ-treated *An. funestus s.s.* rRNA fragments were visualized on a 1% (w/v) denaturing agarose gel. Sizes were estimated by comparison to a 1kb RNA ladder (MWM). Sample RNA was loaded as follows: lane 1 and 6 MWM, lanes 2, and 4 CQ-treated (CQA and B) mosquitoes and lanes 3, and 5 untreated control (A and B) mosquitoes.

3.5.3.2 cDNA quality assessment

The quality of the synthesized cDNA from CQ-treated and untreated mosquitoes was assesed using PCR and agarose gel electrophoresis (Figure 3.28). Figure 3.18 (Section 3.3.2) shows primer binding sites in intron-1 region. All samples, CQ-treated and untreated did not amplify the 403bp intron-1 region in comparison to the gDNA positive control that resulted in a 403bp band (Figure 3.28) and only primer dimers were observed.

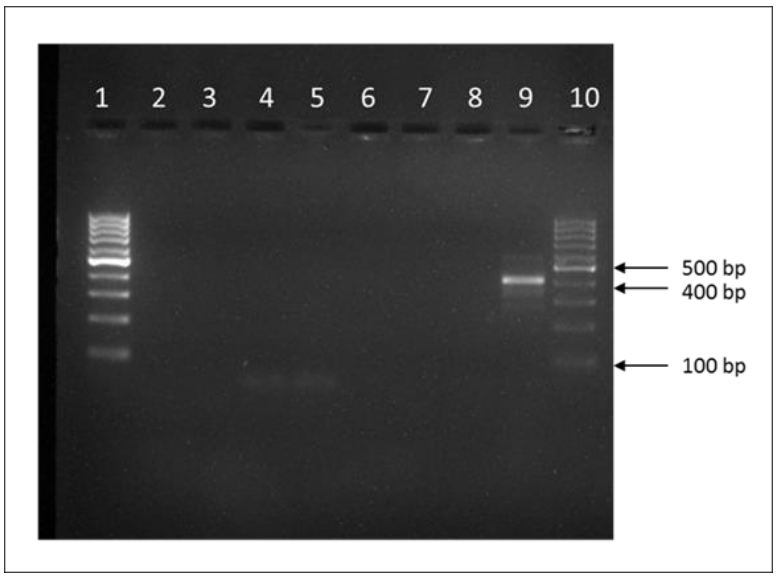

Figure 3.28: Nucleic acid assessment in CQ-treated *An. funestus s.s.* Amplification of intron-1 (403bp) cDNA fragments were visualized on a 2% (w/v) non-denaturing agarose gel, sizes were estimated by comparison to a 100bp DNA ladder (MWM). PCR product was loaded as follows: lanes 1and 10 MWM, lanes 2, 3 and 4 are products from CQ-treated mosquitoes, lanes 5, 6 and 7 are products from untreated mosquitoes, lane 8 is the no template negative control, whereas lane 9 is the gDNA positive control.

3.5.3.3 Expression analysis of *An. funestus s.s.* CTL4 transcript post CQ treatment

The effect of CQ on *An. funestus s.s.* CTL4 transcript was then investigated. Unfortunately, quantification of the *An. funestus s.s.* CTL4 transcript could not be achieved despite optimization. The primer pairs (Table 2.3) that were used have previously been shown to work efficiently in *P. falciparum* infected and uninfected control (Figure 3.22; 3.23). Furthermore, comparison of the efficiency of the primers used (Section 3.4) is summarized (Figure 3.29). Results show that all target samples lie within at least five points of the standard curve and R^2 value greater than 0.995 i.e. 0.999 and 0.998 for RPS26 reference gene used for *An. funestus s.s.* CTL4 quantification (Section 3.4) and CQ-treatment, respectively. However, the efficiency of the CQ-treated and untreated samples was below 90% (Figure 3.29A).

In addition, reactions resulted in good exponential curves and single amplification in the melt peak and curve were achieved, further showing that primer pairs and cycling conditions were working efficiently (Figure 3.29B; C, respectively).

These results also applied to target and other candidate reference genes, where single amplification in melt curve and peak were achieved (Figure 3.30i-ii), R^2 values were between 0.995-0.999, all target samples were within at least five points of the standard curve with a slope of -3.62, -4.16, -4.02 and -3.76 for CTL4, RPS7, RPL19 and ND_5, respectively (Appendix, Section B, Figure B4A-D). The efficiency of each gene was however lower than that required with the highest efficiency being 88.6% (Taylor *et al*., 2010). Thus, reference gene selection and quantification of the *An. funestus s.s.* CTL4 transcript could not be achieved.

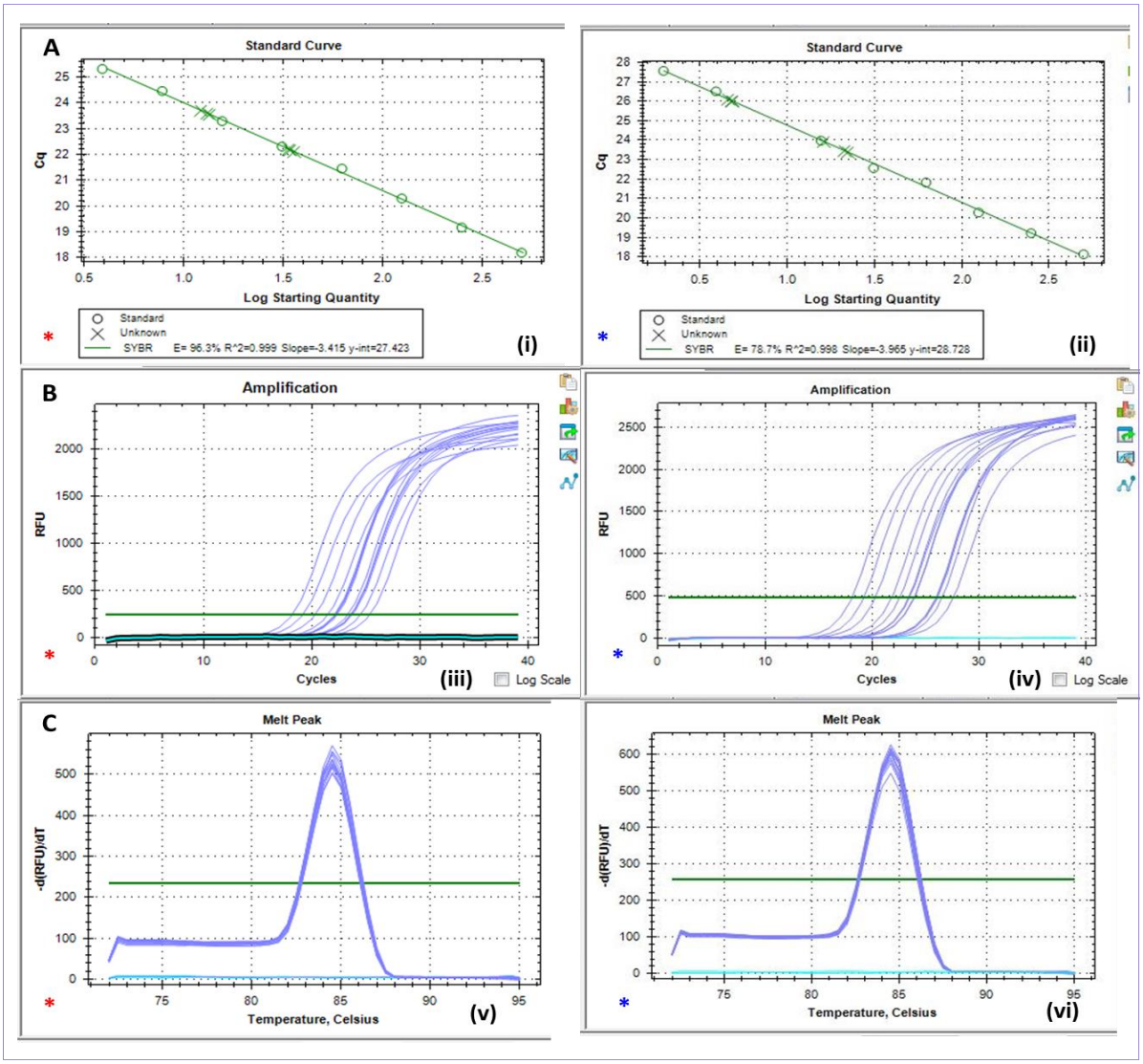

Figure 3.29: Amplification plots for CQ-treated *An. funestus s.s.* CTL4 quantification. Graphical representation of RPS26, **[A (i-ii)]** standard curve where tagert samples lie within the curve, **[B (iii-iv)]** amplification curve showing exponential growth and C_Q values, **[C (v-vi)]** dissociation peaks resulting in amplification of single qPCR products. The red asterisk star represents *P. falciparum* reactions, whereas the blue asterisk star represents CQ-treated reaction.

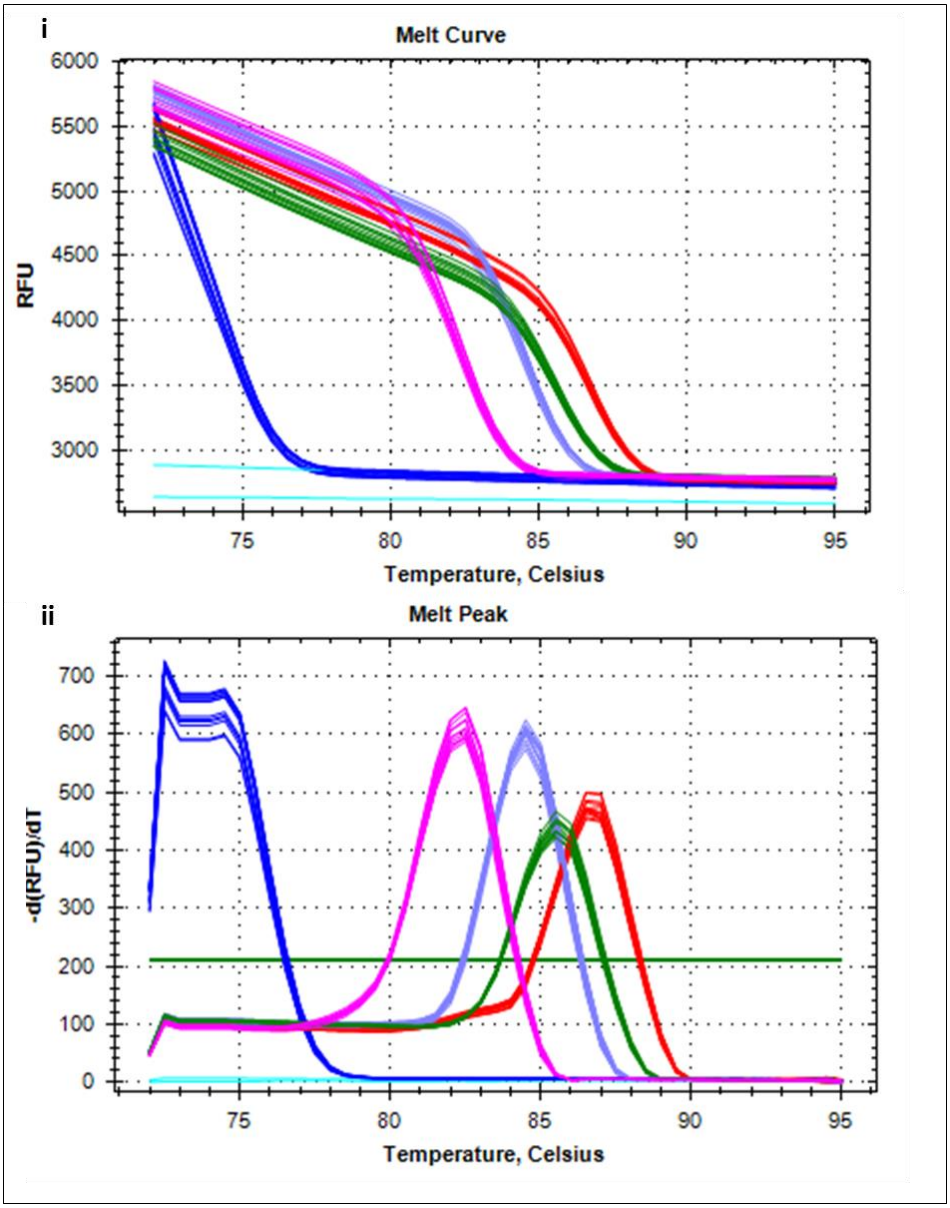

Figure 3.30: Quantification plots of *An. funestus s.s.* after treatment with CQ. Graphical representation of combined genes dissociation (i) curve and (ii) peak showing single peaks indicating amplification of a single qPCR product. NTC are shown by the blue line at the bottom of the curves. Gene identifications are as follows: CTL4 shown in pink, RPS26 shown in blue, RPS7 shown in green, RPL19 shown in red and ND_5 shown in dark blue. The NTC and SYBR + H_2O are shown in light blue at the bottom of the curves.

Additionally, agarose gel electrophoresis and sequencing for the CQ-treated *An. funestus s.s.* was performed to assess whether the correct gene(s) of interest were being amplified and to rule out incorrect amplification, contamination, template degradation or primer inefficacy as the cause of the low qPCR efficiency.

The electrophoresed qPCR products show cDNA profiling with expected single amplicon sizes of 226, 134, 160, 223 and 122bp long for CTL4, RPS7, RPS26, RPL19 and ND_5, respectively (Figure 3.31).

A BLASTn search in Vectorbase resulted in 100% coverage of the edited sequences from the chromatogram (Sanger sequencing) that where aligned with those in the database resulted with a negative E values between 10^{-38} - 10^{-54} and a sequence similarity identity score between 97.8-100%.

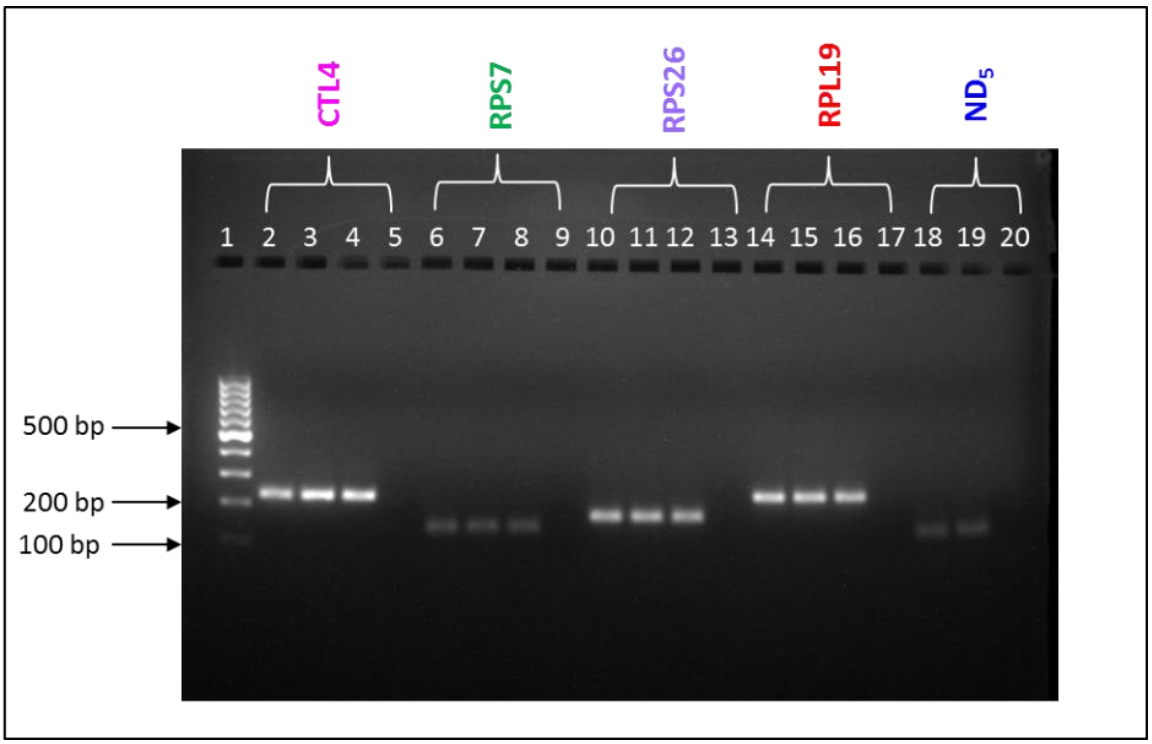

Figure 3.31: Amplification of qPCR products in CQ-treated *An. funestus s.s.* cDNA fragments of qPCR products were visualized in a 2.5% (w/v) non-denaturing agarose gel, sizes were estimated by comparison to a 100bp DNA ladder (MWM). qPCR products were loaded as follows: lanes 1 MWM; lanes 2, 3 and 4 CTL4, lane 5 CTL4 NTC; lanes 6, 7 and 8 RPS7, lane 9 RPS7 NTC; lanes 10, 11 and 12 RPS26, lane 13 RPS26 NTC, lanes 14, 15 and 16 RPL19, lane 17 RPL19 NTC, lanes 18 and 19 ND_5 and lane 20 ND_5 NTC.

CHAPTER FOUR

4 Discussion

Malaria continues to be an important public health issue and one of the leading causes of deaths globally (WHO, 2019). Despite the progress in reducing the burden caused by malaria, Africa still experiences the highest number of cases and deaths globally (WHO, 2019). The emergence of drug resistance by the malaria parasites compromises the efficacy of the current antimalaria drug therapies (WHO, 2019). Moreover, insecticide resistance by members of the anophiline mosquitoes also undermines the current vector management control strategies (WHO, 2019). With these considerations, there is an urgent need for new malaria management control tools that will improve the efficiency or complement the current existing control tools (Ndo *et al*., 2016). The introduction of transgenic vectors to wild *Anopheles* populations in order to disrupt parasite transmission is an approach that is being pursued (Ndo *et al*., 2016). In order to achieve this, an understanding of specific interactions between the *Anopheles* vector and its malaria parasite, and particularly the associated immune response is important. The immune response by the mosquitoes robust immune system has been shown to play a significant role which influences: 1) whether the *Plasmodium* parasite infection can be established in the *Anopheles* vector and 2) whether the ingested parasite committed to sporozoite development can be transmitted to another host (Habtewold *et al*., 2017). Key mechanisms, pathways and molecules/compounds involved in the mosquitos' innate immune system that is critical for the successful development of the *Plasmodium* parasite were highlighted in the Introduction (Sections 1.4-1.11) and any influences that interrupts the parasite from completing its life cycle. As such, one key immune molecule, CTL4 was investigated in this MSc project.

4.1 Characterization of *An. funestus s.s.* CTL4

Invertebrates such as mosquitoes lack an adaptive immune system, so they rely on their innate immune system to defend them against foreign microorganisms and substances. The highly conserved PAMPs on the surface of invading pathogens (parasites, bacteria or fungi) are recognized by the mosquitoes PRR, which in turn trigger various cellular and humoral immune responses (Hillyer, 2010; Kumar *et al*., 2018). As members of PRRs, CTLs play a significant role in pathogen recognition through binding of cognate carbohydrate structures in most cases in a calcium-dependent manner (Drickamer and Taylor, 1993; Zelensky and Gready, 2005).

Several CTLs have been identified in the *An. gambiae* genome (Christophites *et al*., 2002), but their detailed molecular and structural features and function are not well understood. This study reports on a C-type lectin (*Af*CTL4) in *An. funestus s.s.*

The mRNA *Af*CTL4 is 721bp long with a 534bp open reading frame that encodes a 177 amino acid protein with a molecular weight of 20.186kDa (vectorbase.org). Genetic analysis by PCR in this study showed successful amplification and sequencing of segments of the CTL4 exons (Figure 3.12), confirming its presence in laboratory *An. funestus s.s*. The *Af*CTL4 comprises of a signal peptide, which anchors and transports the protein, through cell membranes (Kapp *et al*., 2000; Parker, 2001). Additionally, the signal peptide has 22 amino acid residues comprised of three distinctive features designated as N, H and C region (Figure 3.2). The N region residues is positively charged and located at the amino terminal end of the *Af*CTL4 protein, H region is typically the hydrophobic core of the signal peptide, whereas the C region is known to be involved in the recognition and cleavage by signal peptide (Andrews *et al*., 1992). The signal peptide tags and assists the transportation of the *Af*CTL4 protein to the correct location outside the cell membrane, in this case, during an immune challenge. Only one CTLD is present in the protein and it stretches from 53-177 residues with the following structural features: there are four cysteine residues C^{69}, C^{151}, C^{166} and C^{175} designated as C_1-C_4, which are involved in the stabilization of the CTLD by forming two disulphide bonds between C_1-C_4 and C_2-C_3, and a tri-cysteine that may form a disulphide heterodimer at C^{41}, C^{43} and C^{45} at the N-terminus with *An. funestus s.s* CTLMA2 (Figure 4.1).

Canonical structural motifs include a primary hydrophobic core, which is due to the presence of the β5 that is occupied by a hydrophobic isoleucine (I^{174}), and a negatively-charged glutamic acid (E^{176}). The latter interacts with α2D (mediated by calcium), a small hydrophobic core between α1W; F63 and β2 (β2W) and long loop hydrophobic region formed by β2 (β2W), β3 (β3V) and β4 (β4W). The long loop hydrophobic region has a highly conserved Trp-Ils-Gly-Leu WIGL motif, which is suggested to be involved in the integration of the hydrophobic cores (primary hydrophobic core, small and long loop hydrophobic region) (Zelensky and Gready, 2003). The *Af*CTL4 constitutes this WIGL motif, however with a substitution of leucine to alanine becoming WIGA (Figure 3.3). This is not surprising since they are both hydrophobic amino acids and substitution of other hydrophobic amino acids isoleucine is evident in *Homo sapien*s E-selectin CTL (PDB-igit) (Zelensky and Gready, 2003). The α2 of most CTLDs has a highly conserved glutamic acid (E) that mediates the interaction between α2 and β1 during invasion. The *Af*CTL4 α2 has an aspartic acid, this substitution of the highly conserved glutamic to aspartic acid is also evident in *Homo sapiens*

NKG-2D and CD69 CTLs whose PDB ID is 1kcg and 1e87, respectively (Zelensky and Gready, 2003). Furthermore, at the highly conserved C_2-C_3 at the base of the β3-β4, a β-hairpin with Ala-Glu-Ser-Met (AESM) and another one with Asn-Asn (NN) residues are present in *Af*CTL4 (Figure 4.1) (Zelensky and Gready, 2003; Mitchell *et al*., 2019). In addition, it has been suggested that the β3-β4 disulphide bridges may be responsible for the stabilization of the long loop region since *Caeno-rhabditis elegans* and mammalian CTLD sequences either lack β3, β4 or both cysteine residues, suggesting that they may not be essential for CTLD stabilization (Zelensky and Gready, 2003).

*Af*CTL4 lacks the key canonical QPD and EPN motifs which are involved in galactose and mannose binding respectively, the WND motif is differentiated of tryptophan by alanine (A^{82}). This differentiation may not be true since this motif has been reported to be highly conserved in vertebrates (Iwanga and Lee, 2005). The evolutionary distinction with regards to invertebrates is highlighted by the absence of the WND motif and if present, mutations such as Phe-Arg-Asp (FRD) and Val-Asn-Asp (VND) are observed (Xiu *et al*., 2016). These findings warrant further investigation since *Ae. aegypti* has the WND motif in its CTLD (Figure 3.4B). In addition, Wang *et al*. (2018) reported that invertebrate Japanese spiky, sea cucumber *Apostichopus japonicas* (*Aj*CTL2) has a WND motif in its CTLD. Other invertebrate CTLs containing the WND motif includes *Aedes alboticus* (*Ae. lb* CTL1), *Ae. aegypti* (mosGCTL-1) and *Culex quinquefasciatus* (*Cq* CTL54) (Cheng *et al*., 2014). It has been previously reported that only asparagine and aspartic acid (ND) are involved in calcium coordination, tryptophan (W) contributes to the β4 hydrophobic core (Zelensky and Gready 2003). In this regard, the *Af*CTL4 ND motif (positions 46-47; Figure 3.3) may be a stand-alone motif, since another ND motif is present (positions 107-108; Figure 3.3). The presence of the ND motif suggests that *Af*CTL4 CTLD is characteristic of calcium coordination and carbohydrate binding (Figure 4.2B) (Zelensky and Gready, 2003). In contrast, *An. gambiae* CTL4 does not have any calcium binding affinity (Bishoni *et al*., 2019), as it lacks the ND motif in its sequence (Figure 3.4).

Phylogenic analysis revealed that *Af*CTL4 is a member of the CTL superfamily and it has emerged before members of the *An. gambiae* complex (Figure 3.5). Interestingly, *An. funestus s.s*, whilst distributed in Africa, it is more closely related to vectors that are distributed in Asia, such as *An. minimus* ortholog (Harbach, 2004).

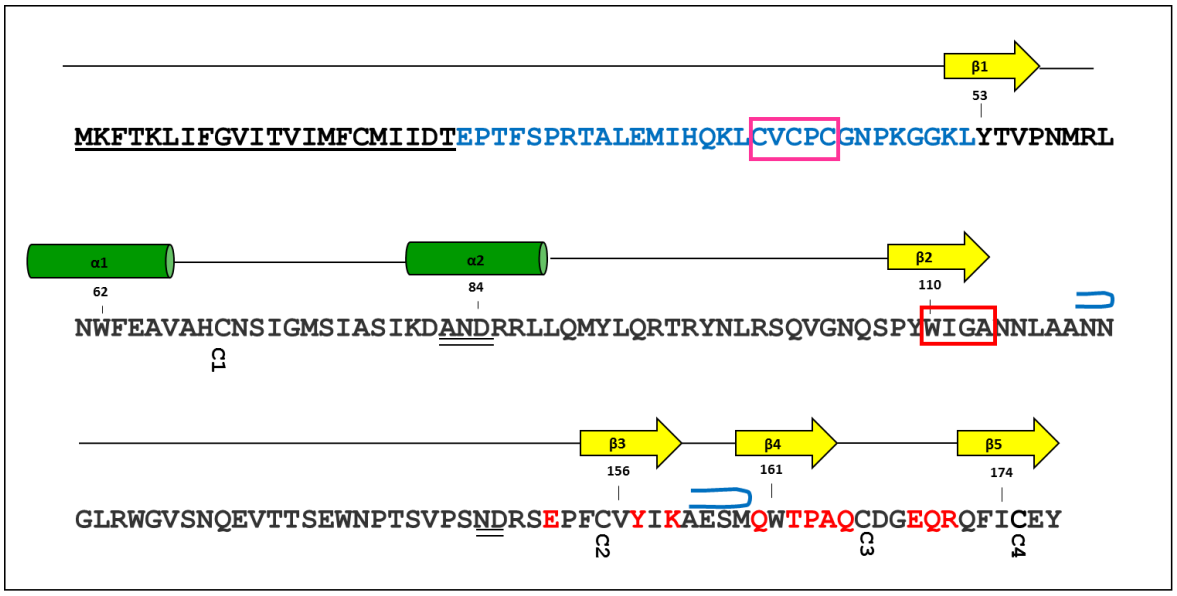

Figure 4.1: Molecular features and secondary structure elements of *An. funestus s.s.* CTL4. Deduced amino acid residues (177bp), signal peptide (1-22) is underlined, tri-cysteine disulphide heterodimer boxed in pink. Functional CTLD begins at β1 (βY) and ends at β5 (βI; E176), AND and ND motifs double underlined, WIGA motif boxed in red and hairpin loops shown in blue. Predicted ligand binding sites shown in red. *Figure drawn by student*.

Homology modelling generally refers to the theoretical construction of a tertiary structure of a protein from its amino acid sequence. This however remains complex as different amino acids have the potential to assume any conformational folding. The conformational characteristics of the tertiary structure of *Af*CTL4 showed that all structures comprised of at least two α helices and two β sheets (Figure 3.6). One major limitation in homology modelling is when the query sequence lacks conserved residues or structural regions to already resolved structures available in PDB. Advances in the field have led to the development of Quark (Xu *et al*., 2012), a template free protein modelling tool where the global fold is generated by the incorporation of *ab initio* algorithm with replica-exchange Monte Carlo (REMC) simulation, which work together to assemble the protein structure. Quark structural prediction is divided into three st ages which involves multiple feature predictions and generation of fragment/s on the query sequence, structural construction using REMC simulation on the bases of semi-reduced protein model and decoy structure clustering and full atomic refinement.The acceptable percentage identity between query and reference sequences used to generate a reliable tertiary structure model includes a cutoff 25%, resolution cutoff 1.8 Åand an R-factor cut off 0.25.

Although it is not advisable to use template free tools, Quark out performed some of the best servers during the Critical Assessment of protein Structure Prediction (CASP9) experiment. Template based RaptorX (Kallberg *et al*., 2012) and Phyre2 (Kelly *et al*., 2015) have a similar approach in assembling the tertiary structure and they both performed well in the CASP9 experiments (Kallberg *et al*., 2012; Kelly *et al*., 2015). Quark produced five models, which it ranked from top $M1_Q$-$M5_Q$ least possible structure, on this bases only three models $M1_Q$, $M2_Q$, $M3_Q$ were analysed. Since RaptorX and Phyre2 predictions are template-based, the resulting models $M1_R$ and $M1_P$ were the only top models resolved from the servers.

One of the keys in understanding biological processes is the availability of a structural model of a protein (Wiederstein and Sippl, 2007). Therefore the assessment of the tertiary structure of a protein predicted experimentally or theoretically is crucial especially for practical uses such as biochemical experiments and rational drug design. All models resolved from Quark, RaptorX and Phyre2 were assessed by Protein Structure Analysis web server (ProSA). All models resolved by Quark were located in the NMR region of previously crystalized protein structures, but their Z-scores varied. The local energy plot showed that model $M3_Q$ adopts a more stable state in comparison to $M1_Q$ and $M2_Q$ were most of their amino acid residues were located in the positive region of the plot that corresponds to erroneous assembly in parts of the protein structure (Figure 3.6A) (Wiederstein and Sippl, 2007). It is interesting that model $M3_Q$ was ranked the least possible structure in comparison to $M1_Q$ and $M2_Q$, but was the most stable. Since models $M1_R$ and $M1_P$ were assembled using crystalized templates including 5e4k and 5aO6 respectively which were ranked top templates by the tools. The 5e4k and 5aO6 Z-score (analysed by ProSA) was -4.19 and -4.1 respectively, which were similar to the -4.05 and -4.09 of the predicted structures by RaptorX and Phyre2, respectively (Figure 3.6 B; C). The local energy plot of models $M1_R$ and $M1_P$ adopts those of templates 5e4k and 5aO6 respectively. One of the advantages of using template based tools is their ability to predict unreliable segments of the protein structure that correspond to residues located in the positive values in the local energy plot. In order to obtain reliable tertiary structures, Killerberg *et al*. (2012) suggests the removal of the disordered regions of the sequence and to assemble the new structure from the remaining residues. Moreover, if more than 50% of the query is predicted to have disordered segments, Phyre2 server states that such a model is unreliable (Kelly *et al*., 2015). The $M1_P$ had a total of 32% of disordered segments implying that the structure was relatively reliable (Figure 3.9) (Kelly *et al*., 2015)

The Ramachandran's plots were further used to assess the quality and assist in the selection of the best theoretical tertiary structure for *Af*CTL4. The plots from PROCHECK (Laskowski *et al*., 1993; 1996) are based on analysis of 118 structures at a resolution of at least 2.0 Angstroms (Å) and over 90% of amino acid residues were expected to occupy the most favourable regions for a model to be considered of good quality. None of the predicted models fulfilled this criterion, however models $M1_R$ and $M1_P$ had over 80% residues in the most favourable region, whilst the other percentages were distributed in the additional and generously allowed region (Figure 3.10B, C). The remaining residues were in the disallowed region (Ramachandran' outliers), which reduces the quality of the structures. However, a few percentages of 0.6% and 2.5% for $M1_R$ and $M1_P$, respectively, values lower than those from the Quark models were outliers. Additionally, the PROCHECK Ramachandran's plot predicted 0.6% and 2.5% residues were located in the disallowed region for crystalized structures 5e4k and 5aO6, respectively. The PDB validation report shows a 0.2% and 0% Ramachandran's outliers for 5e4k and 5aO6, respectively. These discrepancies may be due to the differences in approaches used for construction or calculation. The resolution of the template structures used is 2.58 and 2.5Å for 5e4k and 5aO6, respectively, a value higher than that in PROCHECK criterion (Laskowski *et al*., 1993; 1996). Therefore, based on these analyses, the tertiary structure predicted by RaptorX and Phyre2 were the best models found in this study to best describe the conformational folding of the *Af*CTL4. In support of this study's suggestion, these structures adopt similar conformational folding of the preliminary experimentally determined *An. gambiae* CTL4 (Figure 3.6D) (Bishnoi *et al*., 2019). Additionally, the *Af*CTL4 CTLD fold adopts similar conformational CTLD fold comprising of a double-loop fold, two α-helices and five β sheets, which is stabilized by two highly conserved disulphide bridges as decribed previously (Zelensky and Gready, 2003; Zelensky and Gready, 2005).

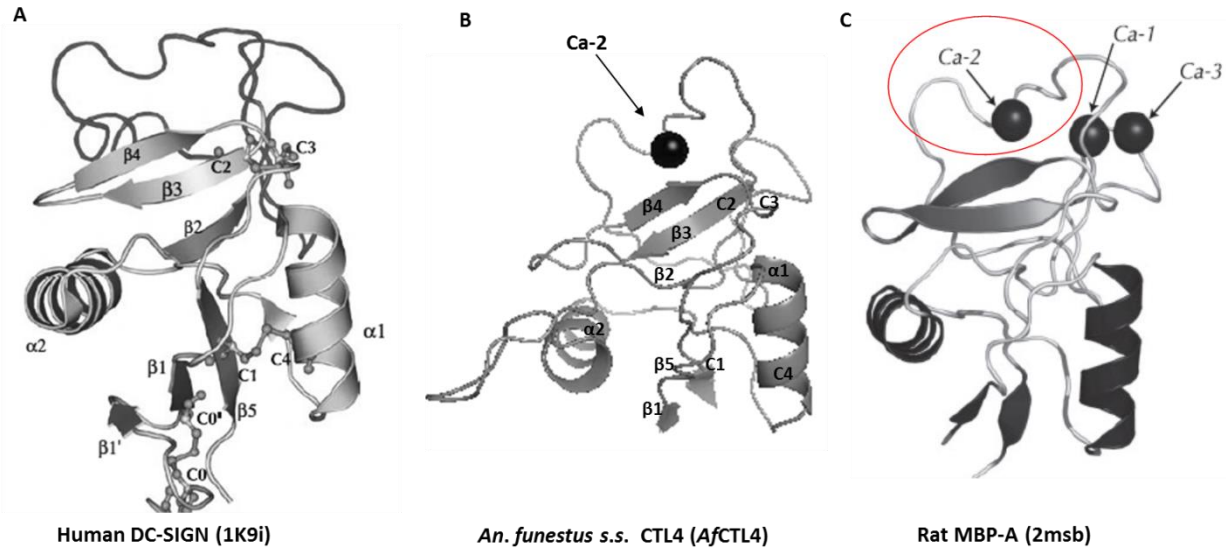

Figure 4.2: C-type lectin domain. Ribbon diagrams for the numbering of the CTLD secondary structure elements and calcium binding sites. (B-C) *An. funestus s.s.* CTL4 and at Rat MBP-A showing three of four typical locations for calcium as black spheres. Secondary elements are numbered according to the universal numbering systems shown in Human DC-SIGN.

4.2 Optimization of the feeding rate

Anopheles funestus s.s. CTL4 has been successfully isolated, this enables for the expression studies to be peformed. Therefore optimization of the feeding rate was essential in order to obtain sufficient blood fed mosquitoes for expression studies. Adult females of the anophiline mosquitoes are anautogenous, a property which forms the fundamental basis for the colonization and maintenance in the mosquito species in the laboratory (Luo, 2014). In early studies, the blood meal for feeding laboratory colonies was obtained from live donated human blood, human volunteers and live animals (Boyd *et al*., 1935; Rozeboom, 1936). This direct blood feeding provided the blood meal in its natural cues of feeding resulting in rapid egg production and colonization (Kasap *et al*., 2003). However, direct feeding caused accidental transmission of mosquito borne diseases (Bailey *et al*., 1978), donated blood carried a risk of blood-borne pathogens whereas the use of live animals has proven to be expensive because their housing requires care and maintenance which is also time consuming (Kasap *et al*., 2003).

In order to reduce these risks, a more convenient cost effective and efficient feeding system was developed. Gonzales and Hansen, (2016) suggested essential requirements that an artificial diet must have in order to successfully replace the vertebrate blood and these include:

1) Females must readily ingest sufficient amount of the blood meal,
2) Vitellogenesis (formation and production of yolk when nutrients get deposited in oocysts) must be supported with large batches of eggs,
3) The mosquitoes behavioural traits and immunity must not be affected and
4) The competitiveness of the progeny must compare with mosquitoes in the wild.

Various types of membranes have been tested in artificial feeding systems for anautogenous insects, membranes such as animal tissue, Parafilm-M® and collagen have been previously used. These include, mesentery bags (Knowlton and Rowe, 1935), rat skin membranes (Woke, 1937), ox-cecum (Bar-Zeev and Smith, 1959), chicken skin (Bishopp and Gilchrist, 1994), collagen (Pothikasikorn *et al*., 2010) and Parafilm-M® (Lyski *et al*., 2011). Although ethics permitted the use of animal skin as membranes, the treatment process of the animal tissue was complicated, expensive and did not consider the welfare of the animal. The use of Parafilm-M® is inexpensive and has an increased feeding rate, however Parafilm-M® breaks easily and it is difficult to stretch to a uniform thickness (Lyski *et al*., 2011). Thus, in this study collagen casing, which was previously reported to have a textured gripping surface for the mosquito was used as a membrane (Lyski *et al*., 2011).

The diet of adult female mosquitoes have prior to a blood meal is important as it can affect their ability to feed. Adults that were provided with plain dH_2O (energy source, sugar water withdrawn) had an increased feeding rate, which was similar to that of the control group (Figure 3.13; Table 3.2). However, the adults that were fully starved resulted in a low feeding rate, which is attributed to by the increased mortality that was observed prior to the blood meal. Since adults provided with dH_2O had a feeding rate similar to the control, it was then used as a standard to determine the starvation period prior to blood meal. It is proposed that females starved for longer periods will have an increased feeding rate. This was proven (Figure 3.14; Table 3. 3), however tolerance to starvation was reached at 72 hours (the time period with the highest feeding rate), and due to the high mortality observed at 96 hours. Despite the mortality observed in adults starved at 96 hours, it was expected that all these adults would feed, however this was not the case since most were too weak to take a blood meal.

The mosquitoes that did feed at 96 hours starvation period died shortly after the blood meal, these observations suggest that the laboratory colony of *An. funestus s.s.* has a tolerance to which it can withstand starvation,. Further investigations must be conducted with this regard.

The blood feeding success rate was investigated in female adults of different ages. The results in this study showed that the blood feeding success rate was not affected by the age at which the mosquito was fed, i.e. there was no interaction between the age of the mosquito and blood feeding rate (Figure 3.15; Table 3.4). Additionally, the average cumulative probability of survival in day 10 (*Plasmodium* oocyst stage in *Anopheles* midgut) reached 82, 79 and 69% ($p = 0.0058$) for ages 5, 10 and 15 days old, respectively. Moreover, the average cumulative probability of survival of 15 days old adult females (*Plasmodium* sporozoite stage in *Anopheles* haemocoel/salivary glands) reached 82, 66 and 50% for ages 5, 10 and 15 days old adults, the survival rate of 15 days old adults continued to drop and reached 46% by day 18 ($p = 0.0058$). These observertions show that the older adults were more susceptible to death and that not all adult females that were blood fed were be able to live throughout the life cycle of the *Plasmodium* parasite. Collectively, these findings have not only upsized the colony in the insectory but also provide preliminary guidelines to follow in order to have the desired number of mosquitos for infection/treatment studies. This in turn can be used to further study vector-parasite interactions in the context of mosquito immunity.

4.3 Nucleic acid assessment in *An. funestus s.s.* provided with *P. falciparum* infected and CQ-treated blood meal

The success of downstream RNA application is dependent on the integrity and quality of the extracted RNA (Machaira *et al*., 2015). However, isolating high quality RNA is challenged by the presence of the ubiquitous ribonucleases that readily degrade the isolated RNA (Macharia *et al*., 2015). Thus, assessing the RNA quality prior to downstream application is mandatory. A denaturing agarose gel was used to assess the integrity of the RNA samples where only a bright band of approximately 2,000bp for 18S, faint 5.8S and 5S rRNA profiling were observed (Figure 3.17; 3.27). Previous studies showed that under denaturing conditions, the 28S rRNA of most insects including Diptera, Hymenoptera and Lepidptera dissociates into two equally sized α- and β-subunits that are produced by a breakage of the hydrogen bond that joins them (Ishikawa and Newburg, 1972). These subunits co-migrate together with the 18S rRNA and display a single bright fragment as observed in this study (Ishikawa and Newburg, 1972).

Furthermore, the dissociation of the 28S rRNA subunit is due to the presence of the Uracil-Adenine-Adenine-Uracil (UAAU) tract located at the 28S β-subunit upstream of the 5' end in the rRNA loop, which acts as a cleavage site (Ogino *et al*., 1990) and a phenomena also known as a hidden break (Winnebeck *et al*., 2010).

During eukaryotic central dogma i.e. from DNA, RNA and to protein, several gene regulation processes takes place, one of which involves the splicing of introns and joining of exons. Prior to mRNA formation, RNA processing results in the removal of introns resulting in an mRNA sequence comprising of exons. With this in mind, when cDNA was synthesized it was expected to be intron free since cDNA is usually obtained from mRNA. Therefore, agarose gel electrophoresis of intron-1 region one of the *Af*CTL4showed no amplification in *P. falciparum* immune challenged vs. non-immune challenges controls and chroroquine-treated and untreated controls (Figure 3.19; 3.28). Amplification of the intron region was evident when gDNA of *An. funestus s.s.* was used as a template. Furthermore, the NanoDrop readings for sample cDNA at A260/A280 absorbance were approximately 1.8, a value generally accepted for pure DNA (Taylor, 2010). These observations confirm that downstream template (cDNA) for quantification of *An. funestus s.s.* CTL4 was from mRNA sequence and not gDNA.

4.4 Confirmation of *P. falciparum* infection in *An. funestus s.s.*

The presence of *P. falciparum* (NF54-strain) was confirmed 24 hours post an infected blood meal. Analysis of the amplicon that codes for the circumsporozite protein (Oakley *et al*., 2018) was amplified. As expected, amplification of the circumsporozoite gene was detected in *An. funestus s.s.* fed with a blood meal infected with *P. falciparum* gametocytes, and no amplification was detected in *An. funestus s.s.* fed with uninfected blood meal (Figure 3.20). These results showed successful infection of laboratory *An. funestus s.s.* by gametocyte-rice *P. falciparum* (NF54-strain) infected blood. In addition, results also highlight the importance of optimising feeding conditions to conduct infection studies in laboratory *Anopheles* vectors using an artificial membrane feeding system.

4.5 Expression analysis of *An. funestus s.s.* CTL4 following immune challenge after *P. falciparum* infected blood meal

Relative quantitative qPCR was used to study the transcript abundance of *Af*CTL4 24 hours post immune and challenge following ingestion of *P. falciparum* infected blood meal. Selection of suitable reference genes for the normalization of *Af*CTL4 mRNA included the identification of potential reference genes and verifying the stability of these potential

reference genes. To achieve this, various mathematical algorithms have been developed with a goal of identifying suitable stable reference genes for gene expression analysis. Bestkeeper (Pfaffl *et al*., 2004), DeltaCt (Silver *et al.,* 2006), GeneNorm (Vandesomple *et al*., 2002), NormFinder (Andersen *et al*., 2004) and RefFinder (Xie *et al*., 2012) are amongst the most commonly used algorithms to select the best suitable reference genes. The use of single or inappropriate reference genes may weaken the detection of the gene of interest (Hellemans *et al*., 2007) and can lead to inaccurate normalization. Vandesomple *et al*. (2002) showed that the use of a single reference gene resulted in an inaccurate expression profile. Moreover, the use of more than one reference gene strengthens the detection of the gene of interest and produces reliable results. Thus, this study selected more than one reference gene, where four reference genes were screened in order to obtain suitable reference (2.5.3.1). Results from NormFinder showed that RPS26, RPS7 and RPL19 based on their low stability (Figure 3.21) values were suitable reference genes for normalization of *Af*CTL4 (Figure 3.21).

Relative quantification of *Af*CTL4 was made possible by the use of fluorescent SYBR Green 1 molecule that binds non-specifically to double stranded DNA (dsDNA). Although SYBR Green 1 has a high affinity for dsDNA, its application is time efficient and excludes the need for designing probes or primers (Biorad, 2006). In order to eliminate non- specific binding of SYBR Green 1, melt curves and peaks (Figure 3.22) were used and showed that amplification of each sample in the assay followed a similar trend, with a single peak that was specific for each amplicon at a certain melting temperature. These curves show that the qPCR was efficie, optimal and reproducible.

There was no non-specific binding or primer dimers that melted at different temperatures (Figure 3.22; 3.30), which further verifies that the qPCR reaction was optimal. Additionally, electrophoresis of the qPCR products showed single specific profiling for each gene, that strongly supports the conclusion that the reaction was running optimally (Figure 3.23; 3.31).

The transcript abundance of mosquito CTL4 has been previously described (Section 1.6.1.5) (Osta *et al*., 2004). This interaction between *An. gambiae* and *P. berghei*, however does not fully describe those that occur in the natural system of the *Anopheles* vector and its human parasite (Boet, 2005). Although the biological materials (*Anopheles* mosquito and *Plasmodium* parasite) used in this study were laboratory reared and cultured, they do provide insight into the natural system of vector-parasite interactions. One of the most critical stages of development for *Plasmodium* parasites in an *Anopheles* mosquito is when they emerge into motile elongated ookinetes which is 20-24 hours post the ingestion of an infected blood meal

(Figure 1.3). During the next 19-36 hours, ookinetes must transverse the basal midgut epithelial cells, this results into major parasite loses (Figure 1.4). Results from the *Af*CTL4 transcript abundance that *Af*CTL4 was not significantly ($p = 0.256$) different between *P. falciparum* immune-challenged mosquitoes and non-immune challenged mosquitoes. These results are in contrast with the study by Osta *et al*. (2004) where it was shown that *An. gambiae* CTL4 expression is up-regulated 24 hours post a *P. berghei* infected blood meal. However, the results of this MSc study do support those reported by Cohuet *et al*. (2006b), which investigated the CTL4 gene expression in *An. gambiae* in response to *P. falciparum* 24 hours post *P. falciparum* infected blood meal. It was reported that there was no significant difference in transcript abundance for CTL4 between *P. falciparum* immune-challenged mosquitoes and non-immune challenged mosquitoes. To verify these findings additional studies are required with studies using natural system combination of vector-parasite interaction.

Despite the incomparable transcript abundance of the mosquito CTL4 in response to *P. falciparum*, it has been shown to significantly contribute in the defense of the mosquito against Gram-negative bacteria; implying that it exhibits pleitropic functions in the mosquito innate immune system (Schnitger *et al*., 2009). In addition, a genome wide study comparing *An. gambiae* transcript abundance in response to *P. berghei* and *P. falciparum* showed co-adaptation of the mosquitoes innate immune system to infection by *P. falciparum*. Invasion by *P. berghei* ookinetes was found to induce the regulation of many genes, with changes in expression of up to 1,102 genes, which corresponded to 81% of the mosquitoes transcriptome. Invasion by *P. falciparum* ookinetes induced a more specific immune response of approximately 3.4% of the mosquitoes' transcriptome (Dong *et al*., 2006b). This might indicate that the *Anopheles* mosquitoes immune system and its human *P. falciparum* parasite have co-evolved together in that invasion by the *P. falciparum* is host specific.

4.6 Larvicidal toxicity

It is essential that vector control at larval stages of the mosquito must be effective against the larvae, with little or no impact on human and animal health, as well as the environment (WHO, 2016). Larvicidal control has been implemented as an intergrated approach to vector control and to reduce the abundance of adult mosquitoes (Filinger and Lindsay, 2011; WHO, 2016). Present day studies on larval control focuses mainly on larvicides of natural plant origin because they are eco-friendly, cheap, easy to administer, biodegradable and have little to no impact on non-target organisms (Baranitharan *et al*., 2019).

Quinolines are alkaloids of plant origin with *N*-based heterocyclic aromatic compounds that have a broad range of bioactivities including: antibacterial, antifungal, antitumor, anti-inflammatory, antiparasitic, antimalarial and insecticidal (Shang *et al*., 2018). The antimalarial drug, CQ is a quinoline derivative that was tested to assess its larvicidal activity against *An. funestus s.s.* larvae. Chloroquine did not have any larval activity against *An. funestus s.s.* larvae, which could be due to the presence of an electron withdrawing group present in the CQ structure (Figure 4.3). This was proposed by Begum *et al*. (2011) who investigated the structure activity relationship of chalcone compounds on larvae, and reported that compounds comprising of an electron donating group in their structure showed high toxicity against *C. quinquefasciatus* larvae compromising/ killing the larvae whereas those with electron withdrawing group do not have larval activity.

The findings of this study are supported by those by Kathrada (2015) where the lack of larvicidal activity by CQ at 0.5µM was observed in CQ derivatives (7-chloroquinoline-4-yl-piperazine-1-yl acetamids and 7-chloroquinoline-4-yl-piperazine-1-yl pyrolidin-2-yl), where these derivatives possessed electron withdrawing groups in their structure and exhibited no larval activity against *An. arabiensis* KGB strain (Figure 4.3). For comparison, the insecticide, DDT was also tested as per WHO recommendations to continuously test efficacy of insecticides (WHO, 2019). As such, abnormalities in the morphology of the *An. funestus s.s.* larvae were microscopically observed in those treated with DDT in comparison to untreated control and CQ-treated larvae (Table 3.6).

In most cases, the overall physical appearance of the larvae incubated in DDT was severely compromised, such as detachment between the head and thorax and loss of abdominal integrity was observed 24 hours post incubation (Table 3.6). Dead larvae either floated at the edges of the cups or sink to the bottom of the cup. These observations show that it is efficient against *An. funestus s.s.* larvae, as reported previously when *An. arabiensis* (KGB-strain) larvae were incubated in 0.5µM DDT, where a 100% mortality was accompanied with compromised morphological appearance (Kathrada, 2015).

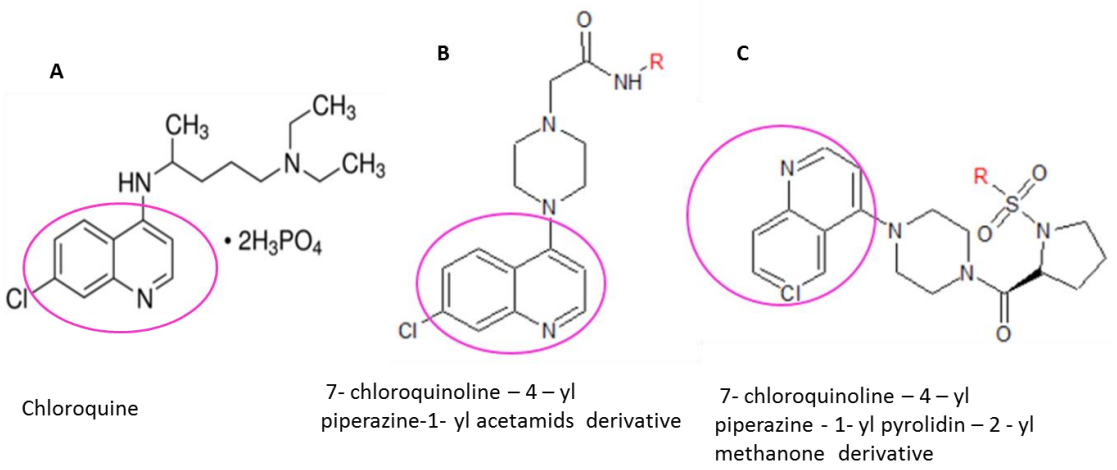

Figure 4.3: Structural similarities between antimalarial compounds. Antimalarial compounds comprising of an electron withdrawing group circled in purple (Kathrada, 2015).

4.7 Expression analysis of *An. funestus s.s.* CTL4 following treatment with CQ

The various mechanisms of action of CQ has been widely studied, however very little is known of its action/s in invertebrates such as mosquitoes (Abrantes *et al*., 2005). The presence of CQ in a blood meal has been linked with an increase in *Plasmodium* parasite infection of the mosquito. Hogh *et al*. (1998) reported that mosquitoes provided with a blood meal from human volunteers treated with 25mg/kg CQ and infected with *P. berghei* and *P. falciparum* gametocytes showed a 4 to 5 fold increase in the mean oocyte number. A similar enhanced infection of mosquitoes by *P. yoelii nigeriensis* (N67-strain) was observed when mice were treated with CQ 12 hours before the mosquitoe's blood meal (Ichiomori *et al*., 1990). These studies suggest that the increase in infectivity to the mosquitoes was a result of CQ interfering with the ability of the mosquito to respond to infection (Abrantes *et al*., 2005).

Abrantes *et al*. (2005) was the first to report on the effect of CQ on the mosquito immune response and showed that mosquitoes provided with a CQ-treated blood meal resulted in the down regulation of transcript abundance of some AMPs and serine proteases of *An. gambiae*. A genome wide transcript abundance study showed that the mosquito immune related genes that were previously known to strongly respond to midgut invasion by *Plasmodium* ookinetes were differentially expressed in the presence of CQ (Abrantes *et al*., 2008). Interestingly, mosquito CTL4 previously shown to protect *P. berghe*i ookinetes against melanization (Osta *et al*., 2004) was together with other immune related genes down regulated in CQ-treated *P. berghe*i infected mosquitoes (Abrantes *et al*., 2008).

Furthermore, mosquitoes provided with a higher dosage (50mg/mL) were excessively engorged with the treated blood meal.

The presence of CQ in blood has a significant impact on the transcript abundance of mosquito immune-related genes, where it is known to down regulate genes involved in adhesion, apoptosis, cytoskeleton, immune and oxidative stress (Abrantes *et al*., 2008). These contribute to the suppression of the well-established robust defence system in *Anopheles* vectors which in turn lead to enhanced *Plasmodium* infectivity in CQ infected mosquitoes (Abrantes *et al*., 2008). In an attempt to investigate the effect that CQ has on *Af*CTL4, a pilot study to determine the dosage of CQ to add in the blood meal was conducted. Mosquitoes provided with a blood meal containing 5mg/mL of CQ resulted in a higher feeding rate in comparison to those with a higher concentration (Figure 3.26). The difference in feeding rate in the control group vs. the CQ-supplemented blood could be largely due to the presence of CQ in the blood meal. Furthermore, the knockdown effect and mortality observed in CQ50 and CQ25 blood fed mosquitoes (Table 3.7) could have been due to the impairment of the innate immune system of the mosquito by the high dosage of CQ in the blood meal. In support of observation in this study, those by Abrantes *et al*. (2005) showed that in the presence of CQ, transcript abundance of some immune genes including antimicrobial peptides and serine proteases previously shown to act against *Plasmodium* invasion of the midgut were down regulated in the presence or absence of infection. Therefore, it is proposed that high doses of CQ in the blood meal compromises the mosquitoes immune response, which eventually leads to death of the *Anopheles* mosquito. The dose-dependent inhibition is not observed at low CQ dosages (Table 3.7). Further investigations are required to investigate this latter effect.

Although amplification of the desired qPCR product was obtained, primers working efficiently and a standard curve that is inclusive of all CQ-treated and untreated samples was obtained, the efficiency of the qPCR was below the accepted 90-100% range (Figure 3.29). Unfortunately relative quantification could not be performed. This low efficiency may be due to contaminating Taq inhibitors in the sample or sequence with secondary structures (Taylor *et al*., 2010). Assays were undertaken to eliminate the contamination and inefficiency of the Taq as the possible reason, but this was not the case since the negative controls (SYBR + water and NTC) did not amplify any product (Figure 3.31). Although dissociation curves showed single product per reaction, it could be that the annealing temperature was not optimal for this treatment and in future to increase reaction efficiency, experiments should be set up such that note is taken on the concentrations of the template in the standard curve and must be adjusted to achive a reaction efficiency within accepted range (Taylor *et al*., 2010).

Alternatively, other reference genes can also be screened. Since whole human blood from three different donors whose medical history is unknown the blood meal could have other factors that may have contributed to the low efficiency because reference genes were changed (data not shown) and the efficiency of the qPCR was still not within the acceptable range 90-105%. In addition, in this study, the process of delivering CQ-treated blood to the mosquitoes was such that CQ was added directly to the blood, whereas in previous studies, CQ-treated blood first passed through a natural biological system of human volunteers (Hogh *et al*., 1998) or mice thereafter provided to mosquitoes (Ichimori *et al*., 1999; Abrantes *et al*., 2005; Silvera *et al*., 2007 and Abrantes *et al*., 2008). Some of the CQ ingested by these mammals is metabolized (Figure 4.4). Hoever, in this study, the mosquitoes received CQ that is not metabolized by any natural system. Most of the available data on the metabolism of CQ has been largely based on studies amongst healthy individuals, where CQ was administered orally as a phosphate salt, thereafter absorbed completely in the gastrointenstial tract (Lee *et al*., 2011; Schrezenmeier and Dorner, 2020). Well absorbed CQ has a bioavailablity of 70-80% following oral administration and a half-life of 40-60 days. As a weak base, CQ accumulates in high concentrations within acid rich vesicles including the lysosome which is an important site for the action of CQ of the kidney, liver, lung and spleen cells (Al-Bari, 2015). Plasma and blood concentration of CQ vary amongst patients. Chloroquine is a substrate for cytochrome P450 enzymes and is partly metabolized in the hepatic cells (Figure 4.4).

The metabolism of CQ begins when CQ is dealkylated by CYP2C8 and CYP3A4 to desethylchloroquine, which is dealkylated by CYP3A5 and CYP2D6 to bisethylchloroquine. CYP1A1 further dealkylates bisethylchloroquine to a transient metabolite, 7-chloro-4-aminoquinoline (Ducharme *et al*., 1996; Projean *et al*., 2003; Schrezenmeier and Dorner, 2020). The elimination of CQ from the body is a slow process, 58% of unmetabolized CQ is exctreted in urine (Schrezenmeier and Dorner, 2020) and 19% is excreted in feaces (McChesnay *et al*., 1967). The effect of CQ on a mammal's immune system is immune-supressing (Section 1.10.3-1.10.4), as is the effect in mosquito immune-related genes (Abrantes *et al*., 2005; Abrantes *et al*., 2008; Silveira *et al*., 2007). Thus, it is proposed that the mechanism of action and metabolism of CQ and other antimalarial drugs in the *Anopheles* vector requires investigations.

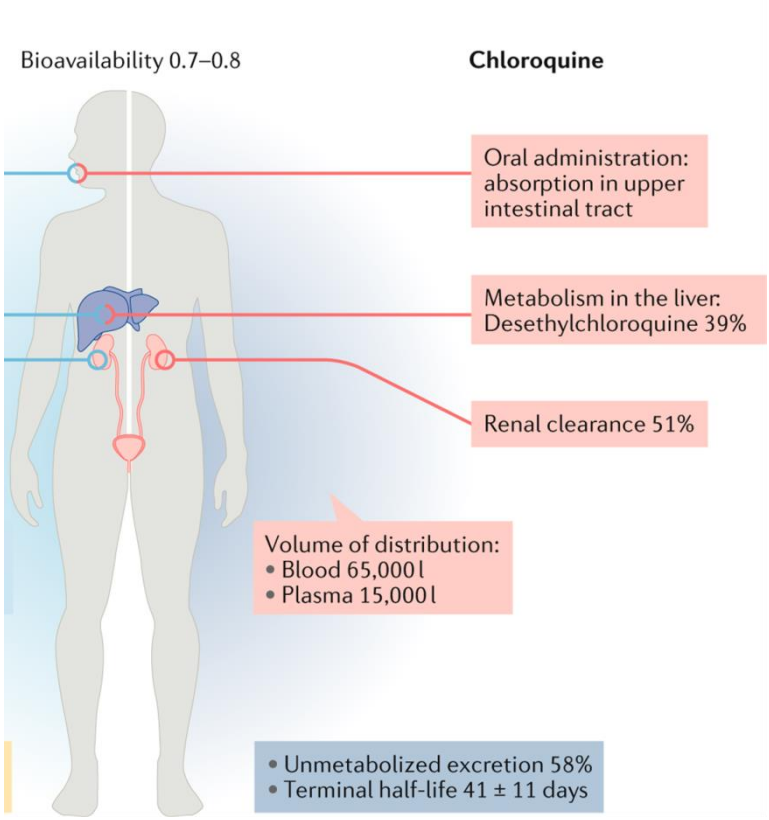

Figure 4.4 : Metabolism of CQ administered orally (Schrezenmeier and Dorner, 2020).

CHAPTER FIVE

5 Conclusion and Recommendations

5.1 Conclusion

The relationship between the malaria parasite and the *Anopheles* vector is essential in understanding the transmission cycle of malaria. The immune system of the *Anopheles* vector has been shown to play an important role in the development of the malaria parasite and transmission to a new host. This study shows the presence of CTL4, a PRR in *An. funestus s.s.* that has a single CTLD which is characteristic of two α-helices, five β-sheets, calcium-binding motifs at site-2 of the CTLD fold is involved in the binding of monosacharride and loops that are stabilized by two disulphide bonds. Infection by *P. falciparum* had no effect on the transcription level of the CTL4 in adult female *An. funestus s.s.* Chloroquine had no larval activity and the *An. funestus s.s.* larvae were able to progress to the adult stages. However, the presence of CQ increased the mortality of *An. funestus s.s.* adults in a dose-dependent manner, confirming the theory that CQ suppresses the immune response of the *Anopheles* vector interfering with signal transduction pathways at transcriptional level. This highlights the importance of understanding the impact that antimalarial drugs, such as CQ and other commonly used prophylactic and treatment drugs have on parasite transmission.

5.2 Recommendations

This study focused on the transcript abundance of CTL4, an immune related gene. A genome wide study has shown that there are other immune related genes that are differentially expressed in *An. gambiae* in response to *P. falciparum* infection (Dong *et al*., 2006b). The role of these genes should also be evaluated in *An. funesus s.s.* such that they can be used in transmission blocking studies and implemented as vector control genes. Since there is little information of CTL4 in other *Anopheline* species, there is a need for sequencing of the CTL4 or other CTLs in other *Anopheline* species. Earlier studies of choloroquine-treated blood meal fed on *Anopheles* vectors suggested that the immune response was impaired by CQ resulting in high *Plasmodium* infection. Our pilot study supports this necessity to further investigate, the impact of CQ on the *Anopheles* vector, which could lead to the elucidation of the mechanism of action of CQ and other aminoquinolines in the *Anopheles* vector. It is proposed that since the *An. funestus s.s.* CTL4 transcript abundance was not successfully determined in CQ-treated mosquitoes, that these experiments must be repeated to verify the observed outcome from this study giving more attention to the choice of reference genes and optimization of the annealing temperature in the qPCR. If the same outcome is determined,

then it is proposed that a more natural *in vivo* system using mice and *P. berghei* is used to deliver CQ and other aminoquinolines. Or alternatively, blood is obtained from patients taking CQ to observe the effects of the metabolites on the vectors' immune system. In addition, to avoid the laborious work and expenses that comes with the care of mice, the development of a "standard" dosage of drug/compound that can be added to the blood meal for artificial membrane feeding system would be beneficial.

CHAPTER SIX

6 References

Abrantes, P., Lopes, L. F., do Rasario, V. E. and Silveria, H. **(2005)**. Effect of chloroquine on the expression of genes involved in the mosquito immune response to *Plasmodium* infection. *Insect Biochemistry and Molecular Biology*, 35, 1124-1132.

Abrantes, P., Dimopoulos, G., Grosso, A. R., do Rosario, V. E. and Silveria, H. **(2008)**. Chloroquine mediacted modulation of *Anopheles gambiea* gene expression. *Insect Biochemistry and Molecular Biology*, 3(7), 1-9.

Akorli, J., Gendrin, M., Pels, N. A. P., Yeboah-Manu, D., Christophides, G. K. and Wilson, M. D. **(2016)**. Seasonality and locality affect the diversity of *Anopheles gambiae* and *Anopheles coluzzii* midgut microbiota from Ghana. *PLOS ONE*, 11(6),1-18.

Al-Bari, M. A. (2015). Chloroquine analogues in drug discovery: new directions of uses, mechanisms of actions and toxic manifestations from malaria to multifarious diseases. *Journal of Antimicrobial Chemotherapy*, 70(6), 1608-1621.

Alano, P. and Billker, O. **(2005)**. Gametocytes and gametes. In *Molecular Approaches to Malaria*. Sherman 1st Ed. ASM Press, Chapter10, 191-219.

Andreadis, T. G. (2005). Evolutionary strategies and adaptations for survival between mosquito-parasitic microsporidia and their intermediate copepod hosts: a comparative examination of *Amblyospora connecticut* and *Hyalinocysta chapmani* (Microsporidia: Amblyosporidae). *Folia Parasitologica*, 52(1-2), 23-35.

Andersen, C. L., Jensen, J. L. and Orntoft, T. F. **(2004)**. Normalization of real-time quantitative reverse transcription-PCR data: a model-based variance estimation approach to identify genes suited for normalization, applied to bladder and colon cancer data sets. *Cancer Research*, 64, 5245-5250.

Andrew, D. W., Young, J. C., Mirels, L. F. and Czarnota, G. J. **(1992)**. The role of the N region in signal sequence and signal-anchor function. *The Journal of Biological Chemistry*, 267(11), 7761-776.

Aoi, W., and Marunaka, Y. **(2014).** Importance of pH homeostasis in metabolic health and diseases: crucial role of membrane proton transport. *BioMed Research International*, 2014, 1-8.

Armenteros, A. J. J., Tsirigos, K. D., Sonderby, C. K., Petersen, T. N., Winther, O., Brunak, S., von Heijne, G. and Nielsen, H. **(2019)**. SignalP 5.0 improves signal peptide predictions using deep neural networks. *Nature Biotechnology*, 37(4):420-423.

Bailey, D.L., Dame, D.A. Munroe, W.L. and Thomas. J.A. **(1978)**. Colony maintenance of *Anopheles albimanus* Wiedemann by feeding preserved blood through a natural membrane. *Mosquito News*, 38, 403-408.

Baranitharan, M., Barbara, S. and Gokulakrishnan. **(2019)**. Phytochemical profiling and larval control of *Erythrina variegate* methanol fraction against malarial and filarial vector. *Advances in Preventive Medicine*, April 16; 2641959.doi: 10.1155/2019/26419591-9. (Access date: 12/02/ 2020).

Bartholomay, L. C. and Michel, K. **(2018)**. Mosquito Immunobiology: The Intersection of Vector Health and Vector Competence. *Annual Review of Entomology*, 63(1), 145-167.

Barron, M. G., Paupy, C., Rahola, N., Akone-Ella, O., Ngangue, M. F., Wilson-Bahun, T. A., Pombi, M., Pierre Kengne, P., Costantini, C., Simard, F., González, J. and Ayala, D. **(2019)**. A new species in the major malaria vector complex sheds light on reticulated species evolution. *Scientific Reports*, (9), 1-13.

Bar-Zeev, M. and Smith. **(1959)**. Action of repellents on mosquitoes feeding through treated membranes or treated blood. *Journal of Economic Entomology*, 52, 263-267.

Bascones-Martinez, A., Mattila, R., Gomez-Font, R. and Meurman, J. H. **(2014)**. Immunomodulatory drugs: oral and systemic adverse effects. *Medicina Oral Patologica Oral Cirugia Bucal*, 19(1), 24-31.

Bauer, H., Kanzok, H. M. and Schirmer, R. H. **(2002)**. Thioredoxin-2 but not thioredoxin-1 is a substrate of thioredoxin peroxidase-1 from *Drosophila melanogaster*. *The Journal of Biological Chemistry*, 277, 17457-17463.

Beenel, J. J., White, S. E. and Shapiro, A. M. **(2005)**. Review of microsporidia-mosquito relationships: from the simple to the complex. *Folia Parasitologica*, 52(1-2), 41-50.

Begum, L. A., Roy, N., Laskar, R. A. and Roy, K. **(2011)**. Mosquito larvicidal studies of some chalcone analogues and their derived products: structure-activity relationships. *Medicinal Chemistry Research*, 20, 184-191.

Bennink, S., Kiesow, M. J. and Pradel, G. **(2016)**. The development of malaria parasites in the mosquito midgut. *Cell Microbiology*, 18(7), 905-918.

Benson, D. A., Cavanaugh, M., Clark, K., Karsch-Mizrachi, I., Lipman, D. J., Ostell, J. and Sayers, E. W. **(2013)**. GeneBank. *Nucleic Acids Research*, 41, D36-42.

Betteridge, D.J. (2000). What is oxidative stress?. *Metabolism*, 49(2 Suppl 1), 3–8.

Bio-Rad Laboratories. (2006). Real-Time PCR Applications Guide. https://www.bio-rad.com/webroot/web/pdf/lsr/literature/Bulletin_5279.pdf (Access date: 06/06/2017)

Billingsley, P. F. and Rudin, W. **(1992)**. The role of the mosquito peritrophic membrane in bloodmeal digestion and infectivity of *Plasmodium* species. *Journal of Parasitology*, 78, 430-440.

Bishnoi, R., Sousa, G. L., Contet, A., Day, C. J., Hou, D. C. F., Profitt, L. A., Singla, D., Jennings, M. P., Valentine, A. M., Povelones, M., and Baxter, R. H. G. **(2019)**. Solution structure, glycan specificity and phenol oxidase inhibitory activity of *Anopheles* C-type lectins CTL4 and CTLMA2. *Scientific Reports*, 9 (15191). https://doi.org/10.1038/s41598-019-51353-z. (Access date: 04/11/2019).

Bishopp, A. and Gilchrist, B. M. **(1994)**. A method for collecting sporozoites of *Plasmodium gallinaceum* by feeding infected *Aedes aegypti* through animal membranes, *Nature*, 153, 713-714.

Blandin, S. Moita, L. F., Köcher, T., Wilm, M., Kafatos, F. C., and Levashina, E. A. **(2002)**. Reverse genetics in the mosquito *Anopheles gambiae*: Targeted disruption of the Defensin gene. *EMBO Reports*, *3*(9), 852-856.

Blandin, S. and Levashina, E. A. **(2004a)**. Mosquito immune response against malaria parasites. *Current Opinion in Immunology*, 16, 16-20.

Blandin, S. Moita, L. F., Kafatos, F. C., Levashina, E. A., Shiao, S.-H., Janse, C. J. and Waters, A. P. **(2004b)**. Complement-like protein TEP1 is a determinant of vectorial capacity in the malaria vector *Anopheles gambiae*. *Cell*, 116(5), 661-670.

Bolling, B. G., Weaver, S. C., Tesh, R. B. and Vasilakis, N. **(2015)**. Insect-specific virus discovery: significance for the arbovirus community. *Viruses*, 7(9), 4911-4928.

Boete, C. (2005). Malaria parasites in mosquitoes: laboratory models, evolutionary temptation and the real world. *Trends in Parasitology*, 21, 445-447.

Boyd, M. F., Stratman-Thomas, W. K. and Kitchen, S. F. **(1935)**. On the relative susceptibility of *Anopheles quadrimaculatus* to *Plasmodium vivax* and *Plasmodium falciparum*. *American Journal of Tropical Medicine and Hygiene*, 15(s1), 485-493.

Brindha, V. (2014). Discovery of Malaria *Plasmodium* in an *Anopheles* mosquito by Ronald Ross - August 20, 1897. *Discovery*, 22(70), 6.

Burke, A., Dandalo, L., Munhenga, G., Dahan-Moss, Y., Mbokazi, F., Ngxongo, S., Coetzee, M., Koekemoer, L. L. and Brooke, B. **(2017)**. A new malaria vector mosquito in South Africa. *Scientific Reports*, 7, 43779. https://doi.org/10.1038/srep43779. (Access date: 05/04/2017).

Burke, A., Dahan-Moss, Y., Duncan, F., Qwabe, B., Coetzee, M., Koekemoer, L. and Brooke, B. **(2019)**. *Anopheles parensis* contributes to residual malaria transmission in South Africa. *Malaria Journal*, 18(257), 1-7.

Burkot, T. R. and Graves P. M. **(2000)**. Malaria, babesiosis, theileriosis and related diseases. Eldrige B. F. and Edman J. D. (eds). Medical Entomology. Springer, Dordrecht. https://doi.org/10.1007/978-94-011-6472-67. (Access date: 14/06/2018).

Cambi, A., Koopman, M. and Figdor, C. G. **(2005)**. How C-type lectins detect pathogens. *Cellular Microbiology*, 7(4), 481-488.

Castillo, J., Strand, M. R. and Robertson, A. **(2009)**. Characterization of hemocytes from the mosquitoes *Anopheles gambiae* and *Aedes aegypti*. *Insect Biochemistry and Molecular Biology*, 36(12), 891-903.

Center for Disease Control and Prevention. (2016). https://www.cdc.gov/malaria/about.biology/index.html. (Access date: 16/03/2019).

Cirimotich, C. M., Dong, Y., Garver, L. S., Sim, S. and Dimopoulos, G. **(2010)**. Mosquito immune defenses against *Plasmodium* infection. *Developmental and Comparative Immunology*, 34, 387-395.

Chemaly, S. M, Chen, C. T. and Van Zyl R. L. **(2007)**. Naturally occurring cobalamins have antimalarial activity. *Journal of Inorganic Biochemistry*, 101(5), 764-773.

Chen, Y., Lien, J., Tseng, L., Cheng, C., Lin, W., Wang, H. and Tsai, K. **(2019)**. Effects of indoor residual spraying and outdoor larval control on *Anopheles coluzzii* from São Tomé and Príncipe, two islands with pre-eliminated malaria. *Malaria Journal*, 18 (405), 1-16.

Cheng, G., Liu, L.,Wang, P., Zhang, Y., Zhao, Y. O., Colpitts, T. M., Feitosa, F., Anderson, J. F. and Fikrig, E. **(2011)**. An in-vivo transfection approach elucidates a role for *Aedes aegypti* thioester-containing proteins in flaviviral infection. *PLoS ONE*, 6 (7), e22786/ 1-7.

Cheng, J., Wang, Y., Li, F., Liu, J., Sun, Y. and Wu, J. **(2014)**. Cloning and characterization of mannose binding C-type lectin gene from salivary gland of *Aedes alboticus*. *Parasites and Vectors*, 7, 1-10.

Chomczynski, P. (1993). A reagent for the single-step simultaneous isolation of RNA, DNA and proteins from cell and tissue samples. *BioTechniques*, 15, 532-537.

Christian, R. N. (2011). The effects of pyrethroid resistance on transcription of metabolic enzymes in a major African malaria vector, *Anopheles funestus*. University of the Witwatersrand. (PhD dissertation) http://hdl.handle.net/10539/10961.

Christophides, G. K., Zdobnov, E.,Barllas- Mury, C.Birney, E., Blandin, S., Blass, C., Brey, P. T., Collins, F. H., Danielli, A., Dimopolous, G., Hetru, C., Hoa, N. T., Hoffmann, J. A., Kanzok, S. M., Letunic, I., Levashina, E. A., Loukeris, T. G., Lycett, G., Meister, S., Michel, K., Moita, L. F., Muller, H. M., Osta, M. A., Paskewitz, S. M.,Rechart, J. M., Rzhetsky, A., Troxler, L., Vernick, K. D., Vlachou, D., Volz, J, von Mering, C., Xu, J., Zheng, L. Bork, P. and Kafatos, F. C. **(2002)**. Immunity-Related Genes and Gene Families in *Anopheles gambiae*. *Science*, 298, 159-165.

Coetzee, M. (2017). Culicidae (mosquitoes). (*in Manual of Afrotropical Diptera*). Suricata Manual of Afrotropicaldiptera, 2, Chapter31, 677-692.

Coetzee, M. (2020). Key to the females of Afrotropical *Anopheles* mosquitoes (Diptera: Culicidae). *Malaria Journal*, 19(1), 70. https://doi.org/10.1186/s12936-020-3144-9 (Acess date: 15/01/21).

Cohuet, A., Simard, F., Toto, J. C., Kengne, P., Coetzee, M. and Fontenille, D. **(2003)**. Species identification within the *Anopheles funestus* group of malaria vectors in Cameroon and evidence for a new species. *The American Journal of Tropical Medicine and Hygiene*, 69 (2), 200-205.

Cohuet, A., Osta, M. A., Morlais, I., Awono-Ambene, P. H., Michel, K., Simard, F., Christophides, G. K., Fontenille, D. and Kafatos, F. C. **(2006)**. *Anopheles* and *Plasmodium*: from laboratory models to natural systems in the field. *European Molecular Biology Organization*, 7(12), 1285-1289.

Collins, F. H., Sakai, R. K., Vernick, K. D., Paskewitz, S., Seeley, D. C., Miller, L. H., Collins, W. E., Campbell, C. C and Gwadz, R. W. **(1986)**. Genetic selection of *Plasmodium*-refractory strain of the malaria vector *Anopheles gambiae*. *Science*, 234(4776), 607-610.

Coranado, L. M., Nadovich, C. T. and Carmenza Spadafora. **(2014)**. Malarial Hemozoin: From target to tool. *Biochimica et Biophysica Acta*, 1840(6), 2032-2041.

Cosgrove, J. B., Wood, R. J., Petric, D., Evans, D. T. and Abbott, R. H. **(1994)**. A convenient mosquito membrane feeding system. *The Journal of the American Mosquito Control Association*, 10(3), 434-436.

Dadzie, S. K., Brenyah, R. and Appawu, M. A. **(2013)**. Role of species composition in malaria transmission by the *Anopheles funestus* group (Diptera: Culcidae) in Ghana. *Journal of Vector Ecology*, 38, 105-110.

Dahalan, F. A., Churcher, T. S., Windbichler, N. and Lawniczak, M. K. N. **(2019)**. The male mosquito contribution towards malaria transmission: mating influences the *Anopheles* female susceptibility to human malaria parasites. *PloS Pathogen*, 15(11), e1008063.

Dambach, P., Louis, V. R., Kaiser, A., Ouedraogo, S., Sié, A., Sauerborn, R., and Becker, N. **(2014)**. Efficacy of *Bacillus thuringiensis* var. *israelensis* against malaria mosquitoes in northwestern Burkina Faso. *Parasites and Vectors*, 7, 1-8.

Das, S., Dong, Y., Garver, L. and Dimopoulos, G. **(2009)**. Specificity of the innate immune system: A closer look at the mosquito pattern-recognition receptor repertoire. *Insect Infection and Immunity*: *Evolution, Ecology, and Mechanisms*. Oxford University Press, 69-85. https://doi.org/10.1093/acpof:oso/978199551354.003.0005. (Access date: 20/02/2018).

de Andrade, L. M., dos Santos Brito, M., Junior, R. F. P., Marchiori, P. E. R., Nóbile, P. M., Martins, A. P. B., Ribeiro, R. V. and Creste, S. **(2017)**. Reference genes for normalization of qPCR assays in sugarcane plants under water deficit. *Plant Methods*, 13(28), 1-9.

Dimopoulos, G., Richman, A., Muller, H. M. and Kafatos, F. C. **(1997)**. Molecular immune responses of the mosquito *Anopheles gambiae* to bacteria and malaria parasites. *Proceedings of the National Academy of Sciences of the United States of America*, 94, 11508-11513.

Dimopoulos, G., Muller, H. M., Levashina, E. A. and Kafatos, F. C. **(2001)**. Innate immune defense against malaria infection in the mosquito. *Current Opinion in Immunology*, 13, 79-88.

Dinglasan, R. R., Devenport, M., Florens, L., Johnson, J. R., McHugh, C. A., Donnelley-Doman, M., Carucci, D. J., Yates III, J. R. and Jacobs-Lorena, M. **(2008)**. The *Anopheles* adult midgut peritrophic matrix proteome. *Insect Biochemistry and Molecular Biology*, 39(2), 125-134.

Dong,Y., Taylor,H. E., and Dimopoulos,G. **(2006a)**. AgDscam, a hypervariable immunoglobulin domain-containing receptor of the *Anopheles gambiae* innate immune system. *PLoS Biology*, 4(7), 1137-1146.

Dong, Y., Aguilar, R., Xi, Z., Warr, E., Mongin, E. and Dimopoulos, G. **(2006b)**. *Anopheles gambiae* immune responses to human and rodent *Plasmodium* parasite species. *PLoS Pathogens*, 2(6), 0513-0525.

Dong, Y. and Dimopoulos, G. **(2009)**. *Anopheles* fibrinogen-related proteins provide expanded pattern recognition capacity against bacteria and malaria parasites. *Journal of Biological Chemistry*, 284(15), 9835-9844.

Drickamer, K. and Taylor, M. E. **(1993)**. Biology of animal lectins. *Annual Review of Cell Biology*, 9, 237-264.

Ecker, A., Lehane, A. M., Clain, J. and Fodock, D. A. **(2012)**. PfCRT and its role in antimalarial drug resistance. *Trends in Parasitology*, 28(11), 504-514.

El-Gebali, S., Mistry, J., Bateman, A., Eddy, S. R., Luciani, A., Potter, S. C., Qureshi, M., Richardson, L. J., Salazar, G. A., Smart, A., Sonnhammer, E. L. L., Hirsh, L., Paladin, L., Piovesan, D., Tosatto, S. C. E. and Finn R. D. **(2019)**. The pfam protein families' database in 2019. *Nucleic Acids Research*, 47(D1), D427-D432.

Fillinger, U. and Lindsay, S.W. **(2011)**. Larval source management for malaria control in Africa: myths and reality. *Malaria Journal*, 10(353),1-10.

Fitch, C. D. (1970). *Plasmodium falciparum* in owl monkeys: drug resistance and chloroquine binding capacity. *Science*, 169, 289-290.

Fantini, J., Di Scala, C., Chahinian, H. and Yahi, N. **(2020)**. Structural and molecular modeling studies reveal a new mechanism of action of chloroquine and hydroxychloroquine against SARS-CoV-2 infection. *International Journal of Antimicrobial Agents*, 14(43), 1-8.

Fontenille, D. and Simard, F. **(2004)**. Unravelling complexities in human malaria transmission dynamics in Africa through a comprehensive knowledge of vector populations. *Comparative Imminology, Microbiology and Infectious Diseases*, 27(5), 357-375.

Foster, W. A. and Walker, E. D. **(2019)**. Mosquitoes (Culicidae)**.** Medical and Veterinary Medicine, 3rd Edition, Academic Press, 261-325.

Fox, R. (1996). Anti-malarial drugs: possible mechanisms of action in autoimmune disease and prospects for drug development. *Lupus*, 5(Suppl 1), S1-S10.

Gao, W., Xiong, Y., Li, Q. and Yang, H. **(2017)**. Inhibition of Toll-Like Receptor signaling as a promising therapy for inflammatory diseases: a journey from molecular to nano therapeutics. *Frontiers Physiology*, 8(508), 1-20.

Garnham, P. C. C. (1966). Malaria parasites and other Haemosporidia. Blackwell Scientific Publications, Oxford. 1(1), 14. https://wellcomecollection.org/works/nta77hfy (Access date: 17/03/2019)

Garver, L. S., Xi, Z., and Dimopoulos, G. **(2008)**. Immunoglobulin superfamily members play an important role in the mosquito immune system. *Developmental and Comparative Immunology*, 32(5), 519-531.

Garver, L. S., Bahia, A. C., Das, S., Souza-Neto, J. A., Shiao, J., Dong, Y., and Dimopoulos, G. **(2012)**. *Anopheles* Imd pathway factors and effectors in infection intensity-dependent anti-*Plasmodium* action. *PLoS Pathogens*, 8(6), 7-9.

Gay, F., Ciceron, L., Litaudon, M., Bustos, M. D., Astagneau, P., Diguet, B., Danis, M. and Gentilini, M. **(1994)**. In-vitro resistance of *Plasmodium falciparum* to qinghaosu derivatives in west Africa. *Lancet*, 343(8901),850-851.

Gbinigie, K. and Frie, K. **(2020)**. Should chloroquine and hydroxychloroquine be used to treat COVID-19? A rapid review. *British Journal of General Practice*, Jun 23;4(2): 1-7. doi: 10.3399/bjgpopen20X101069.

Gillies, M. T. and de Meillon, B. **(1968)**. The Anophelinae of Africa south of the Sahara (Ethiopian Zoogeographical Region). *Publications of the South African Institute for Medical Research*, 54, 1-343.

Gillies, M. T. and Coetzee, M. **(1987)**. A supplement to the Anophelinae of Africa south of the Sahara (Afrotropical Region). *Publications of the South African Institute for Medical Research*, 5, 1-143.

Gimeno, J., Eattock, N., van Deynze, A. and Blumwald, E. **(2014)**. Selection and validation of reference genes for gene expression analysis in Switchgrass (*Panicum virgatum*) using quantitative real-time RT-PCR . *PloS One*, 9(3), 1-12.

Giraldo-Calderón, G. I., Emrich, S. J., MacCallum, R. M., Maslen, G., Dialynas, E., Topalis, P., Ho, N. and Gesing, S., the VectorBase Consortium, Madey, G., Collins, F. H. and Lawson, D. **(2015)**. VectorBase: an updated bioinformatics resource for invertebrate vectors and other organisms related with human diseases. *Nucleic Acids Research*, 43(D1), D707-713.

Golberg, D. E. (1993). Hemoglobin degradation in *Plasmodium*-infected red blood cells. *Serminars in Cell Biology*, 4(5), 355-361.

Gonzalez-Santoyo, I. and Cordoba-Aguliar, A. **(2011)**. Phenoloxidase: a key component of the insect immune system. *Entemologica Experimentalis et Applicata*, 142, 1-16.

Gonzales, K. K. and Hansen, I. A. **(2016)**. Artificial diets for mosquitoes. *International Journal of Environmental Health and Public Health*, 13(1267), 1-13.

Grassmick, R.A. and Rowley,W.A. **(1973)**. Larval mortality of *Culex tarsalis* and *Aedes aegypti* when reared with different concentrations of *Tetrahymena pyriformis. Journal of Invertebrate Pathology*, 22(1),86-93.

Graumans, W., Tadesse, F. G., Andolina, C., van Gemert, G. J., Teelen, K., Lanke, K., Gadisa, E., Yewhalaw, D., van de Vergte-Bolmer, M., Siebelink-Stoter, R., Reuling, I., Sauerwein, R. and Bousema, T. **(2017)**. Semi-high-throughput detection of *Plasmodium falciparum* and *Plasmodium vivax* oocystes in mosquitoes using bead-bearing followed by circumsporozoites ELISA and quantitative PCR. *Malaria Journal*, 16, 356 1-10. https://doi.org/10.1186/s12936-017-2011-9.

Grimstad, P. R., Paulson, S. L. and Craig, G. B., Jr. **(1985)**. Vector competence of *Aedes hendersoni* (Diptera: Culicidae) for La Crosse virus and evidence of a salivary-gland escape barrier. *Journal of Medical Entomology*, 22(44), 447-453.

Gunathilaka, N., Ranathunge, T., Udayanga, L. and Abeyewickreme, W. **(2017)**. Efficacy of blood sources and artificial blood feeding methods in rearing of *Aedes aegypti* (Diptera: Culicidae) for sterile insect technique and incompatible insect technique approaches in Sri Lanka. *BioMed Research International*, 2017(2), 1-7.doi:10.1155/2017/3196924.

Gwadz, R. W., Kaslow, D., Lee, J. Y., Maloy, W. L., Zasloff, M. and Miller, L. H. **(1989)**. Effects of magainins and cecropins on the sporogonic development of malaria parasites in mosquitoes. *Infection and Immunity*, 57(9), 2628-2633.

Habtewold, T., Groom, Z. and Christophides, G. K. **(2017)**. Immune resistance and tolerance strategies in malaria vector and non-vector mosquitoes. *Parasites and Vectors*, 10(186), 1-12.

Hagen, H.E. and Grunewald, J. **(1990)**. Routine blood-feeding of *Aedes aegypti* via a new membrane. *The Journal of the American Control Association*, 6, 535-537.

Harbach, R. E. (2004). The classification of genus *Anopheles* (Diptera: Culicidae): a working hypothesis of phylogenetic relationships. *Bulletin of Entomoligal Research*, 94(6), 537-553.

Hargreaves, K., L. L. Koekemoer, B. D. Brooke, R. H. Hunt, J. Mthembu , and M. Coetzee. **(2000)**. *Anopheles funestus* resistant to pyrethroid insecticides in South Africa. *Medical and Veterinary Entomology*, 14, 181-189.

Hayward, R., Saliba, J. K. and Kirk, K. **(2005)**. The pH of the digestive vacuole of *Plasmodium falciparum* is not associated with chloroquine resistance. *Journal of Cell Science*, 15(119), 1016-1025.

Hellemans, J., Mortier, G., De Paepe, A., Speleman, F. and Vandesompele, J. **(2007)**. qBase relative quantification framework and software for management and automated analysis of real-time quantitative PCR data. *Genome Biology*, 8(2), 1-14.

Hernández-Martínez, S., Lanz-Mendoza, H., Martínez-Barnetche, J., and Rodríguez, M. H. **(2013)**. Antimicrobial properties of *Anopheles albimanus* pericardial cells. *Cell and Tissue Research*, 351(1), 127-137.

Hillyer, J. F., and Christensen, B. M. **(2002)**. Characterization of hemocytes from the yellow fever mosquito, *Aedes aegypti*. *Histochemistry and Cell Biology*, 117(5),431-440.

Hillyer, J. F., Schmidt, S. L. and Christensen, B. M. **(2003)**. Rapid phagocytosis and melanization of bacteria and *Plasmodium* sporozoites by hemocytes of the mosquito *Aedes aegypti*. *Journal of Parasitology*, 89(1), 62-69.

Hillyer, J. F., Barreau, C. and Vernick, K. D. **(2007)**. Efficiency of salivary gland invasion by malaria sporozoites is controlled by rapid sporozoite destruction in the mosquito haemocoel. *International Journal for Parasitology*, 37(6), 673-681.

Hillyer, J. F. (2010). Mosquito immunity. *Advances in Experimental Medicine and Biology*, 708, 218-238.

Hillyer, J. F. and Estévez-Lao, T. Y. **(2010)**. Nitric oxide is an essential component of the hemocyte-mediated mosquito immune response against bacteria. *Developmental Comparative Immunology*, 34(2), 141-149.

Hogh, B., Gamage-Mendis, A., Butcher, G. A. Thompson, R., Begtrup, K., Mendis, C., Enosse, S. M., Dgedge, M., Barreto, J., Eling, W. and Sinden, R. E. **(1998)**. The differing impact of chloroquine and pyremethamine/sulfadoxine upon the infectivity of malaria species to the mosquito vector. *American Journal of Tropical Medicine and Hygiene*, 58(2), 176-182.

Hou, L. and Huang, H. **(2016)**. Immune suppressive properties of artemisinin family drugs. *Pharmacology and Therapeutics*, 166, 123-127.

Hunt, R. H., Brooke, B. D., Pillay, C., Koekemoer, L. L. and Coetzee, M. **(2005)**. Laboratory selection for and characteristics of pyrethroid resistance in the malaria vector *Anopheles funestus*. *Medical and Veterinary Entomology*. 19, 271-275.

Ichimori, K., Curtis, C. F. and Targett, G. A. **(1990)**. The effects of chloroquine on the infectivity of chloroquine-sensitive and resistant populations of *P. yoelii nigeriensis* to mosquitoes. *Parasitology*, 100, 377-381.

Ishikawa, H. and Newburgh, R. W. **(1972)**. Studies of the thermal conversion of 28 S RNA of *Galleria mellonella* (L.) to an 18 S product. *Journal of Molecular Biology*, 64(1), 135-144.

Iwanga, S. and Lee, B. L. **(2005)**. Recent advances in the innate immunity of invertebrate animals. *Journal of Biochemistry and Molecular Biology*, 38, 128-150.

Jones, J. C. (1954). The heart and associated tissues of *Anopheles quadrimaculatus* say (Diptera: Culicidae). *Journal of Morphology*, 94(1), 71-124.

Kallberg, M., Wang, H., Wang, S., Peng, J., Wang, Z., Lu, H. and Xu, J. **(2012)**. Template-based protein structure modeling using the RaptorX web server. *Nature Protocols*, 7(8), 1511-1522.

Kanost, M. R. (1999). Serine proteinase inhibitors in antrhopod immunity. *Developmental amd Comparative Immunology*, 23, 291-301.

Kapp, K., Schrempf, S., Lemberg, M. K. and Dobberstein, B. **(2000)**. Post-Targeting Functions of Signal Peptides. *Protein Transport into the Endoplasmic Reticulum*, Landes Bioscience, 1-16.

Kasap, H., Alptekin, D., Kasap, M., Guzel, A. I. and Luleyap, U. **(2003)**. Artificial blood feeding of *Anopheles Sacharovi* on a membrane apparatus. *The Journal of the American Control Association*, 19(4), 367- 370.

Kathrada, F. (2015). The effect of 7-chloroquinoline derivatives on the life cycle of the malaria parasite. University of the Witwatersrand. (MSc dissertation).

Kawada, H., Dida, G. O., Sonye, G., Njenga, S. M., Mwandawiro, C. and Minakawa, N. **(2012)**. Reconsideration of *Anopheles rivulorum* as a vector of *Plasmodium falciparum* in Western Kenya: some evidence from biting time, blood preference, sporozoite positive rate, and pyrethroid resistance. *Parasites and Vectors*, 5 (230), 1-8.

Kawamoto, F., Alejo-Blanco, R., Fleck, S. L. and Sinden, R. E. **(1991)**. *Plasmodium berghei*: ionic regulation and induction of gametogenesis. *Experimental Parasitology*, 72(1), 33-42.

Kelley, L. A., Mezulis, S., Yates, C. M., Wass, M. N., and Sternberg, M. J. **(2015)**. The Phyre2 web portal for protein modeling, prediction and analysis. *Nature Protocols*, 10(6), 845-858.

Kim, W. S., Choi, W. J., Lee, S., Kim, W. J., Lee, D. C., Sohn, U. D., Shin, H. S. and Kim, W. **(2015)**. Anti-inflammatory, antioxidant and antimicrobial affects of artemisinin axtracts from *Artemisia annua* L. *The Korean Journal of Physiology and Pharmacology*, 19(1), 21-28.

Knowlton, G.F. and J.A. Rowe. **(1935)**. Handling mosquitoes on equine encephalomyelitis investigations. *Journal of Economic Entomology*, 28, 824-829.

Kumar, A., Srivastava, P., Sirisena, P. D. N. N., Dubey, S. K., Kumar, R., Shrinet, J. and Sunil, S. **(2018a)**. Mosquito innate immunity. *Insect*, 9(95), 1-34.

Kumar, S., Stecher, G., Li, M., Knyaz, C. and Tamura, K. **(2018b)**. MEGA X: molecular evolutionary genetics analysis across computing platforms. *Molecular Biology and Evolution*, 35, 1547-1549.

Krogstad, D. J., Gluzman, I. Y., Kyle, D. E., Oduola, A. M. J., Martin, S. K., Milhous, W. K. and Schlesinger, P. H. **(1987)**. Efflux of chloroquine from *Plasmodium falciparum*: mechanism of chloroquine resistance. *Science*, 238: 1283-1285.

Kweka, E. J., Lima, T. C., Marciale, C. M. and de Sousa, D. P. **(2016)**. Larvicidal efficacy of monoterpenes against the larvae of *Anopheles gambiae*. *Asian Pacific Journal of Tropical Biomedicine*, 6, 290-294.

Lagueux, M., Perrodou, E., Levashina, E. A. Capovilla, M. and Hoffmann, J. A. **(2000)**. Constitutive expression of a complement-like protein in toll and JAK gain-of-function mutants of *Drosophila*. *Proceedings of the National Academy* of *Science*. USA, 97, 11427-11432.

Langer, R. C., Li, F., Popov, V., Kurosky, A. and Vintez, J. M. **(2002)**. Monoclonal antibody against the *Plasmodium falciparum* chitinase, PfCHT1, Recognizes a malaria transmission blocking epitope in *Plasmodium gallinaceum* unrelated to chitinase PgCHT1. *Infection and Immunity*, 70(3), 1581-1590.

Laskowski, R. A., MacArthur, M. W., Moss, D. S. and Thornton, J. M. **(1993)**. PROCHECK: a program to check the stereochemical quality of protein structures. *Journal of Applied Crystallography*, 26(2), 283-291.

Laskowski, R. A., Rullmannn, J. A., MacArthur, M. W., Kaptein, R. and Thornton, J. M. **(1996)**. AQUA and PROCHECK-NMR: programs for checking the quality of protein structures solved by NMR. *Journal of Biomolecular NMR*, 8(4), 477-486.

Lee, S. J., Silverman, E. and Bargman, J. M. **(2011)**. The role of antimalarial agents in the treatment of SLE and lupus nephritis. *Nature Reviews Nephrology*, 7, 718-729.

Letunic, I., Doerks, T. and Bork, P. **(2015)**. SMART: recent updates, new developments and status in 2015. *Nucleic Acids Research*, 43, (D1) D257-D260.

Letunic, I. and Bork, P. **(2018)**. 20 years of the SMART protein domain annotation resource. *Nucleic Acids Research*, 46 (D1), D493-D496.

Levashina, E. A., Moita, L. F., Blandin,S. Vriend, G., Lagueux, M and Kafatos, F. C. **(2001)**. Conserved role of a complement-like protein in phagocytosis revealed by dsRNA knockout in cultured cells of the mosquito, *Anopheles gambiae*. *Cell*, 104, 709-718.

Levine, B. and Klionsky, D. J. **(2004)**. Development by self-digestion: molecular mechanisms and biological functions of autophagy. *Developmental Cell*, 6(4), 463-477.

Levine, B., Mizushima, N. and Virgin, H.W. **(2011)**. Autophagy in immunity and inflammation. *Nature*, 469, 323-335.

Li, F., Templeton, T. J., Popov, V., Comer, J. E., Tsuboi, T., Torri, M. and Vintez, J. M. **(2004)**. *Plasmodium* ookinete secreted proteins secreted through a common micronenal pathway are targets of blocking malaria transmission. *Journal of Biological Chemistry*, 279, 26635-26644.

Lo, T. M. (2014). Molecular genetic analysis of *Anopheles* mosquitoes when challenged by *Plasmodium* parasites. University of the Witwatersrand. (PhD dissertation).

Luo, Y. (2014). A novel multiple membrane blood-feeding system for investigating and maintaining *Aedes aegypti* and *Aedes albopictus* mosquitoes. *Journal of Vector Ecology*, 39(2), 271-277.

Lyski, Z. L., Saredy, J. J., Ciano, K. A., Stem, J. and Bowers, D. F. **(2011)**. Blood feeding position increases success of recalcitrant mosquitoes. *Vector Borne Zoonotic Disisease*, 11, 1165-1171.

Macharia, R. W., Ombura, F, F. and Aroko, E. O. **(2015)**. Insects' RNA profiling reveals Absence of ''Hidden Break'' in 28S Ribosomal RNA molecule of Onion Thrips, *Thrips tabaci*. *Journal of Nucleic Acids*, 2015, 1-8.

Mauthe, M., Orhina, I., Rocchia, C., Zhoua, X., Luhre, M., Hijkemaa, K., Coppesa, R. P., Engedale, N., Maraia, M. and Reggioria, F. **(2017)**. Chloroquine inhibits autophagic flux by decreasing autophagosome-lysosome fusion. *Autophagy*, 14(8), 1435-1455.

McChesney, E. W., Fasco, M. J. and Banks, W. F. **(1967)**. The metabolism of chloroquine in man during and after repeated oral dosage. *Journal of Pharmacology and Experimental Therapeutics*, 158, 323-331.

Mitchell, A. L., Attwood, T. K., Babbitt, P. C., Blum, M., Bork, P., Bridge, A., Brown, S. D., Chang, H. Y., El-Gebali, S., Fraser, M. I., Gough, J., Haft, D. R., Huang, H., Letunic, I., Lopez, R., Luciani, A., Madeira, F., Marchler-Bauer, A., Mi, H., Natale, D. A., Necci, M., Nuka, G., Orengo, C., Pandurangan, A. P., Paysan-Lafosse, T., Pesseat, S., Potter, S. C., Qureshi, M. A., Rawlings, N. D., Redaschi, N., Richardson, L, J., Rivoire, C., Salazar, G. A., Sangrador-Vegas, A., Sigrist, C. J. A., Sillitoe, I., Sutton, G. G., Thanki, N., Thomas, P. D., Tosatto, S. C. E., Yong, S. Y. and Finn, R. D. **(2019)**. InterPro in 2019: improving coverage, classification and access to protein sequence annotations. *Nucleic Acids Research*, 47(D1), D352-D360.

Mizushima, N., Levine, B., Cuervo, A. M. and Kilonsky, D. J. **(2008)**. Autophagy fights disease through cellular self-digestion. *Nature*, 451, 1069-1075.

Molina-Cruz, A., DeJong, R. J., Charles, B., Gupta, L., Kumar, S., Jaramillo-Gutierrez, G., and Barillas-Mury, Carolina. **(2008)**. Reactive Oxygen Species Modulate *Anopheles gambiae* Immunity against Bacteria and *Plasmodium*. *The Journal of Biological Chemistry*, 283 (6), 3217-3223.

Nakhleh, J., Moussawi, L. E. and Osta, M. A. **(2017)**. The melanization response in immunity. *Advances in Insect Physiology*, 57, 83-109.

Ndo, C., Kopya, E., Menze-Djatio, B., Toto, J. C., Awono-Ambene, P., Lycett, G. and Wonji, C. S. **(2016)**. High susceptible of wild *Anopheles funestus* to infection with natural *Plasmodium falciparum* gametocytes using membrane feeding assays. *Parasites and Vectors*, 9(341), 1-8.

Nordgard, O., Kvaloy, J. T., Farmen, R. K. and Heikkila, R. **(2006)**. Error propagation in relative real-time reverse transcription polymerase chain reaction quantification models: The balance between accuracy and precision. *Analytical Biochemistry*, 356, 182-193.

Ogino, K., Eda-Fujiwara, H. and Ishikawa, H. **(1990)**. What causes the aphid 28S rRNA to lack the hidden break? *Journal of Molecular Evolution*, 30, 509-513.

Oh, S., Shin, J. H., Jang, E. J., Won, H. Y., Kim, H. K., Jeong, M., Kim, K. S. and Hwang, E. S. **(2016)**. Anti-inflammatory activity of chloroquine and amodiaquine through p21-mediated suppression of T cell proliferation and Th1 cell differentiation. *Biochemical and Biophysical Research Communities*, 472(2), 345-250.

Oakley, M. S., Verma, N., Myers, T. G., Zheng, H., Locke, E., Morin, M. J., Tripathi, A. K., Mlambo, G. and Kumar, S. **(2018)**. Transcriptome analysis based detection of *Plasmodium falciparum* development in *Anopheles stephensi* mosquitoes. *Scientific Reports*, 8(11568), 1-12.

O'Neill, P. M., Barton, V. E., Ward, S. A. and Chadwick, J. **(2012)**. 4-Aminoquinolines: chloroquine, amiodaquine and next generation analogues, *Treatment and Prevention of Malaria*, 19-44.

Osta, M. A., Christophides, G. K and Kafatos, F. C. **(2004)**. Effects of mosquito genes on *Plasmodium* develoment. *Science*, 303(5666), 2030-2032.

Oviedo, M. V. N., Romoser, W. S., James, C. B. L., Mahmood, F. and Reisen, W. K. **(2011)**. Infection dynamics of western equine encephalomyelitis virus (Togaviridae: *Alphavirus*) in four strains of *Culex tarsalis* (Diptera: Culicidae): an immunocytochemical study. *Research and Reports in Tropical Medicine*, 2, 65-77.

Paily, K. P. and Balaraman, K. **(2000)**. Susceptibility of ten species of mosquito larvae to the parasitic nematode *Romanomermis iyengari* and its development. *Medical and Veterinary Entomology*, 14(4), 426-429.

Pan, X., Zhou, G., Wu, J., Bian, G., Lu, P., Raikhel, A. S. and Xi, Z. **(2012)**. *Wolbachia* induces reactive oxygen species (ROS)-dependent activation of the Toll pathway to control dengue virus in the mosquito *Aedes aegypti*. *Proceedings of the National Academy of Sciences*,109(1), E23-31.

Parhizgar, A. R. and Tahghighi, A. **(2017)**. Introducing new antimalarial analogues of chloroquine and amadiaquinine: a narrative review. *Iran Journal of Medical Sciences*, 42(2), 155-128.

Parker, J. (2001). Leader peptide. *Encyclopedia of Genetics*, Academic Press. Southern Illinois University Carbondale, Carbondale, IL, 62901, USA. 1st Ed, 1077-1078. Edited by S. Brenner and J. Miller.

Pfaffl, M. W., Tichopad, A., Prgomet, C. and Neuvians, T. P. **(2004)**. Determination of stable housekeeping genes, differentially regulated target genes and sample integrity: BestKeeper–Excel-based tool using pair-wise correlations. *Biotechnology Letters*, 26, 509-515.

Pinto, S. B., Kafatos, F. C., and Michel, K. **(2008)**. The parasite invasion marker SRPN6 reduces sporozoite numbers in salivary glands of *Anopheles gambiae*. *Cellular Microbiology*, 10(4), 891–898.

Plowe, C. V., Kublin, J. G. and Doumbo, O. K. **(1998)**. *P. falciparum* dihydrofolate reductase and dihydropteroate synthase mutations: epidemiology and role in clinical resistance to antifolates. *Drug Resistance Updates*, 1(6), 389-96.

Pothikasikorn, J., Boonplueang, R., Suebsaeng, C., Kaengraeng, R. and Chereonviriyaphap, T. **(2010)**. Feeding response of *Aedes aegypti* and *Anopheles dirus* using out-of-date human blood in membrane apparatus. *Journal of Vector Ecology*, 35, 149-155.

Pradel, G. (2007). Proteins of malaria parasites sexual stages: expression, funtion and potential for transmission blocking strategies. *Parasitology*, 134, 1911-1929.

Projean, D., Morin, P. E., Tu, T. M. and Ducharme, J. **(2003)**. Identification of CYP3A4 and CYP2C8 as the major cytochrome P450s responsible for morphine N-demethylation in human liver microsomes. *Xenobiotica*, 33(8), 841-854.

Qiagen. (2006). DNeasy blood and tissue handbook. https://www.qiagen.com/ie/resources/resourcedetail?id=68f29296-5a9f-40fa-8b3d-1c148d0b3030&lang=en (Accesse date: 02/11/2018).

Ranson, H., Abdallah, H., Badolo, A., Fulbeogo, W. M., Kerah-Hinzoumbé, C., Yangalbé-Kalnoné, E., Sagnon, N., Simard, F. and Coetzee, M. **(2009)**. Insecticide resistance in *Anopheles gambiae*: data from the first year of a multi-country study highlight the extent of the problem. *Malaria Journal*, 8, 299. https://doi.org/10.1186/1475-2875-8-29.

Rao, X. J., Cao, X., He, Y., Hu, Y., Zhang, X., Chen, Y. R., Blissard, G., Kanost, M. R., Yu, X. Q. and Jiang, H. **(2015)**. Structural features, evolutionary relationships, and transcriptional regulation of C-type lectin-domain proteins in *Manduca sexta*. *Insect Biochemistry and Molecular Biology*, 62, 75-85.

Rich, S. M. and Ayala, F. J. **(2006)**. Evolutionary Origins of Human Malaria Parasites. In *Emerging Infectious Diseases of the 21st Century: Malaria - Genetic and Evolutionary Aspects*. (Eds, Krishna, R. and Dronamraju, P.A.) Springer Science and Business Media, Inc, New York.

Reader, J., Botha, M., Theron, A., Lauterbach, S. B., Rossouw, C. L., Engelbrecht, D., Wepener, M., Smit, A., Leroy, D., Mancama, D., Coetzer, T. L., and Birkholtz, L. M. **(2015)**. Nowhere to hide: interrogating different metabolic parameters of *Plasmodium falciparum* gametocytes in a transmission blocking drug discovery pipeline towards malaria elimination. *Malaria Journal*, 14(1), 213, 1-17. DOI: 10.1186/s12936-015-0718-z

Reader, J. (2021). Van der Watt, M.E., Taylor, D., Le Manach, C., Mittal, N., Ottilie, S., Theron, A., Moyo, P., Erlank, E., Nardini, L., Venter, N., Lauterbach, S., Bezuidenhout, B., Horatscheck, A., van Heerden, A., Spillman, N., Cowell, A., Connacher, J., Opperman, D., Orchard, L., Llinás, M., Istvan, E., Goldberg, D., Boyle, G.A., Calvo, D., Mancama, D., Coetzer, T. L., Winzeler, E. A., Duffy, J., Koekemoer, L.L., Basarab, G., Chibale, K. and Birkholtz., LM. (2020). Multistage and transmission-blocking targeted antimalarials discovered from the open-source MMV Pandemic Response Box. *Nature Communications* 12:269.

Rozeboom, L. E. (1936). The rearing of *Anopheles albimanus* Wiedemann in the laboratory. *American Journal of Tropical Medicine and Hygiene*, 16, 471-478.

Saiyasombat, R., Bolling, B. G., Braul,t A. C., Bartholomay, L. C. and Blitvich, B. J. **(2011)**. Evidence of efficient transovarial transmission of *Culex flavivirus* by *Culex pipiens* (Diptera: Culicidae). *Journal of Medical Entomology*, 48(5),1031-1038.

Sanger, F., Nicklen, S. and Coulson, A. R. **(1977)**. DNA sequencing with chain-terminating inhibitors. *Proceedings of the National Academy of Science of the United States of America*, 74(12), 5463-5467.

Sang, R. C., Gichogo, A., Gachoya, J., Dunster, M. D., Ofula V., Hunt, A. R., Crabtree, M. B., Miller, B. R. and Dunster, L. M. **(2003)**. Isolation of a new flavivirus related to Cell fusing agent virus (CFAV) from field-collected flood-water *Aedes* mosquitoes sampled from adambo in central Kenya. *Archives of Virology*, 148(6), 1085-1093.

Schrezenmeier, E. and Dorner, T. **(2020)**. Mechanisms of action of hydroxychloroquine and chloroquine: implications for rheumatology. *Nature Reviews Rheumatology*, 16, 155-166.

Shang, X., Morris-Natschke, S. L., Liu, Y. Q, Guo, X., Xu, X. S, Goto, M., Li, J. C., Yang, G. Z. and Lee, K. H. **(2018)**. Biologically active quinoline and quinazoline alkaloids part 1. *Medical Research Reviews*, 38(3), 775-828.

Shintani, T. and Klionsky, D. J. **(2004)**. Autophagy in health and disease: a double-edged sword. *Science*, 306(5698), 990-995.

Schitger, A. K., Yassine, H., Kafatos, F. C. and Osta, M. A. **(2009)**. Two C-type Lectins Cooperate to Defend *Anopheles gambiae* against Gram-negative Bacteria. *Journal of Biological Chemistry*, 2284(26), 17616-17624.

Scott, T. W., Lorenz, L. H. and Weaver, S. C. **(1990)**. Susceptibility of *Aedes albopictus* to infection with easterne quinee ncephalomyelitis virus. *Journal of the American Mosquito Control Assocciation*, 6(2), 274-278.

Scott, .J.A., Brogdon, W.G. and Collins, F.H. **(1993)**. Identification of single specimens of the *Anopheles gambiae* complex by the polymerase chain reaction. *The American Society of Tropical Medicine and Hygiene*, 49,520 - 529.

Sebastian, S., Brochet, M., Collins, M. O., Schwach, F., Jones, M. L. and Goulding, D. **(2012)**. A *Plasmodium* calcium-dependent protein kinase controls zygote development and transmission by translationally activating repressed mRNAs. *Cell Host Microbe*, 12, 9-19.

Service, M. W. (1996). *Medical entomology for students*. London. Chapman and Hall. http://www.tandonline.com/toc/rwhi20/. (Access date: 07/05/2020).

Service, M. W. (2008). Introduction to mosquitoes (Culicidae). *Medical entomology for students*.4th Ed. Cambridge University. Press, 1-32.

Shao, L., Devenport, M. and Jacobs-Lorena, M. **(2001)**. The peritrophic matrix of Hematophagous insects. *Archives of Insect Biochemistry and Physiology*. 47(2), 119-125.

Shen, D., Wang, L., Ji, J., Liu, Q. and An, C. **(2018)**. Identification and characterization of C-type lectins in *Ostrinia furnacalis* (Lepodoptera: Pyralidae). *Journal of Insect Science*, 18(2), 24, 1-11.

Shin, S. C. J., Vanderberg, J. P. and Terzakis, J. A. **(1982)**. Direct infection of hepatocytes by sporozoites of *Plasmodium berghei*. *The Journal of Protozology*, 29, 448-454.

Shin, S. N., Zou, Z. and Raikhel, A. S. **(2011)**. A new factor in the *Aedes aegypti* immune response: *CLSP2* modulates melanization. *European Molecular Biology Organization Reports*.12, 983-943.

Sievers, F., Wilm, A., Dineen, D., Gibson, T. J., Karplus, K., Li, W., Lopez, R., McWilliam, H., Remmert, M., Soding, J., Thompson, J. D. and Higgins, D. G. **(2011)**. Fast, scalable generation of high-quality protein multiple sequence alignments using Clustal Omega. *Molecular Systems Biology*, 7(593), 1-6.

Sigma-Aldrich®, 2020a. Chloroquine diphosphate salt. C6628. https://www.sigmaaldrich.com/catalog/product/sigma/c6628?lang=en&region=ZA. (Access date: 17/05/2020**).**

Sigma-Aldrich®, 2020b. 4,4′-DDT. 386340. https://www.sigmaaldrich.com/ZA/en/product/aldrich/386340 . (Access date: 17/05/20).

Sigrist, C. J. A., de Castro, E., Cerutti, L., Cuche, B. A., Hulo, N., Bridge, A., Bougueleret, L. and Xenarios, I. **(2013)**. New and continuing developments at PROSITE. *Nucleic Acids Research*, 41, D344-D347.

Silver, N., Best, S., Jiang, J. and Thein, S. L. **(2006)**. Selection of housekeeping genes for gene expression studies in human reticulocytes using real-time PCR. *BMC Molecular Biology*, 7(33), 1-9.

Silveira, H., Ramos, S., Abrantes, P., Lopes, L. F., do Rosario, V. E. and Abrahamsen. **(2007)**. Effect of chloroquine on gene expression of *Plasmodium yoelii nigeriensis* during its sporogonic development in the mosquito vector. *Malaria Journal*, 6, 84-93. https://doi.org/10.1186/1475-2875-6-84

Simmaco, M., Boman, A., Mangoni, M. L., Mignogna, G., Miele, R., Barra, D. and Boman, H. G. **(1997)**. Effect of glucocorticoids on the synthesis of antimicrobial peptides in amphibian skin. FEBS *Letters*. 416, 273-275.

Simoes, M. L., Mlambo, G., Tripathi, A., Dong, Y. and Dimopoulos, G. **(2017)**. Immune regulation of *Plasmodium* is *Anopheles* species specific and infection intensity dependent. *American Society for Microbiology*, 8(5), 1-13.

Sinka, M. E., Bangs, M. J., Manguin, S., Coetzee, M., Mbogo, C. M., Hemingway, J., Patil, A. P., Temperley, W. H., Gething, P. W., Kabaria, C. W., Okara, R. M., Van Boeckel, T., Godfray, H. C., Harbach, R. E. and Hay, S. I. **(2010)**. The dominant *Anopheles* vectors of human malaria in Africa, Europe and the Middle East: occurrence data, distribution maps and bionomic précis. *Parasites and Vectors*, 3(117), 1-34.

Sippl, M. J. (1993). Recognition of errors in three-dimensional structures of proteins. *Proteins*, 17, 355-362.

Smith, R. C., Vega-Rodroguez, V. and Jacobs-Lorena, M. **(2014)**. The *Plasmodium* bottleneck: malaria parasite losses in the mosquito vector. *The Memorias do Instituto Oswaldo Cruz*. 109, 644-661.

Sologub, L., Kuehn, A., Kern, S., Przyborski, J., Schillig, R. and Pradel, G. **(2011)**. Malaria proteases mediate inside-out egress of gametocytes from red blood cells following parasite transmission to the mosquito. *Cell Microbiology*, 13, 897-912.

Spillings, B. L., Brooke, B., Koekemoer, L.L. Chiphwanya, L., Coetzee, M. and Hunt, R. H. **(2009)**. A new species concealed by *Anopheles funestus* Giles, a major malaria vector in Africa. *American Journal of Tropical Medicine and Hygiene*. 8, 510-515.

Tan, K. L., Vlisidou, I. and Wood, W. **(2014)**. Ecdysone mediates the development of immunity in the *Drosophila* embryo. *Current Biology*. 24, 1145-1152.

ThermoFisher Scientific. (2016). Troubleshooting Sanger sequencing data. https://tools.thermofisher.com/content/sfs/manuals/MAN0014435_Trbleshoot_Sanger_seq_data_UB.pdf?cid=techcomm92 (Accessed date: 14/05/2018)

Taylor, S., Wakem, M., Dijkman, G., Alsarraj, M. and Nguyen, M. **(2010)**. A practical to RT-qPCR-publishing dT that conform to the MIQE guidelines. *Methods*, 50, 1-5.

Valko, M., Rhodes, C. J., Moncol, J., Izakovic, M and Mazur, M. **(2006)**. Free radicals, metals and antioxidants in oxidative stress-induced cancer. *Chemico-Biologico Interactions*, 160(1), 1-40.

Vanderesse, R., Colombeau, L., Frochot, C. and Acherar, S. **(2016)**. Inactivation of malaria parasites in Blood: PDT vs Inhibition of Hemozoin Formation. Chapter11. *Current Topics in Malaria*, 205-233. http://dx.doi.org/10.5772/65053. (Access date: 12/04/2020)

Vandesompele, J., De Preter, K., Pattyn, F., Poppe, B., Van Roy, N., De Paepe, A. and Speleman, F. **(2002)**. Accurate normalization of real-time quantitative RT-PCR data by geometric averaging of multiple internal control genes. *Genome Biology*, 3(7), 1-12.

Varki, A., Cummings, R.D. , Esko, J. D., Freeze, H. H., Stanley, P., Bertozzi, C. R., Hart, G. W. and Etzler, M. E. **(2009)**. Chapter 31 C-type lectins.2nd edition. Cold Spring Harbor (NY): Cold Spring Harbor Laboratory Press.

Vernick, K. D., Fujioka, H., Seeley, D. C., Tandler, B., Aikawa, M. and Miller, L. H. **(1995)**. *Plasmodium gallinaceum*, a refractory mechanism of ookinete killing in the mosquito, *Anopheles gambiae*. *Experimental Parasitology*, 80(4), 583-595.

Vincent, M. J., Bergeron, E., Benjannet, S., Erickson, B. R., Rollin, P. E., Ksiazek, T. G., Seidah, N. G. and Nichol, S. T. **(2005)**. Chloroquine is a potent inhibitor of SARS coronavirus infection and spread. *Virology Journal*, 2(69), 1-10.

Vintez, J. M., Valenzuela, J. G., Specht, C. A., Aravind, L., Langer, R. C., Ribeiro, J. M. and Kaslow, D. C. **(2000)**. Chitinase of the avian malaria parasite *Plasmodium gallinaceum*, a class of enzymes necessary for parasite invasion in the mosquito midgut. *Journal of Biological Chemistry*, 275, 10331-10341.

Vizioli, J., Bulet, P., Hoffmann, J. A., Kafatos, F. C., Muller, H.-M., and Dimopoulos, G. **(2001)**. Gambicin: A novel immune responsive antimicrobial peptide from the malaria vector *Anopheles gambiae*. *Proceedings of the National Academy of Sciences*, 98(22), 12630-12635.

Vogels, C. B. F., Göertz, G. P., Pijlman, G. P., and Koenraadt, C. J. M. **(2017)**. Vector competence of European mosquitoes for west Nile virus. *Emerging Microbes and Infections*, 6(11), 1-13.

Wang, P., Read, M., Sims, P. F. and Hyde, J. E. **(1997)**. Sulfadoxine resistance in the human malaria parasite *Plasmodium falciparum* is determined by mutations in dihydropteroate synthetase and an additional factor associated with folate utilization. *Molecular Microbiology*, 23(5), 979-86.

Wang, Y. H., Hu, Y., Xing, L. S., Jiang, H., Hu, S. N., Raikhel, A. S. and Zou, Z. **(2015)**. A critical role for *CLSP2* in the modulation of antifungal immune response in mosquitoes. *Plos Pathogens*, 11(6), 1-20.

Wang, H., Xue, Z., liu, Z., Wang, W., Wang, F., Wang, Y., Wang, L. and Song, L. **(2018)**. A novel C-type lectin from the sea cucumber *Apostichopus japonicas* (*Aj*CTL2) with preferential binding of D-galactose. *Fish and Shellfish Imunology*, 79, 218-227.

Waterhouse, R. M., Kriventseva EV, Meister, S., Xi, Z., Alvarez, K. S., Bartholomay, L. C., Barillas-Mury, C., Bian, G., Blandin, S., Chritensen, B. M., Dong, Y., Jiang, H., Kanost, M. R., Koutsos, A. C., Levashina, E. A., Li, J., Ligoxyakis, P., MacCallum, R. M., Mayhew, G. F., Mendes, A., Michel, K., Osta, M. A., Paskewitz, S., Shin, A. W., Vlachou, D., Wang, L., Wei, W., Zhengs, L., Zou, Z., Severson, D. W., Raikhel, A. S., Kafatos, F. C., Dimopoulos,

G., Zdobnov, E. M. and Christophides, G. K. **(2007)**. Evolutionary dynamics of immune-related genes and pathways in disease-vector mosquitoes. *Science*, 316(5832), 1738-1743.

Warr, E., Das, S., Dong, Y., and Dimopoulos, G. **(2008)**. The Gram-Negative Bacteria-Binding Protein gene family: Its role in the innate immune system of *Anopheles gambiae* and in anti-*Plasmodium* defence. *Insect Molecular Biology*, 17(1), 39-51.

Warhurst, D. C. (2001). A Molecular Marker for Chloroquine-Resistant Falciparum Malaria. *New England Journal of Medicine*, 344(4), 299-302.

Weiss, W. I., Drickamer, K. and Hendrickson, W. A. **(1992)**. Structure of a C-type mannose-binding protein complexed with an oligosaccharide. *Nature*, 360, 127-134.

Weiss, W. I. and Drickamer, K. **(1994)**. Trimeric structure of a C-type mannose-binding protein. *Structure*, 2(12), 1227-1240.

Wiederstein, M. and Sippl, M. J. **(2007)**. ProSA-web: interactive web service for the recognition of errors in three-dimensional structures of proteins. *Nucleic Acids Research*, 35(*Web Server issue*), W407-W410. https://doi.org/10.1093/nar/gkm290 (Access date: 18/04/2019)

Wilkes, T. J., Matola, Y. G. and Charlwood, J. D. **(1986)**. *Anopheles rivulorum*, a vector of human malaria in Africa. *Medical and Veterinary Entomology*. 10, 108-110.

Wilson, C.M., Serrano, A. E., Wasley, A., Bogenschutz, M. P., Shankar, A.H. and Wirth, D.F. **(1989)**. Amplification of a gene related to mammalian *mdr* genes in drug-resistant *Plasmodium falciparum*. *Science*, 244,1184-1186.

Winnebeck, E. C., Millar, C. D. and Warman, G. R. **(2010)**. Why does insect RNA look degraded?. *Journal of Insect Science*, 10(159), 1-7.

Woke, P.A. (1937). Comparative effects of the blood of different species of vertebrates on egg production of *Aedes aegypti* Linn. *The American Journal of Tropical Medicine*, 17, 729-745.

World Health Organization. (2005). World Health Report Malaria. https://www.who.int/publications/atoz/9241593199/en/. (Access date: 07/06/2017).

World Health Organization. (2013). Larval source management- a supplementary measure for malaria vector control. An operation manual. https://www.who.int/malaria/publications/atoz/9789241505604/en/. (Access date: 20/04/2020).

World Health Organization. (2016). World Health Report Malaria. https://www.who.int/publications-detail/world-malaria-report-2016/report/en/. (Access date: 10/10/2017).

World Health Organization. (2019). World Health Report Malaria. https://www.who.int/publications-detail/world-malaria-report-2019. (Access date: 15/03/2020).

World Health Organization. (2020). World Health Report Malaria. https://www.who.int/teams/global-malaria-programme/reports/world-malaria-report-2021. (Access date: 20/02/22).

Wu, Q., Patocka, J. and Kuca, K. **(2018)**. Insect antimicrobial peptides, a Mini Review. *Toxins*, 10(461), 1-17.

Xie, F., Xiao, P., Chen, D., Xu, L. and Zhang, B. **(2012)**. miRDeepFinder: a miRNA analysis tool for deep sequencing of plant small RNAs. *Plant Molecular Biology*, 80, 75-84.

Xiu, Y., Wang, Y., Bi, J., Liu, Y., Ning, M. and Liu, H. **(2016)**. A novel C-type lectin is involved in the innate immunity of *Macrobrachium nipponense*. *Fish and Shellfish Imunology*, 50, 117-126.

Xu, X., Dong, Y., Abraham, E. A., Kocan, A., Srinivasan, P., Ghosh, A. K., Siden, R. E., Ribeiro, J. M. C., Jacobs-Lorena, M., Kafatos, F. C. and Dimopoulos, G. **(2005)**. Transcriptome analysis of *Anopheles stephensi-Plasmodium berghei* interactions. *Molecular and Biochemical Parasitology*, 142(1), 76-87.

Xu, D. and Zhang, Y. **(2012)**. Ab initio protein structure assembly using continuous structure fragments and optimized knowledge-based force field. *Proteins*, 80, 1715-1735.

Xu, D. and Zhang, Y. **(2013)**. Toward optimal fragment generations for ab initio protein structure assembly. *Proteins*, 81, 229-239.

Yachdav, G., Kloppmann, E., Kajan, L., Hecht, M., Goldberg, T., Hamp, T., Honigschmid, P., Schafferhans, A., Roos, M., Bernhofer, M., Richter, L., Ashkenazy, H., Punta, M., Schlessinger, A., Bromberg, Y., Schneider, R., Vriend, G., Sander, C., Ben-Tal, N. and Rost, B. **(2014)**. PredictProtein-an open resource for online prediction of protein structural and functional features. *Nucleic Acids Research*, 42 (W1), W337-W343.

Zelensky, A. N. and Gready, J. E. **(2003)**. Comparative analysis of structural properties of C-type lectin domain (CTLD). *Proteins*, 52, 466-477.

Zelensky, A. N. and Gready, J. E. **(2005)**. The C-type lectin-like domain superfamily. *Federation of European Biochemistry Societies*, 272(24), 6179-6217.

Zhang, X. W., Xu, W. T., Wang, X. W., M, Y., Zhao, X. F., Yu, X. Q. and Wang, J. X. **(2009)**. A novel C-type lectin with two CRD domains from Chinese shrimp *Fenneropenaeus chinensis* functions as a pattern recognition protein. *Molecular Immunology*, 46, 1626-1637.

7. Appendices

7 Appendix A.1 Clearance certificate for biosafety, protocol number: 20180103.

UNIVERSITY OF THE WITWATERSRAND, JOHANNESBURG

Research Office

INSTITUTIONAL BIOSAFETY COMMITTEE (IBC)
(R 14/16)

CLEARANCE CERTIFICATE **PROTOCOL NUMBER: 20180103**

BRIEF DESCRIPTION OF APPLICATION:

Transcription analysis of an immune factor in a main african malaria vector anopheles funestus

APPLICANT: Miss W Ramashia

SUPERVISOR: Prof RL van Zyl

SCHOOL/DEPARTMENT : Pharmacy and Pharmacology

DATE CONSIDERED: 29 January 2018

EXPIRY DATE: 12 March 2022

DECISION OF COMMITTEE:

1. This clearance certificate expires on 12 March 2022 and may be renewed on application
2. An annual report must be provided on the anniversary date of this certificate, for as long as the project continues
3. Notification of any proposed modifications must be submitted on the attached form
4. Unreported changes to the application may invalidate the clearance given by the IBC

DATE: 12 March 2018

CHAIRPERSON: _____
(Professor J Larkin)

Radiation and Health Physics Unit
University of Witwatersrand
Johannesburg, Republic of South Africa
Tel: +27 (0) 11 717 6931

DECLARATION OF APPLICANT:

To be completed in duplicate and **one copy** returned to the Research Office, Phillip Tobias Building, Room 301, 3rd Floor, 29 Princess of Wales Terrace, Parktown, Faculty of Health Sciences, University.

1. I have read, understood and accepted the approval conditions above
2. I agree to submit a yearly progress report to the Committee and to submit an interim report on the form provided, in the event of any significant unforeseen event, *e.g.* suspension of a drug trial, temporary closure or relocation of my laboratory, etc
3. I note that the University Safety Officer, or his/her representative, may at any reasonable time inspect my laboratory or trial site to ensure compliance with current Health and Safety legislation. I undertake to offer my full co-operation in any such inspection.
4. I have read, understood and will comply with the *recommended standard operating procedures for the handling of biohazardous materials* posted at http://web.wits.ac.za/Academic/Research/Biosafety.htm
5. I declare (delete as appropriate) that:
   a. I have all the approvals required by statute or regulation and by the funding agencies supporting this work, or
   b. that I will not begin work until such approvals are obtained

Signed: _____ **Date:** _____

PLEASE QUOTE THE PROTOCOL NUMBER IN ALL ENQUIRIES

8 Appendix A.2 Clearance certificate for the use of blood: W-CBP-180420-1.

UNIVERSITY OF THE WITWATERSRAND, JOHANNESBURG

HUMAN RESEARCH ETHICS COMMITTEE (MEDICAL

Human Research Ethics Committee (Medical)

Research Office Secretariat:
Faculty of Health Sciences, Phillip Tobias Building, 3rd Floor, Office 301/2/4, 29 Princess of Wales Terrace, Parktown, 2193
Tel +27 (0)11-717-1252 /1234/2656/2700
Private Bag 3, Wits 2050
Office email: HREC-Medical.ResearchOffice@wits.ac.za
Website: www.wits.ac.za/research/about-our-research/ethics-and-research-integrity/

Ref: W-CBP-180420-1 20/04/2018

TO WHOM IT MAY CONCERN:

Waiver: This certifies that the following research does not require clearance from the Human Research Ethics Committee (Medical)

Investigator: Miss Witness Ramashia (student no. 572354) et al

Supervisor: Prof RL van Zyl

Department: Wits Research Institute for Malaria

Project title: Transcription analysis of an immune factor in a main African malaria vector *Anopheles funestus*

Reason: Laboratory analysis. Will use blood to grow the malaria parasite *in vitro*, assess the antimalarial effect of novel compounds and for red blood cell cytotoxicity assays. No human participants will be involved in the study.

Professor CB Penny
Chairperson: Human Research Ethics Committee (Medical)

UNIVERSITY OF THE WITWATERSRAND
OFFICE OF THE DEPUTY VICE CHANCELLOR RESEARCH
20 APR 2018
RESEARCH OFFICE HREC (Medical)
JOHANNESBURG

Copy – HREC (Medical) Secretariat: Zanele Ndlovu and Rhulani Mkansi.

9 Appendix A.3 Clearance certificate for animal ethics, *Anopheles* Waiver 07-2017-O.

UNIVERSITY OF THE WITWATERSRAND, JOHANNESBURG

ANIMAL RESEARCH ETHICS COMMITTEE (AREC)

Registration number: AREC0101210-002

Solomon Mahlangu House
10th Floor, Room 10004
Jorissen Street
Braamfontein, Johannesburg

7 November 2017

To whom it may concern,

Re: Waiver from Animal Ethics Screening Committee of the University of the Witwatersrand

This letter serves to confirm that Associate Professor Robyn van Zyl (Department of Pharmacy and Pharmacology, School of Therapeutic Sciences, University of the Witwatersrand) does not require full animal ethics clearance for her studies which use *Anopheles* mosquito species to evaluate known or novel synthetic and natural compounds as potential insecticides against *Anopheles* species.

Reasons: Mosquito eggs and larva are used in the study. No animals or animal products are used in the study.

Conditions: All approved biosafety and biosecurity SOPs should be adhered to.

Should you require any further information, do not hesitate to contact me.

Yours sincerely,

Kennedy Erlwanger

(Chairman: Animal Research Ethics Committee, University of the Witwatersrand)

Reference: R van Zyl –Anopheles Waiver 07-11-2017-O

Assoc Prof Kennedy H. Erlwanger
School of Physiology
Faculty of Health Sciences, University of the Witwatersrand
7 York Road, Parktown, 2193
SOUTH AFRICA
Tel: +27 (0)11 717 2454
Email: Kennedy.Erlwanger@wits.ac.za

School of Therapeutic Sciences
Pharmacology Division
Department of Pharmacy and Pharmacology

WITS UNIVERSITY

Faculty of Health Sciences · Private Bag 3, Wits, 2050, South Africa
Tel: +27 11 717 2271 · Fax : 0862056385 · E-mail: Robyn.vanZyl@wits.ac.za · www.wits.ac.za

Tuesday, November 21, 2017

To Associate Professor K Erlwanger

re: ANIMAL ETHICS WAIVER FOR MSC STUDENTS

I obtained animal ethics waivers for my MSc students to use *Artemia* species and *Anopheles* larvae with the following two reference numbers:

- *R van Zyl Waiver (Artemia) 07-11-2017-O*
- *R van Zyl –Anopheles Waiver 07-11-2017-O*

The following students will be using both *Artemia* and *Anopheles* in their research:

- Ms Fatima Kathrada [0602240N] – The effect of 7-chloroquinoline derivatives on the life cycle of the malaria parasite.
- Mr Sahil Lala [358351] – The Effect of Quinoline Heterocyclic Derivatives on the Malaria Parasite and *Anopheles Vector.*
- Ms Teboho Malimabe [152675] – The Effect Of Novel Quinoxaline Derivatives On The Life Cycle Of Malaria Parasite And Vector.
- Ms Natasha Jansen van Vuuren [0718672w] – The effect of novel compounds on copper homeostasis in *Plasmodium falciparum* and neuroblastoma cells.
- Mr Thulani Mahlangu [667999] - The chemotherapeutic properties of novel quinazolines and bis–hydrazones compounds.
- Ms Puleng Thabana [609529] - The effect of novel 6-oxo-1,6 dihydropyrimidine and 2-(quinoline-8-yloyxy)acetohydrazone derivatives on the life cycle of the malaria parasite.
- Ms W Ramashia [572354] - Transcription analysis of an immune factor in a main African malaria vector *Anopheles funestus*.

Please could these students use the above two animal ethics numbers for their research as they form part of the larger project I am undertaking.

Yours sincerely,

Associate Professor Robyn van Zyl

Pharmacology Division: Head
Dept of Pharmacy & Pharmacology: Deputy Head
School of Therapeutic Sciences
WITS Research Institute for Malaria (WRIM)
Pharmacology Research Director
Faculty of Health Sciences

WRIM WITS UNIVERSITY

10 Appendix A.4 Clearance certificate for institutional biosafety approval for BSL2: 20180402Lab.

UNIVERSITY OF THE WITWATERSRAND, JOHANNESBURG

Research Office

INSTITUTIONAL BIOSAFETY COMMITTEE
(R 14/16)

CLEARANCE CERTIFICATE **PROTOCOL NUMBER: 20180402Lab**

BRIEF DESCRIPTION OF APPLICATION:

Laboratory situated in room 10M02 10th Floor, Wits Research Institute for Malaria, Medical School

APPLICANT: Professors M/LL Coetzee and Koekemoer

SCHOOL/DEPARTMENT : Molecular Medicine and Haematology

DATE CONSIDERED: By Circulation 29 November 2018

DECISION OF COMMITTEE: Approved unconditionally

These laboratories are considered to meet the standards of the Institutional Biosafety Committee (IBC), for BSL2 approval, as specified in the IBC's published Standard Operating procedures.
Any change to the type of biohazardous agents being handled should be reported to the IBC
DAFF - Reg no 39.2/University of Witwatersrand - 18/041 expiry date 03 December 20-21

1. This clearance certificate expires on 03 December 2023 and may be renewed on application.

DATE OF APPROVAL: 03 December 2019

CHAIRPERSON: James F. S. Larkin 2019.04.15 12:07:53 +02'00'

(Professor J Larkin)

DECLARATION OF APPLICANT:

To be completed in duplicate and **one copy** returned to the University of the Witwatersrand, Faculty of Health Sciences, Research Office, Office 301, Phillip Tobias Building, 29 Princess of Wales Terrace, Parktown,2193.

1. I have read, understood and accepted the approval conditions above
2. I note that the University Safety Officer, or his/her representative, may at any reasonable time inspect my laboratory or trial site to ensure compliance with current Health and Safety legislation. I undertake to offer my full co-operation in any such inspection.
3. I have read, understood and will comply with the *recommended standard operating procedures for the handling of biohazardous materials* posted at http://intranet.wits.ac.za/academic/uro/Pages/Institutional-Biosafety-Committee-(IBC).aspx

Signed: Koekemoer **Date:** 3.12.2019

PLEASE QUOTE THE PROTOCOL NUMBER IN ALL ENQUIRIES

11 Appendix A.5 Clearance certificate for studies on malaria vectors: 20190701-70.

ANIMAL RESEARCH ETHICS COMMITTEE

Registration number: AREC-101210-002

Date: July 1, 2019

Certificate reference: 20190701-7O
Category: O
Re: Waiver from the Animal Research Ethics Committee of the University of the Witwatersran

Reference : Animal Ethics to complete
Re: Waiver from the Animal Research Ethics Committee of the University of the Witwatersrand
HoD applicant : Lizette Koekemoer
Staff number : 09700304
Degree : PhD/Msc Candidates
Study Title : "Studies on malaria vectors".
Department: Wits Research Institute for Malaria;
laboratory
Supervisor: Lizette Koekemoer, Givemore Munhenga, Yael Dahan-Moss, Shune Oliver, Basil Brooke and Maria Kaiser
Email: lizette.koekemoer@wits.ac.za
Address: 7 York Road, Parktown, Johannesburg, 2001
Tel: + 011-717 2486;
Full clearance certificate from the AREC of the University of the Witwatersrand is NOT required.
Reason: This study uses mosquitoes (invertebrates).
Comment/Notes :

1) This is a General Waiver for the PI and listed Supervisors.
2) Individual researchers and MSc & PhD candidates may require Ethics Clearance in the own name according to applicable rules of the Post-Graduate and other Committees.
3) Feeding of the mosquitos should be specified.

Please contact me should you require further information.

GP Candy

Geoffrey Candy PhD
Chair : Animal Research Ethics Committee

Geoffrey P Candy PhD
Professor, Department of Surgery, Faculty of Health Sciences, University of the Witwatersrand, *7 York Road Parktown 2193, Johannesburg; Tel: 27-11-717-2574; Email: geoffrey.candy@wits.ac.za*

12 Appendix A.6

Figure A1 depicts the artificial membrane glass feeding system that was employed during the optimization of the feeding rate of the *An. funestus s.s.* (Section 2.3). Every optimization step was performed in triplicates with two technical replicates.

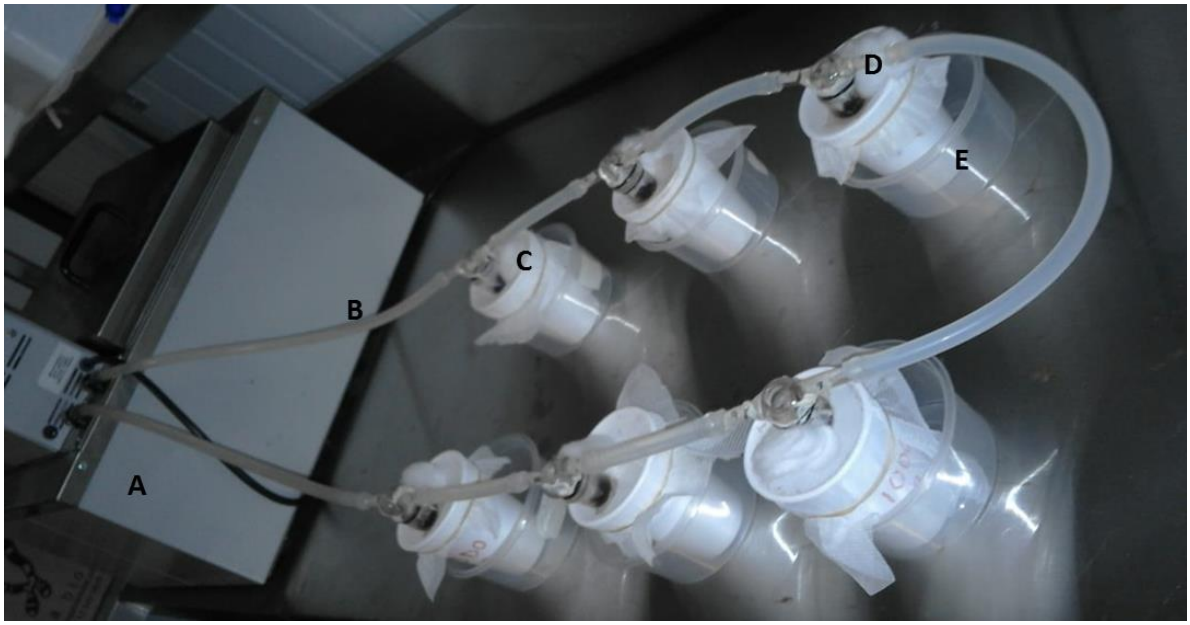

Figure A1: Overview of a multiple artificial glass feeding membrane system in polyester cups. (A) water bath with dH_2O kept at 37°C, **(B)** water inlet and outlet tubes connecting the system and allowing for the flow of water to keep the blood meal warm, **(C)** nylon mesh covering the cages enables the female mosquitoes to use their serrated proboscis to pierce through the mesh and the membrane, temperature of the blood meal regulated at 37°C inside glass feeder and collagen sausage casing, **(D+E)** blood meal and adult female mosquito in 2.5litre cage.

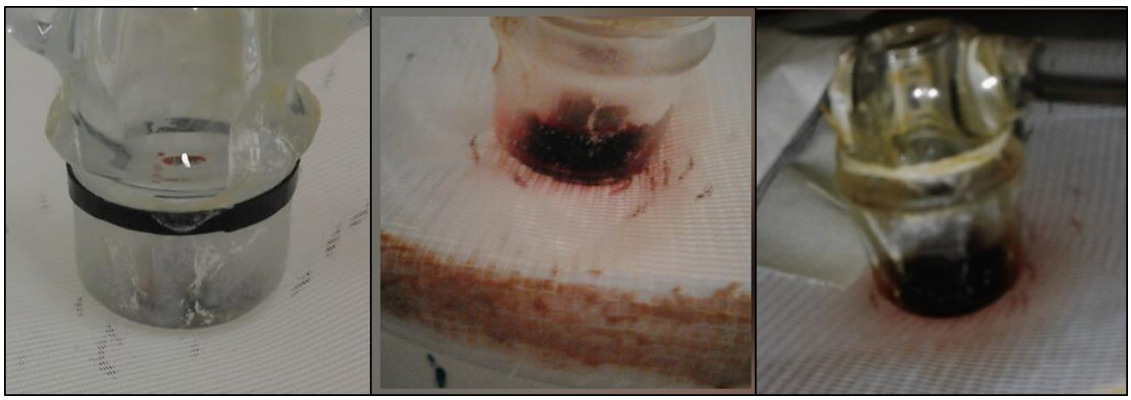

Figure A2: *Anopheles funestus s.s.* during blood meal. Adult female mosquitoes feeding on *P. falciparum* infected and uninfected blood.

13 Appendix B

Table B1 List of C-type lectin containing insects used in the construction of phylogenetic tree Figures 3.5. Selected proteins are identified by their Gene ID and Gene description from VectorBase and GeneBank.

No	Insect	Gene ID	Gene description	% Sequence similarity to *An. funestus*
1.	*Aedes aegypti*	AAEL014382	CTLMA14: mannose binding	27.59
2.	*Anopheles albimanus*	AALB014534	CTL: C-type lectin	41.82
3.	*Anopheles arabiensis*	AARA002455	CTL: C-type lectin	54.8
4.	*Anopheles atroparvus*	AATE017355	CTL: C-type lectin	48.26
5.	*Anopheles christyi*	ACHR008725	CTL: C-type lectin	61.24
6.	*Anopheles coluzzii*	ACOM027875	CTL4: C-type lectin	55.37
7.	*Anopheles darling*	ADAC004009	CTL: C-type lectin	41.07
8.	*Anbopheles dirus*	ADIR003751	CTL: C-type lectin	57.34
9.	*Anopheles funestus*	AFUN010847	CTL4: C-type lectin	100.00
10.	*Anopheles gambiae*	AGAP005335	CTL4: C-type lectin	54.8
11.	*Anopheles maculatus*	AMAM022455	CTL: C-type lectin	65.32
13.	*Anopheles melas*	AMEC014491	CTL: C-type lectin	43.64
14.	*Anopheles merus*	AMEM019544	CTL: C-type lectin	53.67
15.	*Anopheles minimus*	AMIN007380	CTL: C-type lectin	68.57
16.	*Anopheles quadriannulatus*	AQUA007735	CTL4: C-type lectin	54.8
17.	*Anopheles sinensis*	ASIS010487	CTL: C-type lectin	45.88
18.	*Anopheles stephensi*	ASTE002637	CTL: C-type lectin	60.57

A

Controls (Untreated):

	CTL4	RPS7	RPS26	RPL19
1	27.58	22.51	23.6	21.6
2	28.01	22.61	23.56	21.55
3	27.91	22.38	23.71	21.9
4	25.01	20.13	21.84	20.93
5	25.2	20.07	22.11	21.47
6	25.37	20.54	21.9	21.52
7	31.3	25.65	25.27	25.67
8	31.38	25.57	25.4	25.73
9	31.36	25.63	25.34	25.68

Samples (Treated):

	CTL4	RPS7	RPS26	RPL19
1	26.98	20.84	22.1	20.27
2	27.06	21.13	22.18	20.11
3	27.45	21.18	22.11	20.17
4	25.46	19.82	21.1	19.7
5	25.56	19.97	22	20.46
6	25.53	19.72	21.51	19.94
7	28.24	23.43	22.63	22.99
8	28.2	23.41	22.66	23.02
9	28.48	23.48	22.67	23.06

B

Relative Expression Results

Parameter	Value
Iterations	2000

Gene	Type	Reaction Efficiency	Expression	Std. Error	95% C.I.	P(H1)	Result
CTL4	TRG	0.99	0.770	0.417 - 1.597	0.215 - 2.270	0.256	
RPS7	REF	0.94	0.864				
RPS26	REF	0.96	0.992				
RPL19	REF	0.93	1.168				

Interpretation

CTL4 sample group is not different to control group. P(H1)=0.256

Figure B1: Cycle threshold values and normalization of CTL4 for *P. falciparum* infected *An. funestus s.s.* REST 2009 representation of input Ct values and output analysis. (A) Ct values of reference and target genes for *P. falciparum* treated and untreated samples. (B) Relative expression of *An. funestus s.s* CTL4 and reference genes.

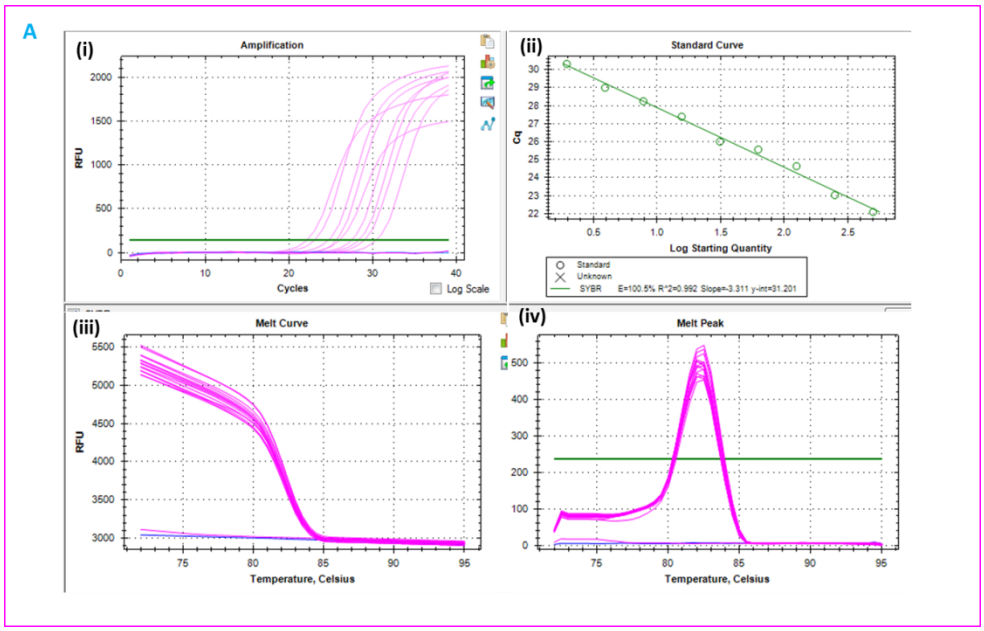

Figure B2A: CTL4 quantification plots of *An. funestus s.s.* immune challenged with *P. falciparum* infected blood meal. Graphical representation of CTL4 depicting **(i)** amplification curve showing exponential growth of the RT-PCR products; **(ii)** standard curve with reaction efficiency 100.5 %, R^2 0.992 and a slope of -3.311 were more than five points of the curve fall in the line of best fit; **(iii-iv)** melt curve and peak showing single peaks indicating amplification of a single RT-PCR product. NTC are shown by the blue line at the bottom of the curves.

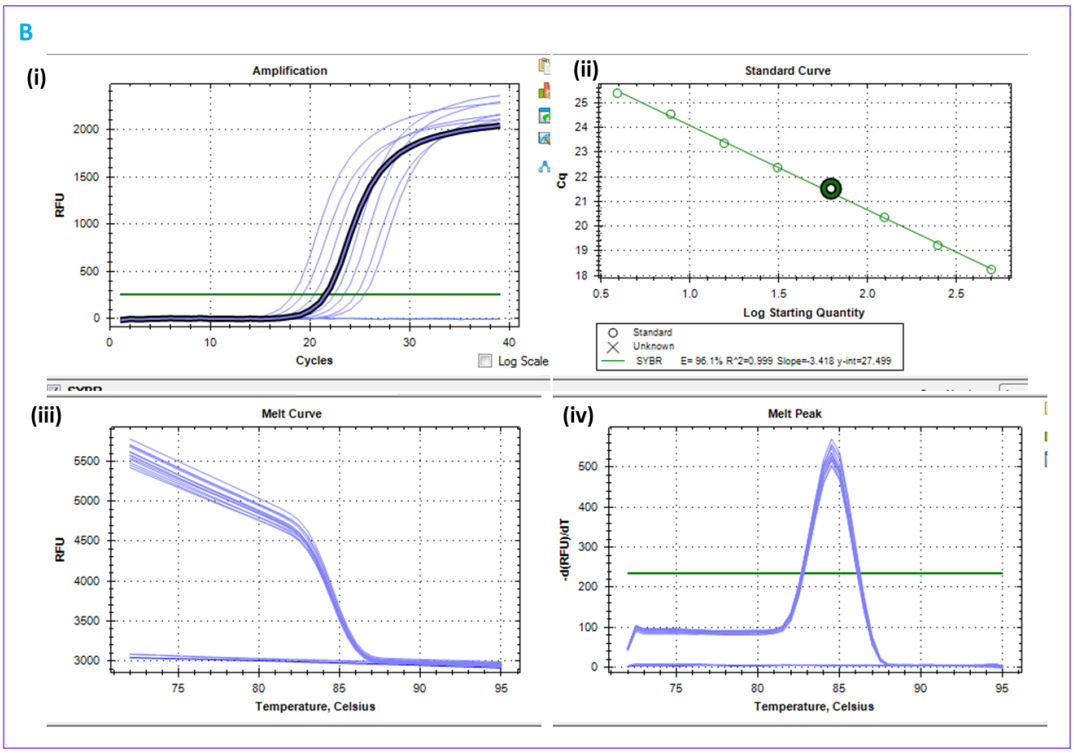

Figure B2B: RPS26 quantification plots of *An. funestus s.s.* immune challenged with *P. falciparum* infected blood meal. Graphical representation of RPS26 depicting **(i)** amplification curve showing exponential growth of the RT-PCR products; **(ii)** standard curve with reaction efficiency 96.1%, R^2 0.999 and a slope of -3.418 were more than five points of the curve fall in the line of best fit; **(iii-iv)** melt curve and peak showing single peaks indicating amplification of a single RT-PCR product. NTC are shown by the blue line at the bottom of the curves.

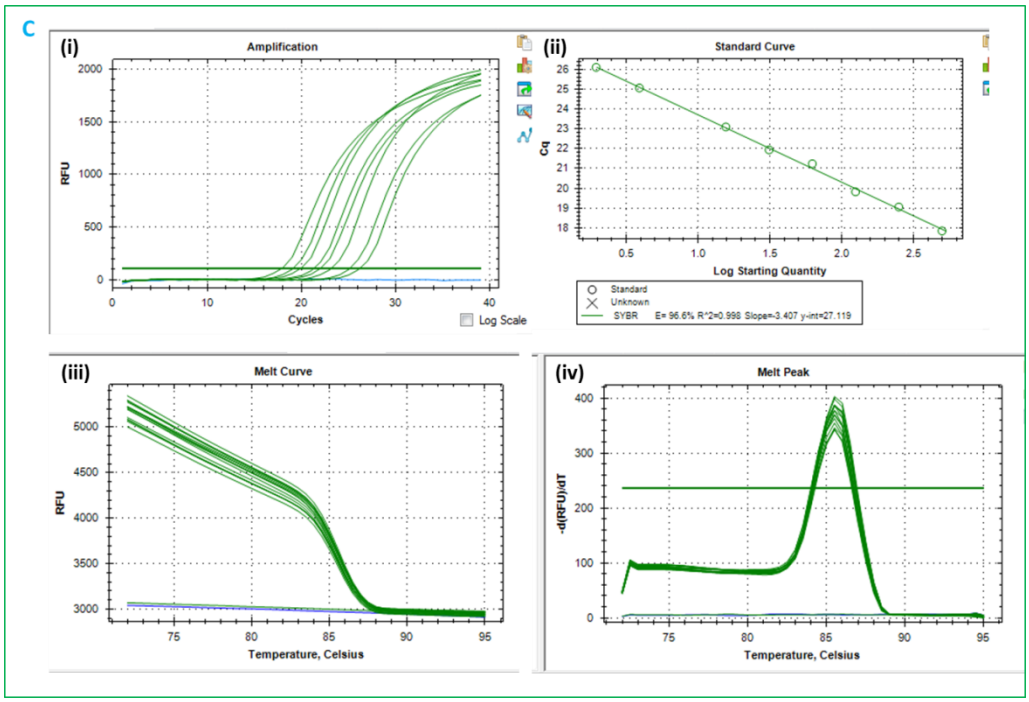

Figure B2C: RPS7 quantification plots of *An. funestus s.s.* immune challenged with *P. falciparum* infected blood meal. Graphical representation of RPS7 depicting **(i)** amplification curve showing exponential growth of the RT-PCR products; **(ii)** standard curve with reaction efficiency 96.6%, R^2 0.998 and a slope of -3.407 were more than five points of the curve fall in the line of best fit; **(iii-iv)** melt curve and peak showing single peaks indicating amplification of a single RT-PCR product. NTC are shown by the blue line at the bottom of the curves.

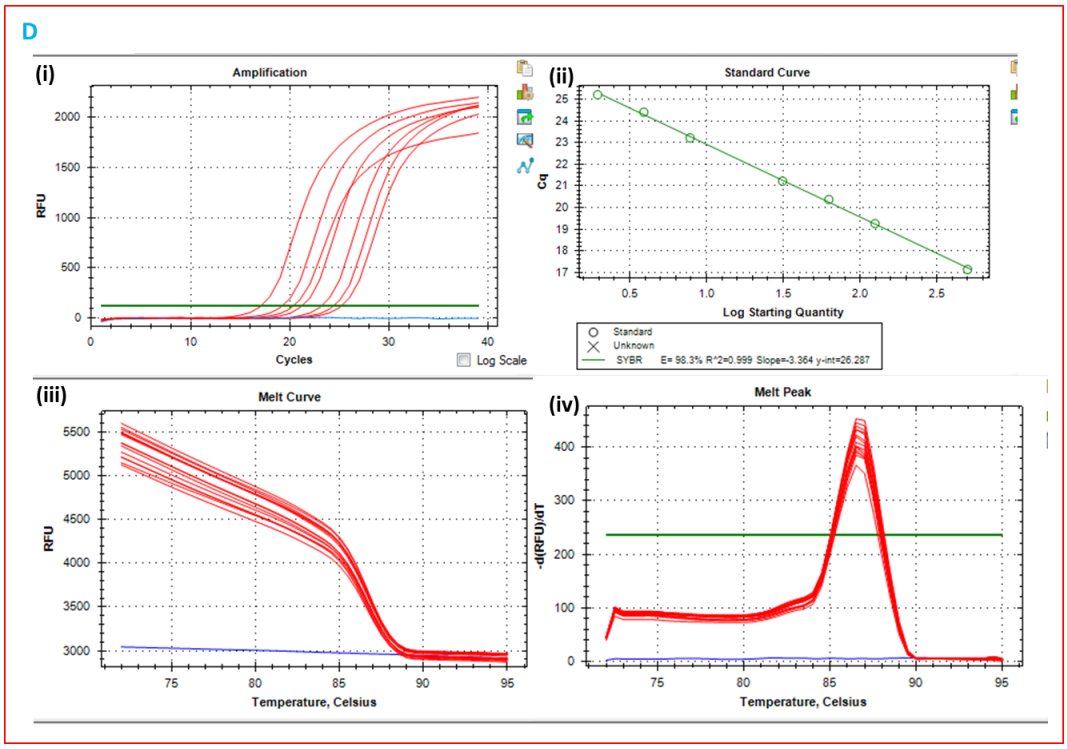

Figure B2D: RPL19 quantification plots of *An. funestus s.s.* immune challenged with *P. falciparum* infected blood meal. Graphical representation of RPL19 depicting **(i)** amplification curve showing exponential growth of the RT-PCR products; **(ii)** standard curve with reaction efficiency 98.3%, R^2 0.999 and a slope of -3.364 were more than five points of the curve fall in the line of best fit; **(iii-iv)** melt curve and peak showing single peaks indicating amplification of a single RT-PCR product. NTC are shown by the blue line at the bottom of the curves.

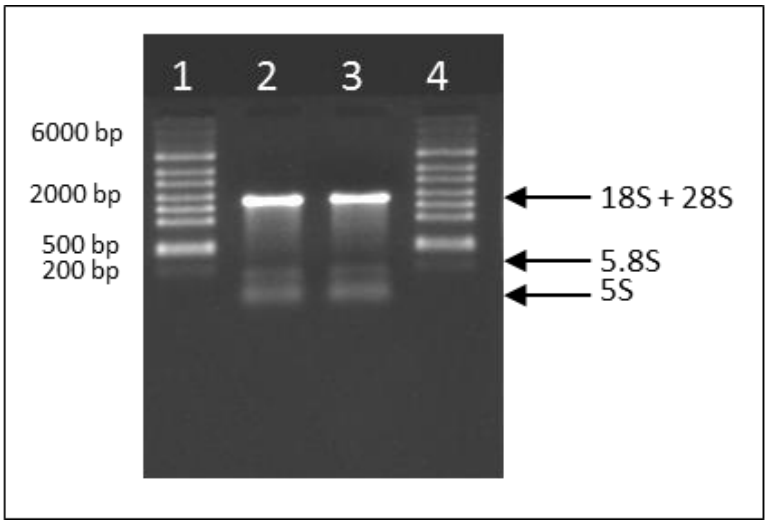

Figure B3: Total extracted rRNA migration patterns in CQ-treated *An. funestus s.s.* rRNA fragments were visualized on a 1% (w/v) denaturing agarose gel. Sizes were estimated by comparison to a 1kb RNA ladder (MWM). Sample RNA was loaded as follows: lane 1 and 4 MWM, lanes 2 CQ-treated mosquitoes and lanes 3 untreated control mosquitoes.

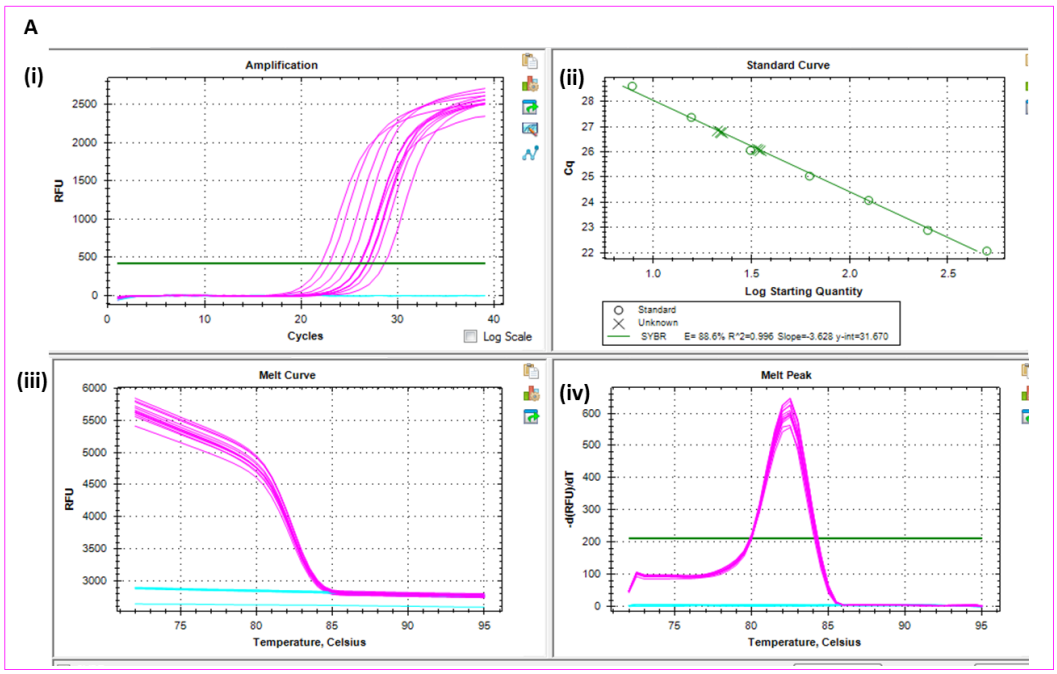

Figure B4A: CTL4 quantification plots of CQ-treated *An. funestus s.s.* Graphical representation of CTL4 depicting **(i)** amplification curve showing exponential growth of the RT-PCR products; **(ii)** standard curve with reaction efficiency 88.6%, R^2 0.996 and a slope of -3.628 were more than five points of the curve fall in the line of best fit and target samples fall within standard curve points **(iii-iv)** melt curve and peak showing single peaks indicating amplification of a single RT-PCR product. NTC are shown by the blue line at the bottom of the curves.

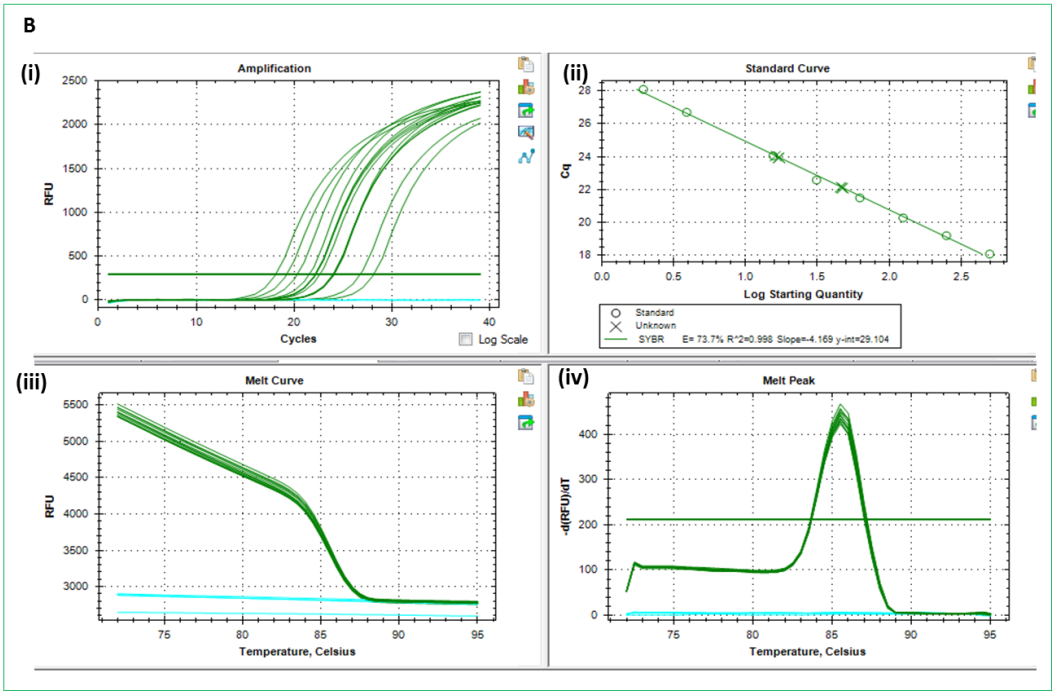

Figure B4B: RPS7 quantification plots of CQ-treated *An. funestus s.s.* Graphical representation of RPS7 depicting **(i)** amplification curve showing exponential growth of the RT-PCR products; **(ii)** standard curve with reaction efficiency 73.7%, R^2 0.998 and a slope of -4.169 were more than five points of the curve fall in the line of best fit and target samples fall within standard curve points **(iii-iv)** melt curve and peak showing single peaks indicating amplification of a single RT-PCR product. NTC are shown by the blue line at the bottom of the curves.

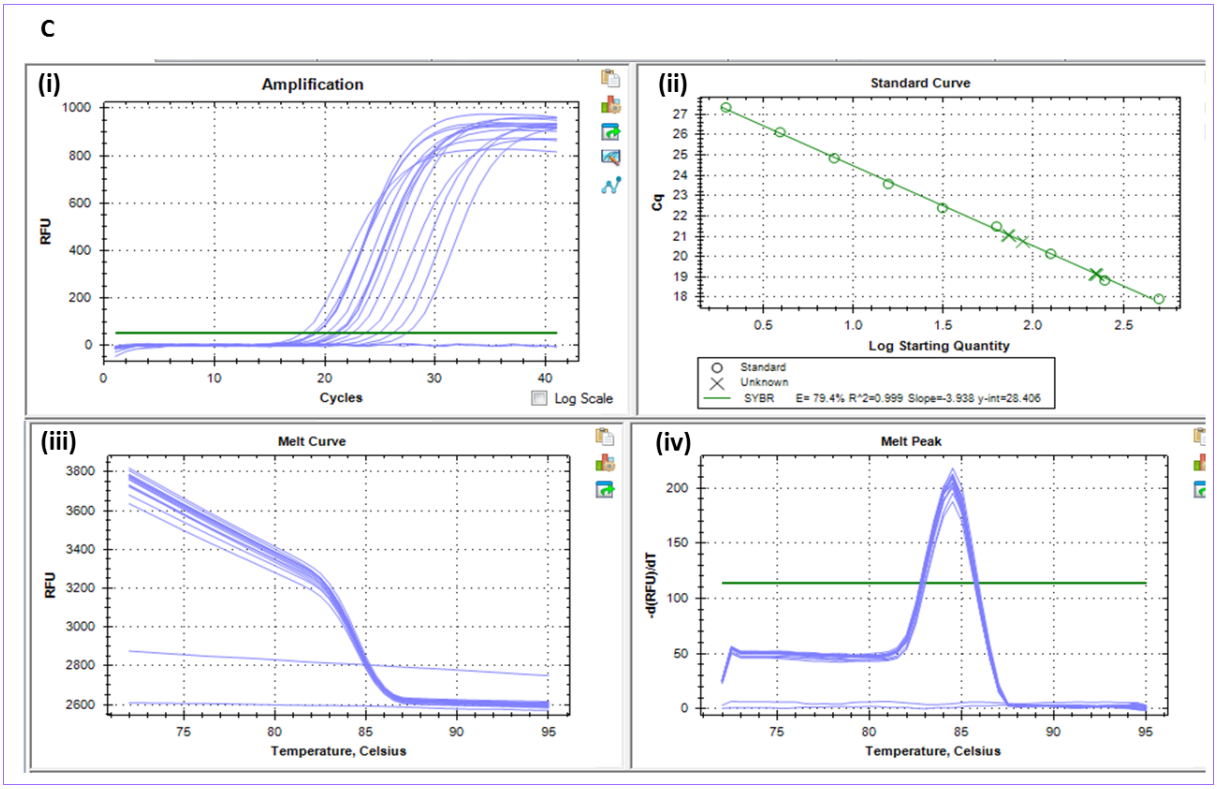

Figure B4C: RPS26 quantification plots of CQ-treated *An. funestus s.s.* Graphical representation of RPS26 depicting **(i)** amplification curve showing exponential growth of the RT-PCR products; **(ii)** standard curve with reaction efficiency 79.4%, R^2 0.999 and a slope of -3.938 were more than five points of the curve fall in the line of best fit and target samples fall within standard curve points **(iii-iv)** melt curve and peak showing single peaks indicating amplification of a single RT-PCR product. NTC are shown by the blue line at the bottom of the curves.

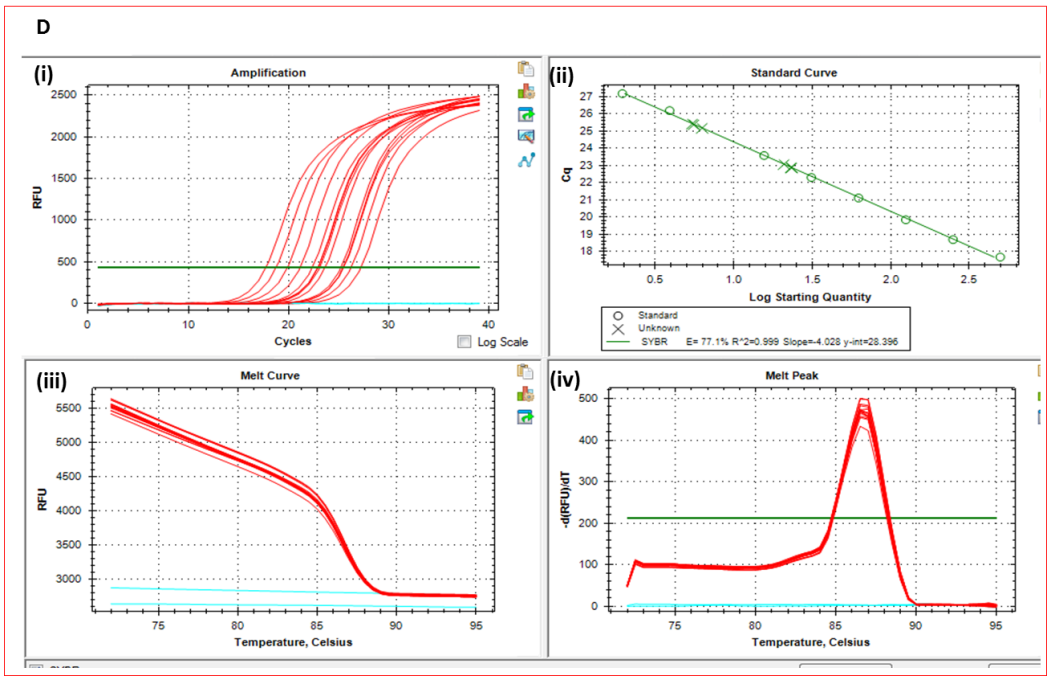

Figure B4D: RPL19 quantification plots of CQ-treated *An. funestus s.s.* Graphical representation of RPL19 depicting **(i)** amplification curve showing exponential growth of the RT-PCR products; **(ii)** standard curve with reaction efficiency 77.1%, R^2 0.999 and a slope of -4.028 were more than five points of the curve fall in the line of best fit and target samples fall within standard curve points **(iii-iv)** melt curve and peak showing single peaks indicating amplification of a single RT-PCR product. NTC are shown by the blue line at the bottom of the curves.

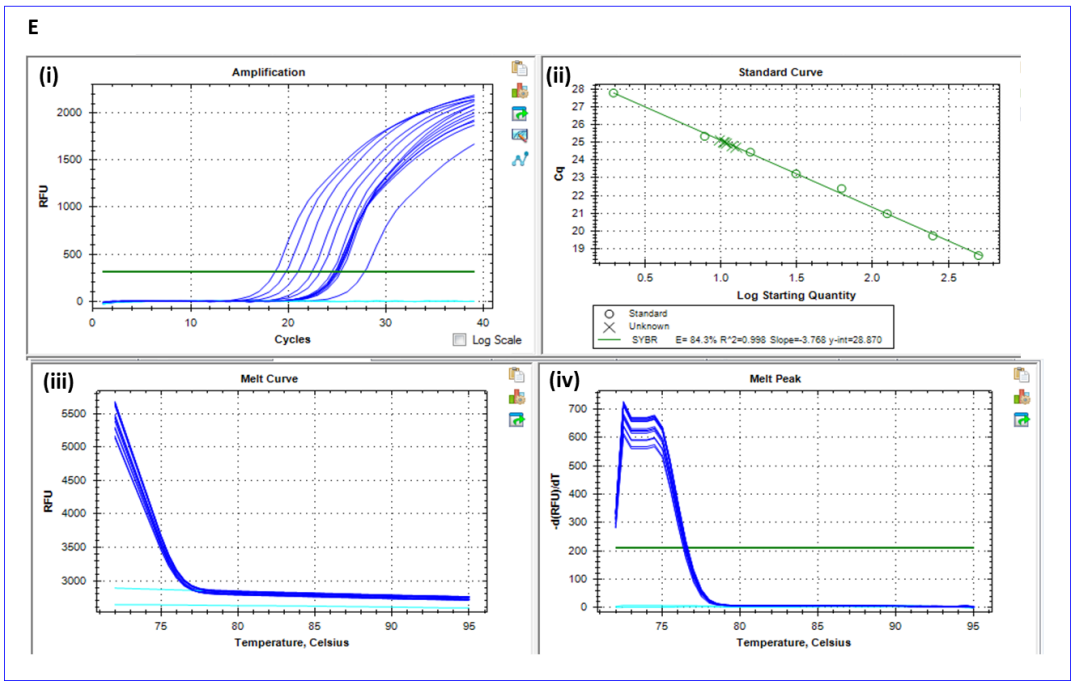

Figure B4E: ND_5 quantification plots of CQ-treated *An. funestus s.s.* Graphical representation of ND_5 depicting **(i)** amplification curve showing exponential growth of the RT-PCR products; **(ii)** standard curve with reaction efficiency 84.3%, R^2 0.998 and a slope of 3.768 were more than five points of the curve fall in the line of best fit and target samples fall within standard curve points **(iii-iv)** melt curve and peak showing single peaks indicating amplification of a single RT-PCR product. NTC are shown by the blue line at the bottom of the curves.